University of Alberta

Post-translational Myristoylation During Cell Death.

By

Dale David Orr Martin

A thesis submitted to the Faculty of Graduate Studies and Research
in partial fulfillment of the requirements for the degree of

Doctor of Philosophy

Department of Cell Biology

Fall 2011

Edmonton, Alberta

ABSTRACT

Myristoylation involves the addition of a 14-carbon fatty acid to the N-terminal glycine of proteins by N-myristoyltransferase. Myristoylation promotes protein-membrane and protein-protein interactions that are crucial for the function of myristoylated proteins. Myristoylation occurs co-translationally on the nascent polypeptide following the removal of the initiator methionine or post-translationally following the proteolytic exposure of an N-terminal glycine.

Herein, we describe how we employed bio-orthogonal myristate analogs that are incorporated into proteins at N-terminal glycines in an N-myristoyltransferase dependent manner, and subsequently, are chemoselectively ligated to various affinity tags that allowed the facile detection of the myristoylated proteins. These methods allowed the detection of myristoylated proteins by western blotting with exposure times ranging from seconds to minutes (~1-5 million faster compared to the incorporation of radioactive myristate into proteins).

Ultimately, we identified 7 post-translationally myristoylated proteins during apoptosis. These include the following caspase cleaved protein products: cell division control protein 6 homolog, cytoplasmic dynein-intermediate chain 2A, Huntingtin (Htt), microtubule-actin crosslinking factor 1, the apoptotic regulator induced myeloid leukemia cell

differentiation protein, protein kinase C epsilon (PKCε) and isoform 1 of YTH domain family protein 2.

Furthermore myristoylated ctPKCε was found to localize to membranes, increase ERK signaling and degradation of the pro-apoptotic protein Bim, which prevented a significant loss of mitochondrial potential of 17% over non-myristoylated ctPKCε in HeLa cells in the presence of apoptotic stimuli. Together, this suggests a possible anti-apoptotic role for post-translationally myristoylated caspase cleaved ctPKCε.

In addition, a 34 amino acid post-translationally myristoylated fragment of Htt released by the cleavage of two caspases was found to localize to ER and lysosomes. Moreover, overexpression of myr-ctHtt$_{N34}$-EGFP induced the formation of autophagosome-like vesicles that were associated with cell death in HeLa cells.

Overall, the new tools described within will enable the field of myristoylation by providing methods to rapidly detect, identify and characterize myristoylated proteins. Already, it has nearly tripled the number of identified post-translationally myristoylated proteins and through the identification of myr-ctHtt and myr-ctPKCε, we have shown the relevance of post-translational myristoylation during apoptosis with plausible implications in the pathophysiology of Huntington's disease.

ACKNOWLEDGEMENTS

First and foremost I would like to thank my supervisor Dr. Luc Berthiaume for accepting me into his lab and for both his guidance and patience during the many years I toiled within his lab. Over the years we have presented our work around the world, submitted a number of papers, with several on the way, and had a great deal of fun while doing so. Thank you so much for this experience.

In addition, I would like to thank my former supervisers, Drs. Douglas Hogue, Bob Ryan, Roger McLeod and Mike Oda, who instilled in me a passion for science and a desire to excel.

I would like to thank my graduate committee members Drs. Michele Barry and Richard Lehner for their guidance. I always left my committee meetings refreshed and excited to continue my projects. I would also like to thank Drs. Stephen Robbins and Thomas Simmen for reading my dissertation and sitting on my examining committee.

One of the most important lessons I have learned about graduate school is to surround your self with good people and I have had the serendipitous pleasure to meet and befriend people both inside and outside of the lab with the utmost integrity. These people have helped hold me up both scientifically and emotionally during the ups and downs of graduate school and life. Without them, I could not have done this. I cannot describe what you mean to me, but I will try.

Throughout my time in the Berthiaume lab, I have had the great pleasure and fortune to work with many talented people. I would like to thank Gareth Lambkin and Greg Plummer for their expertise, help and friendship. I could not have completed this work without the help of our current technician “Super” Megan Yap. Megan is a phenomenal technician whom I owe a great debt of gratitude. Dr. Gonzalo Vilas was my mentor early in my studies and his knowledge still far exceeds mine. It is a pleasure to call him a friend.

Maneka Perinpanayagam was my desk mate, lab mate and is now a friend. I thank her for her help, laughter and great cooking. Ryan Heit is a master of microscopy who has patiently guided me and helped me a lot along the way. Once again, I am grateful for your help and to have you as a friend.

To the undergrads, Chrisselle Ahpin and Jackie Sims, thank you for teaching me patience. Chrisselle contributed a great deal to the TRAMPP story and I must thank her for initiating that project. It has been a pleasure teaching you.

To the members of the lab overall, thank you for making the lab a place of fun, laughter and great science. Over the years, going to the lab everyday has become as comfortable as going home. Remember, the Star fish loves you!

Keith Jackson, Martha Curry, Andrew Goodmanson, Julie Robichaud, Robin Grant, Erin Brown, Rob Tower, Mireille St. Vincent and Kristen Conn have been fantastic friends that have supported me throughout my studies. Thank you Mim and Kristen for all the calming talks and support. You two have been lifesavers.

I would like to thank Kate Scroggins. Thank you for your support during the tumultuous race to the finish. You are the most perceptive, intuitive and understanding person I have met. Everyday that you are in my life I am happier.

Finally, I would like to thank my family; my brothers Craig and Lee and my parents Rick and Gail Martin and my grandparents Marie and Clarence Martin. Mom and Dad, I am the man I am today because of you, your love and the values you have instilled in me. Thank you for helping me reach my goals.

List of Abbreviations

Alk-C14, Alk-Myr	ω-alkynyl-myristate analogue, 13-tetradecynoic acid, Alkyne-myristate
Apaf-1	Apoptotic protease activating factor-1
APT1	Acyl-protein thioesterase-1
ARF	Adenosine diphosphate ribosylation factor
ATG	autophagy related gene
Az-C12	12-azidododecanoate or azido-myristate
Az-biotin	Azido-biotin
Bad	Bcl-2 antagonist of cell death
Baf	Bafilomycin
Bax	Bcl-2-associated X protein
Bcl	B-cell CLL/lymphoma 2
BH	Bcl-2 homology (BH) domains
Bim_{EL}	Bcl-2-interacting mediator of cell death extra long
BSA	Bovine serum albumin
CARD	Caspase recruitment domain
Caspase	Cysteinyl-aspartyl proteases
Cdc6	Cell division control protein 6 homolog
CD-IC2A	Cytoplasmic dynein-intermediate chain 2A
CHAPS	3-[(3-Cholamidopropyl)dimethylammonio]-1-propanesulfonate
CHX	Cycloheximide
CMA	Chaperone-mediated autophagy

ConA	Concanavalin A
CRD	Cysteine rich domain
ct	C-terminally or caspase truncated
$CuSO_4$	Copper(II)Sulphate
DAG	Diacylglyceride
DD	Death domain
DED	Death effector domains
DES	Dihydroceramide delta4 desaturase
DHHC	Aspartate, histidine, histidine, cysteine
DISC	Death inducing signalling complex
DMEM	Dulbecco’s modified Eagle’s medium
DMSO	Dimethyl sulphoxide
dNTP	Deoxyribonucleotide triphosphate
DTT	Dithiothreitol
EDTA	Ethylenediaminetetraacetic acid
Erk1/2	Extracellular signal-regulated kinase 1 and 2
FACS	Fluorescence-activated cell sorting
FADD	Fas-associated death domain
FAFBSA	Fatty acid free BSA
FBS	Fetal bovine serum
FTase	Farnesyl protein transferase
G2A	Glycine to alanine mutation at amino acid position 2
GGTase-1 and -2	Geranylgeranyl prenyltransferase
GPI	Glycosylphosphatidylinositol

GOAT	Ghrelin-O-Acyltransferase
HA	Hemagglutinin
HBSS	Hank’s Balanced Salt Solution (HBSS)
HD	Huntington’s disease (HD)
HEPES	4-(2-hydroxyethyl)-1-piperazineethanesulfonic acid
Hh	Hedgehog
HMA	2-hydroxy-myristic acid
Htt	Huntingtin
IAP	Inhibitor of apoptosis
ICAD	Inhibitor of caspase activated DNAse
IM	Isolation membrane
KH_2PO_4	Potassium phosphate mono-basic
KOH	Potassium hydroxide
LC3	Microtubule-associated protein 1 light chain 3
MACF1	Microtubule-actin crosslinking factor 1
MAPK	Mitogen-activated protein kinase
MARCKS	Myristoylated alanine-rich C-kinase substrate
MBOAT	Membrane bound O-acyl transferase
Mcl-1	Myeloid leukemia cell differentiation protein
MEF	Mouse embryonic fibroblasts
MEK	Mitogen-activated protein kinase or extracellular signal-regulated kinase kinase
$MgCl_2$	Magnesium Chloride
MOMP	Mitochondrial outer membrane permeabilization

mTOR	Mammalian target orthologue of rapamycin
Myr	Myristate, myristic acid
N_{11}-EGFP	11 amino acids appended to the N-terminus of EGFP
N34	34 amino acids
Na_2CO_3	Sodium bicarbonate
NaCl	Sodium chloride
NaOH	Sodium hydroxide
NH_4Cl	Ammonium chloride
NMT	N-myristoyltransferase
PAK2	p21-activated kinase 2
PAS	Phagophore assembly site
PAT	Protein fatty acyl transferases
PBS	Phosphate buffered saline
PCR	Polymerase chain reaction
PI	Phosphoinositide
PI3K	Phosphatidylinositol-3-kinase
PKCε	Protein Kinase C epsilon
PS	Phosphatidylserine
PVDF	Polyvinylidene fluoride
RPMI	Roswell Park Memorial Institute
RIPA	RIPA radioimmunoprecipitation assay
ROS	Reactive oxygen species
SHOC2	Soc-2 suppressor of clear homolog

Smac/DIABLO	Second Mitochondria-derived Activator of Caspases/Direct IAP Binding Protein with Low PI
STS	Staurosporine
TBS	Tris buffered saline
TCEP	Tris-carboxyethylphosphine
TEMED	N,N,N’,N’,-tetramethylenediamine
TMRE	Tetramethylrhodamine, ethyl ester
TNFα	Tumour Necrosis Factor α
TRAMPP	Tandem reporter assay for myristoylated proteins post-translationally
U0126	MEK inhibitor
VDAC	Voltage-dependent anion channel
WT	Wild-type
YTHDF	Isoform 1 of YTH domain family protein 2
z-DEVD-FMK	Caspase-3 inhibitor
z-VA-FMK	Negative caspase inhibitor
z-VAD-FMK	General/pan caspase inhibitor

List of Tables

List of Figures

CHAPTER 1 INTRODUCTION

A version of this chapter has been published in Martin, D.D.O.*, **Beauchamp, E.*, Berthiaume, L.G. (2011) Post-translational myristoylation: fat matters in cellular life and death.** *Biochimie.* 2011 Jan; 93(1):18-31.

*__authors contributed equally.__

1.1. Protein lipidation: an overview

1.1.1. Cholesteroylation, Prenylation and Glypiation

The covalent addition of lipids to proteins plays many roles inside and outside of the cell. It directs proteins to various cellular membranes and sub-membrane domains and promotes protein-protein interactions. In addition, lipidation can directly regulate protein function similar to phosphorylation (Kostiuk et al., 2010; Martin et al., 2010; Resh, 2004). Therefore, lipidation is essential for the function of many proteins. As such, blocking the addition of these lipids to their protein substrates has an inhibitory role on their ultimate functions. Proteins can be co- or post-translationally modified with a wide variety of lipids. The categories of modification are characterized by the identity of the lipid moiety attached, the nature of the covalent bond, the attachment site of the lipid on the protein and the enzymes catalyzing the reactions involved. Five major types of lipid modification are known. Cholesteroylation, prenylation, glypiation and fatty acylation (Nadolski and Linder, 2007) are described immediately below and the addition of phosphatidylethanolamine to the autophagy protein LC3 is described in Section 1.5.4.4.

In cholesteroylation, a cholesterol molecule is esterified to a C-terminal glycine residue via an autocatalytic process (Mann and Beachy, 2000; Porter et al., 1996). To date, Hedgehog (Hh) proteins remain the

only known example of cholesteroylation, but additionally detected cholesteroylated proteins remain to be identified (Porter et al., 1996). During the maturation of Hh through the secretory pathway, its carboxy terminal intein domain mediates the auto-catalytic proteolysis of the protein at the C-terminus between Gly-Cys within the conserved tripeptide sequence Gly-Cys-Phe. Subsequently, cholesterol is covalently linked to the C-terminal glycine via an ester bond, thereby activating the amino terminal signaling domain. Of note, palmitoylation of the Hh protein on its N-terminal cysteine residue via an amide bound complete its processing (Buglino and Resh, 2008).

Prenylation involves the formation of an irreversible thioether bond between either of two specific isoprenoids and one or two C-terminally located cysteine residue(s) by a variety of prenyl transferases (Crowell and Huizinga, 2009). Isoprenoids are polymers of the 5-carbon unit of isopentyl diphosphate and are integral intermediates in the synthesis of cholesterol (McTaggart, 2006). The addition of the 15-carbon and 20-carbon isoprenoids known as farnesyl and geranylgeranyl are referred to as farnesylation and geranylation, respectively. In mammalian cells, each moiety has a specific prenyltransferase, which appends the lipid to the protein: farnesyl protein transferase (FTase) and geranylgeranyl prenyltransferase (GGTase-1 and -2). FTase recognizes cysteine residues within a C-a-a-X motif at the C-terminus. The “a” represents aliphatic residues and X represents serine, methionine, glutamine, or alanine at the

extreme C-terminus of the protein. Substrates of FTase include N-Ras, K-Ras, H-Ras and prelamin A (McTaggart, 2006). When “X” is a leucine residue, the protein will be a substrate for GGTase-1 and its substrates include the small GTPases Rac1, CDC42 and Rho B. The third prenyltransferase, GGTase-2 is specific for the Rab family of small GTPases, which are involved in vesicular trafficking. Generally, they contain 2 C-terminal cysteine residues (X-X-C-C, X-C-X-C, or C-C-X-X) (Basso et al., 2006; Roskoski, 2003).

Following prenylation, the proteins are further modified. First, the final three amino acids (-a-a-X) following the cysteine residue are removed by the endoprotease Ras-converting enzyme 1 (Rce1) (Bergo et al., 2004) and, subsequently, the newly exposed C-terminal isopentylcysteine is carboxymethylated by isopentylcysteine carboxyl transferase (Sinensky, 2000). Likewise, the terminal carboxylic acid moiety is also carboxymethylated in dually geranylgeranylated proteins.

In glypiation, a very large glycolipid moiety referred to as a glycosylphosphatidylinositol (GPI) anchor is added to the C-terminus of a protein. The GPI-anchor is a large bulky molecule consisting of a phosphatidylinositol group, glucosamine, trimannoside and an ethanolamine linker. The GPI moiety is added after a long stretch of hydrophobic amino acids localized to the carboxy terminus of proteins through an amide bond between the ethanolamine groups of the GPI anchor. The addition of the GPI moiety results in the cleavage of the C-

terminal polypeptide backbone. The transamidation reaction is catalysed within the lumen of the endoplasmic reticulum by a GPI-transaminidase complex consisting of the GPI-anchor attachment protein 1 (GAA1), GPI protein 8 (GPI8), and, the class S and class T phosphatidylinositol glycan biosynthesis proteins (PIG-S and PIG-T, respectively) (Mayor and Riezman, 2004; Paulick and Bertozzi, 2008). GPI anchored proteins are found on the luminal side of endocytic secretory vesicles and the exoplasmic leaflet of the plasma membrane. In mammals, the GPI anchor enables proteins to target to the lipid rafts and transduce signals across the lipid bilayer of the plasma membrane such as oxidative burst, Ca^{2+} influx, protein tyrosine phosphorylation, cell proliferation or inhibition of cell growth. Interestingly, despite being linked through an irreversible amide bond, GPI anchorage can be released by endogenous hydrolases that include, phosphoinositide (PI)-phospholipase C, PI-specific phospholipase D and GPI-specific phospholipase C (Mayor and Riezman, 2004).

1.1.2 Fatty Acylation

1.1.2.1 S-Acylation and Rare Fatty Acylations.

Fatty acylation consists, primarily, of the covalent addition of palmitic or myristic fatty acids to proteins. In S-acylation, saturated and unsaturated long chain fatty acids of various carbon chain lengths are

covalently linked via a reversible thioester bond between the fatty acid carboxyl group and the free sulfhydryl group of cysteine residues of a protein. Because palmitic acid is the most abundant fatty acid available in the cell, S-acylation typically corresponds to the reversible attachment of the 16-carbon saturated fatty acid palmitate and is thus most commonly referred to as palmitoylation (Fukata and Fukata, 2010). In some cases, the palmitoyl moiety is linked to proteins via an amide bond on N-terminal cysteine (e.g. Hh proteins) or glycine residues (e.g. G_{α} proteins) (Kleuss and Krause, 2003; Pepinsky et al., 1998).

S-acylation may occur spontaneously both *in vitro* and *in vivo*, or it can be mediated by a myriad of protein fatty acyl transferases (PATs) belonging either to the zDHHC-CRD PATs family or the membrane bound O-acyl transferases (MBOATs) family (Corvi et al., 2001; Kostiuk et al., 2009; Kostiuk et al., 2010; Liang et al., 2004; Resh, 2006). The zDHHC-CRD PATs are multipass proteins containing either 4 or 6 transmembrane domains. The defining sequence elements that makes up the core of the active site consists of a 50 amino acid zinc-finger-like DHHC (aspartate, histidine, histidine, cysteine) cysteine rich domain (CRD) within a cytosolic loop. Mammals possess 23 distinct zDHHC-CRD PATs that carry out the bulk of palmitoylation of proteins in the cytosol. The MBOATs palmitoylate secreted proteins like Wnt and Hh.

Only one protein so far has been identified as a true depalmitoylation enzyme *in vivo*; acyl-protein thioesterase-1 (APT1). APT1

has been shown to depalmitoylate $G\alpha_{13}$ *in vitro* and H/N-Ras *in vivo.* It is thought that APT1 aids in the dynamic properties of palmitoylation thereby providing a possible mechanism for the trafficking of H/N-Ras between the Golgi and plasma membrane. Palmitoylation of H/N-Ras occurs first at the Golgi which provides a stable association with membranes. Subsequently, palmitoylated H/N-Ras traffics to the plasma membrane where it can perform its signaling duties after which it may be depalmitoylated by APT1 and traffic back to the Golgi (Dekker et al., 2010; Siegel et al., 2009).

Alternative forms of fatty acylation have also been reported. The appetite-stimulating peptide hormone ghrelin is known to be acylated on serine 3 with octanoate (Kojima et al., 1999), a reaction catalysed by Ghrelin-O-Acyltransferase (GOAT), a member of the MBOAT family (Yang et al., 2008). Interestingly, because GOAT appears to be regulated by dietary lipids (Kirchner et al., 2009) and octanoylation is essential for ghrelin's physiological activity (Kojima and Kangawa, 2005), GOAT inhibition has become a potential target for appetite suppressants helpful in the treatment of the metabolic syndrome. Furthermore, in addition to being palmitoylated on Cys77 (Willert et al., 2003), the signaling protein Wnt is also modified with the unsaturated fatty acid palmitoleic acid on a highly conserved serine (Ser209). The acylation at both sites is catalyzed by the MBOAT Porcupine (Takada et al., 2006). Recently, a novel form of fatty acylation was detected by tandem MS. For the first time, oleic acid was found to be covalently linked to a Lysine side chain via an amide bond

in the lens membrane protein Aquaporin 0. It is thought that this modification targets the protein to lipid rafts (Schey et al., 2010).

1.1.2.2.1. Myristoylation.

Myristoylation typically consists of the covalent addition of the 14-carbon saturated fatty acid myristate to the N-terminal glycine residue through a stable amide bond (Boutin, 1997; Farazi et al., 2001). The reaction is catalysed by myristoyl-CoA:protein N-myristoyltransferase (NMT) (Towler et al., 1987a). In some rare cases of myristoylation, including the insulin receptor (Hedo et al., 1987) and interleukin 1 α and β (Bursten et al., 1988), myristic acid is also attached to an internal lysine via an amide bond. The enzyme that mediates lysine myristoylation is unknown. Historically, N-myristoylation was initially described as an unusual blocking group, which prevented the direct use of Edman degradation at the N-terminus of the catalytic subunit of cyclic AMP-dependent protein kinase (Carr et al., 1982) and calcineurin B (Aitken et al., 1982). It was later determined by mass spectrometry that the blocking group was myristic acid.

A

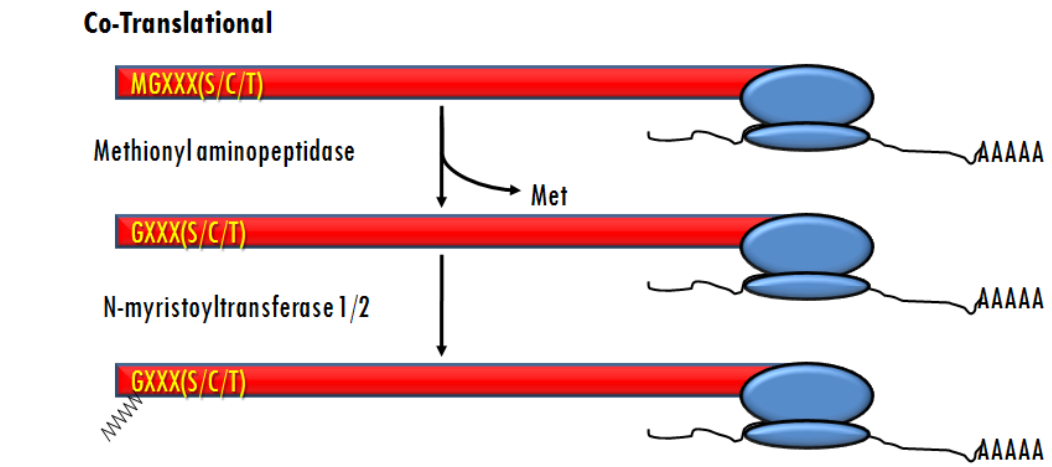

B

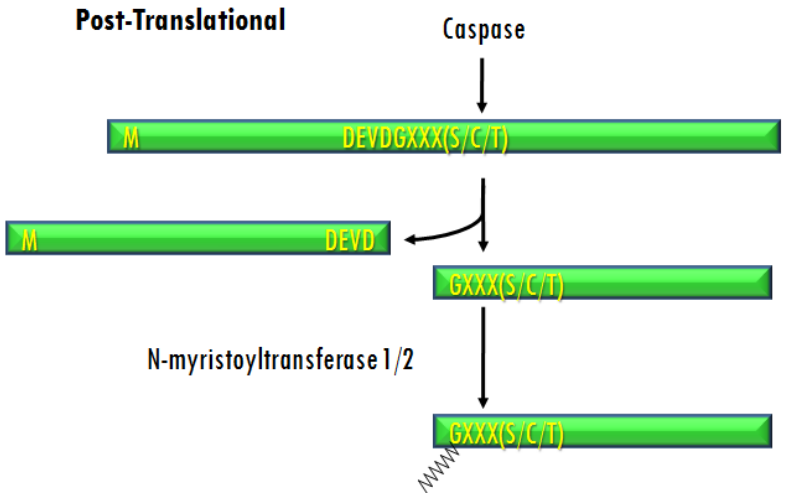

Figure 1.1. - Co- and post-translational attachment of myristate to proteins. Myristoylation involves the covalent addition of the saturated 14-carbon fatty acid myristate to the N-terminal glycine residues of **A** A nascent polypeptide following removal of the initiator Met (co-translational myristoylation) or **B** a cryptic myristoylation site following exposure by caspase cleavage (post-translational myristoylation) (Martin et al., 2010).

Subsequently, N-myristoylation was described as a co-translational modification (Deichaite et al., 1988; Wilcox et al., 1987) that occurs on the nascent polypeptide, as it is being translated by the ribosome, following the removal of the initiator methionine residue (Figure 1.1.A). Interestingly, removal of the initiator methionine by methionine aminopeptidase is a common modification of proteins, occurring in up to 80% of total protein (Matheson et al., 1975). The efficiency of methionine removal is greater when the amino acid residue following the initiator methionine is a glycine residue (Frottin et al., 2006).

However, only specific proteins are myristoylated due to the requirement of specific amino acids to be part of a loose consensus sequence recognized by NMT. Now, it is also well established that myristoylation can also occur post-translationally after caspase cleavage exposes a cryptic internal myristoylation to the action of NMT (Figure 1.1.). Myristoylation can also occur post-translationally on an internal glycine within a cryptic myristoylation consensus sequence exposed by the action of caspases in apoptotic cells (Martin et al., 2008; Sakurai and Utsumi, 2006; Utsumi et al., 2003; Vilas et al., 2006; Yap et al., 2010; Zha et al., 2000) (discussed in detail in the following sections below) (Figure 1.1B). Interestingly, as with the preference of Gly in position 2 for methionyl aminopeptidase, analysis of the caspase-cleaved proteome revealed that there is a higher selectivity for caspases to cleave proteins between an Asp and Gly residue (Dix et al., 2008; Mahrus et al., 2008), thereby

preferentially generating C-terminal products with N-terminal Gly suggesting that there might be numerous cases of post-translational myristoylation yet to be uncovered. Post-translational myristoylation will be discussed in greater detail below.

A large number of myristoylated proteins play key roles in a myriad of cellular signaling pathways [e.g. non-receptor protein tyrosine kinases, heterotrimeric G_{α} proteins, Myristoylated alanine-rich C-kinase substrate (MARCKS) and calcium binding proteins (e.g. Recoverin, Neurocalcin) (Resh, 2006)]. For many of these proteins, the myristoyl moiety contributes to a variety of protein functions including subcellular targeting, protein-protein and protein-membrane interactions required for the activities of these proteins (Johnson et al., 1994). Typically, blocking myristoylation of these proteins reduces their functions. Although myristoylation is required for membrane binding, it is not sufficient to maintain membrane association and must be augmented by downstream interactions in order to provide stable membrane anchoring (Peitzsch and McLaughlin, 1993). This is usually achieved by an adjacent or distant polybasic domain, by one or two nearby palmitoylated cysteine residues or by a protein-lipid binding domain such as the phosphoinositide binding Pleckstrin homology domain (Figure 1.2) (Maurer-Stroh et al., 2004; Resh, 2004). Myristoylation also participates in differential targeting to membranes and sub-membrane domains known as lipid rafts. Localization appears to be directed by adjacent amino acids along with the secondary

binding signal (McCabe and Berthiaume, 1999; McCabe and Berthiaume, 2001).

Although myristate is irreversibly bound to proteins it allows the acylated protein to reversibly sample membranes because of its weak hydrophobic nature. Consequently, the half life of a membrane bound myristoylated peptide is in the order of minutes in comparison to hours for palmitoylated or dually acylated, myristoylated and palmitoylated, peptides (Silvius, 2002).

The dynamic interchange between myristoylated proteins and membranes can be further regulated by a mechanism referred to as “myristoyl switches” (Figure 1.2). For example, a myristoyl moiety may be sequestered into a hydrophobic domain that becomes exposed following a conformational change induced by binding a ligand (McLaughlin and Aderem, 1995). This concept is exemplified by the binding of GTP to the ADP ribosylation factor (ARF) proteins or calcium to recoverin (Figure 1.2), which result in a conformational change that promotes the exposure of the previously hidden myristoyl moiety and subsequent targeting of these proteins to membranes (Ames et al., 1996; Amor et al., 1994). Another variation of the “myristoyl switch” includes the myristoyl electrostatic switch. MARCKS protein contains a myristoylated glycine and a polybasic domain. The positively charged amino acid side chains of the polybasic domain interact with the negatively charged phospholipid headgroups of the membrane. Phosphorylation of serine residues within the polybasic

domain of MARCKS by protein kinase C (PKC) releases the protein from the membrane by reducing the positive charge of the polybasic domain (Seykora et al., 1996).

A variation on the above, linking acylation and phosphorylation, is exemplified by c-Abl and c-Src, which are regulated by a "myristoyl/phosphotyrosine" switch (Hantschel et al., 2003). In c-Abl, the myristoyl moiety is sequestered into a hydrophobic pocket which induces a conformational modification of the protein allowing the docking of the SH2 and SH3 domain onto the kinase domain and auto-inhibition of the enzyme (Nagar et al., 2003). A similar pocket has recently been predicted to exist in the c-Src kinase but, in contrast to c-Abl, myristoylation enhanced c-Src activity (Patwardhan and Resh, 2010). This suggests that myristoylation associated with the other non-receptor tyrosine kinases (e.g. Blk, Lyn, and Fyn) may not just localize these proteins to membranes, but may also regulate their activities.

1.2. N-Myristoyltransferases

In vertebrates, co-translational and post-translational N-myristoylation is catalyzed by two NMTs (Figure 1.1), NMT1 and NMT2, which are members of the GCN5 acetyltransferase superfamily (Dyda et al., 2000). To date, an NCBI database search for NMT annotated

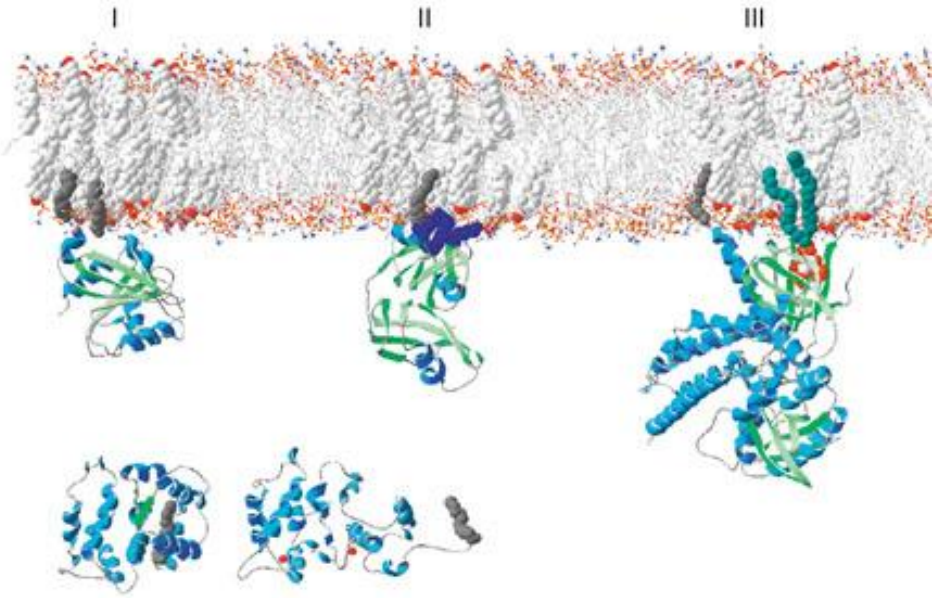

Figure 1.2. - Myristoylation and secondary downstream membrane binding motifs. Schematic representation of the membrane attachment of proteins with a myristoyl anchor (dark gray, space-filling atomic representation) in combination with different co-occurring membrane-attachment factors. Class I, plus palmitoyl anchor (also dark gray, space-filling); class II, plus cluster of positive charges (dark blue, spacefill); class III, plus PIP_2-specific binding domain (PIP_2 in space-filling, alkyl tails in cyan); Two different states of the calcium/myristoyl-switch of recoverin are depicted in the lower left of the figure (calcium ions in red). Visualization is with SwissPdb-Viewer [modified from (Maurer-Stroh et al., 2004)].

entries revealed the presence of the gene encoding for NMT in 53 organisms from taxa spanning animals, plants, apicomplexan parasites (e.g. Plasmodium falciparum), fungi and yeast (Martin et al., 2010). Of these 53 organisms 16 contained both NMT1 and NMT2. NMTs have been purified and cloned from many organisms (Duronio et al., 1989; Giang and Cravatt, 1998; Lodge et al., 1994; Ntwasa et al., 1997; Rioux et al., 2006). However, the most extensively studied NMT comes from *Saccharomyces cerevisiae* and has provided the majority of information regarding the enzymology of the reaction (Towler and Glaser, 1986; Towler et al., 1987a). NMTs perform their catalysis via an ordered Bi Bi reaction mechanism with myristoyl-CoA binding first, peptide binding second, followed by a direct

nucleophilic addition-elimination reaction and the sequential release of CoA and the myristoyl-peptide (Rudnick et al., 1991).

The two genes encoding for the two isoforms of NMT were identified in humans and share about 76% amino acid sequence identity. The two NMTs have unique as well as overlapping substrate specificities (Giang and Cravatt, 1998; Yang et al., 2005). NMT activity is essential for survival. Knockout of NMT in organisms that only express one form of NMT, such as in Drosophila and *S. cerevisiae*, is lethal (Duronio et al., 1989; Ntwasa et al., 2001)). NMT1 is the main NMT expressed during embryogenesis. Consequently, $NMT1^{-/-}$ mice die during embryogenesis. This suggests that NMT2 is not able to rescue N-myristoylation of proteins

for the proper development of the mice embryos. These results indicate that both NMTs must have their own subsets of unique substrates and that NMT1 or some proteins perhaps strictly myristoylated by NMT1 play a crucial role in development (Yang et al., 2005).

NMTs are highly selective for the substrate myristoyl-CoA in enzymatic assays *in vitro* (Bhatnagar et al., 1994; Kishore et al., 1991). This is attributed to the 3D structure of NMT which appears to contain a bent active site cavity that is only large enough to optimally accommodate a 14-carbon fatty acid (Bhatnagar et al., 1999). This leads to a bend in the fatty acid at the vicinity of C5 (Rudnick et al., 1992b). However, different *in vitro* studies have shown that NMT can catalyze the linkage of a synthetic peptide that mimics the N-terminal region of a protein to different fatty acids, such as lauric, tridecanoic, pentadecanoic and palmitic acid (Rudnick et al., 1992b; Rudnick et al., 1990). In the retina, several proteins are heterogeneously myristoylated with the unsaturated fatty acids C14:1 n-9 and C14:2 n-6 (DeMar et al., 1999), but no retinal specific isoform of NMT able to use various fatty acyl-CoA substrates has been identified thus far (Rundle et al., 2004). Although, it has been suggested that the heterogenous N-terminal acylation of retinal proteins arises from the retina's unusual lipid metabolism and the fact that myristate is found is found in low abundance (Bereta and Palczewski, 2011).

Myristoyl-CoA is found at very low concentrations in the cell at approximately 5 nM in animal cells (Faergeman and Knudsen, 1997). Only

0.05% of radiolabeled myristic acid added to rat hepatocytes was found to be dedicated to the N-myristoylation of proteins (Rioux et al., 2002). NMT has been shown to be capable of utilizing palmitic acid as a substrate *in vitro*, albeit at a reduced efficiency compared to myristate (Kishore et al., 1993; Rudnick et al., 1992b; Suzuki et al., 2007). In addition, cellular palmitic acid concentrations are significantly higher than myristic acid. This may suggest that myristoyl-CoA may be available to NMT in specific pools within the cell (Johnson et al., 1994). It has recently been suggested that myristic acid transported by CD36, a class B scavenger receptor found on the surface of many cell types, may be involved in transporting and providing a intracellular pool of myristoyl-CoA for the myristoylation of Fyn, Src and NOS (Isenberg et al., 2007).

1.3. Protein requirements for myristoylation.

The general consensus peptide sequence recognized by NMTs is Gly_2-X_3-X_4-X_5-$(Ser/Thr/Cys)_6$ where X represents most amino acids, except for proline, aromatic or charged residues in position X_3. The amino-terminal Gly residue is absolutely required for myristoylation to occur and substitution of this residue to any other abrogates myristoylation. It is set at position 2 to indicate that it follows either the initiator Met (Position 1) or the internal Asp residue where caspases will cleave. Ser, Thr, Cys are preferred at position X_6, but other amino acids can be tolerated at this

position (e.g. Ala found in Annexin XIII and Gly found in c-Abl tyrosine kinase) (Jackson and Baltimore, 1989; Turnay et al., 2005). Moreover, the combination of amino acids at position X_3, X_6 and X_7 play important roles for the N-myristoylation of the candidate protein (Utsumi et al., 2004). For instance, a Lys residue at position 7 reduces the stringency for certain amino acids at position 3 and is also important in conferring membrane binding properties (Silverman and Resh, 1992; Utsumi et al., 2004). These studies and others have formed the basis for the development of myristoylation prediction models (Boisson et al., 2003; Maurer-Stroh et al., 2002a; Podell and Gribskov, 2004; Sugii et al., 2007). Using computer analysis, the 16 N-terminal residues following the initial methionine were demonstrated to be required for the prediction of the myristoylation status of the protein (Maurer-Stroh et al., 2002b). As such, it was determined that the first 6 amino acids are required for recognition by NMT and are inserted into the binding pocket of the enzyme. The next 3 amino acids are thought to interact with NMT outside of the binding pocket. The final amino acids act as a hydrophilic linker between the enzyme and the rest of the nascent polypepide (Figure 1.3). Using this information with computer algorithms, it is estimated that 0.5 to 3% of the mammalian and plant

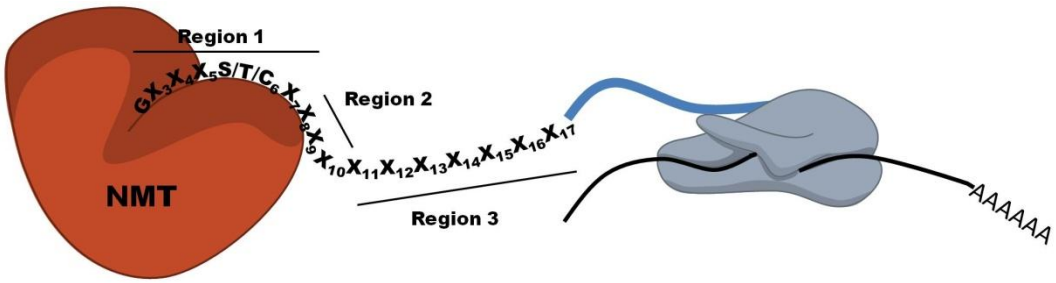

Figure 1.3. - Schematic representation of the interaction between NMT and its protein substrate. The first 17 N-terminal amino acids of an NMT substrate have different types of variability restrictions. Three motif regions have been identified: region 1 (positions 2-7) fits into the binding pocket; region 2 (positions 8-10) interacting with the NMT's surface at the mouth of the catalytic cavity; and region 3 (positions 11-17) comprising a hydrophilic linker.

proteomes consist of myristoylated proteins (Boisson et al., 2003; Maurer-Stroh et al., 2002a; Podell and Gribskov, 2004; Sugii et al., 2007).

1.4. Regulation of myristoylation in health and disease.

The regulation of NMT activity still remains relatively unknown, but it is presumed that levels of NMT activity are necessary and sufficient to efficiently acylate endogenous proteins. However, it has been suggested that NMT activity might be limited by the scarce levels of myristoyl-CoA itself (Colombo et al., 2005; van der Vusse et al., 2002). In this context, it is somewhat paradoxical that NMT levels are elevated in several types of tumours (Selvakumar et al., 2007). In addition, endogenous inhibitors of NMT have been identified. An NMT inhibitor named NMT inhibitor protein 71 (NIP71) was isolated from bovine brain using an *in vitro* NMT assay (King and Sharma, 1993). NIP71 shares 43% identity with the heat shock cognate protein 70 (HSC70). Subsequently, the same group also demonstrated that the glycolytic enzyme enolase is also able to inhibit N-myristoylation *in vitro* (Shrivastav et al., 2003). The molecular interplay between NMT and these inhibitors has yet to be determined.

1.4.1. Crosstalk between myristoylation and phosphorylation.

Phosphorylation of hNMT1 has been shown to regulate the activity of the enzyme. A Tyr100Phe mutation in NMT1 resulted in a 98% decrease of NMT activity (Rajala et al., 2001). However, the extent and the site(s) of phosphorylation are not fully characterized since this mutant was still partially phosphorylated (17% as compared to wild type). Interestingly, NMT was shown to be phosphorylated by Src family tyrosine kinase members of Lyn and Fyn (Rajala et al., 2001) that are, in turn, myristoylated (Selvakumar et al., 2007). In fact, it has been proposed that there is an interaction between the N-terminal domain of hNMT1 and Lyn tyrosine kinase in a phosphorylation dependant manner (Selvakumar et al., 2007). Because, NMT1 and NMT2 have their major amino acid sequence differences at their N-termini (Giang and Cravatt, 1998), this suggests that differential phosphorylation might allow for the fine tuning of the two NMT activities inside the cell.

Interestingly, although the N-terminal region is not required for the activity of NMTs and because it exhibits significant sequence differences between the two enzymes, it has been postulated that the N-terminus allows the differential targeting of NMTs to various cellular compartments, as well as provide access to cellular myristoyl-CoA pools (Rudnick et al., 1992a) and the differential binding to ribosomes (Farazi et al., 2001).

The interactions between NMTs and Src tyrosine kinases underline a possible complex interplay between phosphorylated NMT by its respective myristoylated tyrosine kinases. It is well established that those myristoylated tyrosine kinases ($pp60^{src}$, $pp60^{yes}$, $pp56^{lck}$, $pp59^{fyn/syn}$ and c-Abl) (Cross et al., 1984) display elevated activity in many human cancers (Summy and Gallick, 2003). As stated previously, c-Abl and c-Src activities are intimately linked to their myristoylation statuses (Hantschel et al., 2003). In addition, increased protein and mRNA levels of $pp60^{src}$ were shown in human colon carcinoma, and many human cancer cell lines such as HT29, COLO 201 and COLO 205 (Dehm et al., 2001; Dehm and Bonham, 2004). These data suggested that the regulation of $pp60^{src}$ happens at the level of transcription with two distinct promoters (SRC1A and SRC1α) (Bonham and Fujita, 1993). Inhibition of $pp60^{src}$ myristoylation decreased colony formation, cell proliferation and targeting to the membrane demonstrating the importance of $pp60^{src}$ myristoylation for tumuorigenicity (Shoji et al., 1990). Moreover, myristoylation seems to be critical for the dephosphorylation of $pp60^{src}$ and its subsequent kinase activity (Bagrodia et al., 1993). Myristoylation increases $pp60^{src}$ kinase activity but also regulates the stability of the protein. Recently, it was shown that myristoylation-dependant membrane targeting of $pp60^{src}$ regulates the degradation and ubiquitinylation of the protein (Patwardhan and Resh, 2010) and the myristoyl moiety was recently proposed to possibly reside in a hydrophobic pocket like it does in c-Abl (Hantschel et

al., 2003), but would stimulate rather than inhibit kinase activity (Patwardhan and Resh, 2010).

1.4.2. Myristoylation and cancer.

Magnuson *et al.* (Magnuson et al., 1995) were the first to demonstrate that NMT activity was increased in rat colonic tumors, human colorectal tumours, adenocarcinomas (Raju et al., 1997) and stage B1 tumors, suggesting that NMT is important in the early stages of colonic carcinogenesis (Magnuson et al., 1995). Increased NMT activity correlates with higher expression levels of NMT (Raju et al., 1997), and particularly the second isoform NMT2 (Selvakumar et al., 2006). Increased expression of NMT was also found in gallbladder cancer (Rajala et al., 2000), breast cancer (Shrivastav et al., 2009) and brain tumours (Lu et al., 2005). The overexpression of the myristoylated oncogenic kinases may require increased NMT activity for their proper acylation and, ultimately, function.

1.4.3. Spurious myristoylation in disease.

Recently, spurious myristoylation of the soc-2 suppressor of clear homolog (SHOC2) protein containing a Ser2Gly mutation was documented. Consequently, this mutation was shown to be responsible for a disease phenotype known as Noonan-like syndrome with loose anagen hair, where it was found in twenty five patients (Cordeddu et al., 2009). This syndrome is a rare developmental disorder resulting in reduced growth, facial dysmorphism, cognitive deficits and malignancies (Mazzanti et al., 2003; Schubbert et al., 2007). Mutation of Ser to Gly in SHOC2 lead to incorporation of [^{3}H]-myristic acid at the N-terminal glycine residue. Typically, SHOC2 translocates to the nucleus upon activation. However, the myristoylated mutant was targeted to and remained associated with the plasma membrane. Consequently, membrane bound SHOC2 lead to increased activation of Ras and the mitogen-activated protein kinase (MAPK) pathway, which was thought to promote the disease phenotype seen in Noonan-like syndrome with loose anagen hair. This was the first demonstration of the direct involvement of myristoylation in the development of a human disease and the first example of a spontaneous genetic mutation leading to aberrant myristoylation.

1.4.4. Myristoylation in infectious diseases.

In addition to a myriad of mammalian proteins (Maurer-Stroh et al., 2002a), the covalent attachment of myristate to the N-terminal glycine residue occurs in many viral and even secreted bacterial (Maurer-Stroh and Eisenhaber, 2004) proteins wherein it is essential to these proteins' ultimate function (Boutin, 1997; Farazi et al., 2001). Therefore, NMTs represent attractive therapeutic drug targets. The NMT protein substrate specificity has been well characterized in *S. cerevisiae* using synthetic peptides corresponding to the N-terminus of the protein (Towler et al., 1988a; Towler et al., 1987b; Towler et al., 1988b). Using this system for mammalian NMT1, the first ten amino acids were shown to be sufficient for effective myristoyl-transferase activity. Interestingly, human and yeast NMTs have different yet overlapping substrate specificities (Rocque et al., 1993). The differences were significant enough to allow for the development of selective inhibitors of yNMT (Devadas et al., 1998) paving the way to the design of NMT inhibitors against pathogenic yeasts and fungi such as *Candida albicans*, *Cryptococcus neoformans* and *Histoplasma capsulatum* (Lodge et al., 1994; Wiegand et al., 1992). The fact that the NMT activities appear to be critical for the virulence of *C. albicans* and *C. neoformans* in an immunosuppressed model, again highlights the potential of NMT as a useful therapeutic target. Of note, several parasitic protozoa such as *Leishmania major* and *Leishmania*

donovani (leishmaniasis desease), *Trypanosoma brucei* (African sleeping sickness disease) and *Plasmodium falciparum* (malaria) also possess their own NMT that is essential for their survival (Bowyer et al., 2007; Brannigan et al., 2010; Panethymitaki et al., 2006; Price et al., 2003). Investigations are now focusing on the validation of inhibitors of protozoan NMTs. Different strategies have been used towards the development of these inhibitors and were based on the use of either peptidomimetics able to bind to the NMT active sites or small molecule inhibitors of NMTs. Recently, a pyrazole sulphonamide specific inhibitor of the *T. brucei* NMT has been identified (Frearson et al., 2010). Its selectivity over human NMT is 100-fold and a tight correlation between NMT activity and *T. brucei* proliferation was observed suggesting that NMT activity was the target of this compound. Pyrazole sulphonamide competes with the peptide binding site of NMT. This compound rapidly kills *T. brucei* and eliminates the bloodstream form of *T. brucei*. Moreover, this compound not only works *in vitro*, but also cured all animals in a mouse model of human African trypanosomiasis. Therefore, it shows promising therapeutic properties to treat sleeping sickness.

Of particular note, myristoylation is required for assembly and replication of viruses such as lentiviruses (e.g. HIV) or picornaviridae (Maurer-Stroh and Eisenhaber, 2004). In the case of HIV replication, both the structural proteins Gag and Nef are myristoylated by the host cell NMT. The Gag protein consists of a polyprotein precursor containing

several domains, including a matrix domain, which is myristoylated and directs the protein to the plasma membrane in combination with its polybasic domain (Schultz and Oroszlan, 1983). Subsequently, this anchoring is critical for the downstream cleavage of the polyprotein and the release of the mature myristoylated matrix domain to the cytosol (Spearman et al., 1997). These crucial steps are required for the formation of the viral capsid, as inhibition of myristoylation causes the accumulation of the Gag protein precursor in the cytosol and blocks formation of a competent viral progeny (Furuishi et al., 1997). Recent studies suggest that NMT1 and NMT2 display different affinity for Gag and Nef, allowing the possible development of selective inhibitors (Seaton and Smith, 2008; Takamune et al., 2008). In addition, the competition for the myristoyl-CoA substrate pool appeared to be critical in this pathophysiological situation. It is estimated that the concentration of myristoyl-CoA necessary for the maturation of viral particles is about 1 µM (Boutin, 1997), while the endogenous cellular concentration is about 5 nM (Faergeman and Knudsen, 1997). This suggests that the production of myristoyl-CoA might be a rate-limiting step and that the size of the myristoyl-CoA pool might be regulated during viral infection (Hill and Skowronski, 2005).

Certain types of bacteria are known to inject proteins (via type III secretion) containing an N-terminal glycine, bearing a myristoylation concensus sequence, directly into the cytoplasm of the host cell. The injected protein is then myristoylated by the host NMT and relocalizes to

the plasma membrane. Myristoylation of the protein is essential for maximum virulence (Maurer-Stroh and Eisenhaber, 2004; Nimchuk et al., 2000). This type of myristoylation of type III secreted bacterial proteins was demonstrated in *Pseudomonas syringae* (Nimchuk et al., 2000) and predicted for *Shigella sonnei* (Menard et al., 1994). Drugs targeting eukaryotic acylation of bacterial proteins may represent an interesting strategy to fight plant and animal infections.

Finally, the examples listed above highlight the importance of understanding and characterizing myristoylation under normal and pathological conditions. For instance, because apoptosis ultimately results in caspase activation and is often deregulated in cancer, the importance of characterizing post-translational myristoylation of proteins cleaved by caspases during apoptosis is undeniable, and may be critical to understand the development and progression of cancer and will be discussed in the next section.

1.5. Post-translational myristoylation: Different means to an end.

1.5.1. Post-translational myristoylation during apoptosis.

Until 10 years ago, myristoylation was thought to be exclusively a co-translational process occurring on the nascent polypeptide (Figure 1.1A) (Boutin, 1997; Farazi et al., 2001). However, the pro-apoptotic protein Bid was shown to be post-translationally myristoylated on an internal glycine residue exposed after caspase cleavage during apoptosis (Zha et al., 2000). Since then, additional substrates for post-translational myristoylation during apoptosis have been identified and many more predicted (Martin et al., 2010). Consequently, it is now well established that myristoylation can also occur post-translationally upon caspase cleavage and exposure of an internal glycine within a cryptic myristoylation consensus sequence (Figure 1.1 B) (Martin et al., 2008; Sakurai and Utsumi, 2006; Utsumi et al., 2003; Vilas et al., 2006).

1.5.2. Apoptosis and myristoylation.

Programmed cell death, or apoptosis, is critical for the development and maintenance of organisms and tissue homeostasis. Apoptosis allows an organism to remove unwanted, injured or defective cells through an organized form of cell breakdown that does not include inflammation. This

specialized pathway is tightly regulated and conserved throughout evolution. As such, deregulation of this process can have detrimental consequences (Wyllie, 1997). For instance, unwanted upregulation of apoptosis is associated with tissue and organ damage such as that observed in degenerative disease such as Alzheimer's, Parkinson's and Huntington's disease. In contrast, many forms of cancer originate by bypassing or down regulating the apoptotic pathway (Evan and Vousden, 2001; Leist and Jaattela, 2001; Thompson, 1995).

Apoptosis is physically characterized by cell shrinkage, condensation of DNA and membrane blebbing (Wyllie, 1997; Wyllie et al., 1999). Ultimately, apoptosis leads to the cell breaking into membrane-surrounded fragments, referred to as apoptotic bodies, which are eventually engulfed *in vivo* by "professional" phagocytes that include macrophages and dendritic cells. In cell culture, the apoptotic bodies will lose their plasma membrane integrity followed by complete cell disintegration during late stages of apoptosis, in a process termed secondary necrosis (Wyllie, 1997).

During the onset of apoptosis, hundreds of proteins are specifically cleaved by cysteinyl-aspartyl proteases (caspases) (Nicholson, 1999). Caspases are synthesized as zymogens that become activated following auto-proteolysis or trans-proteolysis by other caspases (Danial, 2007; Sakamaki and Satou, 2009). To date, 11 caspases have been identified in humans including caspases-1 to -10 and caspase-14. Caspases-11 to -13

and caspase-15 have been identified in other mammals such as rodents, the cow *Bos taurus*, and dogs (Sakamaki and Satou, 2009). Caspases are classified into several groups according to their phylogenetic relationships, which correlate to their functional relatedness. Caspases-1, -4, -5, -11, -12 and -13 are involved and required for inflammatory responses. The remaining caspases are involved in regulating apoptosis and are further classified into two groups; initiator (Caspases-2, -8, -9 and -10) and executioner caspases (caspases -3, -6, and -7). They differ both structurally and functionally. Initiator caspases contain longer amino-terminal prodomains, than the executioner caspases, that interact with adaptor proteins. Caspase-8 and -10 contain death effector domains (DED) and caspases-2 and -9 contain a caspase recruitment domain (CARD). Once activated, initiator caspases proteolyze and activate executioner caspases (Sakamaki and Satou, 2009).

Caspase cleavage leads to the activation of pro-apoptotic regulators or the inactivation of many proteins including anti-apoptotic regulators and, in many cases, can lead to changes in localization of the cleaved proteins (Fischer et al., 2003; Nicholson, 1999).

Apoptosis can be triggered through two main pathways that are intricately linked and referred to as the intrinsic and extrinsic pathways (Figure 1.4). The intrinsic pathway is activated through cell stresses such as DNA damage, hypoxia and growth factor deprivation, and is mediated through the mitochondria (Zimmermann et al., 2001). The “point of no

return" correlates to release of cytochrome c following mitochondrial outer membrane permeabilization (MOMP) (Bratton and Cohen, 2001; Danial, 2007; Jiang and Wang, 2004). The intrinsic pathway is primarily regulated by the Bcl-2 family members, which act as "gatekeepers" of cytochrome c release from mitochondria. The Bcl-2 family consists of both pro- and anti-apoptotic members which share conserved regions known as Bcl-2 homology (BH) domains. All of the anti-apoptotic Bcl-2 family members (Bcl-2, Bcl-X_L, Bcl-w and Mcl-1) and a small subset of pro-apoptotic members (Bak, Bax and Bok) contain multiple BH domains. The remaining pro-apoptotic members are referred to as the BH-3 only proteins such as Bim, Bad and Bid (Bratton and Cohen, 2001; Danial, 2007; Kim et al., 2006).

In contrast, extrinsically activated apoptosis is receptor mediated. Typically, binding of a death ligand to its receptor (such as Fas ligand to its receptor Fas in Figure 1.4) leads to trimerization of the receptor and recruitment of the Fas-associated death domain (FADD) adaptor protein (Ramaswamy et al., 2009). FADD contains a death domain (DD) that interacts with the DD of the intracellular portion of the receptor and links the receptor to the inactivated initiator caspases 8 via the adaptor protein's and caspase's DED. In total, the receptor, adaptor protein and caspase complex comprise the death inducing signaling complex (DISC) (Curtin and Cotter, 2003; Khosravi-Far and Esposti, 2004). The DISC, in

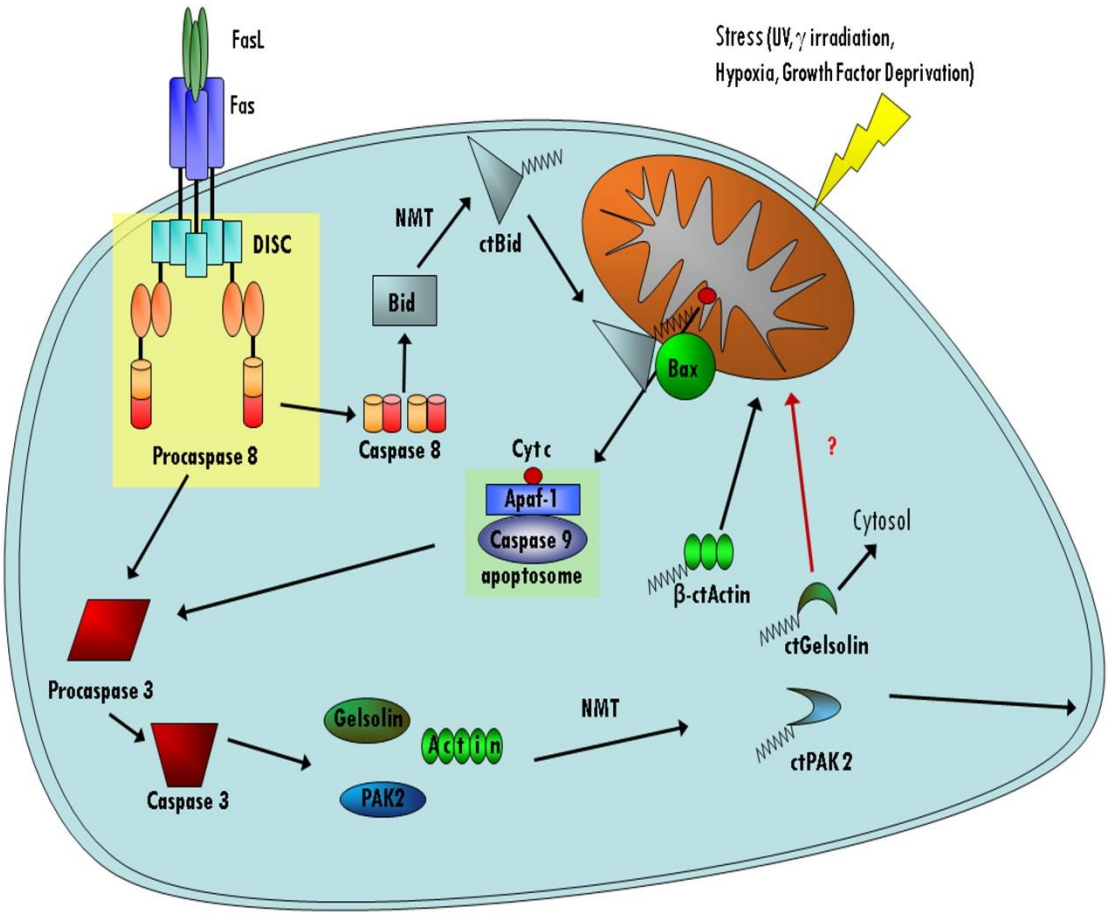

Figure 1.4. - Post-translational myristoylation of proteins during apoptosis. Activation of the extrinsic pathway begins with binding of a death ligand [e.g. Fas ligand (FasL)] to its corresponding death receptor (e.g. Fas). Subsequent binding of adaptor proteins leads to the formation of the death inducing signalling complex (DISC) and activation of caspase-8. Caspase-8 cleaves the pro-apoptotic protein BID, which is then post-translationally myristoylated by NMT at an N-terminally exposed glycine of the C-terminal fragment, which is essential for ctBid's translocation to the mitochondria and progression of apoptosis by the release of cytochrome c. β-Actin, Gelsolin and p21-activated kinase 2 (PAK2) are all cleaved by caspase-3 to yield caspase-truncated (ct) products: ctActin, ctGelsolin and ctPAK2, which are subsequently post-translationally myristoylated. The post-translationally myristoylated caspase-truncated products translocate to their new respective membrane locales to affect apoptosis (Martin et al., 2010).

turn, leads to the proteolytic processing and activation of caspase-8. Subsequently, active caspase-8 will cleave and activate the executioner caspase, caspase-3, which targets a myriad of proteins involved in cell regulation. Another important substrate of the DISC is the pro-apoptotic BH-3 only domain protein Bid (Ramaswamy et al., 2009; Zimmermann et al., 2001). The cleavage of the 21 kDa Bid by caspase-8 results in a 7 kDa and a 15 kDa N-terminal and C-terminal fragments, respectively. As a result of the cleavage, an internal myristoylation motif becomes exposed at the newly exposed amino terminus of the C-terminal or caspase-truncated fragment (ctBid) allowing it to be post-translationally myristoylated by NMT (e.g. Figure 1.1 B) (Mishkind, 2001; Zha et al., 2000). Because the N-terminal fragment of Bid remains associated with the ctBid, myristoylation of ctBid results in the translocation of the complex to mitochondria, promotes the release of cytochrome c, and, ultimately, cell death (Zha et al., 2000).

Another important regulatory factor released by mitochondrial membrane permeabilization includes the pro-apoptotic factor second mitochondrial activator of caspases (Smac; also known as DIABLO). Smac/DIABLO binds the inhibitors of apoptosis proteins (IAPs), which in turn bind and inactivate caspases and prevent apoptosis. Smac/DIABLO binding to IAPs directs them for ubiquitination and degradation by the proteasome, thereby promoting apoptosis (Liston et al., 2003).

When the glycine residue essential for myristoylation was substituted to an alanine (G60A) in ctBid, mitochondrial association of mutant ctBid was drastically reduced to about 30% of wild type levels. Myr-ctBid was also shown to have a higher affinity for mitochondrial membranes and was approximately 350 times more effective than non-myristoylated G60A-ctBID at promoting the maximal release of cytochrome c from purified mitochondria. Cytosolic cytochrome c is important for recruiting and oligomerizing with apaf-1 and another executioner caspase, caspase-9, to form the apoptosome, which, in turn, can also activate caspase-3 (Figure 1.4) (Cain et al., 2000; Zou et al., 1999). As an executioner caspase, caspase-3 has many important substrates, such as the inhibitor of caspase activated DNAse (ICAD) (Nagata, 2000). Cleavage of ICAD releases it from CAD, leading to DNA fragmentation, a key hallmark of apoptosis (Enari et al., 1998). In addition, cleavage of the Rho-associated kinases, ROCK-I, results in the hallmark feature of membrane blebbing (Coleman et al., 2001; Sebbagh et al., 2001). Therefore, the cleavage and subsequent myristoylation of ctBid plays a crucial role in linking the extrinsic and intrinsic cell death pathways.

Additional substrates of caspase-3 include three proteins that were found to be post-translationally myristoylated in separate studies; actin, gelsolin (Sakurai and Utsumi, 2006; Utsumi et al., 2003) and p21-activated kinase 2 (PAK2) (Vilas et al., 2006). First, Utsumi *et. al.* (Utsumi et al., 2003) appended the first nine amino acids immediately following the

caspase cleavage sites of six known substrates that exposed a new N-terminal Gly to the TNFα protein, which was used as a reporter protein. COS-1 cells transiently expressing the TNFα chimeras were metabolically labeled with [^{3}H]-myristate. Incorporation of the radiolabel into both ctActin- and ctGelsolin-TNFα was detected by autoradiography.

Actin is one of the key structural components of the cytoskeleton and plays a crucial role in cell structure, motility, division and organelle movement. Actin can be found in two main forms; globular (G-actin), or monomeric, and filamentous (F-actin), or polymerized (Pollard et al., 2000). Gelsolin is an actin filament-severing protein that regulates actin assembly and disassembly (Burtnick et al., 2004). Interestingly, myr-ctActin-FLAG co-localized with mitochondria, like myr-ctBid, but it was not found to have any effect on cellular morphology, actin networks, nor was any effect on apoptosis established (Sakurai and Utsumi, 2006; Utsumi et al., 2003).

In a follow up study by the same authors, myr-ctGelsolin-HA was shown to be primarily cytosolic. Indeed, cell fractionation studies showed ctGelsolin-HA predominantly in the cytosolic fraction regardless if it was myristoylated or not. In addition, myr-ctGelsolin was also concluded to be cytosolic based on indirect immunofluorescence data (Sakurai and Utsumi, 2006). Despite displaying no obvious membrane localization, cells expressing myr-ctGelsolin had an increased protection from apoptosis induced by the topoisomerase inhibitor etoposide, when compared to non-

myr-ctGelsolin or vector alone. Once again, this demonstrates the importance of post-translational myristoylation in regulating the function of caspase-cleaved proteins during apoptosis. Interestingly, previous studies have shown that both the full length form and ctGelsolin were anti-apoptotic through a mechanism that is thought to involve the voltage-dependent anion channel (VDAC) at the mitochondrial membrane (Koya et al., 2000; Kusano et al., 2000). In that context, it would be interesting to compare the potency of full-length versus caspase-cleaved myristoylated gelsolin in order to assess whether myristoylation augments the ability of gelsolin to suppress apoptosis. Interestingly, ctBid is also thought to promote apoptosis by associating with VDAC and promoting an open pore conformation (Rostovtseva et al., 2004). Although it should be noted that in that study, post-translational myristoylation was blocked by the presence of an N-terminal epitope tag on ctBid. It may be of interest to determine whether myr-ctActin, which translocates to the mitochondria, also interacts with the VDAC. Of note, it has been suggested that destabilization of the interaction between cardiolipin and the mitochondrial permeability transition pore, of which the VDAC is a main component, promotes an open conformation of the pore during apoptosis to allow the release of cytochrome c (Wright et al., 2004). In the absence of cardiolipin, Bid does not localize to the mitochondria (Wright et al., 2004). These results suggest that post-translationally myristoylated proteins may be

directed to the VDAC in a cardiolipin dependent manner to regulate the open/closed formation of the pore complex (Martin et al., 2010).

In addition to ctBid, ctActin and ctGelsolin, our laboratory has identified another post-translationally myristoylated protein: PAK2 (Vilas et al., 2006). PAK2 is a Ser/Thr kinase whose activity is regulated by the small GTPases Rac and Cdc42 (Knaus et al., 1995). In dividing cells PAK2 activity stimulates cell growth, cell motility and cell survival (Bokoch, 2003). In apoptotic cells, PAK2 is cleaved by caspase-3 resulting in the release of the highly pro-apoptotic constitutively active C-terminal kinase domain from the N-terminal regulatory domain (Rudel and Bokoch, 1997). The newly exposed N-terminal glycine of the caspase-cleaved PAK2 kinase domain (ctPAK2) is subsequently post-translationally myristoylated (Vilas et al., 2006). It was observed that myr-ctPAK2 was a more potent activator of apoptosis than its non-myristoylated counterpart. Indeed, after 12 hours of transient transfection of ctPAK2-Myc, more than 50% of myr-ctPAK2-Myc expressing cells were apoptotic compared to only 23% in both the vector control and G2A-ctPAK2-Myc transfected cells. While WTctPAK-Myc induced 50% of cell death within 12 hours, the non-myristoylated G2A mutant reached a maximal cell death of 50% after 24 hours. In addition, a concomitant 5-fold and 3.5 fold increase in phosphorylation of the stress-activated signaling kinase JNK was observed in cells expressing the myristoylated- and non-myristoylated ctPAK2 respectively, over vector alone. Conversely, the myristoylated

form of ctPAK2 was found to be hypophosphorylated compared to its non-myristoylated counterpart suggesting that loss of myristoylation lead to a dysregulation of PAK2 phosphorylation. In addition, myr-ctPAK2 was found to localize to plasma membrane ruffles and early endosomes while the non-myristoylated ctPAK2 remained primarily cytosolic, thus suggesting once more that myristoylation leads to membrane localization and enhanced biological activity. Interestingly, and excitingly, cellular death induced by expression of myr-ctPAK2 bypassed several key hallmarks of apoptosis. For example, cells undergoing myr-ctPAK2 mediated cell death did not release cytochrome c from the mitochondria nor lose mitochondrial potential. In addition, these cells did not expose phosphatidylserine at the cell surface during the cell death process. These observations suggest that myr-ctPAK2 mediates its actions downstream of the mitochondrial “step”.

Because post-translational myristoylation potentiates the pro-apoptotic activity of ctBid and ctPAK2, post-translational myristoylation of caspase cleaved proteins could represent an elegant means developed by the cell to expand the functionality of its encoded proteins.

1.5.3. Potential roles for co-translational myristoylation and myristate in the regulation of apoptosis.

Myristoylation may also play an important role in the metabolism of sphingolipids and ceramides, two types of molecules known to be involved in the regulation of apoptosis. For instance, several proteins involved in these pathways contain N-terminal glycines that may be myristoylated, such as ceramide kinase (Sugiura et al., 2002) and neutral sphingomyelinase (Chatterjee et al., 1999). In fact, dihydroceramide delta4 desaturase (DES) has been shown to be myristoylated and its activity is even upregulated when “free” myristate is added to cells (Beauchamp et al., 2007). Myristoylation of DES targets the enzyme to mitochondria where sphingolipid metabolism may be altered (Beauchamp et al., 2009). Furthermore, this acylation induces ceramide production, cytochrome c release from mitochondria and, consequently, apoptosis in COS-7 cells. It is well known that ceramides induce apoptosis by targeting mitochondrial metabolism via the formation of channels in the outer mitochondrial membrane and release of cytochrome c (Stiban et al., 2006). Ceramides also interact with key components of the electron transport chain (Gudz et al., 1997) and induce the production of ROS species (Garcia-Ruiz et al., 1997) leading to the induction of apoptosis. Consequently, changes in myristate concentrations may alter the outer mitochondrial membrane composition in phospholipids and cardiolipins by structurally altering their

fatty acid constituents and, therefore, change the mitochondrial membrane permeability (Martin et al., 2010).

Recently, our laboratory has shown that both NMT-1 and -2 are cleaved during apoptosis, with caspase-8 mediated NMT1 cleavage preceding the cleavage of NMT2 by caspase-3. NMT1 activity decreased by as much as 40% at 8 hours following induction of apoptosis, while NMT2 activity was not significantly reduced, suggesting that caspase cleavage does not abrogate catalytic activity but might alter substrate specificity. Indeed, a drastic change in the myristoylation profile in apoptotic cells was observed. This was attributed to the exposure of new myristoylation sites revealed by caspase cleavage. Interestingly, chemical inhibition of NMTs potentiated apoptosis in Jurkat T cells suggesting that NMTs have an overall pro-survival role in these cells. Of note, Ducker *et al.* (Ducker et al., 2005) found that siRNA-mediated depletion of NMT2 upregulated apoptosis 2.5 fold greater than NMT1 depletion, and also promoted expression of pro-apoptotic Bcl proteins. This further suggests that NMT2 may be responsible for post-translational myristoylation.

Overall, it appears that both co- and post-translational myristoylated proteins play important roles in the regulation of mitochondrial integrity and the generation of pro-death or pro-survival signals. Altogether these are key components of the cell's ability to make life and death decisions.

HYPOTHESIS: Post-translational myristoylation alters the function of select caspase-cleaved proteins through changes in cellular location to elicit profound effects on apoptosis and disease.

1.5.4. Alternative forms of cell death.

It is important to note that alternative forms of cell death do exist. Non-apoptotic programmed cell death includes autophagy with cell death, necroptosis, pyrotosis and paraptosis. With the exception of autophagy, these alternative forms of programmed cell death are not well described.

1.5.4.1. Paraptosis

'Para' means 'next to' and suggests that this is an apoptotic-like pathway. Paraptosis is a caspase-9 dependent cell death pathway, but does not involve the apoptosome, as in the archetypal apoptosis. It is associated with extensive cytoplasmic vacuolation, ER swelling and mitochondrial swelling with an absence of caspase activation and nuclear changes. It is programmable though, as it requires the upregulation of specific genes (Kar et al., 2009; Sperandio et al., 2000).

1.5.4.2. Pyroptosis

Pyroptosis is an inflammatory form of programmed cell death primarily described in macrophages in response to microbial infection. Unlike apoptosis, it is caspase-1 dependent and relies on the formation of

a pyroptosome that consists of an oligomer comprised of the adapter protein apoptosis-associated speck-like protein containing a CARD (ASC). Like apoptosis, DNA fragmentation occurs, but not in the classical form of nucleosomes and does not involve CAD, as described above. In addition, mitochondrial integrity does not appear to be affected and, consequently, cytochrome c is not released. Ultimately, cells undergoing pyroptosis rupture to release pro-inflammatory intracellular contents. (Bergsbaken et al., 2009; Hornung et al., 2009).

1.5.4.3. Necroptosis

Similarly, necrosis is commonly thought of as an unregulated means of cell death that is characteristically described by membrane rupture and the release of the intracellular contents. Recently, it has been shown that necrosis can be a programmed event and is referred to as necroptosis (Vandenabeele et al., 2010). Necroptosis has been used to describe one particular form of programmed necrosis that depends on the Ser/Thr kinase activity of RIP1 kinase. RIP1 is the essential component of the necrosome, which also contains caspase-8. However, if caspase-8 is active, the cell will undergo traditional programmed cell death or apoptosis, but if caspase-8 is inhibited the cell will undergo necrosis (Galluzzi and Kroemer, 2008; Vandenabeele et al., 2010).

1.5.4.4. Autophagy

Autophagy is primarily a protective stress-induced catabolic pathway, conserved among all eukaryotes, for the cell to remove defective

proteins and organelles through the lysosome. However, when autophagy is excessively induced, it can result in autophagic cell death, which is referred to as type II programmed cell death (Chen and Klionsky, 2011; Todde et al., 2009). Unlike the other alternative forms of cell death, autophagy has been studied extensively and is more understood.

Autophagy is divided into three main types based on how the cargo is delivered to the lysosome; microautophagy, macroautophagy and chaperone-mediated autophagy (CMA) (Figure 1.5). Microautophagy (Figure 1.5B) involves the translocation of cytoplasmic materials across the lysosomal membrane by direct engulfment by the lysosome membrane The molecular components that participate in this autophagic process in mammals remain unknown (Kaushik et al., 2010). In CMA (Figure 1.5C), individual soluble proteins that contain a KFERQ motif are specifically selected by chaperone proteins, unfolded and translocated across the lysosome membrane one-by-one (Kon and Cuervo, 2010). Internalization of substrate proteins by this pathway is attained through the coordinated function of chaperones on both sides of the lysosomal membrane and a membrane protein (the lysosome-associated membrane protein type 2A or LAMP-2A) that acts both as a receptor and as an essential component of the translocation complex (Kaushik et al., 2010). Macroautophagy is characterized by the formation of cytosolic double-membrane vesicles, referred to as autophagosomes, which encapsulate cytosolic components (Figure 1.5.A). Subsequently, autophagosomes fuse with lysosomes to

form autolysosomes and degrade their contents to be reused by the cell (Kimura et al., 2007; Tanida, 2011).

Macroautophagy is the major lysosomal degradation pathway and, for all intents and purposes, is typically referred to as autophagy. Mechanistically, macroautophagy begins with the formation of a cup-shaped or Ω-shaped membrane referred to as an omegasome. Subsequently, a cisterna or fold in the membrane will form and is known as the isolation membrane (IM) (Axe et al., 2008; Juhasz and Neufeld, 2006; Tanida, 2011). The site of formation of the omegasome is referred to as the pre-autophagosomal structure, or phagophore assembly site (PAS). The PAS serves as the platform for the autophagosome. The site of assembly still remains controversial and data suggests that phagosomes originate from the ER (Axe et al., 2008), mitochondria (Hailey et al., 2010) or the plasma membrane (Ravikumar et al., 2010a). An alternative hypothesis includes the *de novo* formation of autophagosomes in the cytosol (Ravikumar et al., 2010b; Tanida, 2011).

The members of the autophagy related gene (ATG) family are recruited to the membrane in three main protein complexes; an autophagy specific phosphatidylinositol-3-kinase (PI3K) complex (Beclin1, Vps34, p150, Atg14), the Ulk1 kinase complex (ULK1, Atg13 and FIP200) and two-closely linked ubiquitin-like protein conjugation systems (Kaushik et al., 2010; Ravikumar et al., 2010b; Tanida, 2011). These processes are further controlled upstream by the nutrient-sensing kinase mTOR

(mammalian target orthologue of rapamycin) (Figure 1.5.A) (Kaushik et al., 2010).

Initially, mobilization of the initiation complex to the membrane serves as the point of nucleation for the autophagosome. Lipid phosphorylation by the Class III PI3K Vps34 is essential for the recruitment of ATG proteins that comprise the ubiquitin-like conjugation systems (Axe et al., 2008; Tanida, 2011). They are said to be “ubiquitin-like” because they rely on ligases that activate substrate and ligand, which enzymatically catalyse their conjugation (Kaushik et al., 2010). In the first system, the ubiquitin-like protein Atg12 is activated by the E1 ubiquitin activating enzyme-like Atg7. Atg12 is then transferred to the E2-ubiquitin conjugating enzyme-like enzyme Atg10 and, ultimately, covalently linked between its C-terminus and a lysine side chain of Atg5. The Atg12-Atg5 complex is then free to conjugate with Atg16L through the coiled-coil domains of Atg16L to generate a large tetramer approximately 800 kDa in size. This complex is essential for the elongation of the pre-autophagosome, but dissociates from the fully formed autophagosome (Axe et al., 2008; Ravikumar et al., 2010b; Tanida, 2011).

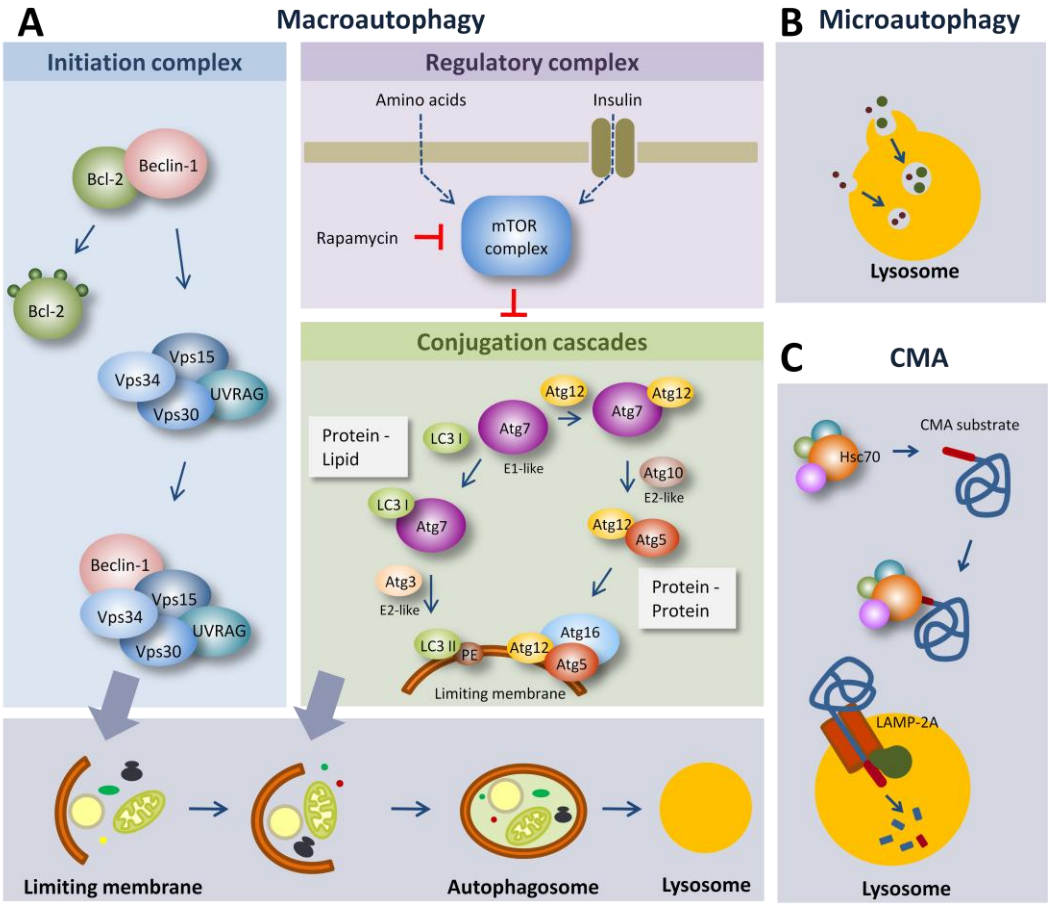

Figure 1.5. – Outline of the 3 forms of autophagy. A Induction of macroautophagy leads to the translocation of a protein kinase type III complex (the initiation complex) towards the sites of autophagosome formation. The major negative regulator of macroautophagy, the mTOR protein kinase complex, is also depicted. **B** Microautophagy mediates the internalization of cytosolic cargo – proteins and organelles – through invaginations of the lysosomal membrane. **C** In chaperone-mediated autophagy (CMA), only soluble cytosolic protein substrates are selectively targeted to the lysosomal membrane by a cytosolic chaperone and they require unfolding before reaching the lysosomal lumen [Image provided by Dr. Ana-Maria Cuervo and published in (Kaushik et al., 2010)].

The second conjugation system ultimately leads to a lipidated form of LC3 (microtubule-associated protein 1 light chain 3). First, the carboxy terminus of the precursor form of LC3 is removed by the protease Atg4B to produce LC3-I. Subsequently, in a reaction involving Atg7 and Atg3 (E2-like), phosphatidylethanolamine is added to the C-terminal Gly of LC3 to generate LC3-II. The difference in levels of the two isoforms is typically used to evaluate the induction of autophagy; increased levels of LC3-II over LC3-I is indicative of activated autophagy (Klionsky et al., 2008a). In addition, GFP-LC3 is the predominant marker to follow the formation of autophagosomes in cell culture, while GFP-LC3-I is cytosolic, GFP-LC3-II is localised to punctate vesicular structures during autophagy (Klionsky et al., 2008a). LC3-II is specifically targeted to the elongating autophagosome membrane and remains on the complete autophagosomes until fusion with lysosomes (Kimura et al., 2009; Kimura et al., 2007; Ravikumar et al., 2010b). Subsequently, LC3-II on the cytoplasmic face of the autophagosome is delipidated by ATG4 and recycled or degraded within the lumen of the lysosome (Kimura et al., 2007; Satoo et al., 2009). Additionally, the multispanning transmembrane protein Atg9, which cycles between the *trans* Golgi network and endosomes is also important for elongation (Takahashi et al., 2011; Tanida, 2011).

Autophagy occurs in virtually all nucleated cells at a basal constitutive level to maintain homeostasis (Marino et al., 2010; Todde et

al., 2009). In addition to stress response, autophagy is also involved in development, senescence, lifespan extension, immunity and defense against microbial invasion (Todde et al., 2009). Alternatively, it is also associated with various pathophysiologies including cancer, myopathies, heart and liver diseases, gastrointestinal disorders and neurodegeneration (Chen and Klionsky, 2011; Todde et al., 2009). Several tumour suppressors are associated with autophagy; Beclin 1, DAP-kinase, and PTEN. As such, autophagy has frequently been found to be down regulated during cancer and has, therefore, become a target for chemotherapy (Gozuacik and Kimchi, 2004). However, it has been recently discovered that pancreatic cancer has a distinct dependence on autophagy for tumour progression. Inhibition of autophagy in pancreatic cells leads to tumour regression and prolonged survival in cancer xenografts and genetic mouse models (Yang et al., 2011). Although many neurodegenerative diseases have different origins, many share common features including the accumulation of altered proteins and, in some cases, aggregation of these proteins. When proteins aggregate they can only be removed by a bulk degradation pathway such as autophagy (Martinez-Vicente and Cuervo, 2007; Rubinsztein, 2006).

1.6. Detection of myristoylation: click chemistry and the solution to long film exposures.

1.6.1. Detection using radioactive fatty acids.

The key roles played by co- and post-translationally myristoylated proteins in the generation of pro-survival or pro-death signals warrants the identification of the co- and post-translational myristoylated protein proteomes or "myristoylomes". Indeed, in addition to the previously identified post-translationally myristoylated proteins, we have observed the presence of nine other post-translationally myristoylated proteins using metabolic labelling of apoptotic Jurkat cell lysates with [^{3}H]-myristic acid (Vilas et al., 2006). However, the use of radioactive [^{3}H]-myristic acid has a low sensitivity, is very time consuming, expensive and represents a health hazard. Overall, progress in the identification and characterization of myristoylated proteins has been impeded by the long exposure times required to monitor incorporation of radioactive myristate into proteins (typically 1–3 months). Still using [^{3}H]-myristic acid as a label, the Utsumi laboratory recently developed cell free assays that utilize rabbit reticulocyte lysates or insect cell lysates for the synthesis and labeling of potentially myristoylated proteins (Sakurai and Utsumi, 2006; Suzuki et al., 2007; Suzuki et al., 2010). In their paper, using these cell free systems myristoylation detection was reduced to days/weeks film exposure using

fluorography. This allowed for the identification of 27 myristoylated proteins, of which 18 were new myristoylated proteins (Suzuki et al., 2010). Despite identifying a number of novel myristoylated proteins, this approach was rather time consuming and still relied on metabolic labelling techniques linked to rather lengthy fluorographic film exposures and an exhaustive mass spectrometric/proteomic approach.

To alleviate the lengthy fluorographic exposures inherent to the use of [^{3}H]-myristic acid to label cells, an [^{125}I]-iodomyristate has also been synthesized and used to reduce exposure time to days or less, but this requires the handling of large quantities (mCi) of the hazardous high energy ^{125}I radioisotope (Berthiaume et al., 1994; Deichaite et al., 1993; Kostiuk et al., 2010). Unfortunately, this compound is not commercially available and must be generated in the laboratory (Kostiuk et al., 2009; Kostiuk et al., 2010).

Specific Aim I: Develop a non-radioactive detection method.

Due to the long exposure times and health hazards associated with the use of radioactive fatty acids, we sought to develop a non-radioactive detection method. As such, we decided to adapt the previously described Staudinger ligation to specifically biotinylate myristoylated proteins (Saxon and Bertozzi, 2000). The Staudinger ligation exploits the very specific reaction between a phosphine and an azide. As such, alkyl azides can be

covalently linked to a triarylphosphine linked to an affinity tag of choice (e.g. the FLAG epitope or biotin). Recently, the specific chemoselective Staudinger ligation between an alkyl-azide and a triarylphosphine has been effectively adapted to study glycosylation and farnesylation using a variety of bio-orthogonal azido analogs in a reaction termed the Staudinger ligation (Figure 3.1.) (Kho et al., 2004; Saxon and Bertozzi, 2000). Azido-analogs have historically been chosen because they remain inert in the biological milieu, they are nonpolar and specifically react with phosphines. In addition, the isosteric myristate analog 12-azidododecanoate (azido-myristate or Az-C12) has been previously shown to be non-toxic to cells when treated for up to 10 days.

Subsequently, our lab and others have developed another non-radioactive chemical ligation detection method that relies on the Cu (I)-catalyzed [3+2] Huisgen cycloaddition reaction (commonly referred to as 'click chemistry'). In our case, we carry out click chemistry with an ω-alkynyl-myristate analog (Alk-C14) used to label cells and, primarily, an azido-biotin probe (Yap et al., 2010).

The use of both methods to detect co- and post-translational myristoylation and to identify new candidates for post-translational myristoylation will be further described within this thesis.

Specific Aim II: Identify new substrates for post-translational myristoylation during apoptosis.

Herein, I will describe how we successfully combined *in silico* analysis to identify putative substrates for post-translational myristoylation with our novel non-radioactive detection methods to identify seven new strong candidates for post-translational myristoylation. These include the following caspase cleaved protein products: cell division control protein 6 homolog (Cdc6), cytoplasmic dynein-intermediate chain 2A (CD-IC2A), Huntingtin (Htt), microtubule-actin crosslinking factor 1 (MACF1), the apoptotic regulator induced myeloid leukemia cell differentiation protein (Mcl-1), protein kinase C epsilon (PKCε) and isoform 1 of YTH domain family protein 2 (YTHDF2).

Specific Aim III: Characterization of the roles of newly identified post-translationally myristoylated proteins in apoptosis.

The ultimate goal of this project was to characterize the role of post-translationally myristoylated proteins in apoptosis. As such, based on our experience gained during the study of the caspase cleaved serine/threonine kinase: ctPAK2 during apoptosis (Vilas et al., 2006) and the significance of Huntingtin protein on the progression of Huntington's disease, I chose to characterize the role of post-translational myristoylation of another caspase-cleaved protein kinase: ctPKCε and ctHtt in living and dying cells as further described below.

1.7. Biology of newly identified post-translationally myristoylated proteins.

1.7.1. Protein Kinase C epsilon (PKCε).

PKCs encompass a family of phospholipid-dependent serine/threonine kinases with a myriad of subcellular substrates that correspond to a variety of physiological roles. The enzyme activity is conserved from yeast to mammals (Durgan et al., 2008). To date, a total of 9 protein kinase C (PKC) isoforms have been described (Newton and Messing, 2010). They are categorized into 3 groups based on their activation profiles. The classical or conventional PKCs (cPKCs; PKCα, PKCβI, PKCβII and PKCγ) are activated after binding Ca^{+2} and diacylglycerol (DAG) or phosphatidylserine (PS). The novel PKCs (nPKCs; PKCδ, PKCε, PKCη, and PKCθ) are Ca^{+2}-independent and DAG-dependent while the atypical PKCs (aPKCs; PKCζ and PKCλ) are Ca^{+2} and DAG-independent, but PS can regulate their activity (Mackay and Twelves, 2007).

PKCε is a novel PKC and, consequently, Ca^{+2}-independent, but DAG- and PS-dependent. Activation of PKCε occurs in two steps. The enzyme is first 'primed' by phosphorylation, which is required for PKCε to become responsive to secondary signals, such as DAG. Phosphorylation

occurs primarily at 3 sites that lie within conserved regions among the PKCs within the catalytic domain: Thr566 in the activation loop, Ser729 in the hydrophobic tail at the C-terminus, and Thr-710 at an autophosphorylation loop (Figure 1.6.) (Akita, 2002; Cenni et al., 2002; Durgan et al., 2008). Phospholipid-dependent kinase 1 (PDK1) is responsible for phosphorylating Thr566 in the activation loop, whereas the remaining two sites are autophosphorylated. Phosphorylation of Thr566 is thought to be the rate-limiting step in the activation of PKCε (Cenni et al., 2002). Three additional sites of phosphorylation have recently been discovered with the N-terminal regulatory domain, but their contribution to activity has not been elucidated (Durgan et al., 2008). However, PKCε-dependent phosphorylation of Ser368 has been shown to play a role in 14-3-3β binding and cytokinesis in mouse embryonic fibroblasts (MEF) (Cenni et al., 2002; Saurin et al., 2008).

The hypophosphorylated or immature form of PKCε is found associated with the anchoring protein centrosome and Golgi localized Protein kinase N associated protein (GC-NAP) via its catalytic domain. Phosphorylation at Thr-566 and Ser-729 appear to be conferred at the Golgi/centrosome. The mature phosphorylated form of PKCε can be further stimulated by multiple secondary signals, which affect its subcellular localization. In response to DAG or tridecanoic acids PKCε translocates to the plasma membrane, whereas if it is stimulated by arachidonic acids or linoleic acids the enzyme will associate with Golgi-

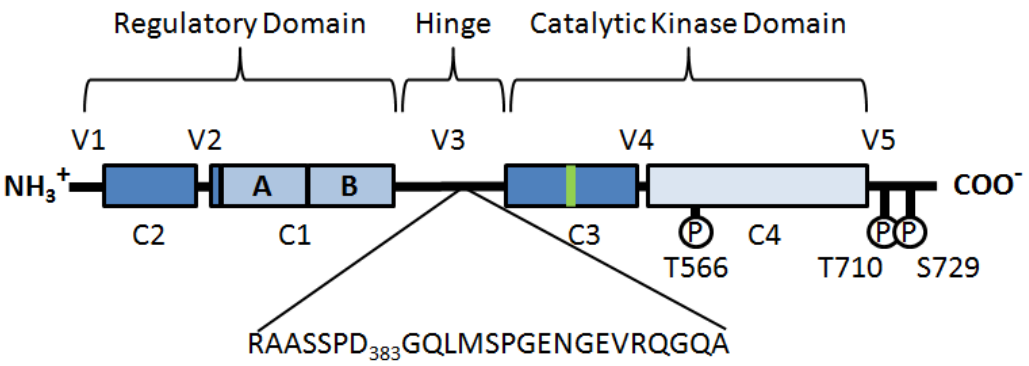

Figure 1.6 – Schematic representation of PKCε. PKCε is comprised of three primary domains; the N-terminal regulatory domain and the C-terminal kinase domain linked together by the Hinge domain. DAG and phorbol esters might have different CIA versus CIB selectivity. CIB seems to be important for fatty acid-induced targeting of the isotype. The phosphorylation of Thr-566 in the activation loop is essential for enzymatic activity. Phosphorylation at Thr-710 and Ser-729 is also necessary for stability and to 'prime' the kinase for binding to second messengers. The green bar represents the ATP binding site Lys-437. The kinase is cleaved by caspase-3 at Asp383 to release the constitutively active C-terminal kinase domain with an N-terminal glycine that is predicted to be myristoylated.

networks (Akita, 2002). In addition to the Golgi and plasma membrane, PKCε has also been detected in the nucleus (Martelli et al., 2006; Xu and Rumsby, 2004) and associated with mitochondria (Baines et al., 2002). In addition, a unique feature within PKCε is an actin-binding domain in the N-terminal regulatory domain, which appears to negatively regulate actin (Li et al., 2006). Actin binding by PKCε is thought to contribute to neurotransmitter exocytosis (Akita, 2002).

PKCε plays a role primarily in proliferation and differentiation, but has also been shown to contribute to cell adhesion and motility, cytoskeleton remodeling, vesicle trafficking and apoptosis (Akita, 2002). Overexpression of PKCε leads to increased proliferation and cell survival. Consequently, a unique feature of PKCε compared to the other PKCs is that it is the only isoform that is oncogenic when overexpressed (Akita, 2002; Garczarczyk et al., 2009; Gorin and Pan, 2009). In fact, it is emerging as a biomarker for oncogenesis (Gorin and Pan, 2009). *In vitro* studies have shown that overexpression of PKCε increases proliferation, motility, and invasion of fibroblasts or immortalized epithelial cells. In addition, in *in vivo* studies using xenografts and transgenic animal models, overexpressing PKCε resulted in metastatic disease. For instance, in mice injected with NIH 3T3 cells overexpressing PKCε all animals developed tumours

(Gorin and Pan, 2009; Mischak et al., 1993). Most importantly, PKCε has been found to be overexpressed in tumour-derived cell lines and histopathological tumour specimens and from various organ sites. PKCε is highly expressed in glioma cell lines and high grade gliomas. Silencing of the enzyme induces apoptosis in glioma cells and primary glioma cultures (Griner and Kazanietz, 2007). Its proliferative, cell survival promoting and oncogenic properties are associated through its activation of the MAPK pathway through Raf-1 and Ras-signaling (Akita, 2002).

PKCε is primarily responsible for the phosphorylation of the Ser/Thr kinase Raf-1. Typically, this leads to activation of the MAPK signaling pathway that, through several downstream effectors, ultimately activates extracellular signal-regulated kinase 1 and 2 (Erk-1/2), which regulates proliferation, differentiation and the cell cycle (Cagnol and Chambard, 2010). Furthermore, Raf-1 activation has been linked to phosphorylation of Akt, which is anti-apoptotic (Majewski et al., 2004). In addition, Raf-1 has been shown to translocate to mitochondria and phosphorylate the pro-apoptotic protein Bad. It also interacts with the anti-apoptotic protein Bcl-2 (Jin et al., 2005). Erk-1/2 has also been shown to phosphorylate and inactivate both Bim and Bad (Luciano et al., 2003). It is thought that PKCε mediates its anti-apoptotic effects through these signaling pathways (Akita, 2002; Bertolotto et al., 2000; Garczarczyk et al., 2009).

Like PAK2, PKCε's N-terminal domain acts as the regulatory domain, but is lost following caspase cleavage during apoptosis resulting

in the release of a constitutively active C-terminal kinase domain (Akita, 2002; Basu et al., 2002; Koriyama et al., 1999; Saurin et al., 2008). PKCε has two caspase cleavage sites at Asp383 and Asp451 (Basu et al., 2002). However, the first site of cleavage and the predominantly cleaved site is Asp383 in the hinge domain between the regulatory and kinase domains (Basu et al., 2002; Mizuno et al., 1997). This exposes an N-terminal Gly residue contained within a predicted myristoylation concensus sequence (Martin et al., 2010; Martin et al., 2008). The second cleavage occurs downstream of the ATP binding site thereby inactivating the kinase domain (Basu et al., 2002; Koriyama et al., 1999). To date, the caspase activated C-terminal domain has not been a main point of focus and the reports about its role in apoptosis are conflicting. Hoppe *et al.* (Hoppe et al., 2001) found that expression of the full-length enzyme as well as the C-terminal kinase domain had no effect on apoptosis. However, they used AKR-2B cells, which do not express PKCδ. It has been shown that there is an interplay between the two isoforms that regulate apoptosis in many cells (Griner and Kazanietz, 2007). Leverrier *et al.* (Leverrier et al., 2002) suggest that the catalytic domain of PKCε plays a positive feedback role to promote the activation of caspase-3 and cleavage of PKCδ in the rat GH3B6 pituitary adenoma cell line (Leverrier et al., 2002). In this case, calpain cleaved PKCε was used, which correlates upstream of Asp383 and would not be myristoylated. Alternatively, Basu *et al.* (Basu et al., 2002) found that an Asp383Ala mutation not only reduced the anti-

apoptotic effect mediated by PKCε, but it potentiated the effect of TNFα-induced apoptosis.

I, therefore, hypothesize that myristoylation of the caspase-activated C-terminal kinase domain of PKCε may substitute the lipid-binding domains (found in the N-terminus) necessary to relocate the kinase domain to various membranes within the cell.

1.7.2. Huntingtin and Huntington's disease.

Huntingtin (Htt) is a large 3144 amino acid protein (approximately 350 kDa) that is ubiquitously expressed and found associated with a number of intracellular compartments including the Golgi complex, nucleus, mitochondria, microtubules and vesicular structures in neuritis and at synapses (Pattison et al., 2006; Sarkar and Rubinsztein, 2008). It is comprised of five HEAT repeat domains (named for the proteins where they were first described: Huntingtin, elongation factor 3, the PR65/A subunit of protein phosphatase 2A, and lipid kinase TOR), which are sites for protein-protein interactions, punctuated by unstructured domains including two PEST (Proline, Glutamic acid, Serine, Threonine rich) domains containing proteolytic sensitive regions (Figure 1.7) (Ehrnhoefer et al., 2011; Schilling et al., 2006; Xia et al., 2003).

Htt is indispensable for cell survival and may mediate protective effect by associating with PAK2 and preventing its cleavage to its proapoptotic form (described above) (Luo and Rubinsztein, 2009). Alternatively, it increases levels of brain derived neurotrophic factor (BDNF), which is essential for the maintenance and differentiation of neurons in the brain (Ehrnhoefer et al., 2011; Gauthier et al., 2004). However, mutated Htt is the causative agent of Huntington's disease (HD) (Group, 1993; Pattison et al., 2006; Sarkar and Rubinsztein, 2008).

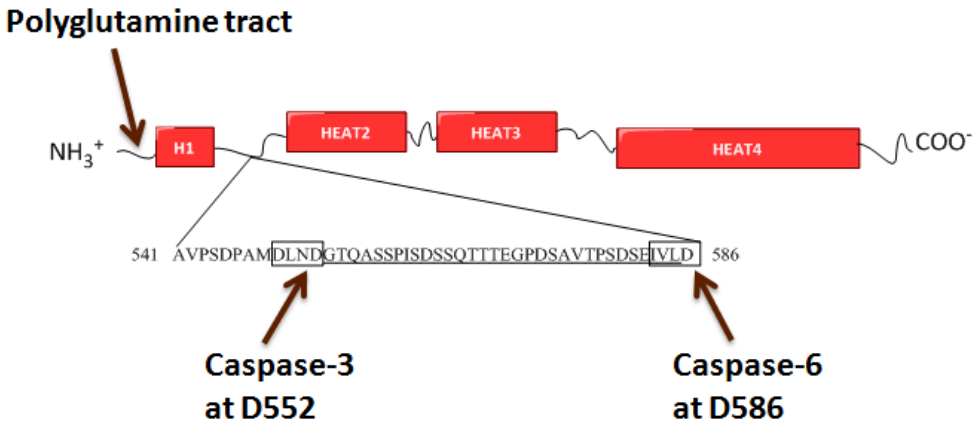

Figure 1.7. – Schematic representation of Huntingtin. The 3144 amino acid protein is comprised of five HEAT domains, punctuated by unstructured domains. The polyglutamine tract associated with HD when there are greater than 35 glutamine repeats is located at the N-terminus. The site of cleavage by caspase-2/-3 and caspase-6 are indicated with the amino acid sequence of the released fragment that is predicted to be myristoylated at Gly553.

HD is an autosomal dominant disease that affects the central nervous system that leads to the dysfunction and cell death of neuronal cells, particularly of striatal neurons, which play a key role in initiating and controlling movements of the body, limbs and eyes. Consequently, the disease is characterized by a loss of cognitive ability and motor skills, eventually leading to dementia and changes in personality. It is also associated with severe motor dysfunction that leads to uncoordinated movement known as chorea. Ultimately, the disease leads to death typically within 10 to 20 years after the appearance of the first diagnosable symptoms. The average age of onset is about 35 to 40 years, but juvenile causes have been detected as early as 5 years of age (Ehrnhoefer et al., 2011; Pattison et al., 2006; Sarkar and Rubinsztein, 2008).

HD is caused by an extended CAG (cytosine-adenosine-guanine) repeat encoding for glutamine (Q) in exon 1 of the IT15 Htt gene (Huntington's Disease Collaborative Research Group 1993). Tandem repeats of greater than 35 Q causes the disease, although a repeat of 39 or higher essentially makes the disease inevitable. In fact, the age of onset indirectly correlates to the number of tandem repeats. Consequently, children with juvenile onset HD have greater than 100 Q repeats. Normal Htt protein typically has 15Q (Huntington's Disease Collaborative Research Group1993; Pattison et al., 2006; Sarkar and Rubinsztein, 2008).

The site of the first glutamine in the expansion is located near the N-terminus at amino acid 17 and is followed by a proline rich region (amino acids 40-70), which is important for protein-protein interactions. The polyglutamine tract of mutant Htt presumably causes the protein to form insoluble aggregates found in the nucleus and other compartments (DiFiglia et al., 1997; Ehrnhoefer et al., 2011; Huntington's Disease Collaborative Research Group 1993). Whether the aggregates themselves are toxic is still debatable. As in Parkinson's disease the intermediate filaments may be toxic, while the final aggregates may be protective (Ehrnhoefer et al., 2011).

Both wildtype and mutant Htt undergo a number of post-translational modifications that appear to regulate protein function and the disease phenotype including, SUMOylation, ubiquitination, acetylation, palmitoylation, phosphorylation and proteolytic cleavage (Ehrnhoefer et al., 2011; Fryer and Zoghbi, 2006; Jeong et al., 2009; Ratovitski et al., 2009; Schilling et al., 2006; Yanai et al., 2006). Therefore, the modifying enzymes may provide targets for treating Huntington's disease. Of note, inhibition of palmitoylation on Cys214 by mutation of the cysteine residue leads to increased inclusion formation, increased nuclear localization and increased toxicity in neurons in mice (Yanai et al., 2006). The palmitoyltransferase responsible for palmitoylation of Htt is HIP14. Downregulation of HIP14 in mouse neurons expressing wild-type and mutant Htt with an extended polyQ tract increases inclusion formation,

whereas overexpression of HIP14 substantially reduces inclusions. Interestingly, the increase in Q in mutant Htt leads to a decrease in palmitoylation of Htt (Yanai et al., 2006). Similarly, phosphorylation at all known sites is diminished in mutant Htt compared to wild type (Ehrnhoefer et al., 2011). SUMOylation and ubiquitination share a dynamic interplay between the same lysine targets within Htt. Ubiquitination has been linked to reduced toxicity of mutant Htt, presumably via increased degradation by the proteasome, whereas SUMOylation stabilizes the proteins, reduces aggregation, and exacerbates transcriptional dysregulation by mutant Htt. Of note, the E3 ligase Rhes (Ras homolog enriched in striatum), which is highly expressed in striatum, has been implicated in SUMOylation of Htt with a greater affinity for mutant over wildtype (Ehrnhoefer et al., 2011). This may explain the selective pathology of HD that results in the significant loss of up to 60% in the striatum (Pattison et al., 2006).

Acetylation has long been viewed as a means to regulate transcription by modification of histones. However, new concepts are emerging. For instance, acetylation of Lys444 appears to direct mutant Htt to autophagosomes for degradation (Jeong et al., 2009). Mutant Htt is preferentially acetylated compared to wildtype and is associated with an increase in autophagy in cell culture, mouse models and patient brains (Ehrnhoefer et al., 2011). Htt labeled vacuoles display the same ultrastructural features of early and late autophagosomes and Htt-enriched cytoplasmic vacuoles appear to be more abundant in cells expressing

mutant Htt (Kegel et al., 2000; Sarkar and Rubinsztein, 2008). However, a recent study has shown that there is a deficiency in cargo recognition in autophagy in HD (Martinez-Vicente et al., 2010). They suggest that the inefficient engulfment of cytosolic components by autophagosomes is responsible for the slower turnover, functional decay and accumulation of autophagosomes in HD.

Htt also undergoes several proteolytic cleavages by caspases (Figure 1.7.) (Fryer and Zoghbi, 2006; Graham et al., 2006; Kim et al., 2001; Wellington et al., 2002). Elevated caspase activity has been detected in neuronal cells expressing mutant Htt (Ehrnhoefer et al., 2011). There are two primary sites of caspase cleavage in Htt, Asp552 and Asp586. Position 552 is cleaved by both caspase-2 and -3 while position 586 is cleaved by caspase-6 (Figure 1.7.) (Wellington et al., 2002; Wellington et al., 2000). There does not appear to be preferential cleavage for wildtype or mutant Htt, but the cleavage of mutant Htt may increase caspase-6 activity, thereby potentiating the effects of mutant Htt (Graham et al., 2006). In neurons, caspase-3 and -6 play a role in synaptic plasticity, memory and learning, suggesting that these caspases cleave Htt during normal cell processes and not just during apoptosis suggesting that they may contribute to the progressive nature of the disease (Ehrnhoefer et al., 2011). The age-dependent increase of caspase-6 activity in the brain could, therefore, further contribute to this feedback loop to promote neurodegeneration. Of note, cleavage of mutant Htt by

caspase-6 is critical for its cytotoxicity. Inhibition of caspase-6 cleavage of mutant Htt in mice significantly reduces toxicity of mutant Htt. In fact, mutant Htt appears to reacquire the protective effect against excitotoxic injury seen in wild type Htt in neurons.

Interestingly, both caspase cleavage sites result in N-terminal glycines. However, only the Gly553, corresponding to caspase-3, is predicted to be myristoylated (Martin et al., 2010). This results in the release of a 34 amino acid fragment of Htt (Htt_{N34}) corresponding to the region between the two caspase cleavage sites. Although blocking cleavage of Asp552 did not appear to improve the HD phenotype in mice, this proteolytic event can be detected *in vivo* and may play an important role downstream of the cleavage at Asp586 (Ehrnhoefer et al., 2011; Graham et al., 2006; Kim et al., 2001).

In each case, the post-translational modifications of Htt tightly regulate the physiological role of Htt in cells and abrogation of these modifications appears to be intricately linked to the progression of HD. Therefore, it is likely that post-translational myristoylation of the Gly553 in mutant Htt protein may act as a membrane binding signal for the C-terminal fragments of Htt and, like fatty acylation by palmitate, may influence the formation of Htt aggregates and, consequently, neurodegeneration in HD.

CHAPTER 2

MATERIALS AND METHODS

2.1. MATERIALS

Table 2.1. Reagents

Name	**Source**
β-mercaptoethanol	Sigma-Aldrich
2-hydroxy-myristic acid (HMA)	Sigma-Aldrich
3-[(3-Cholamidopropyl)dimethylammonio]-1-propanesulfonate (CHAPS)	Sigma-Aldrich
Acrylamide	Bio-Rad
Agar	Invitrogen, Gibco
Agarose, electrophoresis grade	Rose Scientific
Albumin	Pierce
Alkyne-myristate (13-tetradecynoic acid, Alk-Myr, Alk-C14)	OMM Scientific, custom synthesis
Ammonium chloride (NH_4Cl)	Sigma-Aldrich
Ammonium persulphate	Bio-Rad
Azido-biotin (Az-biotin)	Dr. Carolyn Bertozzi, OMM Scientific, custom synthesis
Azido-myristate (12-azidododecanoic acid, Az-C12, Az-Myr)	Dr. John Falck Laboratory
Bacto-tryptone	Difco
Bacto-yeast extract	Difco
Bafilomycin (Baf)	Sigma-Aldrich
Bicinchoninic acid (BCA) Protein Assay Reagent	Pierce
Bis-acrylamide (N,N'- Methylene-bis-Acrylamide)	Bio-Rad
Bovine serum albumin (BSA) fatty acid free	Sigma-Aldrich
Bovine serum albumin (BSA) fraction V	Sigma-Aldrich
Bromophenol blue	BDH
Complete^{TM} protease inhibitors	Roche
Coomassie Brilliant Blue R-250	ICN
Copper(II)Sulphate ($CuSO_4$)	Sigma-Aldrich
Cycloheximide (CHX)	Sigma-Aldrich
DH5α Competent *E. coli* cells	Invitrogen
Deoxyribonuctelotide triphosphate (dNTP)	Fermentas
Dimethyl sulphoxide (DMSO)	Sigma-Aldrich
Dithiothreitol (DTT)	Sigma-Aldrich
Dulbecco's modified Eagle's medium (DMEM)	Life Technologies
ECL Plus	GE Healthcare
Ethanol	Commercial Alcohols
Ethylenediaminetetraacetic acid (EDTA)	Sigma-Aldrich
Fetal bovine serum (FBS)	Life Technologies
FLAG-phosphine	Dr. Carolyn Bertozzi

Table 2.1. Reagents (continued)

Name	**Source**
FuGENE 6 transfection reagent	Roche Applied Science
Gelatin	Fisher Scientific
GeneClean® Turbo PCR purification kit	Q-Biogene
Glacial acetic acid	Fisher
L-Glutamine	Gibco
Glycerol	BDH
Glycine	Bio-Rad
Hank's Balanced Salt Solution (HBSS)	Invitrogen
Hydrochloric acid	Fisher
ImageQuant software	GE Healthcare
Immobilon-P Polyvinylidene fluoride (PVDF) membrane	Millipore Corporation
Isopropanol	Fisher
LysoTracker® Red DND-99	Invitrogen
Magnesium Chloride ($MgCl_2$)	Fisher
Mannitol	Sigma-Aldrich
Methanol	Fisher
MitoTracker Red CM-H_2Xros	Molecular Probes
N,N,N',N',-tetramethylenediamine (TEMED)	Invitrogen
4-(2-hydroxyethyl)-1-piperazineethanesulfonic acid (HEPES)	Invitrogen
NeutrAvidin™-HRP	Pierce
Nitrocellulose membrane (0.45 micron pore)	Bio-Rad
Nonidet P-40 (NP40)/IGEPAL CA-630	Sigma-Aldrich
Nuclease-free water	Fermentas
Paraformaldehyde	Sigma-Aldrich
Peltier Thermo Cycler	MJ Research
Phenylmethylsulfonyl fluoride (PMSF)	Sigma-Aldrich
Phosphine-biotin	Dr. Carolyn Bertozzi
Phosphorimager screen	GE Healthcare
PhosSTOP® Phosphatase inhibitor cocktail	Roche
PNK Buffer	NEB
Poly-L-lysine	Sigma-Aldrich
Potassium hydroxide (KOH)	Sigma-Aldrich
Potassium phosphate mono-basic (KH_2PO_4)	Sigma-Aldrich
Prolong Antifade Solution	Molecular Probes
Protein G-Sepharose CL-4B	GE Healthcare
Roswell Park Memorial Institute (RPMI) media	Gibco
Sepharose CL-4B	Sigma-Aldrich

Table 2.1 Reagents (continued)

Name	**Source**
Skim milk	Carnation
Sodium bicarbonate (Na_2CO_3)	Sigma-Aldrich
Sodium chloride (NaCl)	Sigma-Aldrich
Sodium citrate	Sigma-Aldrich
Sodium deoxycholate	Sigma-Aldrich
Sodium dodecyl sulphate (SDS)	Bio-Rad
Sodium hydroxide (NaOH)	Sigma-Aldrich
Staurosporine (STS)	Sigma-Aldrich
Sucrose	BDH
Tetramethylrhodamine, ethyl ester (*TMRE*)	Invitrogen
Trichloroacetic acid (TCA)	Sigma-Aldrich
Tricine	Bio-Rad
Tris base	Roche
Tris (benzyltriazolylmethyl)amine (TBTA)	Sigma-Aldrich
Tris-carboxyethylphosphine (TCEP)	Sigma-Aldrich
Triton X-100	BDH
Trypsin (0.25% w/v)	Life technologies
Tumour Necrosis Factor α; human (TNFα)	PeproTech
Tween 20 (polyoxyethylenesorbitan monolaureate)	Caledon
U0126 (MEK inhibitor)	Cell Signaling
Urea	Bio-Rad
Yeast extract	Difco
z-DEVD-FMK (caspase-3 inhibitor)	BD Biosciences
z-VA-FMK (negative caspase inhibitor)	BD Biosciences
z-VAD-FMK (general/pan caspase inhibitor)	BD Biosciences

Table 2.2 Commonly Used Media and Buffers

Name	**Composition**
2.5X MS solution	525 mM mannitol, 175 mM sucrose, 12.5 mM Tris-HCl pH 7.4, 12.5 mM EDTA
1X Blotto Solution	0.1% Tween 20, 150 mM NaCl, 50 mM Tris-HCl pH 7.5
Coomassie Blue Gel Destaining solution	10% glacial acetic acid, 45% methanol in MQ water
Coomassie Blue Gel Staining solution	0.25% Coomasie Brilliant Blue R-250, 10% glacial acetic acid, 45% methanol in MQ water
Laemmli 5X SDS-PAGE loading buffer	300 mM Tris-HCl pH 6.8, 50% glycerol, 10% SDS, 0.1% Bromophenol Blue, 1 M DTT or 5% β-mercaptoethanol
Laemmli Running Buffer	1% SDS, 0.025M Tris pH 8.8, 0.2M Glycine
Laemmli Separating Gel Buffer	0.4% SDS, 1.5M TrisHCl pH 8.3
Laemmli Stacking Gel Buffer	0.4% SDS, 0.5M TrisHCl pH 6.8
LB	1% tryptone, 0.5% yeast extract, 1% NaCl
MgRS hypotonic buffer	10 mM NaCl, 1.5 mM $MgCl_2$, 10 mM Tris-HCl pH 7.4, 1X Complete Protease Inhibitor
Phosphate buffered saline (PBS)	1.4 M NaCl, 30 mM KCl, 10 mM Na_2HPO_4-$7H_2O$, 14 mM KH_2PO_4
Phosphine reaction buffer	0.1 M sodium phosphate pH 7.2, 1% SDS
RIPA buffer	50 mM Tris-HCl pH 8.0, 150 mM NaCl, 1% NP-40, 0.5% sodium deoxycholate, 2 mM $MgCl_2$, 2 mM EDTA and Complete protease inhibitor
SOC Media	2% w/v bacto-tryptone, 0.5% w/v bacto-yeast, 8.56mM NaCl, 2.5mM KCl, 10 mM $MgCl_2$, 20 mM glucose
TAE	40 mM Tris-acetate pH 8.0, 1 mM EDTA
Tris buffered saline (TBS)	140 mM NaCl, 25 mM Tris-HCl pH 7.5
TE buffer	10 mM Tris-HCl pH8.0, 1 mM EDTA
Transfer Buffer	0.04 M Glycine, 0.05M Tris, 20% methanol

Table 2.3 Radiochemicals

Radiochemical	**Source**
[9,10(n)-^{3}H]-Myristic acid	GE Healthcare
[9,10(*n*)-^{3}H]-Palmitic acid	GE Healthcare

Table 2.4 Antibodies and fluorescently tagged markers

Antibody	**Species**	**Use**	**Source**	**Catalog number**
anti-phospho-Bad (Ser112)	Rabbit	WB	Cell Signaling	5284
anti-Bim	Rabbit	WB	Cell Signaling	2819
anti-phospho-Bim (Ser69)	Rabbit	WB	Cell Signaling	4581
anti-cleaved caspase-3	Rabbit	WB	Cell Signaling	9665
anti-phospho-ERK (Thr202/Tyr204)	Rabbit	WB	Cell Signaling	4376
anti-GAPDH	Rabbit	WB	Berthiaume laboratory	N/A
anti-GFP	Goat	IP	Eusera	EU4
anti-GFP-sepharose	Goat	IP	Berthiaume Laboratory	
anti-GFP	Rabbit	WB	Eusera	EU1
anti-HA (clone 12CA5)	Mouse	WB	Roche	11583816001
anti-HA (3F10)	Rat	IF	Roche	11867423001
anti-HA-Sepharose	Rat	IP	Roche	11815016001
anti-mouse-HRP	Sheep	WB	GE Healthcare	NXA931-1ML
anti-mouse-Alexa 594	Chicken	IF	Invitrogen	A-2120
anti-PAK(C-19)	Goat	WB, IP	Santa Cruz Biotechnology	sc-1519
anti-PAK2 (R-41)	Rabbit	WB, IP	Berthiaume Laboratory	N/A
anti-PARP	Rabbit	WB	Berthiaume laboratory	N/A
anti-PKCε	Rabbit	WB	Santa Cruz	sc-214
anti-rabbit-FITC	Goat	IF	Jackson Immuno-Research Laboratories	111-095-003
anti-rabbit HRP	Goat	WB	GE Healthcare	RPN2108
anti-rat Alexa 488	Goat	IF	Invitrogen	A11006

WB: western blot IP: immunoprecipitation IF: immunofluorescence HRP: horse radish peroxidase

Table 2.4 Antibodies and fluorescently tagged markers (Continued)

Antibody	Species	Use	Source	Catalog number
Concanavalin A (ConA)	N/A	IF	Invitrogen	C825
Phalloidin-Alexa Fluor 594	N/A	IF	Molecular Probes	A12381

WB: western blot IP: immunoprecipitation IF: immunofluorescence HRP: horse radish peroxidase

Table 2.5 Selective Antibiotics

Antibiotic	Source
Ampicillin	Calbiochem
Carbenicillin	Calbiochem
Kanamycin	Calbiochem
Penicillin G (sodium salt)	Life Technologies
Streptomycin sulfate	Life Technologies

Table 2.6 DNA Modifying Enzymes

Enzyme	Source
Calf intestinal alkaline phosphatase (CIP)	New England BioLabs, Fermentas
High Fidelity Polymerase system	Fermentas
Restriction Endonucleases, Fast Digest	New England BioLabs, Fermentas
T4 DNA Ligase	New England BioLabs, Fermentas

Table 2.7 Plasmids used in this study

Plasmid	Source
pcDNA3.1(+)	Invitrogen
pEGFP-N1	Invitrogen
tdTomato-C1	Invitrogen
ER-RFP	Invitrogen
LAMP1-RFP	Addgene
RFP-LC3	Addgene

Table 2.7 Plasmids used in this study (Continued)

Plasmid	Source
Cathepsin B-BFP	Dr. Michael Davidson
Arf1-mCherry	Dr. Paul Melacon
Htt1-588-eYFP	Dr. Ray Truant
EGFP-Bim(EL)	Dr. Ing Swie Goping
Yes-N_{11}-GFP	Dr. Luc Berthiaume
FL-ctPAK2-EGFP	Dr. Luc Berthiaume
ctPAK2-N_{15}-EGFP	Dr. Luc Berthiaume
PKCε cDNA	Origene
ctPKCε-HA	This work
ctHtt-N34-EGFP	This work
ΔMet-Fyn-EGFP	This work
ctAtrophin-N_{11}-EGFP	This work
ctBap31-N_{11}-EGFP	This work
ctCalcineurin-N_{11}-EGFP	This work
ctCD-IC2A-N_{11}-EGFP	This work
ctGCLC-N_{11}-EGFP	This work
ctMst3-N_{11}-EGFP	This work
ctPAK2-N_{11}-EGFP	This work
ctPKCε-N_{11}-EGFP	This work
ctPKCζ-N_{11}-EGFP	This work
ctSTAT1-N_{11}-EGFP	This work
pTRAMPP-B3AT	This work
pTRAMPP-Bap31	This work
pTRAMPP-CDC6	This work
pTRAMPP-CD-IC2A	This work
pTRAMPP-GATA1	This work
pTRAMPP-GCLC	This work
pTRAMPP-Htt	This work
pTRAMPP-LEDGEF	This work
pTRAMPP-MACF	This work
pTRAMPP-Max	This work
pTRAMPP-Mcl1	This work
pTRAMPP-Mst3	This work
pTRAMPP-PAK2	This work
pTRAMPP-PKCε	This work
pTRAMPP-RBPF	This work
pTRAMPP-YTHDF2	This work

Table 2.8: List of oligonucleotide primers used for PCR for potentially post-translationally myristoylated proteins using EGFP-N1 (All oligos were acquired from MWG Biotech):

Oligo Name	**Oligonucleotide sequence (5′ to 3′)**
TKLTEER-ΔMet-EGFP For	AACTGCAGACCAAGCTGACCGAGGAGCGCGTGAGCAAGGGCGAGGAGCTGTTCACC
BssH II For	CGGCAACTACAAGACGCGCGCCGAGG
BssH II Rev	CCTCGGCGCGCGTCTTGTAGTTGCCG
	STOP
EGFP Rev	TGATCTAGAGTCGCGGCCGCTTTACTTGTACAGCTCGTCC
PKCε	CCCTCGAGGACATGGGCCAGCTGATGAGCCCCGGCGAGAACGGCACCAAGCTGACCGAGGAGCGCGTG
PKCζ	CCCTCGAGGACATGGGCATCAAGATCAGCCAGGGCCTGGGCCTGACCAAGCTGACCGAGGAGCGCGTG
Atrophin-1	CCCTCGAGGACATGGGCCGCAGCCTCAACGACGACGGCAGCAGCACCAAGCTGACCGAGGAGCGCGTG
Calcineurin	CCCTCGAGGACATGGGCGCCACCGCCGCCGCCCGCAAGGAAGTCACCAAGCTGACCGAGGAGCGCGTG
CD-IC2A	CCCTCGAGGACATGGGCGCCGTGGGCAGCCGCACCCTCCACTGGACCAAGCTGACCGAGGAGCGCGTG
STAT-1	CCCTCGAGGACATGGGCCCCAAGGGCACCGGCTACATCAAGACCACCAAGCTGACCGAGGAGCGCGTG
GCLC	CCCTCGAGGACATGGGCTGCGGCAAGGCCCAGAACAGCACCGAGACCAAGCTGACCGAGGAGCGCGTG
Bap31	CCCTCGAGGACATGGGCGGCAAGCTGGACGTCGGCAACGCCGAAACCAAGCTGACCGAGGAGCGCGTG
WT PAK2	CCCTCGAGGACATGGGCGCCGCCAAGTCCCTGGACAAGCAGAAGACCAAGCTGACCGAGGAGCGCGTG
G2A PAK2	CCCTCGAGGACATGGCCGCCGCCAAGTCCCTGGACAAGCAGAAGACCAAGCTGACCGAGGAGCGCGTG

Table 2.9: PCR primers for pTRAMPP-PAK2

Oligo Name	**Oligonucleotide sequence (5′ to 3′)**
Rev A (for)	GGCATGGACGAGCTGTACAAGTTAGGAGGAACT GGAAGTGGA
Rev td Tom A (rev)	TCCACTACCAGTTCCTCCTAACTTGTACAGCTCGT CCATGCCGTACAG
Rev B (for)	TACAAGTTAGGAGGAACTGGAAGTGGATCCGGA GATGAGGTCGACGCGT
Rev td Tom B (rev)	ACGCGTCGACCTCATCTCCCGATCCACTTCCAGT TCCTCCTAACTTGTACTTGTA

Table 2.10: Oligonucleotides for insertion into pTRAMPP-PAK2. Underline indicates site of new restriction endonuclease site.

Oligo Name	**Oligonucleotide sequence (5′ to 3′)**	**New RE site introduced**
WT PAK2	TCGACGGCGCCGCCAAGAGCCTGGACAAG CAGAAGACCA	N/A
WT PKCε for	TCGACGGCCAGCTGATGAGCCCCGGCGAAA ACGGTACCA	KpnI
WT PKCε rev	AGCTTGGTACCGTTTTCGCCGGGGCTCATC AGCTGGCCG	KpnI
WT CD-IC2 for	TCGACGGCGCCGTGGGATCCCGCACCCTC CACTGGACCA	BamHI
WT CD-IC2 rev	AGCTTGGTCCAGTGGAGGGTGCGGGATCCC ACGGCGCCG	
WT Mst3 for	TCGACGGCCAGGCCAGCGGCGGATCCGAC AGCGGCACCA	BamHI
WT Mst3 rev	AGCTTGGTGCCGCTGTCGGATCCGCCGCTG GCCTGGCCG	

Table 2.10 (Continued): Oligonucleotides for insertion into pTRAMPP-PAK2. Underline indicates site of new restriction endonuclease site.

Oligo Name	**Oligonucleotide sequence (5′ to 3′)**	**New RE site introduced**
WT PKC ζ for	TCGACGGCATCAAGATCAGCCAG GGCCTAGGCCTGACCA	Stu I
WT PKC ζ rev	AGCTTGGTCAGGCCTAGGCCCTG GCTGATCTTGATGCCG	
WT GCLC for	TCGACGGCTGCGGCAAGGCCCAG AATTCCACCGAGACCA	EcoRI
WT GCLC rev	AGCTTGGTCTCGGTGGAATTCTGG GCCTTGCCGCAGCCG	
WT Bap31 for	TCGACGGCGGCAAGCTGGACGTC GGCAACGCCGAAACCA	N/A
WT Bap31 rev	AGCTTGGTTTCGGCGTTGCCGAC GTCCAGCTTGCCGCCG	
WT MEKK1 for	TCGACGGCCAGCAGGACAGCTTC CTGCAGGCCAGCACCA	PstI
WT MEKK1 rev	AGCTTGGTGCTGGCCTGCAGGAA GCTGTCCTGCTGGCCG	
WT Htt for	TCGACGGTACCCAGGCCAGCAGC CCCATCAGCGACACCA	KpnI
WT Htt rev	AGCTTGGTGTCGCTGATGGGGCT GCTGGCCTGGGTACCG	
WT Max for	TCGACGGCGGATCCGACAGCAGC AGCGAAAGCGAAACCA	BamHI
WT Max rev	AGCTTGGTTTCGCTTTCGCTGCTG CTGTCGGATCCGCCG	
WT CDC6 for	TCGACGGCAACCGCATGACCCTG AGCCAGGAAGGTACCA	KpnI
WT CDC6 rev	AGCTTGGTACCTTCCTGGCTCAGG GTCATGCGGTTGCCG	

Table 2.10 (Continued): Oligonucleotides for insertion into pTRAMPP-PAK2. Underline indicates site of new restriction endonuclease site.

Oligo Name	**Oligonucleotide sequence (5′ to 3′)**	**New RE site introduced**
WT GATA-1 for	TCGACGGCAAGGGATCCACCAGC TTCCTGGAAACCACCA	BamHI
WT GATA-1 rev	AGCTTGGTGGTTTCCAGGAAGCT GGTGGATCCCTTGCCG	
WT LEDGF for	TCGACGGCAACCAGCCCCAGCAC AACGGCGAAAGCACCA	N/A
WT LEDGF rev	AGCTTGGTGCTTTCGCCGTTGTGC TGGGGCTGGTTGCCG	
WT B3AT for	TCGACGGCGGTACCGAAGGCCAC AGCCCCAGCGGCACCA	KpnI
WT B3AT rev	AGCTTGGTGCCGCTGGGGCTGTG GCCTTCGGTACCGCCG	
WT RNA-binding protein FUS (RBPF) for	TCGACGGCAAGGAATTCAGCGGC AACCCCATCAAGACCA	EcoRI
WT RNA-binding protein FUS (RBPF) rev	AGCTTGGTCTTGATGGGGTTGCC GCTGAATTCCTTGCCG	
WT YTHDF2 for	TCGACGGCAACGGCGTGGGCCAG AGCCAGGCCGGTACCA	KpnI
WT YTHDF2 rev	AGCTTGGTACCGGCCTGGCTCTG GCCCACGCCGTTGCCG	
WT MACF1 for	TCGACGGATCCGACGCCAGCCAG CTGCTGCACCAGACCA	BamHI
WT MACF1 rev	AGCTTGGTCTGGTGCAGCAGCTG GCTGGCGTCGGATCCG	

Table 2.10 (Continued): Oligonucleotides for insertion into pTRAMPP-PAK2. Underline indicates site of new restriction endonuclease site.

Oligo Name	**Oligonucleotide sequence (5′ to 3′)**	**New RE site introduced**
PAK2:G2A For	TCGACGCGGCCGCCAAGAGCCTGGACAAGCAGAAGACCA	NotI
PAK2:G2A Rev	AGCTTGGTCTTCTGCTTGTCCAGGCTCTTGGCGGCCGCG	NotI
G2A CD-IC2 for	TCGACGCCGCCGTGGGATCCCGCACCCTCCACTGGACCA	BamHI
G2A CD-IC2 rev	AGCTTGGTCCAGTGGAGGGTGCGGGATCCCACGGCGGCG	
G2A CDC6 for	TCGACGCCAACCGCATGACCCTGAGCCAGGAAGGTACCA	KpnI
G2A CDC6 rev	AGCTTGGTACCTTCCTGGCTCAGGGTCATGCGGTTGGCG	
G2A Htt for	TCGACGCCACCCAGGCCAGCAGCCCCATCAGCGACACCA	
G2A Htt rev	AGCTTGGTGTCGCTGATGGGGCTGCTGGCCTGGGTGGCG	
G2A Mcl-1 for	TCGACGCCTCTCTTCCGTCGACTCCTCCTCCTGCCACCA	SalI
G2A Mcl-1 rev	AGCTTGGTGGCAGGAGGAGGAGTCGACGGAAGAGAGGCG	
G2A MACF for	TCGACGCCTCCGACGCTAGCCAGCTGCTGCACCAGACCA	NheI/BmtI
MACF G2A rev	AGCTTGGTCTGGTGCAGCAGCTGGCTAGCGTCGGAGGCG	
G2A YTHDF2 for	TCGACGcCAACGGCGTGGGCCAGAGCCAGGCCGGTACCA	KpnI
G2A YTHDF2 rev	AGCTTGGTACCGGCCTGGCTCTGGCCCACGCCGTTGgCG	

Table 2.10 (Continued): Oligonucleotides for insertion into pTRAMPP-PAK2. Underline indicates site of new restriction endonuclease site.

Oligo Name	Oligonucleotide sequence (5′ to 3′)	New RE site introduced
G2A PKCε for	TCGACGCCCAGCTGATGAGCCCC GGCGAAAACGGtACCA	KpnI
G2A PKCε rev	AGCTTGGTACCGTTTTCGCCGGG GCTCATCAGCTGGGCG	

Table 2.11: PCR primers for the generation of ctPKCε-HA

Oligo Name	Oligonucleotide sequence (5′ to 3′)	RE site used
WTctPKCε for	CGGGATCCGAAATGGGCCAGCTG ATGAGCCCCGGTGAGAAT	BamHI
G2ActPKCε for	CGGGATCCGAAATGGCCCAGCTG ATGAGCCCCGGTGAGAAT	BamHI
Rev PKCe with HA tag	CCGCTCGAGCTATGCATAGTCTG GTACGTCGTATGGATAGGGCATCA GGTCTTCACCAAAGTAGGAGAAAC C	XhoI

Table 2.12: Oligonucleotides used for the generation of ctHtt$_{N34}$-EGFP

Oligo Name	Oligonucleotide sequence (5′ to 3′)	RE Used
WTctHtt for	TCGACAGATCTACCATGGGCACTCA GGCTAGCAGTCCAATCAGTGACAG TAGTCAGACTACTACTGAAGGCCCA GACAGTGCCGTGACTCCAAGTGAC AGTAGTGAAATCGTGCTGACCA	SalI BglII HindIII
WTctHtt rev	AGCTTGGTCAGCACGATTTCACTAC TGTCACTTGGAGTCACGGCACTGT CTGGGCCTTCAGTAGTAGTCTGACT ACTGTCACTGATTGGACTGCTAGCC TGAGTGCCCATGGTAGATCTG	SalI BglII HindIII
G2ActHtt for	GATCTACCATGGCCACTCAGGCTA G	BglI BmtI
G2ActHtt rev	CCTGAGTGGCCATGGTA	BglI BmtI

Table 2.13 Cell Lines used in this study

Cell	Description	Source
Jurkat	Human, peripheral blood, leukemia, T cell	Dr. Michele Barry (University of Alberta)
COS-7	African green monkey, kidney cell	ATCC
HeLa	Human, adenocarcinoma cervical cells	Dr. Thomas Simmen (University of Alberta)
ST14A	Rat, embryonic striatal cells	Dr. Simonetta Sipione (University of Alberta)

2.2. METHODOLOGY

2.2.1. Polymerase chain reaction (PCR).

Where indicated, cDNA was amplified using the High Fidelity Polymerase system using the indicated primers listed in Tables 2.8. - 2.12. In 100 µL total nuclease-free water, 50 µM primers were added to 5% (v/v) DMSO, 0.2 mM dNTPs, 500 ng of template DNA and 2.5-5 U of polymerase. Typically, reactions were performed for 30-35 cycles in a Peltier Thermal Cycler. Subsequently, template DNA was digested by the addition of 1 µL of DpnI endonuclease restriction enzyme and incubated overnight at 37°C. Site-directed mutagenesis was performed by overlap extension PCR.

2.2.2. PCR purification and restriction endonuclease digestion.

PCR products were purified from contaminating PCR components using QIAquick® PCR purification Kit (Qiagen). Purified PCR products were eluted in 30 µL of nuclease-free water (Fermentas). 14 µL of PCR product was subjected to restriction endonuclease digestion in a total volume of 20 µL and 10 U of the required restriction enzymes. 0.1 mg/mL of BSA was added when required.

2.2.3. Agarose gel electrophoresis and DNA fragment isolation.

Electrophoresis grade agarose (GibcoBRL) [0.75%-2% (w/v)] was dissolved in TAE buffer (Table 2.2) by heating. DNA samples were mixed with DNA gel loading dye (Table 2.2) and separated by electrophoresis in the agarose gel. Subsequently, the gel was incubated in 0.5 µg/mL of ethidium bromide for 10-20 mins at RT. DNA was visualized using a Ultra-violet gel transilluminator (Fisher Biotech Electrophoresis Systems) or a FluoroChem FC imaging system (Alpha Innotech Corporation).

The GENECLEAN® Turbo PCR purification kit (Q-BIOgene) was used to purify PCR products from agarose gels as per the manufacturer's instructions. PCR products were eluted in 30-60 µL nuclease-free water.

2.2.4. Ligation.

The gel extracted DNA inserts and vectors were combined in an approximately 2.5:1 (v/v) ratio with T4 DNA ligase in the supplier's buffer and ligated for 1 hour at RT or overnight at 4°C.

2.2.5. Molecular Cloning Strategies.

2.2.5.1. Generation of the co-translational EGFP reporter protein to test potentially post-translationally myristoylated proteins (ctSubstrate-N_{11}-EGFP).

First, the hydrophilic linker TKLTEER, which can facilitate the myristoylation of short sequences (McCabe and Berthiaume, 1999) was appended to the N-terminus pEGFP-N1 by PCR using Fermentas High Fidelity PCR mix. At this point, the initiator methionine of EGFP was deleted to prevent a potential alternate translation start site. In addition, a silent mutation was introduced at position 327 (C to G) to introduce a central BssHII restriction endonuclease site to facilitate future cloning projects. This plasmid (TKLTEER-ΔMet-EGFP) served as the template to add the first 10 amino acid sequences of the nine predicted "myristoylatable" candidate proteins to the N-terminus of pEGFP-N1 using PCR and the primers in Table 2.8. The nomenclature for these constructs is ct'substrate'-N_{11}-EGFP (e.g. WTctPAK2-N_{11}-EGFP, Figure 3.7). All sequences were verified by automated DNA sequencing (MWG Biotech).

2.2.5.2. Genetic engineering of a vector encoding for the expression of a caspase cleavable tandem fluorescent reporter protein for analysis of myristoylated proteins post-translationally: pTRAMPP.

The WTctPAK2-N_{11}-EGFP vector described above was used as a template for the construction of the tandem reporter protein. First, the initiator methionine was replaced with an aspartate and a SalI endonuclease restriction site at the 5´ end and a HindIII site was introduced in the DNA sequence encoding for the TKLTEER amino acid linker sequence by PCR extension using Fermentas High Fidelity PCR mix (Primers presented in Table 2.9). Next, the hydrophilic linker, with a 5´ BspEI restriction site, and the remainder of the caspase-3 cleavage site (SGLGGTGSGSGDEV) of PAK2 were introduced at the C-terminus of tdTomato by PCR extension (Ai et al., 2008). A KpnI restriction site was introduced at the C-terminus of EGFP at this point. The product of the latter PCR reaction was inserted into the tdTomato-C1 plasmid using the BspEI and KpnI digestion sites (Figure 4.1).

The non-myristoylatable G2A construct was generated by annealing the 5´-phosphorylated oligonucleotides (Table 2.10) that contained SalI and HindIII overhangs and introduced a new NotI site. Briefly, 100 µM of each oligonucleotide was incubated in PNK buffer (NEB, Ipswich, MA, USA) and 0.5 M NaCl and heated to 95°C for 2 min in a thermocycler and allowed to cool to 4°C at a rate of 0.1°C/s. The oligos

were ligated into SalI and HindIII digested and agarose gel purified tdTom-DEVD-WTctPAK2-N_{10}-EGFP (pTRAMPP-WTctPAK2). The inserts were diluted 1:100 and ligated into the vector at a ratio of 3:1. The new NotI site was used to confirm insertion and the sequence was verified by DNA sequencing (Eurofins MWG Operon). All other constructs were generated similarly using 5′-phosphorylated oligonucleotides Table 2.10. Constructs in which a new restriction site could not be inserted were cloned into the G2A construct and loss of the NotI site was used to confirm insertion prior to DNA sequencing.

2.2.5.3. Cloning of ctPKCε-N_{11}-EGFP and ctPKCε-HA in pcDNA3.1(+)

PKCε cDNA was obtained from ATCC and amplified using a 5′ primer bearing a BamHI restriction enzyme site and a Kozak sequence, and a 3′ primer containing a XhoI restriction endonuclease site and a sequence encoding for the HA epitope tag (Table 2.11). The amplified PCR product was subcloned into pcDNA3.1(+) to produce ctPKCε C-terminally tagged with HA (Figure 4.6.). All constructs were verified by automated DNA sequencing (MWG Biotech).

2.2.5.4. Cloning of ctHttN34-EGFP into pEGFP-N1

WT-ctHtt$_{N34}$-EGFP was generated in a similar fashion as pTRAMPP. Phosphorylated oligonucleotides (Table 2.12) correlating to the full-length 34 amino acid fragment of Htt, excluding the Asp residue from the caspase-6 site and including an initiator Met, were ligated into the pTRAMPP vector using SalI and HindIII. Subsequently, the ctHtt$_{N34}$-EGFP portion was shuttled into the pEGFP-N1 vector using BglI and NotI (Figure 5.2). Phosphorylated oligonucleotides corresponding to G2A-ctHtt$_{N34}$-EGFP was ligated in WT-ctHtt$_{N34}$-EGFP using BglI and BmtI, thereby substituting the essential Gly to and Ala.

2.2.6. Bacterial transformation.

Typically, approximately 50-500 ng cold DNA was combined with 10-50 µL of chemically competent DH5α cells on ice for 30 min prior to transformation. The DNA-bacterial mixture was heat shocked by placing the mixture at 42°C for 45 seconds followed by a 5 min recovery on ice. 180 µL of SOC media was added and incubated for 45 min shaking at 37°C. Finally, the DNA-DH5α mixture was spread on pre-warmed LB agar plates containing the appropriate selective antibiotic.

2.2.7. Cell culture.

COS-7, HeLa, and ST14A cells were maintained in DMEM while Jurkat cells were cultured in RPMI medium at 37°C and 5% CO_2 in a humidified incubator. All the maintenance media were supplemented with 10% fetal bovine serum (FBS), 100 U/mL penicillin and 0.1 mg/mL streptomycin and 2 mM L-Glutamine.

2.2.8. Cell transfection.

Cells were transiently transfected with the indicated constructs using FuGene 6 transfection reagent per manufacturer's instructions in DMEM or RPMI supplemented with 10% FBS and 100 U/mL penicillin and 0.1 mg/mL streptomycin and 2 mM L-glutamine unless otherwise indicated. Typically, transfection reagent-DNA complex was left in the medium for the duration of the experiments.

2.2.9. Electrophoresis and western blotting.

Protein samples were prepared in 1X SDS-PAGE sample loading buffer, unless otherwise indicated. Subsequently, the samples were heated at 100°C for 5 min. Protein were separated on Laemmli SDS-

PAGE gels (Laemmli, 1970) of different percentages ranging from 8 to 12.5 %, based on the separation requirements of the experiments.

After electrophoresis, proteins were transferred onto Immobilon-P PVDF membranes for up to 2 h at 100 V in a Bio-Rad Trans Blot apparatus. For immunodetection, membranes were blocked for 1 h at room temperature with 0.1% Tween 20 in Blotto containing either 5% skim milk or 5% BSA with gentle rocking or overnight at 4°C. After incubation with the indicated primary antibodies, the membranes were subjected to 3 cycles of 6 washes of 5 mins each alternating between 2 washes with PBS followed by 2 washes with 0.1% Tween 20 in PBS and, finally, 2 washes with PBS. Subsequently, the membranes were incubated with the corresponding HRP-conjugated secondary antibodies, washed as described above and processed for ECL detection.

2.2.10. Potassium hydroxide treatment of PVDF membranes.

When PVDF membranes were treated with KOH, protein samples were loaded in duplicate on separate SDS-PAGE gels. After electrophoresis and blotting, the duplicate membranes were soaked in 100 mL of 0.2 M KOH or 0.2 M Tris-HCl pH 7.0 at 25°C for 16 h with gentle shaking. Treated membranes were washed thoroughly with PBS before probing with NeutrAvidin™-HRP/ECL.

2.2.11. Metabolic labeling of cells.

2.2.11.1. Radiolabeling of cells and detection of radiolabeled proteins.

Transiently transfected COS-7 cells were deprived of fatty acids by incubating in serum free DMEM supplemented with 0.1% fatty acid free BSA. [9,10(*n*)-^{3}H] Myristic acid and [9,10(*n*)-^{3}H] palmitic acid (500 μCi) were saponified by 20% molar excess of potassium hydroxide at 65°C for 15 min. Saponified fatty acids were dissolved and incubated in 0.1% fatty acid free BSA in DMEM for 15 min at 37°C, followed by 5 min at 65°C then returned to 37°C before adding to the cells. Cells were radiolabeled for 4 h at 37°C then lyzed with 0.1% SDS-RIPA buffer. Radiolabeled proteins were immunoprecipitated as described below with goat anti-GFP sepharose beads rocking overnight at 4°C. Immunocomplexes were separated by reducing SDS-PAGE, blotted onto PVDF membranes and detected by rabbit anti-GFP serum (1:10,000-1:50,000). PVDF membranes containing radiolabeled proteins were air-dried and exposed to Biomax MS film for 50 days at -80°C.

2.2.11.2. Metabolic labeling of Jurkat cells with Azido-myristate to detect endogenous post-translationally myristoylated proteins.

A modified version for the metabolic labeling of Jurkat cells with [^{3}H]myristate was used for azido-myristate (Vilas et al., 2006). Approximately, 1.0x10^7 Jurkat cells were incubated for 1 h at 37°C in the presence or absence of 1 mM HMA, a NMT inhibitor that does not inhibit protein palmitoylation (Galbiati et al., 1996; Nadler et al., 1993), in RPMI without FBS or antibiotics but supplemented with 1.0% fatty acid free BSA. 40 μM azido-myristate or DMSO vehicle were added to the cells and incubated for 3 h prior to induction of apoptosis by the addition of 2.5 μM staurosporine (STS) and 5 μg/mL cycloheximide (CHX) (Vilas et al., 2006). After 4 h, cells were subjected to hypotonic lysis, as described below, and the post-nuclear supernatant was separated into cytosolic and membrane fractions (Vilas et al., 2006). Typically, 100-200 μg of protein was precipitated with acetone, dissolved in reaction buffer, conjugated with 250 μM phosphine-biotin and analyzed by western blotting as described above.

Endogenous caspase cleaved [^{3}H]myr- or azido-myr-ctPAK2 were immunoprecipitated from whole Jurkat cell. Immune complexes were recovered with protein-G-sepharose as above, eluted with 100 μl phosphine reaction buffer at 80°C for 20 min, conjugated to 250 μM phosphine-biotin and the reaction products were analyzed by western

blotting, as described above. Where indicated, the membranes were treated with either 0.2 M Tris-HCl pH 7.0 or 0.2 M KOH as described above.

2.2.11.3. Non-radioactive metabolic labelling of cells with azido-myristate to detect exogenously expressed myristoylated chimeric EGFPs using a biotinylated phosphine.

The ctPAK2-N_{15}-EGFP and Yes-N_{11}-EGFP constructs were from previous work (Vilas et al., 2006). COS-7 cells were transiently transfected with the pEGFP-N1 vectors expressing the various chimeric EGFPs using Fugene 6 in DMEM in the absence of FBS or antibiotics but supplemented with 1% fatty acid free BSA (Sigma-Aldrich). At 10 h post transfection, 40 µM 12-azidododecanoate (azido-myristate) in DMSO or vehicle alone were added to the media, and incubated for 12-14 h. The cells were washed with cold PBS, harvested and lysed with 0.8 mL of 1% SDS-RIPA buffer (50 mM Tris-HCl pH 8.0, 150 mM NaCl, 1% NP-40, 0.5% sodium deoxycholate, 2 mM $MgCl_2$, 2 mM EDTA and complete protease inhibitor (Roche)) followed by two rounds of sonication at an output of approximately 5.5. The supernatants of a 16 000 x g (10 min at 4°C) centrifugation were collected and precipitated with three volumes of ice cold acetone overnight at -20°C. The precipitates were washed once with one volume of ice cold acetone, dried and resuspended in phosphine

reaction buffer (0.1 M Na phosphate pH 7.2, 1% SDS). Typically, 200-300 µg of protein were conjugated with 250 µM phosphine-biotin or phosphine-FLAG (from a 5 mM stock in 30% DMF in reaction buffer kept under argon gas) for 10 h at room temperature. Following acetone precipitation, the dried pellet was solubilized in 1% SDS-RIPA, diluted to 0.1% SDS-RIPA and pre-cleared with protein-G-sepharose (GE Healthcare) rocking for 45 min at 4°C. Chimeric EGFPs were immunoprecipitated with 0.5 µg affinity purified goat anti-GFP per 100 µg of lysate for 16 h at 4°C followed by addition of protein-G-sepharose for 2 h at 4°C. Following extensive washing with 0.1% SDS-RIPA, the immune complexes were boiled for 5 min in SDS-sample buffer, separated by SDS-PAGE and electro-transferred to PVDF membranes. Where indicated, the membranes were treated with either 0.2 M Tris-HCl pH 7.0 or 0.2 M KOH, as described above and biotinylated azido-myristoylated proteins were detected using neutravidin-HRP or the appropriate anti-FLAG antibodies followed by ECL-Plus detection (GE Healthcare). EGFP was detected on membranes using rabbit anti-GFP serum.

2.2.12. Metabolic labeling of cells with ω-alkynyl- and ω-azido-fatty acids.

The labeling protocol was modified from Martin *et al.* (Martin et al., 2008). Cells were deprived of fatty acids by incubating in their respective

media supplemented with either 5% dextran-coated charcoal treated fetal bovine serum (DCC-FBS) or 1% fatty acid free BSA (Sigma Aldrich) for 1 h prior to labeling. The ω-azido-fatty acids, ω-alkynyl-fatty acids or fatty acids were dissolved in DMSO to generate 20 to 100 mM stock solutions. To facilitate cellular uptake, prior to labeling, fatty acids were saponified by incubation with a 20% molar excess of potassium hydroxide at 65°C for 15 min. A 20 X solution was made by dissolving the saponified fatty acids in pre-warmed serum-free culture media containing 20% fatty acid-free BSA at 37°C, followed by an additional 15 min incubation at 37°C. After deprivation of fatty acids, cells were washed with warm phosphate-buffered saline (PBS) and incubated in fresh media without supplement. One twentieth volume of the 20X fatty acid-BSA conjugate in serum-free media was added to the cells, typically 200 µL to 3.8 mL media, so that the final concentration of BSA is 1% and the fatty acids were at the indicated concentrations. In control experiments, mock DMSO or unlabeled fatty acids were subjected to the saponification and conjugation to BSA as described above. Cells were labeled for times indicated at 37°C in a 5% CO2 humidified incubator. The inhibitor of N-myristoylation 2-hydroxy-myristate (HMA) was also saponified and conjugated to BSA prior to addition to cells.

2.2.13. Detection of ω-alkynyl-fatty acid labeled proteins using click chemistry.

Cell lysates or immunoprecipitated proteins were adjusted to 1% SDS and incubated with 100 μM tris-(benzyltriazolylmethyl)amine (TBTA), 1 mM $CuSO_4$, 1 mM tris-carboxyethylphosphine (TCEP) and 100 μM azido-biotin or 3-azido-7-hydroxycoumarin at 37°C in darkness for 30 mins. Reactions containing the azido-biotin were stopped by the addition of 10 volumes of ice-cold acetone and proteins were precipitated at -20°C for 1 hour or overnight. Precipitated proteins were spun down at 16,000 x g for 15 mins and resuspended in 1X SDS-PAGE sample buffer containing 20 mM DTT. Reactions containing the 3-azido-7-hydroxycoumarin were stopped by addition of one fifth volume 5X SDS-PAGE sample buffer. Samples were heated at 95°C for 5 mins then analyzed by SDS-PAGE. Gels containing the products of the fluorogenic reactions with the 3-azido-7-hydroxycoumarin were scanned with a Storm 840 Phosphorimager in the Blue fluorescence mode. Membranes were probed as described above. Figure results are representative of two or more experiments.

2.2.14. Immunoprecipitation.

2.2.14.1. GFP chimeras

Cells were washed with cold PBS, harvested and lysed with cold EDTA-free RIPA buffer (0.1% SDS, 50 mM Tris-HCl pH 7.4, 150 mM NaCl, 1% Igepal CA-630, 0.5% sodium-deoxycholate, 2 mM $MgCl_2$, EDTA-free complete protease inhibitor [Roche]) by rocking for 15 mins at 4°C. When click chemistry was to be performed following immunoprecipitation, the Tris-HCl was replaced with 50 mM HEPES pH 7.4 in RIPA buffer. Cell lysates were centrifuged at 16,000 x g for 10 mins at 4°C and the post-nuclear supernatants were collected. GFP fusion proteins were immunoprecipitated with affinity purified goat anti-GFP cross-linked to sepharose beads (www.eusera.com) by rocking for 2 h or overnight at 4°C. The beads were extensively washed with 0.1% SDS-RIPA, resuspended in 50 mM HEPES pH 7.4 with 1% SDS, and heated for 15 mins at 80°C. The supernatants containing the fusion proteins were collected.

2.2.14.2. Endogenous PAK2

Endogenous caspase cleaved [^{3}H]myr- or azido-myr-ctPAK2 were immunoprecipitated from whole Jurkat cell lysates induced to undergo

apoptosis for 6 h, using either 3 μg of goat anti-γPAK (C-19) antibody (Santa Cruz Biotechnology) or 3.3 μL of R-41 rabbit anti-ctPAK2 per 200 μg of lysate proteins. R-41 antiserum was from our laboratory stocks and reacts with an epitope mapping to the C terminus of human PAK2.

2.2.15. Sub-cellular fractionation.

Non-adherent Jurkat cells were collected by centrifugation at 1, 000 x g for 5 mins at RT, followed by a PBS wash. For adherent cells, the media was discarded and the cells washed with PBS. Subsequently, cells were collected by trypsinization and scraped off the plates using a cell lifter and harvested. Cells were spun down at 1,000 x g for 5 mins at 4°C, resuspended and swelled in hypotonic buffer, Mg Resuspension Buffer (MgRSB) for 20 mins on ice and homogenized with 30 strokes using the tight pestle in a Dounce homogenizer. Following the addition of 0.4 volumes of EDTA-free 2.5X MS buffer to the homogenate, the cells were homogenized with 10 more strokes. The homogenate was centrifuged at 1,000 x g for 5 min at 4°C. The post-nuclear supernatant (Tot) was collected. The pellet, containing mostly nuclei, was washed once with 1X MS and homogenized in 1X HB containing with 10 additional strokes. The post-nuclear supernatant was centrifuged at 1,000 x g for an additional 5 min at 4°C. The supernatant was collected and combined with Tot. The combined homogenate was centrifuged at 100,000 x g for 30 min at 4°C in

a Beckman TLA 120.2 rotor, resulting in cytosolic fraction (Sup) and a light membrane pellet (Pel). The pellets were solubilized in 1X HB with 1% SDS.

2.2.16. Identification of potentially post-translationally myristoylated proteins.

Putative internal myristoylation sequences adjacent to known caspase cleavage sites were identified from a published list of caspase substrates (Fischer et al., 2003). Myristoylation candidate sequences were recognized using two prediction algorithms provided on http://www.expasy.org/tools/myristoylator/ (Bologna et al., 2004) and http://mendel.imp.ac.at/myristate/SUPLpredictor.htm (Bologna et al., 2004; Eisenhaber et al., 2003; Maurer-Stroh and Eisenhaber, 2004).

2.2.17. Induction of apoptosis and post-translational myristoylation of pTRAMPP chimera proteins.

COS-7 cells were transiently transfected with pTRAMPP-WT- and G2A-ctPAK2 or WT and G2ActPAK2-N_{11}-EGFP for 20 h using Fugene6 (Roche). Apoptosis was induced with 1 µM STS and 5 µg/mL of CHX for 4 h unless otherwise indicated. For labeling studies, the media was exchanged with DMEM supplemented with 1% fatty acid free BSA at 19 h

post transfection and starved for 1 h prior to the addition of 25 µM alkyne-myristate, as described previously, followed by another 30 min incubation prior to inducing apoptosis. Where indicated, the general caspase inhibitor z-VAD-Fmk was used at 20 µM and added prior to the addition of alkyne-myristate. Following lysis in 0.1% SDS-RIPA buffer, GFP proteins were immunoprecipitated using goat anti-GFP linked to sepharose. The beads were washed extensively in lysis buffer and resuspended in click chemistry buffer and incubated at 37°C in darkness for 30 min. The immunoprecipitates were released from the beads by heating for 5 mins at 95°C in 2x SDS-PAGE sample buffer with 100 mM DTT. Incorporation of the alkyne-myristate into proteins was monitored after conjugation to azido-biotin by Western blotting with NeutraAvidin^{TM}-HRP/ECL. Where indicated, the membranes were treated with either 0.1 M Tris-HCl pH 7.0 or 0.1 M KOH overnight prior to probing with NeutraAvidin^{TM}-HRP/ECL.

2.2.18. Microscopy.

2.2.18.1. Fixed cell microscopy

For immunocytochemistry, transfected COS-7 were grown in six well tissue culture plates each one containing a glass coverslip (no.1 thickness, Fisher Scientific) previously coated with 5 µg/ml poly-L-lysine. Cells were

washed twice in PBS, fixed in 4% paraformaldehyde in PBS pH 7.4, for 20 min, washed twice with PBS and then processed as follows.

For immunocytochemistry of COS-7, cells were quenched with 50 mM NH_4Cl for 10 min and permeabilized with 0.1% Triton X-100 in PBS pH 7.4 for 1 min at room temperature, followed by a 30 min block with 0.2% gelatin in PBS pH 7.4. For co-localization of HA chimeras, various organelles and cellular structures, cells were incubated for 1 hour at 37°C in a humidified chamber with rat anti-HA (1:500) and mouse anti-tubulin (1:500) to detect the HA epitope and tubulin, respectively.

After 3 washes containing 0.2% gelatin in PBS pH 7.4, the slides were incubated with the secondary antibodies goat anti-mouse-Alexa Fluor 488 (1:500), and chicken anti-rabbit-Alexa Fluor 594 were was used to detect anti-HA and anti-tubulin antibodies, respectively. Phalloidin-Alexa Fluor 594 (3 units/coverslip) and and ConA-Texas Red (1:500) were used to, actin cytoskeleton, and the ER and Golgi, respectively. All antibodies and fluorophores used were diluted in 0.2% gelatin in PBS pH 7.4.

After processing, all coverslips were mounted in Prolong Antifade Solution (Molecular Probes) and observed by confocal laser scanning microscopy on a Zeiss 510 NLO laser scanning confocal microscope.

2.2.18.2. Live Cell Microscopy

For live cell microscopy, cells were plated on Poly-D-Lysine coated 35 mm glass bottom dishes (MatTek Corporation, Ashland, MA, USA) and transiently transfected with the indicated fluorescently tagged proteins using Fugene6 as recommended by the suppliers.

2.2.18.2.1 Wide field Live Cell Microscopy

Z-stacks of observed cells were acquired by 0.26-0.3 µm step size using a Zeiss Observer Z1 microscope and Axiovision software (Axiovision, version 4.8). Cells were illuminated by a Kublan HXP 120 C lamp using bright field illumination with GFP and Rhodamine filter cubes. Cells were maintained at 37°C and 5% CO_2 using both a Pecon CO_2 module S1 and Tempmodule S1.

For pTRAMPP cell death assays, HeLa cells were transfected for 18 h with the indicated constructs. Subsequently, media was replaced with 1 mL of fresh warm media containing. After 30 min, 1 mL of media was added containing a final concentration of 100 ng/mL TNFα and 5 ug/mL CHX. Acquisition continued until all cells in focus completed apoptosis or 5 h had elapsed.

When viewing ctHtt-N_{34}-EGFP, ST14A and HeLa cells were transfected for 24 or 48 h as indicated. Mitochondrial potential was detected with MitoTracker Red CM-H2XRos (1 µM) as recommended by the supplier. Lysosomes were stained using (1 µM) LysoTracker® Red.

2.2.18.2.2. Spinning Disk Live Cell Confocal Microscopy

Spinning disk confocal microscopy was performed on an UltraView Vox Confocal Imaging System (PerkinElmer, Woodbridge, ON, Canada) attached to a Leica DMI6000B microscope. Images were acquired on an ImagEM camera (Hamamatsu Corporation, Bridgewater, NJ, USA). Excitation radiation was provided by a 488nm laser line paired with a W55 527nm emission filter (PerkinElmer). The growth environment was maintained inside of a Universal ASI Stage Water Jacketed Incubator (Okolab, Ottaviano, NA, Italy). The atmosphere was kept at 19% O_2 and 5% CO_2 by paired DGTO2BX and DGTCO2BX gas mixers (Okolab). Temperature was measured by a TP00-1 thermometer (Okolab), maintained by a Ecoline Staredition E103 water bath (LAUDA, Lauda-Königshofen, Germany) controlled by TempControl Basic software (Okolab).

Where indicated, cells co-expressing ctHtt-N_{34}-EGFP and ER-RFP for 20 h were starved by replacing DMEM media with HBSS media for an additional 4 h. Furthermore, in HeLa cells co-expressing ctHtt-N_{34}-EGFP,

RFP-LC3 and Cathepsin B-BFP, 0.5 µM Baf was added for an additional 24 h after 24 h post-transfection to inhibit autophagosome fusion with lysosomes.

2.2.16.2.3. Deconvolution

Deconvolution of microscopic Z-stacks was performed using Huygens Professional software (Scientific Volume Imaging B.V., Hilversum, Netherlands). The software used a theoretical point spread function, an estimated signal to noise ratio, automatic background estimation, automatic bleaching correction, automatic brick mode, optimized iteration mode, automatic padding mode, a quality change threshold of 0.1%, for a maximum of 40 during CMLE. Where indicated, deconvolved images were reconstructed into 3D representations using Bitplane's Imaris (Imaris x64, version 6.4.2).

2.2.18.3. Immunoelectron Microscopy

HeLa cells transiently expressing Htt_{N34}-EGFP or EGFP alone for 24 h were prepared for immunoelectron microscopy (Manolea et al., 2010). The cells were pelleted and fixed in a mixture of 2% glutaraldehyde and 2% paraformaldehyde in Dulbecco-PBS (D-PBS) for 20 min at 37°C. The fixed cells were rinsed in D-PBS and then dehydrated with alcohol

series (30, 50, 70, and 80% ethyl-alcohol) and infiltrated with LR White (London Resin, Berkshire, United Kingdom). The infiltrated cells were embedded into gelatin capsules and polymerized under UV for 24 h at 4°C. Ultrathin sections of 60 nm were cut and loaded on a 300-mesh nickel grid without coating. Immunolabeling with anti-GFP IgG was performed. The ultrathin sections on the grid were initially blocked with 5% bovine serum albumin in D-PBS for 10 min and incubated with the first primary rabbit antibody, anti-GFP IgG (1:10,000), for 2 h. The secondary antibody bearing 18 nm-colloidal gold–conjugated donkey anti-rabbit IgG (1:10) was also incubated for 1.5 h each. All antibodies were diluted with bovine serum albumin (1% final volume) in D-PBS, and the staining was performed at room temperature. After immunolabeling, ultrathin sections were contrasted with 2% aqueous uranyl acetate for 15 min. The grids were examined in a Philips 410 (Mahwah, NJ) transmission electron microscope, at 80 kV equipped with a charge-coupled device camera (MegaView III, Soft Imaging System, Olympus, Melville, NY).

2.2.19. Cell signaling assays.

Unless indicated otherwise, COS-7 cells were transiently transfected with the indicated plasmids for 18 h. Co-transfections were performed at a ratio of 10:1 (µg:µg) of pcDNA3.1(+) based plasmids to EGFP plasmids to ensure that cells expressing EGFP plasmids also

contained pcDNA3.1(+) plasmids. The specific MEK inhibitor U0126 (10 μM) or vehicle (DMSO) was added for up to 6 h. Cells were washed once with PBS and resuspended in 0.1 % SDS-RIPA with complete protease inhibitors, and PhosSTOP phosphatase inhibitor cocktail (Roche) when evaluating the phosphorylation status of proteins. Cells were collected and incubated rocking for 15 min at 4°C followed by centrifugation at 16,000 x g for 10 min. Protein concentrations were determined using a BCA assay and absorbance was read on a Vmax Kinetic Microplate reader (Molecular Devices) plate reader at 562 nm.

2.2.20. Fluorescence activated cell sorting (FACS).

Cells were plated at a density of 1.0 x 10^5 several hours prior to transfection and grown for indicated times. Cells were incubated with tetramethylrhodamine, ethyl ester (TMRE) for 30 min. Where indicated, cells were induced to undergo cell death by the addition of 150 ng/mL of mouse anti-Fas antibody (clone CH11, Millipore, Billerica, MA, U.S.A.) and 5 μg/mL CHX for 4 hours. Cells expressing EGFP that retain TMRE were counted by fluorescence activated cell sorting (FACS) on a FACScan (Becton Dickson). In cells co-expressing ctPKCε-HA, the data is presented as mean TMRE fluorescence of GFP fluorescing cells normalized to control cells expressing EGFP and vector alone in the absence of an apoptotic stimulus. Otherwise, the data is presented as the percentage of

cells retaining TMRE. Error bars are representative of standard deviation. After determining equal variance by performing an F-test on pooled data a two-tailed Student's t-test was performed on each group.

CHAPTER 3

Development of chemoselective non-radioactive detection methods for myristoylation.

Versions of this chapter have been published in:

1) **Dale D. O. Martin**, Gonzalo L. Vilas, Jennifer A. Prescher, Gurram Rajaiah, John R. Falck, Carolyn R. Bertozzi and Luc G. Berthiaume (2008) **Rapid detection, discovery, and identification of post-translationally myristoylated proteins during apoptosis using a bio-orthogonal azido-myristate analog.** *The FASEB Journal.* 22:797-806.

2) Megan C. Yap, Morris A. Kostiuk, **Dale D. O. Martin**, Maneka A. Perinpanayagam, Pieter G. Hak, Anjaiah Siddam, Janaki R. Majjigapu, Gurram Rajaiah, Bernd O. Keller, Jennifer A. Prescher, Peng Wu, Carolyn R. Bertozzi, John R. Falck and Luc G. Berthiaume (2010) **Rapid and selective detection of fatty acylated proteins using ω-alkynyl-fatty acids and click chemistry.** *J. Lipid Res.* 51(6):1566-80.

-Rights for reproduction were obtained from the publishers.

3.1. Rationale

Post-translational myristoylation of caspase-cleaved proteins has rapidly emerged as a novel means to regulate substrates of programmed cell death (Sakurai and Utsumi, 2006; Utsumi et al., 2003; Vilas et al., 2006; Zha et al., 2000). As described above, several regulators of apoptosis are post-translationally myristoylated including ctBid, ctPAK2 and ctGelsolin. Myr-ctBid and myr-ctPAK2 are both pro-apoptotic while, paradoxically, myr-ctGelsolin is anti-apoptotic. Regardless of the effect on apoptosis, post-translational myristoylation of each of these caspase substrates is fundamental to their functions within apoptosis.

The programmed cleavage of hundreds of proteins during apoptosis (Fischer et al., 2003; Mahrus et al., 2008) warrants the search for additional post-translationally myristoylated proteins and the characterization of their involvement in the regulated demise of the cell. However, the identification and characterization of myristoylated proteins is a tedious process that has long been impeded by the requirement of metabolic labeling of cells with radioactive myristate (^{3}H- or ^{14}C-). This process requires lengthy fluorographic or autoradiographic exposure time to detect radioactive myristate incorporation into proteins, typically weeks to months. Although [^{125}I]iodo-fatty acid analogs have been developed to reduce exposure time needed to detect myristoylated or palmitoylated proteins (Deichaite et al., 1993), this technique requires the handling of large quantities (mCi) of the hazardous high energy ^{125}I radioisotope. This

isotope can still require days to process by autoradiography. Therefore, the need for a nonradioactive methodology able to reliably detect myristoylated proteins is very desirable.

Recently, a new method involving the specific chemoselective ligation between an alkyl-azide and a triarylphosphine has been effectively adapted to study glycosylation and farnesylation using a variety of bio-orthogonal azido analogs in a reaction termed the Staudinger ligation (Figure 3.1) (Kho et al., 2004; Saxon and Bertozzi, 2000). The Staudinger ligation exploits the very specific reaction between a phosphine and an azide. As such, alkyl azides can be covalently linked to a triarylphosphine linked to an affinity tag of choice (e.g. the FLAG epitope or biotin). Azido-analogs have been chosen because they specifically react with phosphines. In addition, they remain inert in the biological milieu and they are nonpolar, thereby ensuring specificity for phosphine groups (Devadas et al., 1998; Kho et al., 2004; Saxon and Bertozzi, 2000). Furthermore, the isosteric myristate analog 12-azidododecanoate (azido-myristate or Az-C12) has been previously shown to be non-toxic to cells when treated for up to 10 days (Devadas et al., 1998).

Herein, I will describe how I have adapted the principle of this methodology to efficiently detect exogenously and endogenously myristoylated proteins using a bio-orthogonal azido-myristate analog and tagged triarylphosphines.

3.2. Results

3.2.1. Phosphine-biotin/FLAG-mediated detection of azido-myristoylated exogenous and endogenous proteins via Western blot analysis.

To reduce exposure time required to detect and characterize myristoylated proteins using radioactive fatty acids, we sought to develop an alternative nonradioactive chemical detection protocol in which a bio-orthogonal azido analog of myristate could be incorporated into proteins upon metabolic labeling and detected by chemoselective ligation to a tagged triarylphosphine (Figure 3.1). Based on a previous study using various azido-myristate analogs with varying numbers of carbons to inhibit viral infections, 12-azidododecanoate was found to be the most isosteric analog and was well suited for use by NMT (Devadas et al., 1998). In addition, in preliminary studies, 12-azidododecanoate appeared to incorporate more efficiently than its 10-carbon counterpart, 10-azidodecanoic acid (Figure 3.2.) in Jurkat cells. The result appeared to be more predominant in cells induced to undergo apoptosis with staurosporine (STS) and in which protein translation was inhibited with cycloheximide (CHX) (Figure 3.2., red arrows). STS is a general kinase inhibitor that induces the intrinsic apoptotic pathway (Antonsson and Persson, 2009).

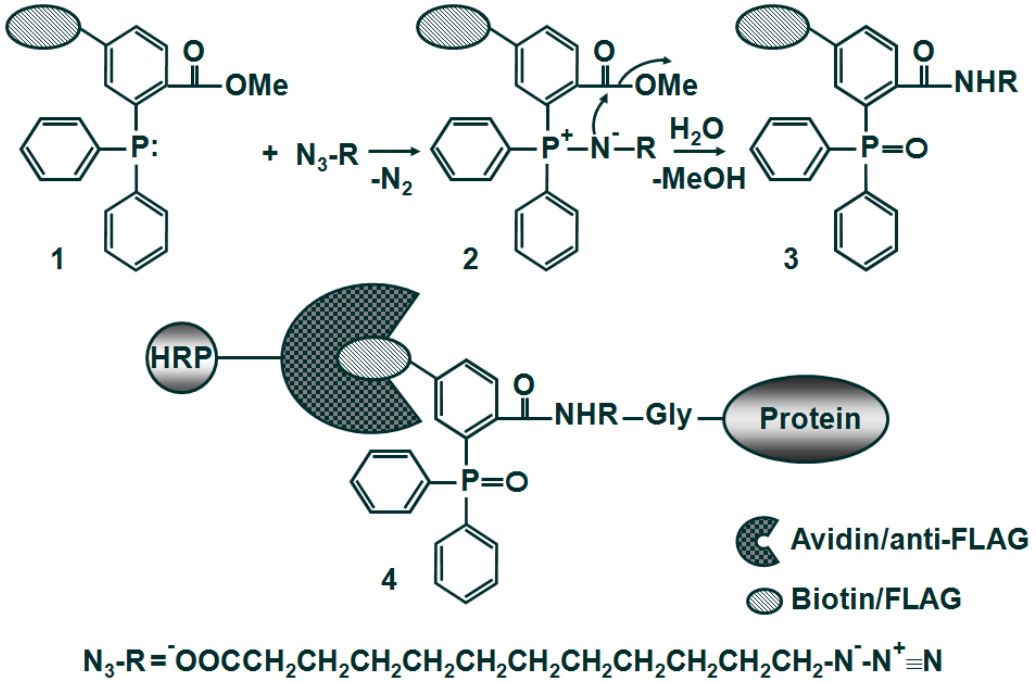

Figure 3.1. Schematic of the Staudinger ligation. The triarylphosphine (*1*) specifically reacts with the azide moiety of azido-myristate to generate an aza-ylide intermediate (*2*), which cyclizes and is subsequently hydrolyzed to form the final product (*3*) that contains the triarylphosphine covalenty linked to the azido-myristate. In cells, the azido-myristate is added to proteins at an N-terminally exposed Gly by NMT. On solubilization of cells, the azido-myristoylated proteins are ligated to the tagged (biotin or FLAG epitope) triarylphosphine (*4*) *via* the Staudinger ligation.

As such, we sought to demonstrate the incorporation of 12-azidododecanoate (azido-myristate or Az-C12) into a variety of known myristoylated proteins.

In the first series of experiments (Figure 3.3A), we employed a well established method of studying exogenously expressed myristoylatable proteins. As such, the first 15 amino acids of ctPAK2, following the caspase cleavage site, were appended to the N-terminus of EGFP with an initiator methionine (Vilas et al., 2006). Alternatively, a non-myristoylatable form was generated wherein the essential N-terminal Gly residue was substituted with an Ala (G2A).

Subsequently, COS-7 cells were transiently transfected with the above-described EGFP constructs and metabolically labeled with the azido-myristate analog. Upon immunoprecipitation with anti-GFP, the immunocomplexes were reacted with phosphine-biotin. Incorporation of the analog was assessed by Western blotting using NeutrAvidin™-HRP, a 'neutral' form of avidin that specifically binds biotin (Bayer and Wilchek, 1990).

In Figure 3.3.A, incorporation of the azido-myristate analog was only detected in the WT, but not in the non-myristoylatable G2A form, nor EGFP alone. These results reflect that of traditional metabolic labeling with [^{3}H]-myristic acid (Figure 3.3.B). This demonstrates that the azido-myristate analog, like [^{3}H]-myristic acid, can be specifically incorporated into N-terminal glycines within myristoylation concensus sequences. Of

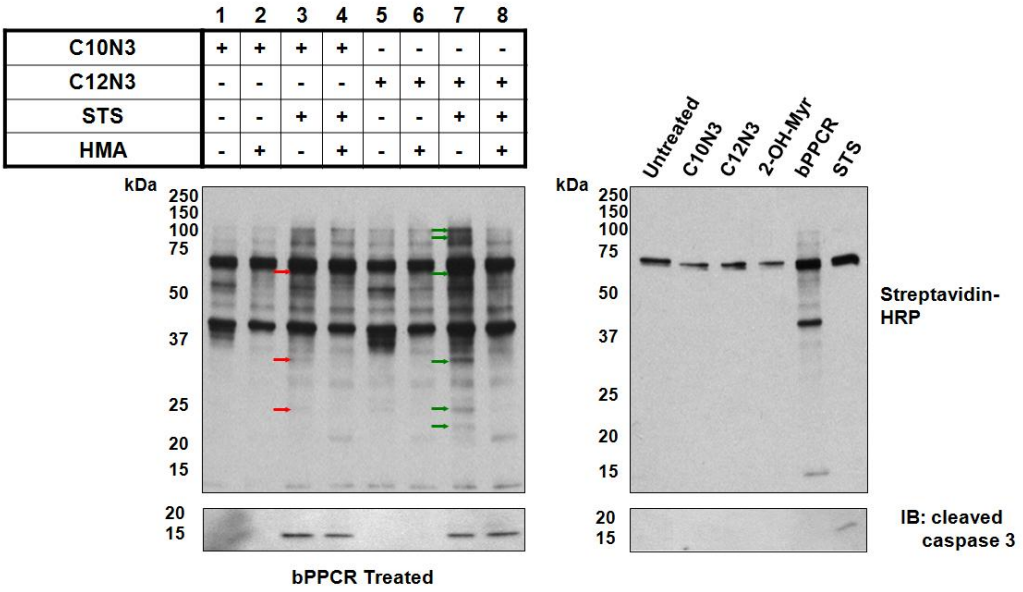

Figure 3.2. – Azido-myristoylated proteins labeled via the Staudinger ligation and detected with streptavidin-HRP. Jurkat cells labeled with 20 μM azido-myristate analogs (C10N3 or C12N3) in the presence or absence of 2-OH myr were induced to undergo apoptosis by the addition of STS. Cells solubilized in 2% SDS-RIPA buffer were incubated with 250 μM biotin phosphine capture reagent (bPPCR) for 10 h at RT. Lysates were separated by 12.5 % SDS-PAGE, transferred to PVDF membranes and probed with streptavidin-HRP. The membranes were stripped and re-probed for activated cleaved caspase 3. Red and green arrows indicate proteins that have incorporated Az-C10 and Az-C12 post-translationally, respectively.

note, detection with azido-myristate was in the order of minutes compared to 50 days using [^{3}H]-myristic acid. Interestingly, when transfected cells were labeled metabolically with azido-palmitate, acylation of WT-ctPAK2-N_{15}-EGFP also was detected, albeit to a much lower extent (Figure 3.3.A). This phenomenon can also be seen when using [^{3}H]-palmitic acid (Figure 3.3.B), again to a much lesser extent, which may be attributed to the lower sensitivity of radiolabeling. Incorporation of the palmitate moieties may be contributed to metabolic interconversion of palmitate into myristate (especially using a 10 h labeling period) and its subsequent incorporation into proteins. This has been suggested previously (McCabe and Berthiaume, 1999). Alternatively, despite NMT's high selectivity for myristoyl-CoA, which normally excludes transfer of palmitate from palmitoyl-CoA (Rudnick et al., 1992b; Rudnick et al., 1990), NMT may be able to use azido-palmitoyl-CoA more efficiently than palmitoyl-CoA, but less efficiently than azido-myristoyl-CoA. To investigate whether the fatty-acyl moieties were incorporated into the EGFP chimeras *via* a thioester or amide bond, PVDF membranes were soaked in 0.2 M KOH for a total of 16 h, a treatment known to hydrolyze radiolabeled fatty acids incorporated into proteins *via* a thioester bond (Armah and Mensa-Wilmot, 1999; Vilas et al., 2006; Zhao et al., 2000). Regardless of the analog used, the label incorporated into WT-ctPAK2-N_{15}-EGFP, but not G2A-ctPAK2-N_{15}-EGFP, was apparently totally resistant to alkali treatment, indicating that the fatty acid moieties

A

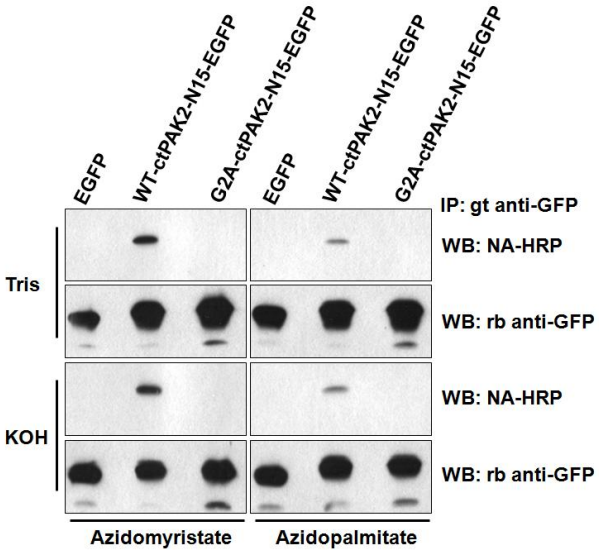

B

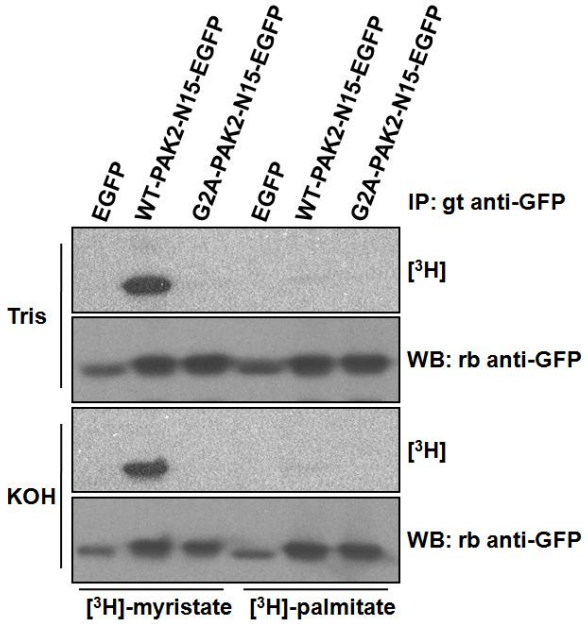

Figure 3.3. – Azido-myristate is specifically incorporated into N-terminal glycines. COS-7 cells transiently expressing truncated (first 15 amino acids only) WT-ctPAK2-N_{15}-EGFP, G2A-ctPAK2-N_{15}-EGFP, or EGFP were labeled with **A** azido-myristate or azido-palmitate and conjugated to phosphine-biotin and detected using NeutrAvidin-HRP or **B** labeled with [^{3}H]-myristic acid or [^{3}H]-palmitic acid and exposed to autoradiography for 50 days. Where indicated, the PVDF membranes were incubated in 0.2 M Tris pH 7.0 or 0.2 M KOH solutions.

were attached to the chimeras *via* an amide bond and not an alkali-sensitive thioester bond.

In Figure 3.4.A, we demonstrate that phosphine-FLAG can be an effective substitute for phosphine-biotin and yields highly similar results and conclusions. In this case, the 34 kDa C-terminal portion of the known post-translationally myristoylated protein caspase-cleaved PAK2 (ctPAK2) and its nonmyristoylatable G2A counterpart were fused to the N-terminus of EGFP, yielding an ~59 kDa fusion protein (WT-FL-ctPAK2-EGFP and G2A-FL-ctPAK2-EGFP, respectively, where FL-ct stands for the full length C-terminal fragment).

Once again, only the WT-FL-ctPAK2-EGFP (Figure 3.4.A) chimera incorporated azido-myristate, while the G2A-FL-ctPAK2-EGFP mutant did not. Of note, azido-myristoylated proteins could typically be detected in under-a-minute exposure to film, often only seconds. The fact that an ~59 kDa band (indicated by an asterisk) can be readily detected in lysates of cells transfected with vector expressing WT-FL-ctPAK2-EGFP (Figure 3.4.A), but not in the lysates of cells expressing G2A-FL-ctPAK2-EGFP, further illustrates the sensitivity of the new method.

In the final study using exogenously expressed proteins, we employed the use of additional EGFP chimeras. This time, the first ten amino acids of the dually acylated protein non-receptor tyrosine kinase Yes was used (Yes-N_{11}-EGFP) (Figure 3.4.B) (McCabe and Berthiaume, 1999). Yes is co-translationally myristoylated on its N-terminal Gly and

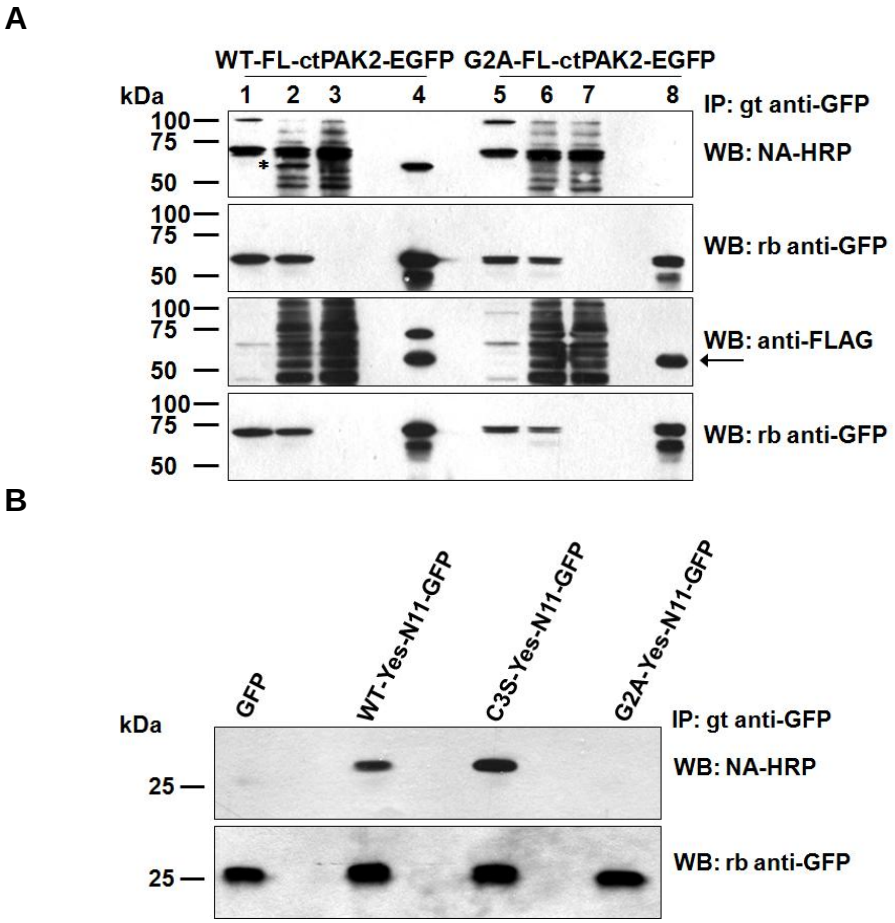

Figure 3.4. - Incorporation of azido-myristate into proteins exogenously expressed in COS-7 cells as detected by chemoselective ligation with phosphine-biotin and phosphine-FLAG. **A** The lysates of COS-7 cells expressing wild-type full-length ctPAK2 with a C-terminal EGFP tag (WT-FL-ctPAK2-EGFP) or the nonmyristoylatable G2A-FL-ctPAK2-EGFP labeled with azido-myristate were left untreated (lanes 1, 5) or conjugated with phosphine-biotin or phosphine-FLAG (lanes 2–4, 6–8). The biotin and FLAG covalently attached to the azido-myristate analog were detected in the lysates (lanes 2, 3, 6, 7) and immunoprecipitated proteins (lanes 4, 8) by Western blotting using NeutrAvidin-HRP (NA-HRP) or anti-FLAG antibodies and ECL. Lanes 3 and 7 represent the postimmunoprecipitation supernatants. Anti-GFP immunoblots demonstrate the presence of WT-FL-ctPAK2-EGFPs and G2A-FL-ctPAK2-EGFPs in similar amounts. The asterisk marks the detection of the azido-myristoylated WT-FL-ctPAK2-EGFP in the crude cell lysate (lane 2) by NA-HRP but not in the corresponding postimmunoprecipitated supernatant (lane 3); the arrow indicates a nonspecific band. **B** Azido-myristate labeling of COS-7 cells expressing truncated (first 11 amino acids) WT-Yes-N_{11}-EGFP, C3S-Yes-N_{11}-EGFP, G2A-Yes-N_{11}-EGFP (McCabe and Berthiaume, 1999), or EGFP were handled as in *A*.

post-translationally palmitoylated on the adjacent Cys residue. Similar to ctPAK2-N15-EGFP, the azido-myristate analog was efficiently incorporated into WT-Yes- and C3S-Yes-N_{11}-GFP and detected in a matter of seconds (Figure 3.4.B). In McCabe *et al.* (McCabe and Berthiaume, 1999) detection of myristoylation required a 1-month exposure using [^{3}H]-myristate as a label. Anti-GFP blots attest to the similar presence of the EGFP chimeras in the various lanes.

To investigate whether our method could detect endogenously myristoylated proteins and perhaps facilitate the identification of new post-translationally myristoylated proteins in cells undergoing apoptosis, we sought to compare the detection of ctPAK2 myristoylation using azido-myristate or [^{3}H]-myristate as labels (Figure 3.5.). We found that, like [^{3}H]-myristate, the incorporation of azido-myristate into immunoprecipitated ctPAK2 was abolished in the presence of the NMT inhibitor HMA (Paige et al., 1990) (Figure 3.5.), suggesting that the azido-myristate is recognized as a substrate by the highly selective NMT (Farazi et al., 2001). Of note, when incorporated into cells, HMA is metabolically activated to 2-hydroxymyristoyl-CoA, a specific inhibitor of NMT that does not inhibit protein palmitoylation (Galbiati et al., 1996; Nadler et al., 1993; Paige et al., 1990). While preventing the incorporation of [^{3}H]-myristate or azido-myristate into ctPAK2 in cells induced to undergo apoptosis (Figure 3.5.A.), HMA did not impair caspase 3-mediated PAK2 cleavage on STS treatment (Figure 3.2.). The

A

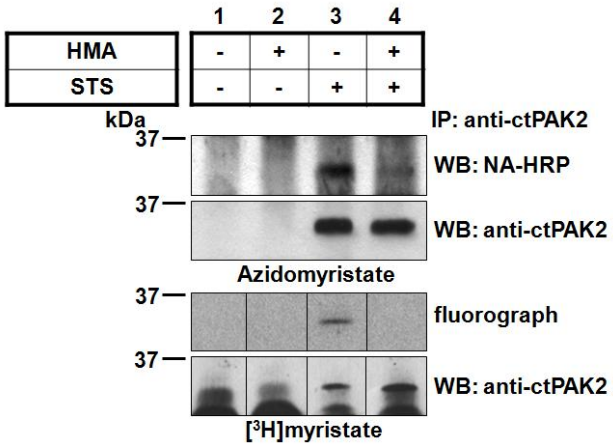

B

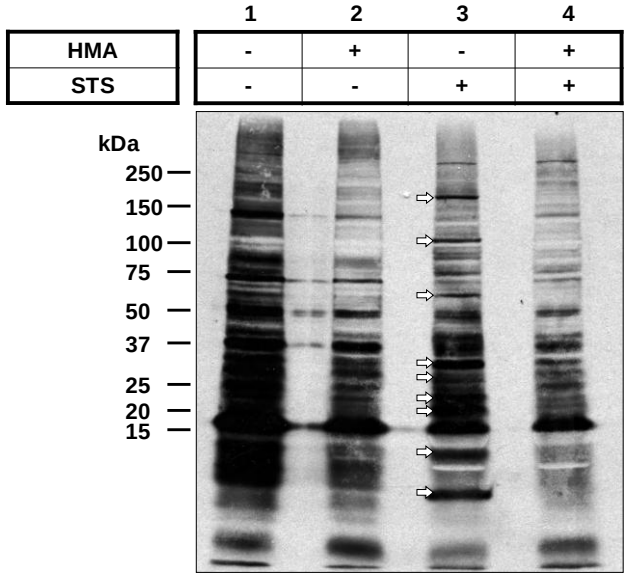

Figure 3.5. Myristoylation of endogenous ctPAK2 in Jurkat cells. Jurkat cells metabolically labeled with **A** azido-myristate or [^{3}H]-myristate were induced to undergo apoptosis with STS/CHX (lanes 3, 4) in the presence or absence of HMA (lanes 2, 4) (Vilas et al., 2006). Endogenous ctPAK2 was immunoprecipitated and conjugated to phosphine-biotin for the nonradioactive detection, then separated by SDS-PAGE, and incorporation of azido-myristate was assessed by Western blot analysis with NeutrAvidin-HRP using a 5-s exposure and incorporation of [^{3}H]-myristate *via* a 2-month fluorographic exposure (composite gel). The post-immunoprecipitation supernatants from the [^{3}H]-myristate samples in **A** were separated by SDS-PAGE and subjected to fluorography for 1 month. **B** The arrows highlight the presence of at least 9 putative post-translationally myristoylated proteins in apoptotic Jurkat cells [Figure 3.5.B was contributed by Dr. Gonzalo Vilas and published in (Martin, Vilas et al. 2008)].

myristoylation of endogenous ctPAK2 myristoylation was detected after a 5 s exposure on Western blot processing with NeutrAvidin-HRP/ECL, while the detection of the incorporation of [^{3}H]-myristate into ctPAK2 required a 65-day exposure using a conventional fluorographic method (Figure 3.5.A).

Overall, our results indicate that a bio-orthogonal azido-myristate analog can be incorporated into proteins *via* an amide bond and used to detect exogenously or endogenously expressed myristoylated proteins in a matter of seconds using phosphine-biotin instead of the typical 1–3 month fluorographic exposure to film required for the detection of [^{3}H]-myristoylated proteins (McCabe and Berthiaume, 1999; Vilas et al., 2006). This difference represents over a million-fold improvement in detection speed.

3.2.2. Azido-myristate incorporation into proteins and its detection with phosphine-biotin demonstrates the existence of several endogenous post-translationally myristoylated proteins in Jurkat T cells.

To investigate if post-translational myristoylation is a widely used modification process during the onset of apoptosis, metabolically radiolabeled Jurkat T cell proteins contained in the post-PAK2-immunoprecipitation supernatants from the previous experiment were

analyzed by SDS-PAGE followed by fluorography. The fluorogram (1-month exposure) in Figure 3.5.B demonstrates that on induction of apoptosis with STS and CHX, at least 9 proteins appear to exhibit post-translational myristoylation (Figure 3.5.B, lane 3). Because HMA inhibits NMT but not palmitoyl transferases, proteins corresponding to bands whose incorporation of [^{3}H]-myristate was drastically reduced in the presence of the NMT inhibitor HMA on induction of apoptosis with STS/CHX (Figure 3.5.B, lane 4) were considered as post-translationally myristoylated proteins.

In comparison, we metabolically labeled Jurkat T cells undergoing STS/CHX-mediated apoptosis with the azido-myristate analog in the presence or absence of HMA. To reduce the complexity of the samples, postnuclear supernatants of cell lysates were fractionated into membrane and cytosolic fractions following metabolic labeling and hypotonic lysis. Figure 3.6. shows that at least 15 and 13 proteins appear to be post- and co-translationally myristoylated, respectively, as judged by the appearance of prominent bands on a short exposure (1 min) of the membrane to film. Interestingly, the vast majority of post-translationally azidomyristoylated proteins (11 of 15) were found in the cytosolic fraction while most co-translationally azidomyristoylated proteins (8 of 13) were found in the membrane fraction. Untreated cells (no azido-myristate, no phosphine-biotin; Figure 3.6, lanes 1, 7) showed 3 endogenous bands in the cytosolic fraction, and up to 8 proteins were detected by the NeutrAvidin-HRP in the

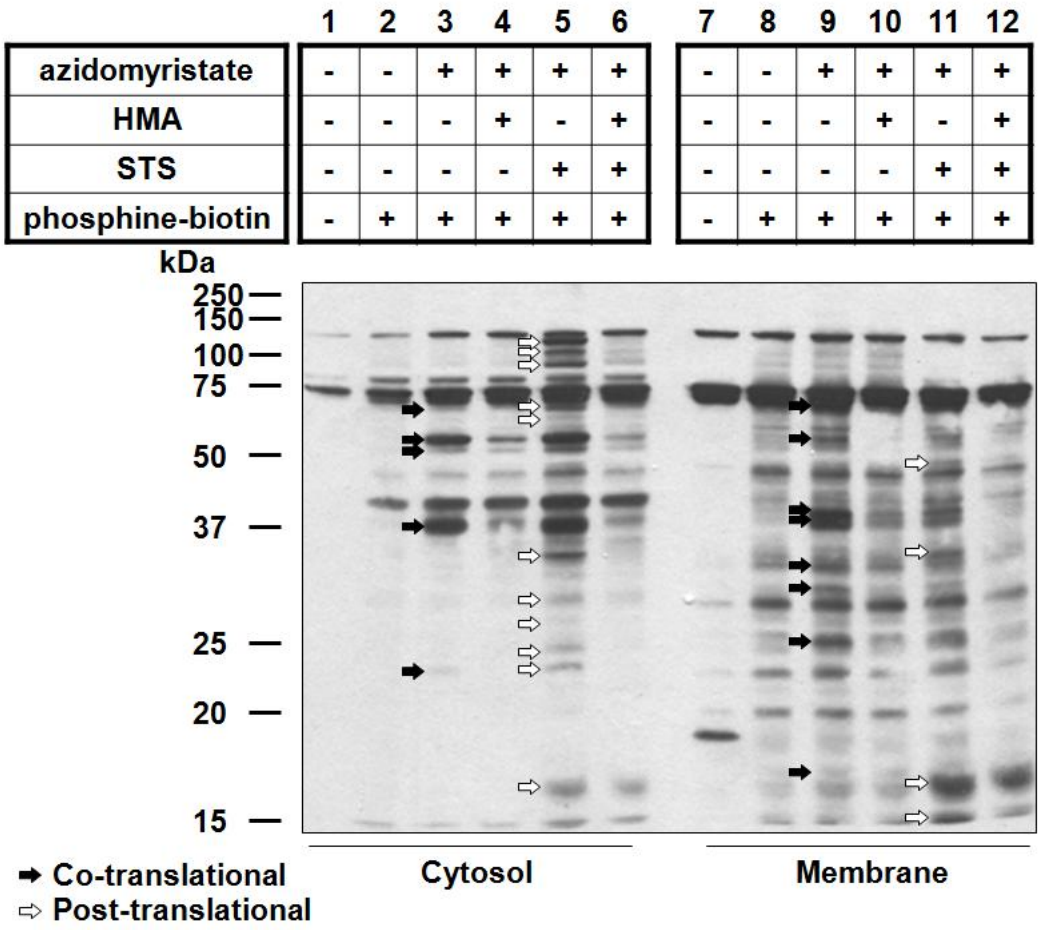

Figure 3.6. - Detection of co- and post-translational azidomyristoylation of endogenous proteins in Jurkat cells using phosphine-biotin. Jurkat cells were metabolically labeled with azido-myristate and induced to undergo apoptosis with STS/CHX (lanes 5, 6, 11, 12) in the presence or absence of HMA (lanes 4, 6, 10, 12), followed by hypotonic lysis and fractionation. The cytosolic (lanes 1–6) and membrane (lanes 7–12) fractions of the postnuclear supernatant were conjugated with the phosphine-biotin (lanes 2–6, 8–12) and subjected to Western blot analysis. Biotinylated, azidomyristoylated proteins were detected with NeutrAvidin-HRP, using a 1-min exposure. Co- (lanes 3, 8) and post-translationally (lanes 5, 11) myristoylated proteins are indicated by black and white arrows, respectively.

membrane fraction; these likely correspond to endogenously biotinylated carboxylases or their proteolytic fragments. We found that the membranous fractions presented a consistently higher background than the cytosolic ones. This might be a consequence of the hydrophobic nature of the 3 aryl groups of the phosphine moiety of the phosphine-biotin or the result of indirect detection of azido-labeled phospholipids nonspecifically bound to membrane proteins. Regardless, these results, in addition to the radioactive data (Figure 3.5.B), indicate that there are additional proteins that are post-translationally myristoylated during apoptosis and that this phenomenon might play an important role in the regulation of apoptosis.

The fact that numerous proteins are post-translationally myristoylated during apoptosis illustrates the need for their identification and the characterization of their roles during this process. Toward this end, we used our azido-myristate analog to label COS-7 cells transiently transfected with vectors expressing various N-terminal EGFP chimeras containing the first 10 amino acids of caspase-cleaved proteins containing putative myristoylation sites directly adjacent to their cleavage site (Table 3.1.).

3.2.3. Development of a strategy for the rapid identification of potentially post-translationally myristoylated proteins.

We identified potential substrates for post-translational myristoyl-

Table 3.1. **List of known and predicted post-translationally myristoylatable proteins.** The C-terminal amino acid sequences downstream of known caspase cleavage sites were subjected to computational analysis to predict myristoylation [E = denotes prediction based on (Bologna et al., 2004; Eisenhaber et al., 2003)**.** Known substrates of post-translational myristoylation were included for comparison (β-actin, Bid, Gelsolin and PAK2). This table is modified from (Fischer et al., 2003)

Substrate	Physiological Role	Cleavage Effect	Cleavage Sequence (Caspase/Myristoylation)	Prediction of Myristoylation	Proven *in vivo*
β -actin	Cytoskeleton	Inactivated	ELPD/GQVITGNE	Twilight Zone (E)	Yes
Bid	Apoptosis activator	Activated	LQTD/GNRSSHSR	Medium Confidence (B) Reliable (E)	Yes
Gelsolin	Severs & nucleates actin	Inactivated	DQTD/GLGLSYLS	Medium Confidence (B) Reliable (E)	Yes
p21-activated kinase 2 (PAK2)	Cytoskeletal dynamics, activated by Rac & Cdc42	Activated	SHVD/GAAKSLDK	High Confidence (B) Twilight Zone (E)	Yes
Atrophin-1	Polyglutamine tract protein defective in Dentatorubral pallidalysian atrophy	Aggregates	DSLD/GRSLNDDG	Low Confidence (B)	No
B-cell receptor-associated protein 31 (p28 Bap31)	Bcl-2 adaptor at the ER, originally identified as B-cell receptor-associated protein	Inactivated	AAVD/GGKLDVGN	Low Confidence (B)	No
Calcineurin	Calmodulin-dependent phosphatase involved in NFAT activation and cytokine synthesis	Activated	DGFD/GATAAARK	Reliable (E)	No
Cytoplasmic dynein intermediate chain (CD-IC)	Mediates dynein/dynactin interaction	Inactivated	DSGD/GAVGSRTL	Medium Confidence (B) Reliable (E)	No
Glutamate-L-cysteine ligase (GCL)	Rate-limiting enzyme in glutathione synthesis	Inactivated	AAVD/GCGKAQNT	Reliable (E)	No
Myc-associated factor X (Max)	Basic helix-loop-helix/leucine zipper protein that plays a role in the activity of c-Myc	Inactivated	SAFD/GGSDSSSE	High Confidence (B) Twilight Zone (E)	No
Mammalian STE20-like protein kinase (Mst3)	Stress signalling	Activated	AETD/GQASGGSD	Twilight Zone (E)	No
Protein Kinase C epsilon (PKC ε)	Cell signalling (various)	Activated	SSPD/GQLMSPGE	High Confidence (B)	No
Protein Kinase C zeta (PKC ζ)	Cell signalling (various)	Activated	DGMD/GIKISQGL	High Confidence (B)	No
Signal transducer and activator of transciption -1 (STAT-1)	Transcription factor for IFN, IL & growth factors	Inactivated	MELD/GPKGTGYI	High Confidence (B)	No

lation by locating internal myristoylation consensus sequences directly downstream of identified caspase cleavage sites (Fischer et al., 2003). To do so, the complete carboxyl terminal sequences downstream of the caspase cleavage site were subjected to computational prediction analysis based on myristoylator and NMT-the Myr Predictor algorithms (Bologna et al., 2004; Eisenhaber et al., 2003). Of more than 280 proteins identified as caspase substrates (Fischer et al., 2003), 48 occurred immediately upstream of a glycine residue, and 9 of these proteins received favorable scores for myristoylation and were identified as putative candidates for post-translational myristoylation (Table 3.1.). The first 10 amino acids downstream of the caspase cleavage sites of these 9 proteins were appended after an initiator methionine to the N-terminus of EGFP at the cDNA level, as we reported earlier (McCabe and Berthiaume, 1999) (Figure 3.7.A).

When COS-7 cells were transiently transfected with vectors expressing the indicated EGFP chimeras in the presence of the azido-myristate analog, 5 of the 9 immunoprecipitated EGFP chimeras tested appeared to incorporate the azido-myristate analog. Figure 3.7B shows that ctBap31-, ctCD-IC2A-, ctGCLC-, ctMST3-, and ctPKCε-N_{11}-EGFPs, as well as the positive control WT-ctPAK2-N_{11}-EGFP, all incorporated significant, albeit different, amounts of the azido-myristate as judged by the positive detection of phosphine-biotin with NeutrAvidin-HRP on the membrane. The signals were the strongest in ctPKCε-N_{11}-EGFP

A

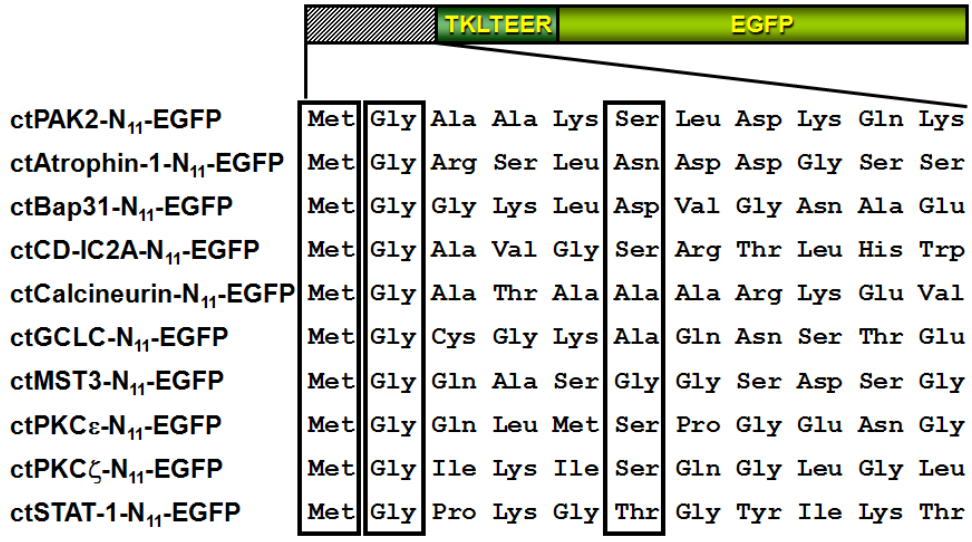

B

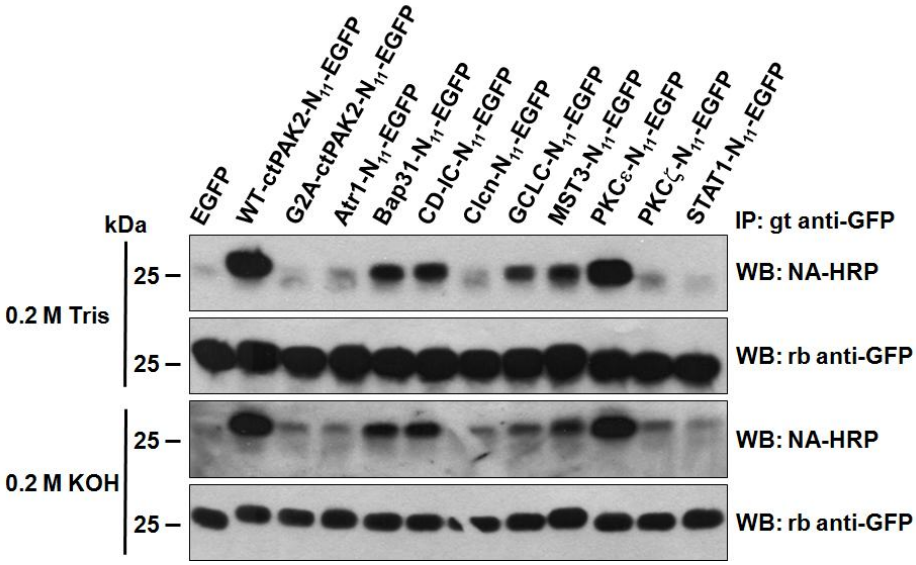

Figure 3.7. - Azidomyristoylation of putative post-translationally myristoylatable proteins. A Representation of the N_{11}-EGFP chimeras bearing the first 10 amino acids of the predicted putative substrates of post-translational myristoylation with an initiator methionine and a TKLTEER hydrophilic linker. The initiator methionine, essential Gly in position 2, and preferred amino acids at position 6 (Ser, Thr, Cys) are boxed. **B** EGFP chimeras were transiently expressed in COS-7 cells and labeled with azido-myristate. The immunoprecipitated EGFP chimeras were reacted with phosphine-biotin and detected by Western blotting with NeutrAvidin-HRP after the membranes were treated with 0.2 M Tris pH 7.0 or 0.2 M KOH. Chimeric ctPAK2-, ctCD-IC2A-, ctPKCε-, ctMST3-, ctBap31-, and ctGCLC-N_{11}-EGFPs all gave significant signals on films to varying intensity.

and WT-ctPAK2-N_{11}-EGFP. In contrast, ctAtr1-, ctCalcineurin-, ctPKCζ-, and ctSTAT1-N_{11}-EGFP, as well as our negative control, the nonmyristoylatable G2A-ctPAK2-N_{11}-EGFP, did not appear to incorporate the azido-myristate analog as no reactive band was found on development of the film. The incorporation of the azido-myristate analog was resistant to alkali hydrolysis and, therefore, believed to occur *via* an amide bond. All chimeric EGFPs were expressed at similar levels (Figure 3.7.B).

To further assess the extent of myristoylation of these 5 sequences of amino acids appended to EGFP, we used confocal microscopy to look at transiently transfected COS-7 cells (Figure 3.8.). We previously have shown that myristoylation of short chimeric GFP constructs is sufficient to confer endomembrane binding and nuclear exclusion to the GFP reporter (McCabe and Berthiaume, 1999). We show that ctCD-IC2A-N_{11}-EGFP and ctPKCε-N_{11}-EGFP as well as WT-ctPAK2-N_{11}-EGFP presented significant perinuclear membrane association and nuclear exclusion while the extent of apparent membrane association and nuclear exclusion is significantly lower for ctBap31-, ctGCLC-, and ctMST3-N_{11}-EGFPs. We believe the extent of nuclear exclusion and endomembrane localization to be highly indicative of the extent of myristoylation. It appears that the localization of ctPKCζ-N_{11}-EGFP (Figure 3.8.), which did not incorporate the azido-myristate (Figure 3.7.B), was like that of G2A-ctPAK2-N_{11}-EGFP, which was indistinguishable from that of EGFP (found largely in the nucleus) (McCabe and Berthiaume, 1999).

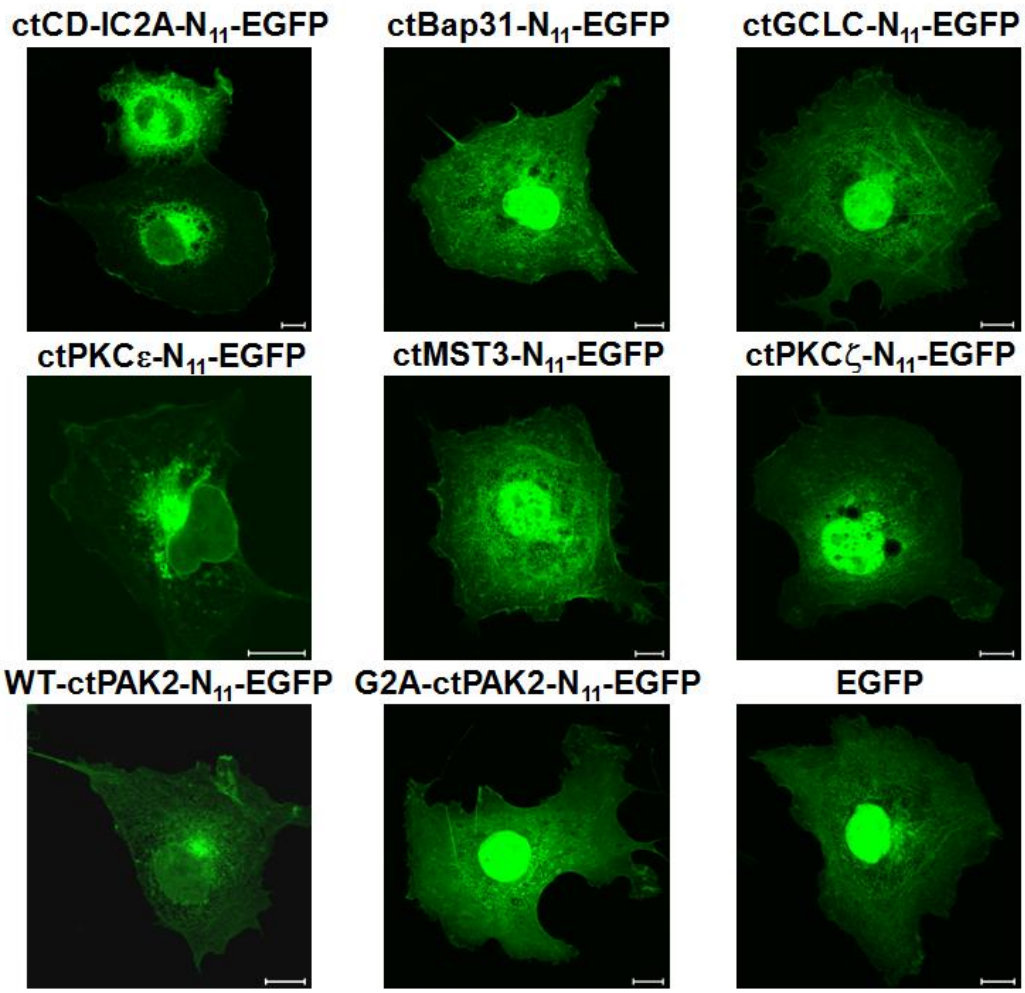

Figure 3.8. Fixed cell confocal microscopy of EGFP chimeras. COS-7 cells transiently expressing the significantly azidomyristoylated chimeric EGFPs identified in *B*, the nonmyristoylatable ctPKCζ- or G2A-ctPAK2-N_{11}-EGFP, and EGFP were fixed and photographed by fluorescence confocal microscopy. Scale bars = 10 μm.

When appended to the hydrophilic N-terminus of a reporter protein, the first 10 amino acids of a known myristoylated protein usually are sufficient to confer myristoylation by NMT and are excellent indicators of protein N-myristoylation (McCabe and Berthiaume, 1999; Utsumi et al., 2003). Altogether, ctCD-IC2A and ctPKCε therefore appear to be our most likely candidates as novel post-translationally myristoylatable substrates for NMT inside cells while ctGCLC, ctBap31, and ctMST3 may be only partially myristoylated. The significance of the post-translational myristoylation of these proteins is currently being investigated.

3.3. Discussion

We developed an alternative and highly sensitive detection method to study the myristoylation of proteins to replace the time consuming, expensive, hazardous, and laborious labeling of cells with radioactive fatty acids. This alternative method takes advantage of the Staudinger ligation's unique chemoselective reactivity that can covalently link alkyl azides, such as azido-myristate, to a tagged triarylphosphine *via* an amide bond, thereby allowing specific probing of azidomyristoylated proteins within the cell (Saxon and Bertozzi, 2000). Indeed, the fact that neither alkyl azides nor phosphines are found in the biological milieu and that they do not react with cellular nucleophiles at ambient temperatures makes them ideal for *in vivo* labeling and subsequent tagging of post-translationally modified proteins (Kho et al., 2004; Saxon and Bertozzi, 2000; Saxon et al., 2002; Sprung et al., 2005). Important to the biological study of myristoylation, 12-azidododecanoate is an alkyl azide analog of myristate that, like most alkyl azides, has been shown previously to be nontoxic to cells and animals (Devadas et al., 1998). Furthermore, 12-azidododecanoate also is efficiently converted to its azidomyristoyl-CoA derivative by fatty acyl CoA synthetase (Devadas et al., 1998), which is a prerequisite to its use by NMT.

Herein, we demonstrate that the isosteric analog of myristate (Devadas et al., 1998), azido-myristate (12-azidododecanoate) can be specifically incorporated in a co- or post-translational fashion *via* an alkali-

resistant amide bond at the N-terminal glycine of exogenously or endogenously expressed proteins and readily detected with the phosphine-biotin using NeutrAvidin/ECL. Recently, Hang *et al.* (Hang et al., 2007) also demonstrated that a variety of azido-fatty acid analogs can be used as chemical probes to monitor protein fatty acylation using the Staudinger ligation, therefore establishing the proof-of-principle for such a methodology. Of relevance to our study, they also showed that 12-azidododecanoate (azido-myristate) is preferentially incorporated into proteins *via* an amide bond (Hang et al., 2007). In our study, we established the proof-of-principle in greater detail and exploited this new technique to demonstrate the existence of several post-translationally myristoylated proteins in Jurkat T cells undergoing apoptosis. Furthermore, we designed a strategy that allowed us to successfully identify new post-translationally myristoylated proteins.

Our strategy is based on several studies that showed that the first 10–15 N-terminal amino acids of a known myristoylated protein are sufficient to confer myristoylation when appended to reporter proteins such as tumor necrosis factor (TNF) or GFP (McCabe and Berthiaume, 1999; McCabe and Berthiaume, 2001; Utsumi et al., 2003; Utsumi et al., 2001). Since we showed that the myristoylation of short chimeric WT-ctPAK2-N_{15}-EGFP and WT-Yes-N_{11}-GFP can readily be detected using azido-myristate cell labeling and reaction with phosphine-biotin (Figures 3.3. and 3.4.), we first identified internal myristoylation sites adjacent to caspase

cleavage sites using computational prediction analysis (Bologna et al., 2004; Eisenhaber et al., 2003) and, second, incorporated these predicted NMT substrate sequences at the N-terminus of EGFP at the cDNA level (Table 3.1.). Finally, using our nonradioactive azido-myristate labeling/phosphine-biotin-based detection method, we assessed the myristoylation status of the chimeric EGFP proteins transiently expressed in COS-7 cells. In doing so, we identified ctBap31-, ctCD-IC2A-, ctGCLC-, ctMST3-, and ctPKCε-N_{11}-EGFP as potential new substrates for NMT and reconfirmed the myristoylation of ctPAK2-N_{11}-EGFP. In our assay, ctPKCζ-N_{11}-EGFP was not a substrate for NMT, confirming the results of Utsumi *et al.* (Utsumi et al., 2003) using tumor necrosis factor as a reporter protein and [^{3}H]myristate as the label.

ctCD-IC2A-N_{11}-EGFP and ctPKCε-N_{11}-EGFP provided the strongest signal *via* Western blot analysis and were almost completely excluded from the nucleus like ctPAK2-N_{11}-EGFP as visualized by confocal microscopy (Figures 3.7. and 3.8.) and, therefore, are likely very efficiently myristoylated and represent strong candidates for post-translational myristoylation of their respective full-length proteins in apoptotic cells. In contrast, despite the significant incorporation of azido-myristate into ctBap31-, ctGCLC-, and ctMST3-N_{11}-EGFP as assessed by Western blot analysis, these chimeras did not show significant nuclear exclusion, suggesting that they are only partially myristoylated, although this may still be of significance inside cells. It is possible that their

endogenous counterparts may act as more desirable substrates for NMT or that there may be some unknown interferences in our system because we were using reporter constructs, which required co-translational myristoylation of chimeric reporters as a means to assess the myristoylation status of naturally post-translationally myristoylated proteins. Furthermore, there are two NMT isoforms (NMT-1 and NMT-2) expressed in mammalian cells, which differ primarily at their N-termini. While the NMT-1 N-terminus is thought to be responsible for ribosome interactions required for co-translational myristoylation, NMT-2 is more cytosolic (Farazi et al., 2001; Giang and Cravatt, 1998). The two isoforms have both overlapping and nonoverlapping substrate specificities (Ducker et al., 2005). Presently, we do not know which isoform is required for post-translational myristoylation, but based on localization studies and recent evidence that NMT-2 interacts with caspase 3 and Bcl-2, we hypothesize that NMT-2 may be the primary enzyme involved in post-translational myristoylation (Giang and Cravatt, 1998; Selvakumar et al., 2006).

Like other previously identified post-translationally myristoylated proteins, the proteins we identified are kinases, proapoptotic proteins, or regulators of the cytoskeleton structure (Utsumi et al., 2003; Vilas et al., 2006; Zha et al., 2000). Like ctPAK2, caspase cleavage of PKCε results in the loss of the N-terminal regulatory domain to generate a constitutively active C-terminal kinase domain (Basu et al., 2002). PKCε contains two caspase cleavage sites at Asp383 and Asp451. The former appears to be

the primary site of cleavage and is located within the hinge domain, between the regulatory and kinase domains, whereas cleavage at the second site is delayed and is found within the catalytic domain (Basu et al., 2002). PKCε is a calcium-independent and diacylglycerol (DAG)-dependent kinase and post-translational myristoylation of ctPKCε at the primary caspase cleavage site (Asp383) may substitute the DAG-binding domain (found in the N-terminus) to relocate the kinase domain to a new site within the cell where it could phosphorylate and regulate the activity of specific proteins during apoptosis.

The effect of myristoylation on the C-terminal kinase domain of PKCε will be described in Chapter 4. The possible effect of post-translational myristoylation on the remaining candidates will be discussed in Chapter 6.

Using this alternative detection methodology, we also demonstrate the existence of at least 15 proteins that undergo post-translational myristoylation in apoptotic Jurkat T cells (Figure 3.6.). This result suggests that post-translational myristoylation of caspase-cleaved proteins represents a mechanism widely used to regulate cell death. While the majority of co-translationally myristoylated proteins were found in the membrane fraction (Figure 3.6) as assessed by our methodology, the majority of the post-translationally myristoylated proteins were found in the cytosolic fraction, perhaps suggesting alternative roles for myristoylation other than membrane tethering.

Because the azide moiety bound to myristate can be ligated with high chemoselectivity with a tagged phosphine *via* a highly stable amide bond, one of the most exciting future applications of this methodology resides in the proteomic identification of the complete set of myristoylated proteins in living and dying cells via affinity chromatography and identification by mass spectrometry. Although this methodology is designed as a chemical tool to label, discover, and identify myristoylated proteins, it is important to note that the biophysical properties of azido-myristate likely differ from that of myristate, and this dissimilarity obviously potentially restricts the use of azido-myristate in subcellular localization studies.

The ease, high sensitivity, and power of our new methodology to detect and identify new myristoylated proteins is undeniable and will greatly facilitate the study of the biology of co- and post-translational myristoylation of proteins in cells and eventually animals with the potential of unraveling new roles for this type of post-translational protein modification.

CHAPTER 4

Tandem reporter assay for myristoylated proteins post-translationally (TRAMPP) identifies novel substrates for post-translational myristoylation: PKC epsilon, a case study.

A version of this chapter has been submitted for publication:

1) **Dale D. O. Martin**, Chrisselle Y. Ahpin, Ryan J. Heit, Maneka A. Perinpanayagam, Megan C. Yap, Richard A. Veldhoen, Ing Swie Goping and Luc G. Berthiaume (2011) **Tandem reporter assay for myristoylated proteins post-translationally (TRAMPP) identifies novel substrates for post-translational myristoylation: PKC epsilon; a case study.** *The FASEB Journal.*

4.1. Rationale.

Previously, we demonstrated the existence of approximately 15-20 post-translationally myristoylated proteins in apoptotic Jurkat T cells [Figure 3.6.; (Martin et al., 2008; Yap et al., 2010)]. Because of the significant number of post-translationally myristoylated proteins and the fact that some have pro-apoptotic roles (e.g. myr-ctBid and myr-ctPAK2) while others have anti-apoptotic functions (e.g. myr-ct-gelsolin), we think post-translational myristoylation is emerging as a novel form of regulation for caspase-cleaved proteins during apoptosis (Martin et al., 2008; Sakurai and Utsumi, 2006; Utsumi et al., 2003; Vilas et al., 2006; Zha et al., 2000).

The emergence of this novel type of post-translational modification of proteins as a potential regulator of apoptosis led us to develop a strategy to identify additional substrates of post-translational myristoylation [Chapter 3; (Martin et al., 2008; Yap et al., 2010)]. First, our laboratory and others developed a non-radioactive method that uses an azido-myristate analog that can be chemically ligated to a triarylphosphine-biotin by the Staudinger ligation (Hang et al., 2007; Martin et al., 2008). This new method allowed the detection of azido-myristoylated proteins reacted with a triarylphosphine-biotin using NeutrAvidin conjugated to HRP and standard western blotting techniques, as well as the identification of multiple new potential substrates for post-translation myristoylation identified by prediction analysis programs (Bologna et al., 2004; Eisenhaber et al., 2004; Fischer et al., 2003). In Chapter 3 (Martin et al.,

2008), the first ten amino acids downstream of the caspase cleavage site of proteins identified as potentially myristoylatable by *in silico* analysis were appended to the N-terminus of EGFP with an initiator methionine as described previously (Martin et al., 2008; McCabe and Berthiaume, 1999). Of the ten substrates tested, strong incorporation of the myristate analog was found in the caspase cleaved cytoplasmic dynein-intermediate chain 2A (CD-IC2A) and PKCε [Figure 3.7; (Martin et al., 2008)]. To a lesser extent, the myristate analog was also incorporated into mammalian STE20-like protein kinase 3 (MST3), glutamate-cysteine ligase catalytic subunit (GCLC) and B-cell receptor-associated protein 31 (Bap31). The extent of myristoylation also corresponded to the intra-cellular distributions of chimeric EGFPs as assessed by confocal microscopy. While constructs that strongly incorporated the azido-myristate analog were primarily localized onto membranes and excluded from the nucleus [Figure 3.8; (Martin et al., 2008)], a property of myristoylated proteins (McCabe and Berthiaume, 1999), others that incorporated the analog less efficiently were found primarily in the cytosol and were not efficiently excluded from the nucleus. As noted previously, one explanation for the variations in myristate analog incorporation and differences in intra-cellular localization is that we employed a co-translational myristoylation assay to assess post-translational myristoylation. Indeed, perhaps the EGFP chimeras in our previous study were not appropriate substrates for methionine aminopeptidase, which removes the initiator methionine in co-translational

myristoylation (Matheson et al., 1975).

In order to overcome this potential caveat we sought to develop an alternative post-translational assay that would rely on caspase cleavage of a given substrate. As such, we generated a tandem reporter assay for myristoylation of proteins post-translationally (pTRAMPP). Briefly, the reporter protein consists of tdTomato (Red) -DEVD-"a test myr-sequence"-EGFP (Green) (tdTom-DEVD- N_{10}-EGFP; Figure 4.1A). The engineering of this vector was inspired from that of dual biosensors used to study caspase cleavage of engineered caspase cleavage sites inserted in between fluorescent proteins (Ai et al., 2008; Tyas et al., 2000). Our version allows for the facile insertion of DNA sequences encoding for putative myristoylatable protein sequences identified by computational prediction analysis downstream of a hydrophilic linker and the caspase-3 consensus sequence "DEVD" (Figure 4.1.A). Following induction of apoptosis, the reporter protein is cleaved by caspases, which frees a new N-terminus exposed to the action of NMTs. We combined the use of the pTRAMPP constructs with a newer detection methodology developed in our laboratory and others (Charron et al., 2009; Hannoush and Arenas-Ramirez, 2009; Yap et al., 2010). The new detection method is based on the incorporation of an alkynyl myristate analog (Alk-C14) into N-terminal Gly residues, like azido-myristate (Az-C12). In this case, the chemical ligation detection method relies on the Cu (I)-catalyzed [3+2] Huisgen cycloaddition reaction (commonly referred to as 'click chemistry'), which

covalently links Alk-Myr to an azido-biotin probe (Figure 4.1.B). By combining our post-translational myristoylation assay with our new detection method we were able to validate the post-translational myristoylation of ctCD-IC2- and ctPKCε-N_{10}-EGFP while ruling out ctMST3-, ctGCLC- and ctBap31-N_{10}-EGFP as potential substrates. In addition, we identified caspase cleaved and exposed sequences of cell division control protein 6 homolog (Cdc6), microtubule-actin crosslinking factor 1 (MACF1), the apoptotic regulator induced myeloid leukemia cell differentiation protein (Mcl-1), Huntingtin (Htt) and isoform 1 of YTH domain family protein 2 (YTHDF2) as putative new substrates for post-translational myristoylation.

Due to the robust incorporation of myristate analog into the ctPKCε chimera detected previously [Figure 3.7.; (Martin et al., 2008) and confirmed herein, we sought to elucidate the effect of myristoylation of ctPKCε in cells as a case study. PKCε is a novel PKC and that is Ca^{+2}-independent, but DAG dependent (Akita, 2002). PKCε plays a role primarily in proliferation and differentiation, but has been shown to contribute to cell adhesion and motility, cytoskeleton remodeling, vesicle trafficking and apoptosis (Akita, 2002). A unique feature of PKCε compared to the other PKCs is that it is the only isoform that is oncogenic when overexpressed (Akita, 2002; Garczarczyk et al., 2009). Like PAK2,

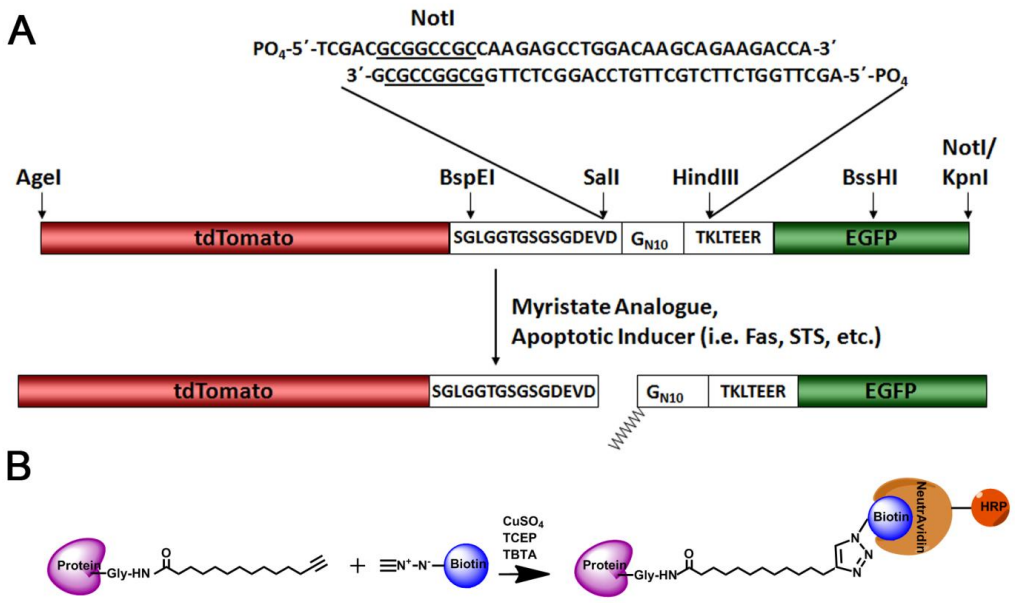

Figure 4.1. – Schematic representation of the tandem fluorescent reporter protein and 'click' chemistry. A Important restriction enzyme sites are indicated. The caspase cleavage site is marked by the DEVD and the orientation of the fluorescent proteins as well as the location of the sequences of interest to be inserted are indicated. The DNA sequence at the top represents the G/A oligonucleotide to be inserted into the WTctPAK2 sequence and illustrates how the test myristoylation sequences were inserted. The site of post-translational myristoylation on the newly exposed glycine of the caspase released EGFP product is shown at the bottom. **B** Proteins acylated with ω–alkynyl-myristate analog are detected using copper(I)-catalyzed azide-alkyne [3 + 2] cycloaddition (click chemistry) with an azido-biotin.

its N-terminal domain acts as the regulatory domain but is lost following caspase cleavage resulting in the release of a constitutively active C-terminal kinase domain (Akita, 2002; Basu et al., 2002; Koriyama et al., 1999; Saurin et al., 2008). PKCε has two caspase cleavage sites at Asp383 and Asp451(Basu et al., 2002). However, the first site of cleavage and the predominantly cleaved site is D383 in the hinge domain between the regulatory and kinase domains. The second cleavage occurs downstream of the ATP binding site thereby inactivating the kinase domain (Basu et al., 2002; Koriyama et al., 1999). To date, the caspase activated C-terminal domain has not been a main point of focus. There is evidence suggesting that it has an anti-apoptotic effect while one study reports that it plays a positive feedback role to promote the activation of caspase-3 (Leverrier et al., 2002). We hypothesized that myristoylation of the caspase-activated C-terminal kinase domain may substitute for the DAG-binding domain (found in the N-terminus) necessary to relocate the kinase domain to various membranes within the cell.

Herein we describe the myristoylation of exogenously expressed caspase-activated C-terminal PKCε (ctPKCε) bearing an HA-tag. We found that myr-ctPKCε-HA incorporated the alkyne-myristate analog specifically at its N-terminal glycine residue. In turn, it is localized to various membranes while non-myr-ctPKCε-HA was mostly cytosolic. In comparison to expression of non-myr-ctPKCε-HA in HeLa cells, expression of the myr-ctPKCε-HA led to an increase in MAPK signaling

through the ERK1/2 pathway resulting in a concomitant phosphorylation of the pro-apoptotic protein Bim as well as a decrease in total Bim levels. Activation of the survival pathway Erk and the decrease of the pro-apoptotic protein Bim were associated with increased TMRE retention in HeLa cells in both the absence and presence of apoptotic stimulus. Together, this suggests a possible anti-apoptotic role for post-translationally myristoylated caspase cleaved ctPKCε.

4.2. Results

4.2.1. Proof of concept for the TRAMPP assay.

In order to assess post-translational myristoylation, we generated a caspase-cleavable tandem fluorescent reporter protein called Tandem Reporter Assay for Myristoylation of Proteins Post-translationally (TRAMPP). The reporter protein is made of tdTomato (Red) -DEVD-“a test myristoylation sequence”-EGFP (Green) (Figure 4.1.A). This vector allows for the facile insertion of DNA sequences encoding the first ten amino acids for putative myristoylatable protein sequences identified by computational prediction analysis downstream of the caspase-3 consensus sequence “DEVD” (Table 4.1.). Following induction of apoptosis of COS-7 cells appropriately transfected with the various pTRAMPPs, the expressed reporter protein is cleaved by caspases, which frees a new N-terminus exposed to the action of NMTs. As such, we can detect myristoylation by incorporation of an alkynyl myristate analog and chemical ligation to an azido-biotin tag (Yap et al., 2010) (Figure 4.1.B). To facilitate easy insertion of myristoylatable sequences, we included SalI and HindIII restriction enzyme sites in which hybridized 5´-phosphorylated oligonucleotides could be inserted. Each new insert included a new restriction endonuclease site for quick confirmation of proper insertion (Table 2.1.). We chose tdTomato as the non-myristoylated cytosolic

counterpart to GFP for its larger molecular weight, which would allow clear separation by SDS-PAGE.

To establish our proof-of-concept, we first transiently transfected COS-7 cells with pTRAMPP-ctPAK2 for 22 h, then cycloheximide (CHX) was added to inhibit translation and staurosporine (STS) was added to induce apoptosis. As shown in Figure 4.2.A, the construct is efficiently processed during apoptosis. The anti-GFP antibody detects 2 bands; 87 kDa and ~27 kDa. These sizes correlate to the full-length uncut chimeric protein and the C-terminal cleavage fragment corresponding to EGFP.

Next, we sought to determine whether the WT-ctPAK2 chimera could incorporate a myristate analog post-translationally. To do so, COS-7 cells were transiently transfected with pTRAMPP encoding for the myristoylatable WT-ctPAK2 or its non-myristoylatable form in which the essential glycine was substituted to an alanine (G2A) for 21 h. Prior to the induction of apoptosis by the addition of CHX and STS, the cells were starved for 1 h in media without FBS, but supplemented with 1% fatty acid free BSA followed by addition of 25 μM alkyne-myristate conjugated to BSA for 30 mins. After 4 h of apoptosis the chimeric proteins were immunoprecipitated with anti-GFP and the alkyne-myristoylated proteins reacted with azido-biotin via Cu^{+2}-catalysed click chemistry as described in Chapter 2. As can be seen in Figure 4.2.B, the alkyne-myristate was efficiently incorporated into the ~26 kDa fragment that corresponds to the caspase-cleaved C-terminal EGFP product released by cleavage of

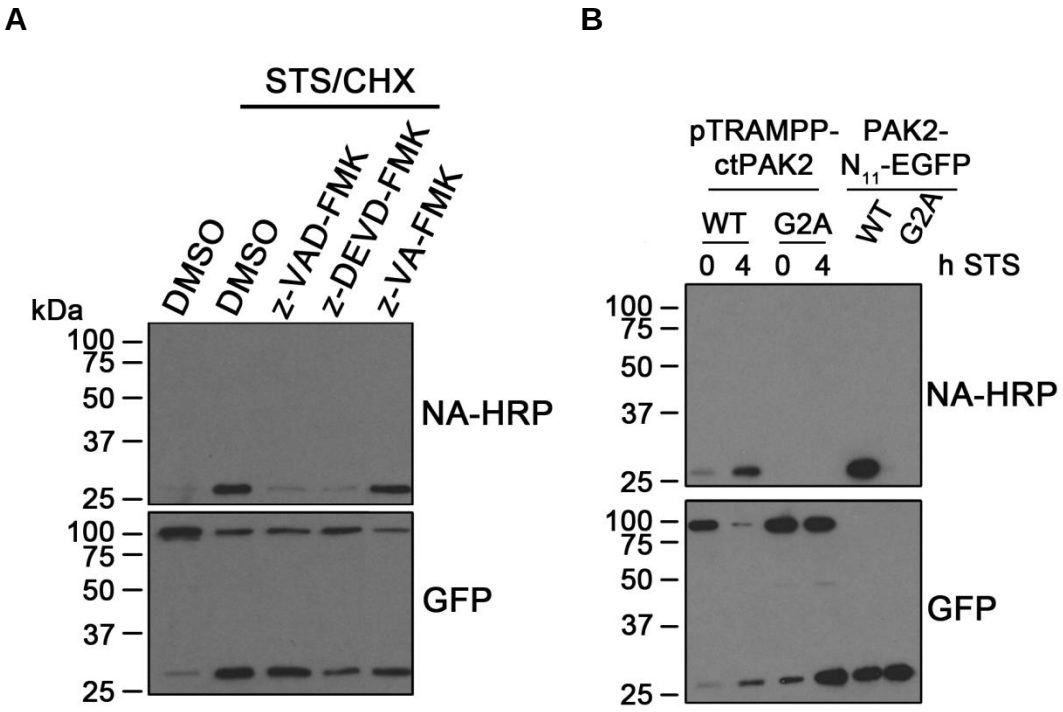

Figure 4.2. – **Proof of concept; post-translational myristoylation of pTRAMPP-ctPAK2. A** Cleavage of the reporter protein and incorporation of Alk-myr post-translationally in the presence of 20 µM general caspase inhibitor (z-VAD-FMK), caspase-3 inhibitor (z-DEVD-FMK) or a negative control for caspase inhibition (z-VA-FMK) after treatment with STS and CHX. The top, middle and bottom bands represent the full-length protein, N-terminal tdTomato-DEVD- and the C-terminal myrG-N10-EGFP fragments, respectively. **B** Post-translational myristoylation of the WT reporter protein following caspase-cleavage. The co-translational myristoylation of WTctPAK2-N_{11}-EGFP is included as a control for myristoylation and click chemistry.

pTRAMPP-WT-ctPAK2 in cells treated with STS/CHX. No incorporationwas detected in non-apoptotic cells or in the non-myristoylatable G2A-ctPAK2-EGFP mutant cleavage product. Furthermore, the level of myristoylation was comparable to that of cells transfected with a vector encoding for the expression of its co-translationally myristoylatable WT-ctPAK2-N_{11}-EGFP counterpart, as described previously (Martin et al., 2008). These data demonstrate that our tandem fluorescent reporter can be exploited to detect post-translational myristoylation of a known post-translationally myristoylated protein and establishes our proof-of-concept. Confirmation that the alkyne-myristate labeling is a caspase dependent event was demonstrated by a strong decrease in incorporation of alkyne-myristate in the presence of a general caspase inhibitor or caspase-3 inhibitor (Figure 4.2.A).

4.2.2. Live cell imaging following the cleavage and post-translational myristoylation of pTRAMPP-ctPAK2.

Typically, when an N-myristoylatable sequence is appended to the N-terminus of EGFP, the chimeric EGFP will be relocated to membranes and excluded from the nucleus as opposed to the usual cytosolic and nuclear localization of EGFP (Martin et al., 2008). When we attempted to visualize the localization of our tandem fluorescent proteins in COS-7 cells undergoing STS/CHX mediated apoptosis using live cell microscopy we did not see the classical hallmark features of apoptosis (e.g. cell retraction,

rounding-up and formation of apoptotic bodies) (Wyllie, 1997; Wyllie et al., 1999). Consequently, HeLa cells were transfected with pTRAMPP-ctPAK2 and treated with TNFα/CHX to induce apoptosis via the extrinsic pathway, which resulted in more typical morphological characteristics of apoptosis. HeLa cells transiently expressing pTRAMPP-WT- and -G2A-ctPAK2 were treated with TNFα for up to 5 h. Prior to the induction of apoptosis, cells bearing intact pTRAMPP-WT-ctPAK2 showed a near complete overlap of the green and red fluorescence (Figure 4.3.A). Once the cells began to retract and round-up, the separation of red and green fluorescence started to appear. However, once apoptotic bodies formed, a clear separation between the red and green fluorescent signals was detected wherein the green fluorescence (myr-EGFP) was found both at the center and periphery of the apoptotic bodies while the red fluorescence was retained in the cytosolic compartments. Therefore, these results suggest that the myristoylated EGFP fragment localizes to membranes while the tdTomato fragment remains cytosolic. Our pTRAMPP-ctPAK2 construct, therefore, allowed the visualization of post-translational myristoylation as it occurs in a dying cell for the first time. In contrast, in HeLa cells expressing pTRAMPP-G2A-ctPAK2 there was no apparent separation of red and green fluorescent signals at any time (Figure 4.3B), suggesting that the non-myristoylated EGFP fragment remains cytosolic like tdTomato. Of particular note, the tdTomato fluorescence has a maturation half-life of 1 h. During this time tdTomato will transition through an intermediate

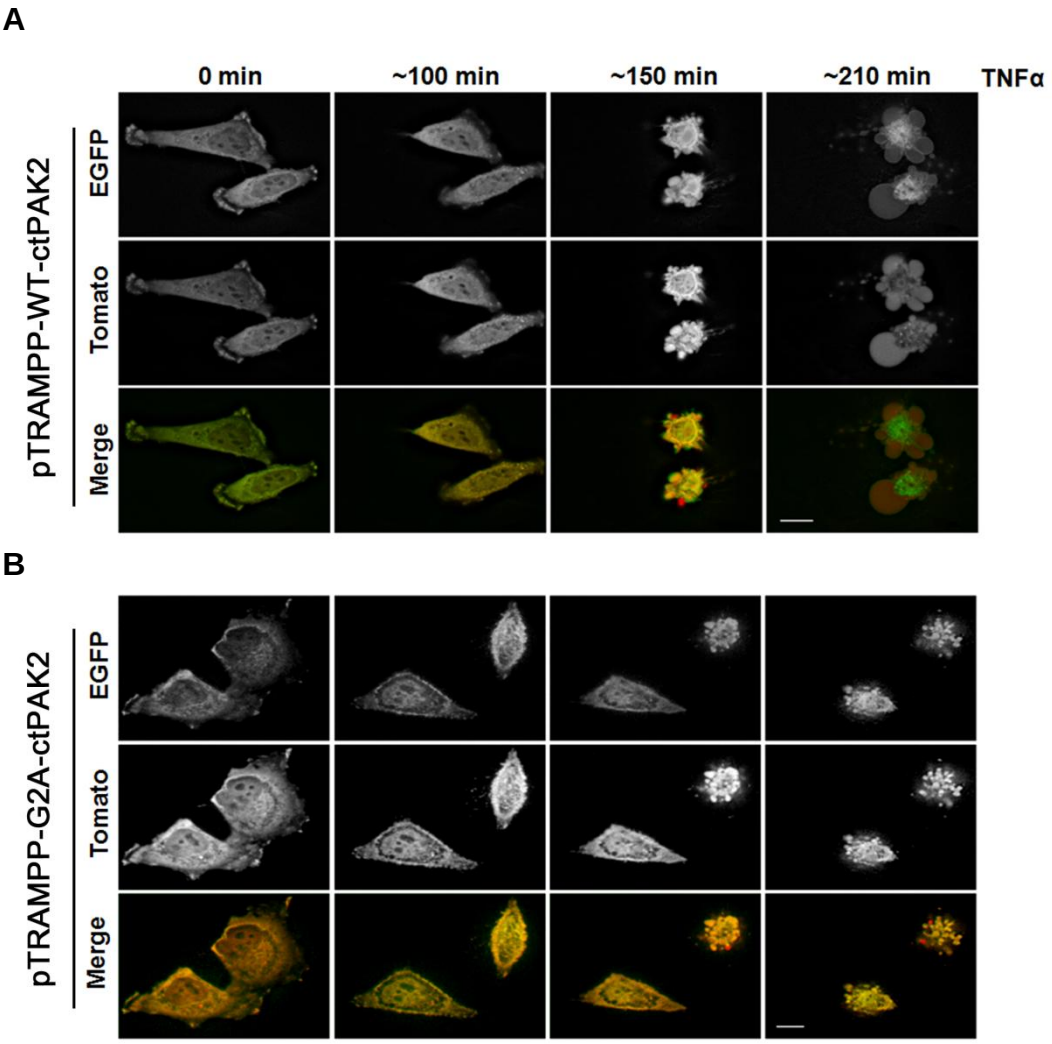

Figure 4.3. – **Imaging post-translational myristoylation of pTRAMPP-ctPAK2 in live HeLa cells.** HeLa cells transiently expressing **A** pTRAMPP-WT-PAK2 or **B** pTRAMPP-G2A-PAK2 were induced to undergo cell death with TNFα and CHX. Z-stack images were collected via wide field microscopy every 3 mins for approximately 4 h. Subsequently, the images were deconvolved using with Mediacybernitcs' Autoquant Software (Autoquant X, version X2.1.1). A clear separation of the red and green fluorophores can be seen in apoptotic bodies in **A** pTRAMPP-WT-ctPAK2 expressing cells, whereas no separation was detected when myristoylation of the EGFP fragment was abrogated in the pTRAMPP – G2A-ctPAK2 expressing cells **B**.

chromophore stage where it will fluoresce green (Shaner et al., 2005). In our experiments, translation of new protein is inhibited by the addition of CHX. As such, the clear separation seen at the later stages does not seem to be affected by this transition from green to red fluorescence.

4.2.3. Identification of post-translationally myristoylated proteins using pTRAMPP.

Next, we sought to identify potential substrates for post-translational myristoylation. In our previous report (Martin et al., 2008), post-translationally myristoylated substrates were identified by looking for myristoylation consensus sequences adjacent to known caspase-cleavage sites described in a review containing all the known caspase substrates at the time (Fischer et al., 2003). Since then, several reports have dramatically increased the number of known caspase substrates and their cleavage sites have been deposited in an easy to use database; CASBAH (Dix et al., 2008; Luthi and Martin, 2007; Mahrus et al., 2008). Consequently, by repeating the same search with the expanded database, we have identified 16 new potential post-translationally myristoylatable proteins in which the caspase cleavage exposes an N-terminal myristoylation concensus sequence that is predicted to be myristoylated *in silico* (Table 4.1.) (Bologna et al., 2004; Eisenhaber et al., 2004; Martin et al., 2010). As such, we chose to investigate the post-translational

Table 4.1. – Updated list of proven, putative and predicted post-translationally myristoylated proteins. Group I – Proven post-translationally myristoylated proteins (Sakurai and Utsumi, 2006; Utsumi et al., 2003; Vilas et al., 2006; Zha et al., 2000). Group II – Putative post-translationally myristoylated proteins identified in Martin *et al.* (Martin et al., 2008). Group III – Caspase cleaved proteins from CASBAH (Luthi and Martin, 2007) and Dix *et al.* (Dix et al., 2008) predicted to post-translationally myristoylated by NMT predictor [E denotes = (Eisenhaber et al., 2004)] and Myristoylator [B denotes = (Bologna et al., 2004)].

Substrate	Physiological Role	Cleavage Effect	Cleavage Sequence (Caspase/Myristoylation)	Prediction of Myristoylation
Group I - Proven				
β-actin	Cytoskeleton	Inactivated	ELPD(244)/GQVITIGNER	Twilight Zone (E)
Bid	Apoptosis activator	Activated	LQTD(59)/GNRSSHSRLG	Medium Confidence (B) Reliable (E)
Gelsolin	Severs & nucleates actin	Inactivated	DQTD(403)/GLGLSYLSSH	Medium Confidence (B) Reliable (E)
p21-activated kinase 2 (PAK2)	Cytoskeletal dynamics, activated by Rac & Cdc42	Activated	SHVD(212)/GAAKSLDKQK	High Confidence (B) Twilight Zone (E)
Group II - Putative				
B-cell receptor-associated protein 31 (p28 Bap31)	Bcl-2 adaptor at the ER, originally identified as B-cell receptor-associated protein	Inactivated	AAVD(163)/GGKLDVGNAE	Low Confidence (B)
Cytoplasmic dynein intermediate chain (CD-IC2A)	Mediates dynein/dynactin interaction	Inactivated	DSGD(99)/GAVGSRTLHW	Medium Confidence (B) Reliable (E)
Glutamate-L-cysteine ligase (GCL)	Rate-limiting enzyme in glutathione synthesis	Inactivated	AAVD(499)*/GCGKAQNSTE	Reliable (E)
Mammalian STE20-like protein kinase (MST3)	Stress signalling	Activated	AETD(325)*/GQASGGSDSG	Twilight Zone (E)
Protein Kinase C epsilon (PKCe)	Cell signalling (various)	Activated	SSPD(383)/GQLMSPGENG	High Confidence (B)
Group III - Predicted				
Band 3 anion transport protein, Chromobox protein homolog 1, Heterochromatin protein 1 homolog beta (B3AT)	Required for the formation of heterochromatin	Decreased binding to protein 4.2	EQGD(205)/GGTEGHSPSG	Twilight Zone (E)
Cell division cycle 6 homolog (CDC6)	Required for prereplicative complex formation	Inactivated	SEVD(442)*/GNRMTLSQEG	High Confidence (B)
Zinc finger protein multitype 1 (GATA-1)	Erythropoeitic transcription factor	Inactivated	EDLD(125)/GKGSTSFLET	Twilight Zone (E)
Huntingtin (Htt)	Polyglutamine tract protein defective in Huntington's disease	Aggregates	DLND(552)/GTQASSPISD	High Confidence (B) Reliable (E)
Lens epithelium derived growth factor (LEDGF)	Transcriptional coactivator	Inactivated	DAQD(486)/GNQPQHNGES	High Confidence (B)
Microtuble-actin crosslinking factor 1 (MACF1)	Cytoskeletal linker protein that associates with both actin and microtubules	Unknown	DAPD(3022)*/GSDASQLLHQ	High Confidence (12) Reliable (E)
Myc-associated factor X (Max)	Basic helix-loop-helix/leucine zipper protein that plays a role in the activity of c-Myc	Inactivated	SAFD(135)/GGSDSSSESE	High Confidence (B) Twilight Zone (13)
Induced myeloid leukemia cell differentiation protein (MCL-1)	Bcl-2-related protein, anti-apoptotic	Pro-apoptotic	TSTD(157)GSL PSTPPPA	High Confidence (B) Reliable (E)
RNA-binding protein FUS (RBPF)	Oncogene FUS, Oncogene TLS, Translocated in liposarcoma protein, DNA-pairing protein	Unknown	DWFD(355)/GKEFSGNPIK	High Confidence (B)
Isoform 1 of YTH domain family protein 2 (YTHDF2)	Unknown	Unknown	NGVD(367)/GNGVGQSQAG	Medium Confidence (B) Reliable (E)

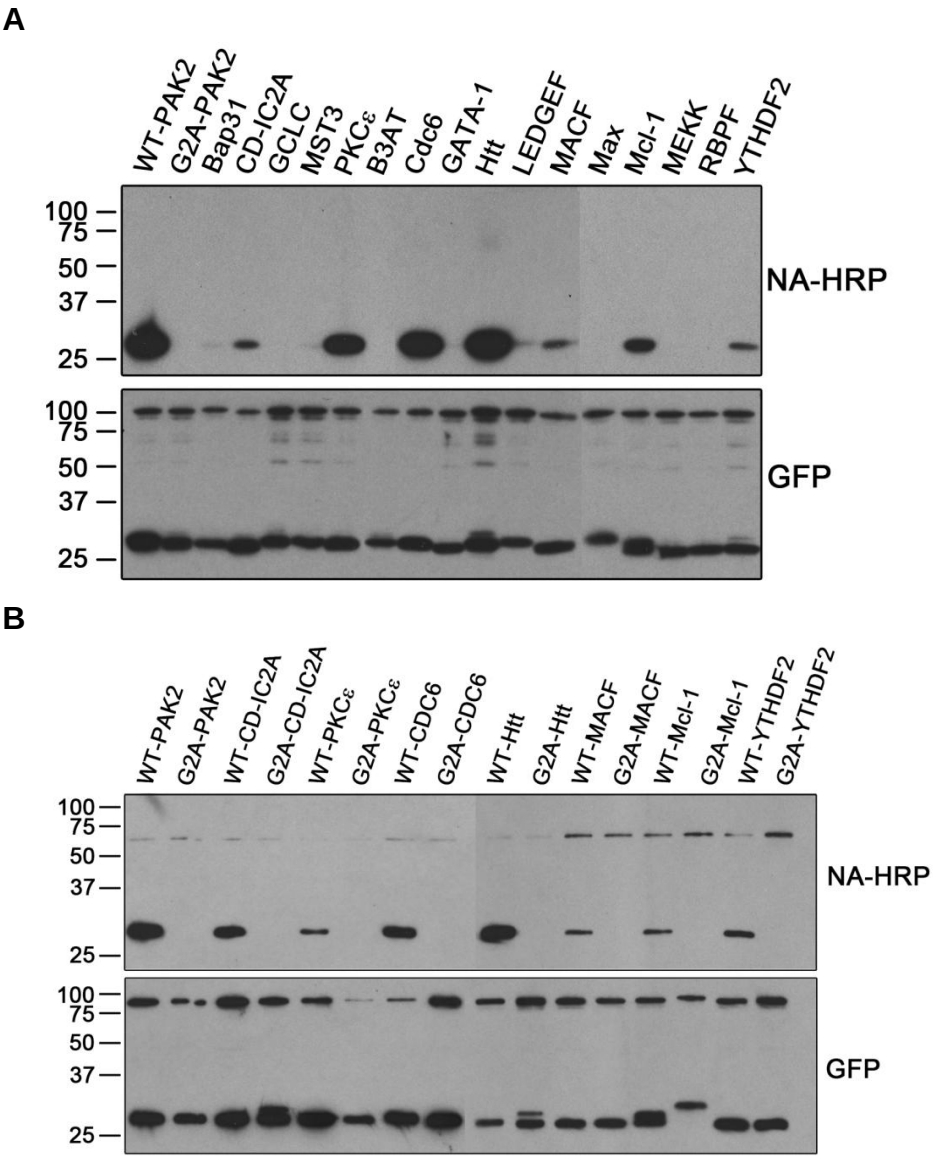

Figure 4.4. – Post-translational myristoylation of predicted post-translationally myristoylated proteins. **A** tdTom-DEVD-N_{10}-EGFP chimeras were transiently expressed in COS-7 cells and labeled with alkynyl-myristate. The immunoprecipitated EGFP chimeras were reacted with azido-biotin by click chemistry and detected by Western blotting with NeutrAvidin-HRP after the membranes were treated with 0.2 M Tris pH 7.0 or 0.2 M KOH. Chimeric ctPAK2-, ctCD-IC2A-, ctPKCε-, ct-Mcl-1, ct-YTHDF2, ct-MACF, ctHtt-, and ctCdc6-N_{10}-EGFPs all gave significant ECL signals on films, although of varying intensity. **B** Myristoylation of the putative post-translationally myristoylated proteins was confirmed by substituting the essential glycine to alanine. In each case, substitution of glycine to alanine completely abrogated myristoylation.

myristoylation of the candidates that appeared to have the greatest possibility to be post-translationally myristoylated based on our previous experience. In addition, we sought to confirm the post-translational myristoylation of the five proteins identified previously using a co-translational myristoylation assay [Figure 3.7.; (Martin et al., 2008)].

In Figure 4.4A, we show that alkyne-myristate was incorporated in a robust fashion in ctCD-IC2A and ctPKCε EGFP chimeras, thereby demonstrating that these are still strong candidates for post-translational myristoylation. However, little to no post-translational incorporation of alkyne-myristate was detected in ctBap31-, ctMST3- and ctGCLC-EGFP chimeras, which had all produced a weak myristoylation signal when studied previously (Martin et al., 2008). Therefore, these results demonstrate that ctCD-IC2A and ctPKCε are likely still strong candidates for post-translational myristoylated proteins while ctBap31, ctMST3 and ctGCLC are likely not significantly myristoylated. Likewise, ctGATA1, ctLEDGEF or ctMEKK1 are not myristoylatable substrates.

In addition, when we used pTRAMPPs encoding for various test sequences, we found that the ctCdc6 and ctHtt chimeras were strongly myristoylated post-translationally and to a lesser extent ctMcl-1, ctMACF and ctYTHFD2. Furthermore, when the essential glycine of these candidate substrates was substituted with an alanine there was no incorporation of the alkyne-myristate (Figure 4.4.B) demonstrating that incorporation of the analog is specific for N-terminal glycines and

represents N-terminal myristoylation of these chimeras. Of note, the relative incorporation of alkynyl-myristate into the caspase cleaved pTRAMPP constructs varied between experiments (e.g. compare the intensity of signal of WT-PKCε between Figure 4.4.A and 4.4.B). The aberrant migration of some of the non-myristoylatable EGFP constructs could not be explained, but the DNA sequences of these constructs were verified more than once.

4.2.4. Myristoylation of recombinant ctPKCε.

Due to the robust signals acquired from our previous study [Figure 3.7; (Martin et al., 2008)] and the results described above we sought to further investigate myristoylation of constitutively active ctPKCε. In order to confirm the myristoylation of ctPKCε-N_{11}-EGFP, the essential N-terminal glycine was replaced with an alanine (Figure 4.5A). Substitution of the glycine for an alanine in ctPKCε-N_{11}-EGFP completely abrogated myristoylation of the chimeric protein (Figure 4.5B) as well as membrane binding and nuclear exclusion when observed with confocal microscopy (Figure 4.5C). These results further reinforced the possibility that ctPKCε is a *bona fide* post-translationally myristoylated protein.

The role of myristoylation of the full length C-terminal PKCε (ctPKCε) was thus investigated next. To do so, we appended an HA-tag to the C-terminus and an initiator methionine at the N-terminus (WT-ctPKCε-

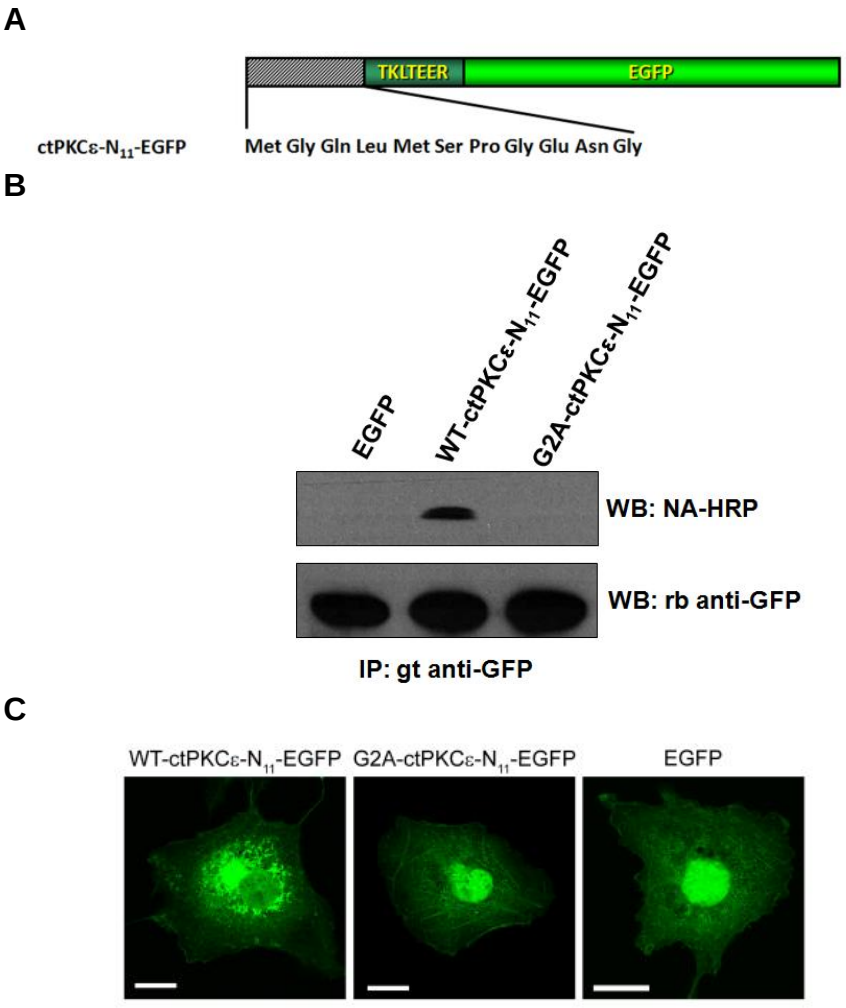

Figure 4.5. – Azido-myristoylation and localization of ctPKCε-N_{11}-EGFP. A Representation of the ctPKCε-N_{11}-EGFP chimera bearing the first 10 amino acids of ctPKCε with an initiator methionine and a TKLTEER hydrophilic linker. **B** ctPKCε-N_{11}-EGFP chimeras were transiently expressed in COS-7 cells and labeled with azido-myristate as described before. The immunoprecipitated EGFP chimeras were reacted with phosphine-biotin and detected by western blotting with NeutrAvidin-HRP (NA-HRP). **C** COS-7 cells transiently expressing the ctPKCε-N_{11}-EGFP were fixed and visualized by fluorescence confocal microscopy.

HA, Figure 4.6A). A non-myristoylatable form of the epitope-tagged protein was generated in which the essential glycine at position 2 was substituted with an alanine (G2A-ctPKCε-HA). As with the short EGFP chimeras, we observed the incorporation of alkyne-myristate into WT-ctPKCε-HA, but not into the G2A-ctPKCε-HA (Figure 4.6B). Several attempts to immunoprecipitate endogenous ctPKCε were unsuccessful and, therefore, myristoylation of the endogenous protein has not been verified. However, considering that ctPAK2 and ct-gelsolin were originally assessed similarly, we believe that the endogenous ctPKCε is very likely to be myristoylated.

4.2.5. Localization of ctPKCε-HA.

Using confocal microscopy, WT-ctPKCε-HA had a similar distribution profile as WT-ctPKCε-N_{11}-EGFP (Compare Figures 4.5.C and 4.6.C). It displayed strong perinuclear localization, a reticulated pattern as well as a strong signal at the plasma membrane including membrane ruffles (Figure 4.7.A). Interestingly, WT-ctPKCε-HA was also found in the nucleus. Localization of activated full length PKCε within the nucleus, at the Golgi, ER and plasma membrane has been documented (Akita, 2002; Garczarczyk et al., 2009; Sallese et al., 2006; Xu et al., 2009). Co-localization of WT-ctPKCε-HA was observed along plasma membrane ruffles (inset) with the actin-binding protein phalloidin (Figure 4.7.A). In addition, co-localization was demonstrated with tubulin, but only with the

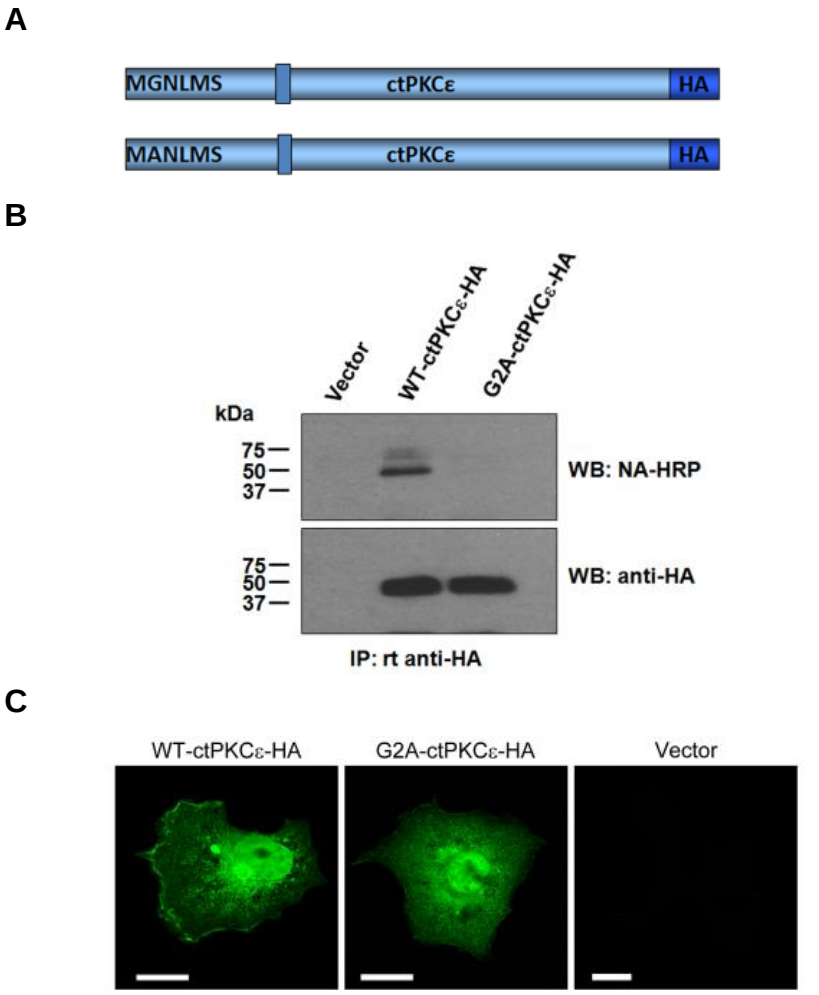

Figure 4.6. - **Azido-myristoylation and localization of ctPKCε-HA. A** Schematic representation of the myristoylatable (G) and the non-myristoylatable (A) forms of the C-terminal constitutively active kinase domain of PKCε (ctPKCε) with a C-terminal HA tag. **B** COS-7 cells transiently transfected with the indicated plasmids were labeled with azido-myristate. Anti-HA immunocomplexes from solubilized transfected cells were reacted with biotin-phosphine and incorporation of the label was detected using NA-HRP. **C** The localization of ctPKCε-HA constructs was visualized in fixed COS-7 cells by immunofluorescence. Scale bars equal to 10 μm.

microtubule organization centre (MTOC), which correlates with Golgi localization (Kronebusch and Singer, 1987). To further investigate the Golgi localization, we used the lectin concanavalin A (ConA), which binds the internal and non-reducing terminal alpha-mannosyl groups found in the Golgi and ER (Guasch et al., 1993; Shnyder and Hubbard, 2002) and found the greatest degree of co-localization. This clearly suggests that myr-ctPKCε-HA localizes to Golgi and ER. Typically, the non-myristoylatable form, G2A-ctPKCε-HA, was dispersed within the cytosol with a strong nuclear staining, although in some cases G2A-ctPKCε-HA was found to be completely excluded from the nucleus while remaining primarily cytosolic (Figure 4.7A). In some cases, the distribution of G2A-ctPKCε-HA was similar to the wild type protein.

Upon hypotonic lysis and subcellular fractionation, WT-ctPKCε-HA and G2A-ctPKCε-HA were both found predominantly in the membrane fraction with a small proportion in the cytosolic fraction (Figure 4.7B). However, there did appear to be a smaller amount of WT-ctPKCε-HA that consistently appeared to be slightly more enriched in the membrane fraction than its non-myristoylated ctPKCε-HA counterpart. Myristoylated and palmitoylated WT-Yes-N_{11}-GFP was found predominantly in the pellet while myristoylated-C3S-Yes-GFP was partially found in the supernatant and non-acylated G2A-Yes-GFP was strictly found in the supernatant as previously published (McCabe and Berthiaume, 1999). These constructs

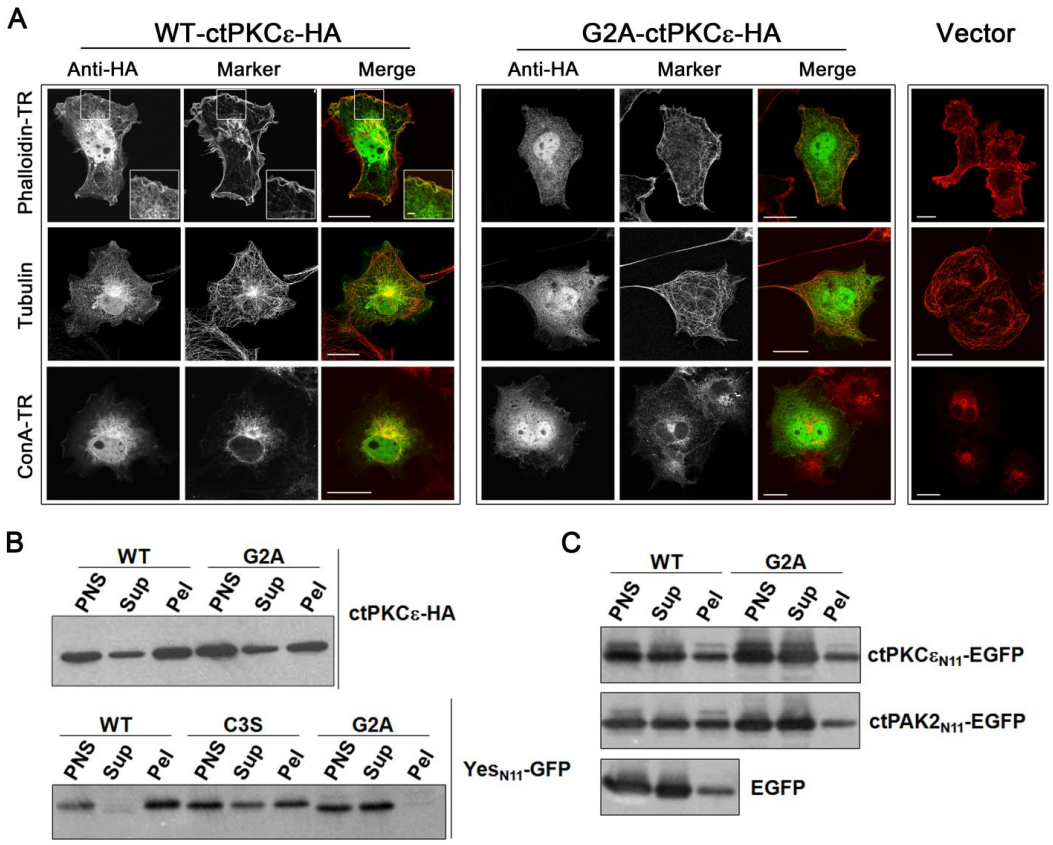

Figure 4.7. – Localization and distribution of myristoylated and non-myristoylated ctPKCε-HA in COS-7 cells. A Co-localization of ctPKCε-HA and various membrane markers was visualized in COS-7 cells by immunofluorescence. Transfected cells were fixed, immunostained with anti-HA antibodies and photographed by fluorescence confocal microscopy. Anti-mannosidase II antibodies were used as a Golgi marker. Phalloidin-FITC was used to stain actin filaments and the lectin concanavalin A (ConA) conjugated to Texas Red was used to detect Golgi and ER membranes. Scale bars equal to 10 μm. **B** COS-7 cells were transiently transfected with ctPKCε-HA and mono- (C3S), dually- (WT) or non-acylated (G2A) forms of Yes-N_{11}-GFP. The cells were subjected to hypotonic lysis and the cytosolic (Sup) and membrane (Pel) fractions were separated by ultracentrifugation of the post-nuclear supernatant (PNS). **C** COS-7 cells were prepared as in **B** using plasmids expressing ctPKCε-N_{11}-EGFP and ctPAK2-N_{11}-EGFP.

validated our fractionation protocol (Figure 5B, lower panel). Overall the distribution of WT-ctPKCε-HA resembled that of a myristoylated GFP chimera lacking its second anchoring signal, Yes(C3S)-N_{11}-GFP (Figure 5B, lower panel). To test whether the sequence responsible for myristoylation was sufficient for membrane targeting and binding, cells expressing ctPKCε-N_{11}-EGFP were also subjected to hypotonic lysis and fractionation. As shown in Figure 4.7.C, the distribution of ctPKCε-N_{11}-EGFP is very different from ctPKCε-HA (Figure 4.7.B, upper panel). Both the wild type and the non-myristoylated forms were predominantly found in the cytosolic fractions, similar to EGFP alone (Figure 4.7.C, lower panel). A similar construct bearing the first 10 amino acids of ctPAK2 appended to EGFP (WTctPAK2-N_{11}-EGFP) was nearly equally distributed between the soluble and membrane fractions whereas its non-myristoylatable form G2ActPAK2-N_{11}-EGFP was predominantly cytosolic and distributed similar to the two ctPKCε-N_{11}-EGFP proteins or EGFP alone (Figure 4.7.C). These results are consistent with the presence of strong membrane binding signal in the C-terminal portion of ctPKCε.

4.2.6. Cell signaling effect of exogenously expressed ctPKCε-HA.

PKCε can regulate many pathways depending on its mode of activation and cell type, but its most documented role is described in the activation of the MAPK Erk1/2 pathway through phosphorylation and

activation of Raf-1 (Akita, 2002). When COS-7 cells were transiently transfected with myristoylatable and non-myristoylatable forms of ctPKCε-HA there was an obvious increase in Erk1/2 phosphorylation and, consequently, activation when compared to untransfected cells or cells transfected with vector alone (Figure 4.8A). Expression of the myristoylatable form of ctPKCε-HA lead to a more perceptible increase in phosphorylation than its non-myristoylatable form (Figure 4.8.A), particularly at 24 h post-transfection. The Erk1/2 signaling pathway is associated with cell survival and the strong activation of the Erk1/2 pathway, therefore, suggests that myr-ctPKCε-HA may promote cell survival.

Based on the possibility that myr-ctPKCε-HA may promote cell survival through Erk activation, we further characterized possible downstream targets of the BH3-only members of the Bcl-2-related protein family. Erk1/2 activation can lead to phosphorylation of Bim at Ser69, targeting it for ubiquitination and its subsequent degradation by the proteasome (Luciano et al., 2003).

Interestingly, in cells transiently expressing ctPKCε-HA, Bim migrated at a higher molecular weight than when vector alone was used for transfection (Figure 4.8.A) suggesting it is phosphorylated in the presence of ctPKCε-HA. This was confirmed using antibodies specific for phosphorylated Ser69. Cells expressing both forms of ctPKCε-HA contained phosphorylated Bim at Ser69, whereas no phosphorylated

A

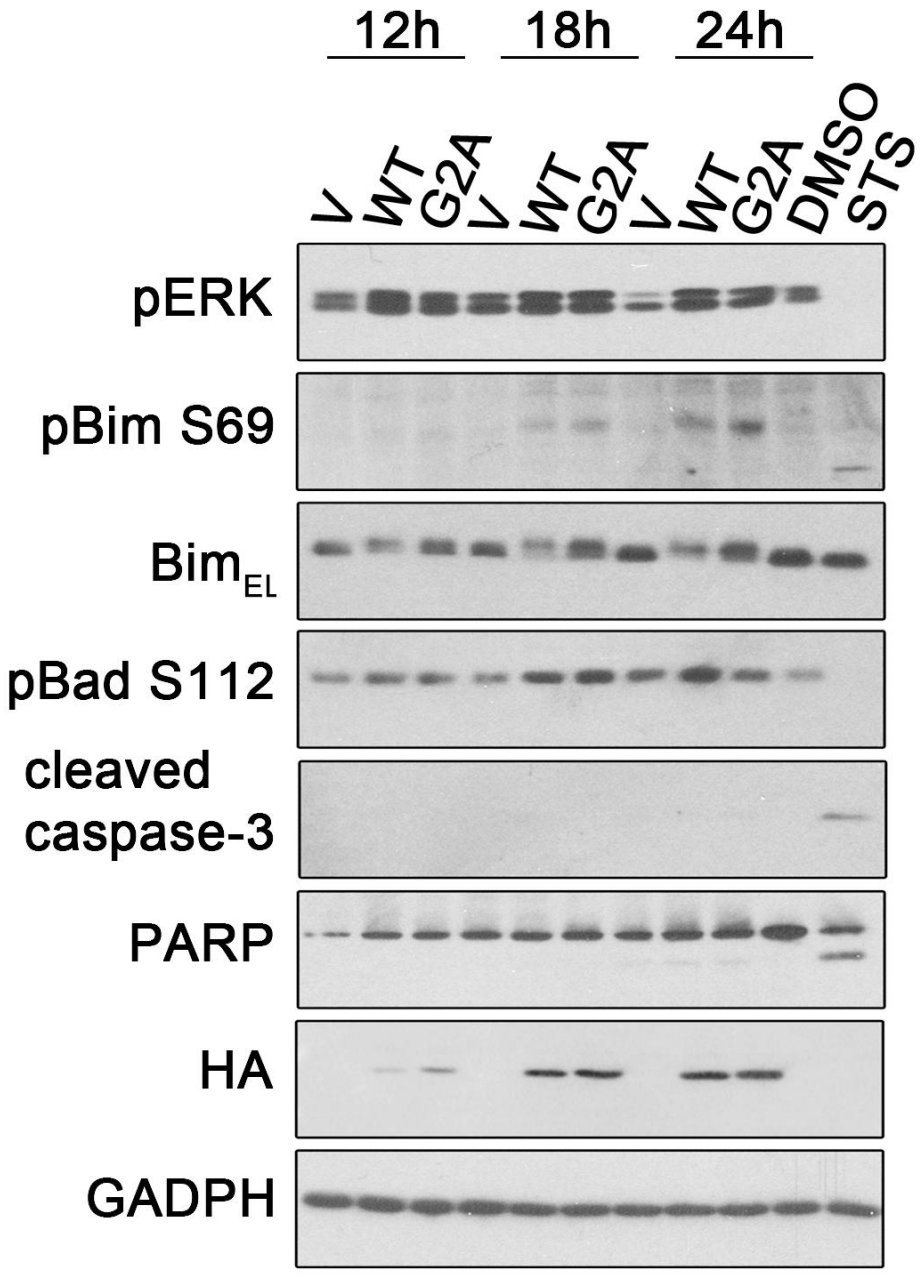
12h
18h
24h
V
WT
G2A
V
WT
G2A
V
WT
G2A
DMSO
STS
pERK
pBim S69
Bim$_{EL}$
pBad S112
cleaved caspase-3
PARP
HA
GADPH

B

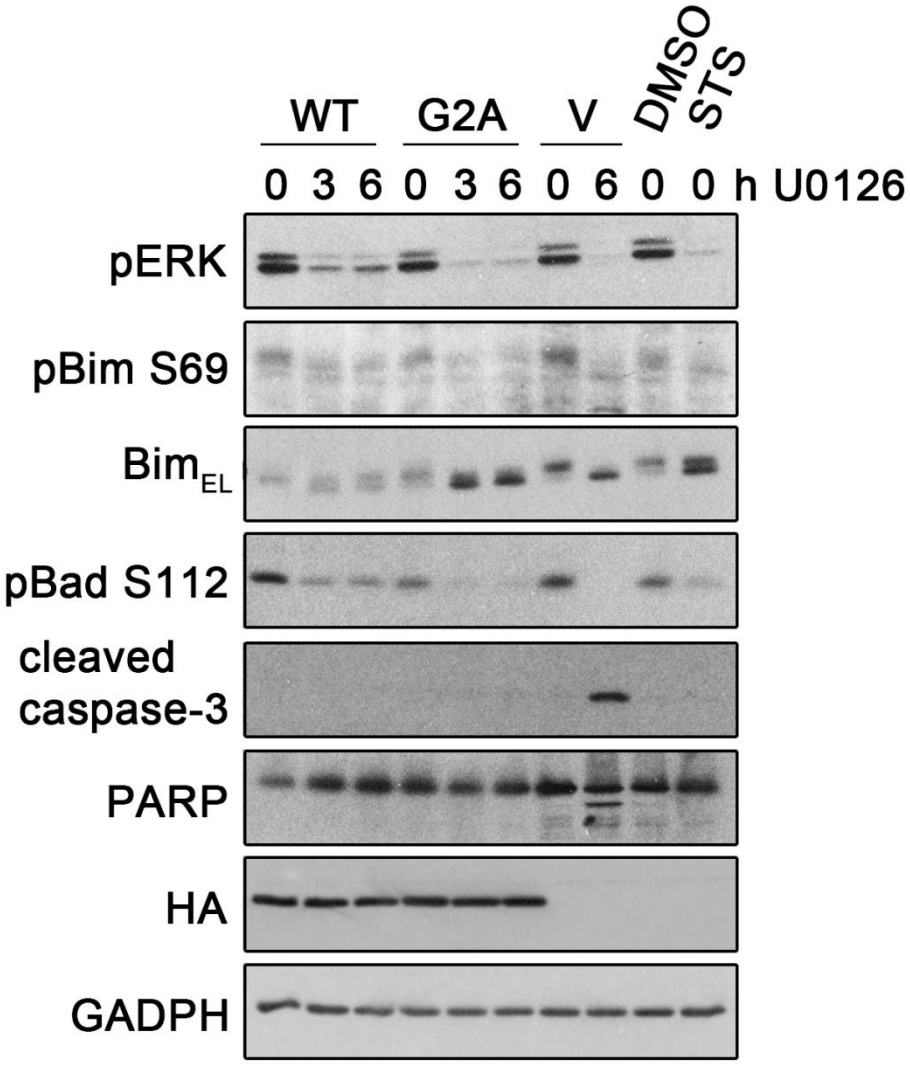
WT
G2A
V
DMSO
STS
0 3 6 0 3 6 0 6 0 0 h U0126
pERK
pBim S69
Bim$_{EL}$
pBad S112
cleaved caspase-3
PARP
HA
GADPH

C

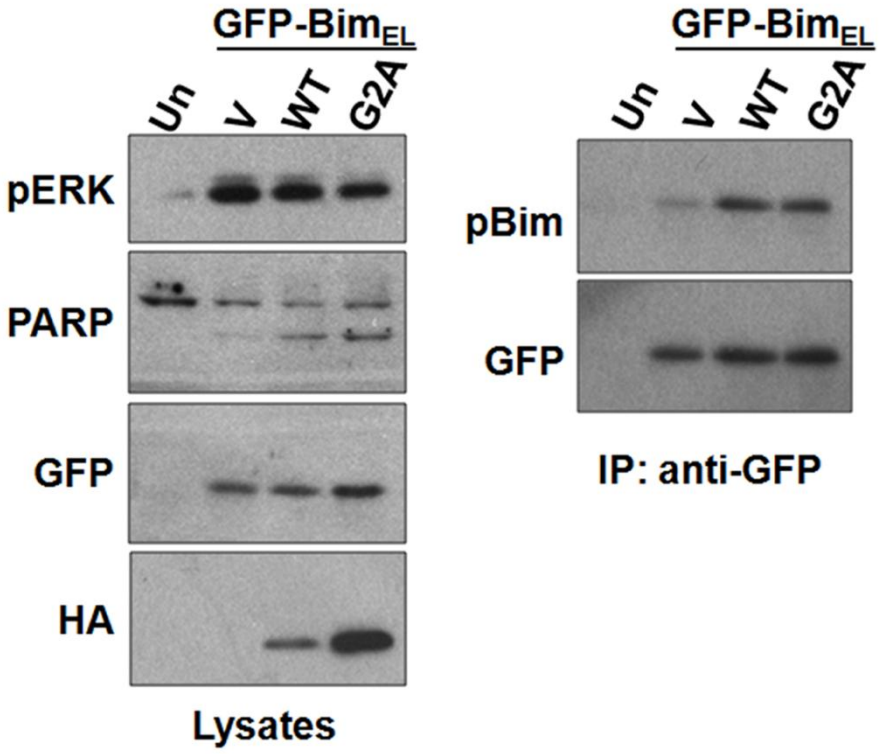

Figure 4.8. – Effect of transient transfection of myristoylatable and non-myristoylatable forms of ctPKCε-HA on COS-7 cells. A COS-7 cells were transiently transfected with myristoylatable and non-myristoylatable forms ctPKCε-HA, or vector alone for 12 h, 18h or 24 h. Mock transfected cells were treated 1 µM STS and 5 µg/mL CHX, or DMSO alone 4 h. Cells were lysed in 0.1% SDS-RIPA with protease and phosphatase inhibitors, separated by SDS-PAGE and analyzed by western blot using phospho-specific antibodies. Antibodies specific for active cleaved caspase-3 were used to detect activation of the apoptotic pathway and anti-HA antibodies indicate the levels of ctPKCε-HA. GAPDH antibodies were used as a loading control. **B** Cells were prepared as described above and incubated with 10 µM of the MEK inhibitor U0126 for 0 h, 3 h or 6 h at 18 h post-transfection. **C** Phosphorylation of Ser69 in Bim$_{EL}$ is associated with protecting mitochondrial integrity in cells expressing myr-ctPKCε-HA. COS-7 cells were co-transfected with ctPKCε-HA or vector alone and N-terminally GFP-tagged Bim (GFP-Bim$_{EL}$) at a 10:1 ratio, respectively. GFP-Bim was immunoprecipitated and probed for phosphorylation at Ser69.

Ser69 was detected in cells transfected with vector only (Figure 4.8A). In addition, Bim levels were noticeably lowered in the presence of myr-ctPKCε-HA compared to non-myristoylated ctPKCε-HA or vector alone. These results are highly reminiscent of previous study showing a mobility shift in Bim and a decrease in Bim levels when Erk1/2 was activated (Luciano et al., 2003). Together, these results suggest that both forms of ctPKCε-HA promote the phosphorylation of Bim, but myristoylation of ctPKCε-HA promotes the degradation of Bim. (Figure 4.8.A, Bim panel). Furthermore, when the specific MEK inhibitor U0126 was present, Bim migrated at a lower molecular weight suggesting it was not phosphorylated, which was confirmed by the decrease in Ser69 phosphorylation. In addition, the apparent levels of Bim increased in the presence of the MEK inhibitor suggests it was not targeted as efficiently for proteasomal degradation (Figure 4.8.B). Inhibition of MEK1/2 by U0126 suggests that phosphorylation of Bim is mediated through Erk. This observation further validated the implication of ctPKCε-HA–dependent activation of the MAPK pathway leading to a pro-survival response. Of note, the most noticeable increase in Bim levels was associated with the non-myristoylated ctPKCε-HA suggesting that both myristoylated and non-myristoylated ctPKCε-HA phosphorylate Bim, but myr-ctPKCε-HA stimulates degradation. Final confirmation of ctPKCε-HA mediated phosphorylation of Bim_{EL} was confirmed when GFP-Bim_{EL} was co-expressed with ctPKCε-HA. An increase in phosphorylation of

immunoprecipitated GFP-Bim_{EL} at Ser69 was detected when in the presence of ctPKCε-HA compared to vector alone or untransfected (Figure 4.8.C).

Erk can also directly activate p90RSK, which, in turn, can lead to the phosphorylation of Ser112 of the pro-apoptotic protein Bad. Phosphorylation at Ser112 promotes Bad's association with 14.3.3 proteins, which sequesters Bad away from the mitochondria, thereby preventing apoptosis (Tan et al., 1999). Similar to what we saw with Bim phosphorylation, an increase in phosphorylation of Ser112 of Bad was observed when myr-ctPKCε-HA was present compared to G2A-ctPKCε-HA or vector alone at 24 hours (Figure 4.8.A). Again, this phosphorylation was reduced in the presence of U0126 suggesting that this is an Erk-mediated response (Figure 4.8.B). These results imply that myr-ctPKCε-HA also regulates the phosphorylation status of Bad at Ser112 through the ERK MAPK pathway.

Both Bim and Bad are pro-apoptotic proteins that mediate their apoptotic effects through the mitochondrion by promoting the release of cytochrome c through interactions with anti-apoptotic proteins. Therefore, we measured the effect of ctPKCε-HA on mitochondrial potential by measuring TMRE levels in HeLa cells expressing ctPKCε-HA by fluorescence activated cell sorting (FACS) (Figure 4.9.). The mean total fluorescence of cells expressing EGFP and, therefore, ctPKCε-HA was normalized to cells transfected with empty vector and EGFP. Surprisingly,

A

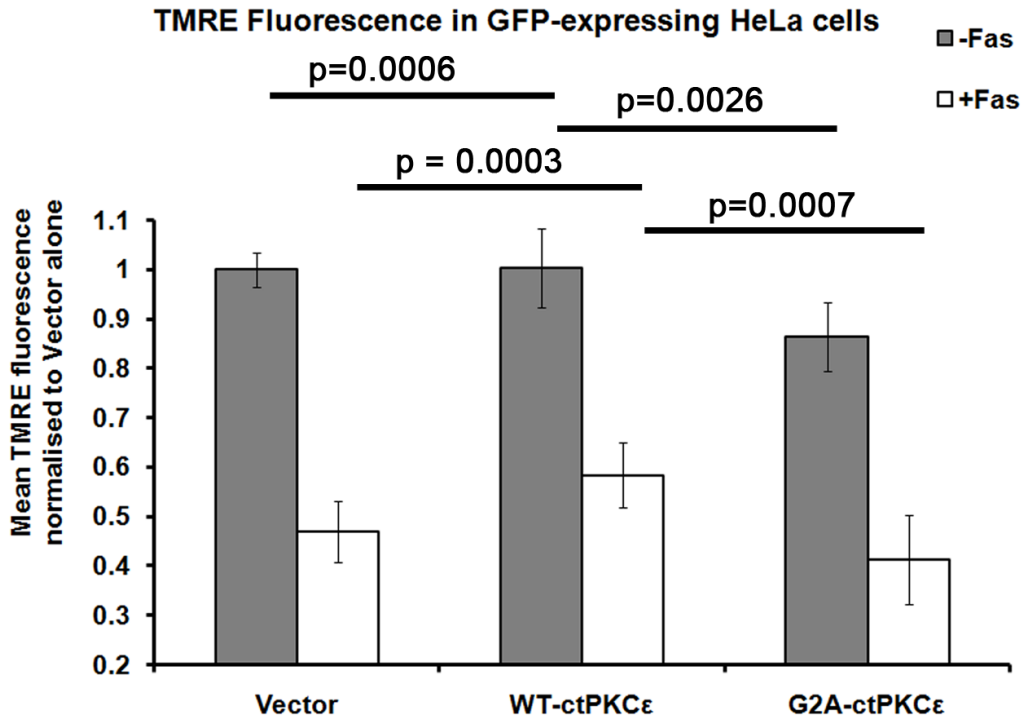
TMRE Fluorescence in GFP-expressing HeLa cells
-Fas
+Fas
p=0.0006
p=0.0026
p = 0.0003
p=0.0007
Mean TMRE fluorescence normalised to Vector alone
1.1
1
0.9
0.8
0.7
0.6
0.5
0.4
0.3
0.2
Vector
WT-ctPKCε
G2A-ctPKCε

B

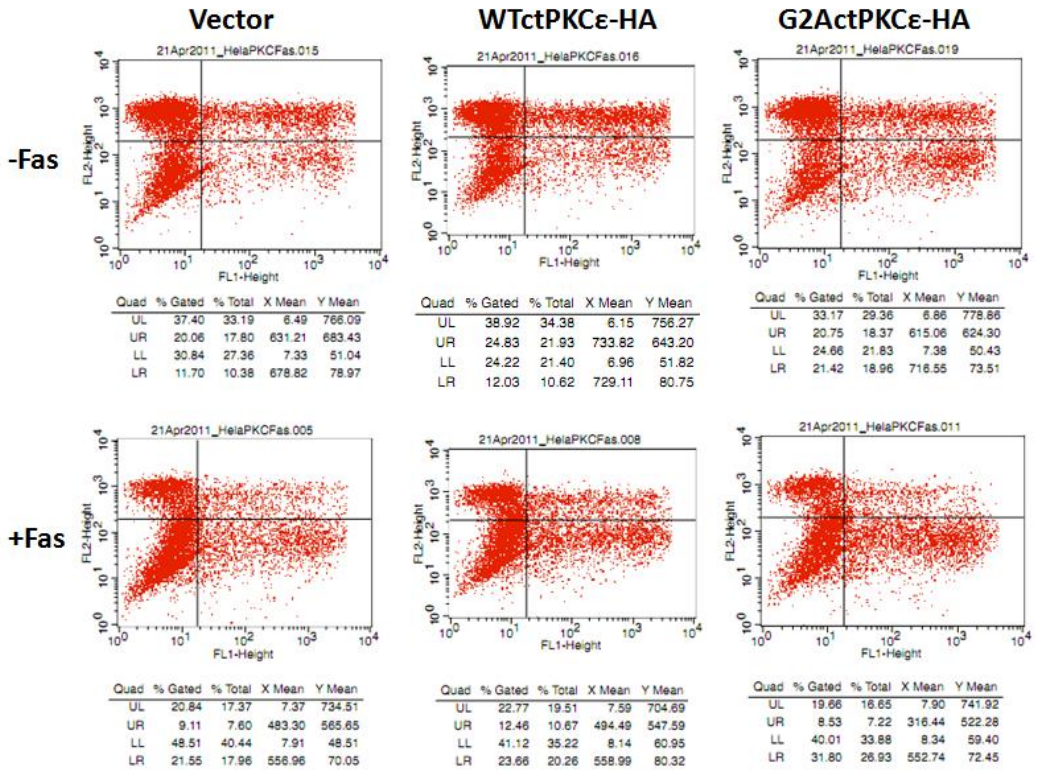
Vector
WTctPKCε-HA
G2ActPKCε-HA
-Fas
+Fas
21Apr2011_HelaPKCFas.015
21Apr2011_HelaPKCFas.016
21Apr2011_HelaPKCFas.019
21Apr2011_HelaPKCFas.005
21Apr2011_HelaPKCFas.008
21Apr2011_HelaPKCFas.011
FL1-Height
FL2-Height
Quad % Gated % Total X Mean Y Mean
UL 37.40 33.19 6.49 766.09
UR 20.06 17.80 631.21 683.43
LL 30.84 27.36 7.33 51.04
LR 11.70 10.38 678.82 78.97
Quad % Gated % Total X Mean Y Mean
UL 38.92 34.38 6.15 756.27
UR 24.83 21.93 733.82 643.20
LL 24.22 21.40 6.96 51.82
LR 12.03 10.62 729.11 80.75
Quad % Gated % Total X Mean Y Mean
UL 33.17 29.36 6.86 778.86
UR 20.75 18.37 615.06 624.30
LL 24.66 21.83 7.38 50.43
LR 21.42 18.96 716.55 73.51
Quad % Gated % Total X Mean Y Mean
UL 20.84 17.37 7.37 734.51
UR 9.11 7.60 483.30 565.65
LL 48.51 40.44 7.91 48.51
LR 21.55 17.96 556.96 70.05
Quad % Gated % Total X Mean Y Mean
UL 22.77 19.51 7.59 704.69
UR 12.46 10.67 494.49 547.59
LL 41.12 35.22 8.14 60.95
LR 23.66 20.26 558.99 80.32
Quad % Gated % Total X Mean Y Mean
UL 19.66 16.65 7.90 741.92
UR 8.53 7.22 316.44 522.28
LL 40.01 33.88 8.34 59.40
LR 31.80 26.93 552.74 72.45

Figure 4.9. - Myr-ctPKCε-HA prevents the loss of mitochondrial potential in cells induced to undergo cell death. A HeLa cells transiently co-expressing EGFP with empty vector (pcDNA3.1(+)), WT-ctPKCε-HA, or G2A-ctPKCε-HA were labeled with the mitchondrial potential marker TMRE. Loss of TMRE was measured by FACS analysis 24 h post transfection in the presence (white bars) or absence (grey bars) of anti-Fas antibody and CHX for 4 h. Data is represented as TMRE retention in EGFP expressing cells normalised to untreated vector and is representative of 8 experiments. Error bars represent standard deviation. **B** Example of representative data from FACS analysis. FL-1 and FL-2 represent GFP and TMRE fluorescence, respectively.

after 24 hours transient expression, HeLa cells expressing G2A-ctPKCε-HA retained significantly less TMRE than myr-ctPKCε-HA (p=0.0026) and vector (p=0.0006) alone. The decrease in TMRE and electrochemical potential suggests that G2A-ctPKCε-HA is mildly toxic to cells (Figure 4.9.D; grey bars). When cells were induced to undergo cell death mediated by 4 h anti-Fas treatment (Figure 4.9., white bars) cells expressing WTctPKCε-HA retained significantly more TMRE compared to G2ActPKCε-HA (17.2%, p=0.0007) or vector alone (11.5 %, p=0.0003). Once again, cells expressing G2ActPKCε-HA retained the least amount of TMRE. This suggests that myristoylation of WTctPKCε-HA mediates its protective effect by mediating the activation of the Erk1/2 pathway to promote the phosphorylation of both Bim and Bad, which leads to Bim degradation via the proteasome and Bad sequestration from the mitochondria by 14.3.3. proteins. Overall, myristoylated WTctPKCε-HA protects mitochondrial integrity and mediates a pro-survival effect.

4.3. Discussion

We previously developed alternative non-radioactive detection methods for the identification of both co- and post-translationally myristoylated proteins (Martin et al., 2008; Yap et al., 2009). The combination of *in silico* identification of potential substrates for post-translational myristoylation combined with our sensitive chemical biology labeling techniques allowed for the identification of new substrates for post-translational myristoylation during apoptosis (Martin et al., 2008). However, due to the suspected potential artifacts of using a co-translational assay to measure a post-translational modification, we sought to develop a sensitive post-translational detection method for post-translationally myristoylated proteins. Herein, we described the successful use of a caspase-cleavable tandem fluorescent reporter assay for the detection and of post-translational myristoylation (pTRAMPP), the identification of several new potential post-translationally myristoylated substrates and the characterization of the role of myristoylation in one of them, caspase-cleaved ctPKCε, as a case study.

Initially, an oligonucleotide duplex encoding for the first ten amino acids downstream of the endogenous caspase cleavage site of PAK2 was inserted downstream of the canonical caspase-3 cleavage site located between the fluorescent proteins tdTomato and EGFP in the pTRAMPP vector (Figure 4.1.A). The resulting pTRAMPP-ctPAK2 chimera was

shown to undergo caspase-dependent cleavage when expressed in COS-7 cells induced to undergo apoptosis. This cleavage exposed an N-terminal Gly on the C-terminal PAK2-N_{11}-EGFP fragment and incorporation of alkynyl-myristate analog on that N-terminal glycine residue in a post-translational fashion (Figure 4.2). The myristoylated ctPAK2-N10-EGFP portion appeared to be directed to membranes during apoptosis and segregated into peripheral membranes of apoptotic bodies away from the tdTomato component of the TRAMPP vector, which remained primarily in the cytosol (Figure 4.3.A). In the non-myristoylated G2A-PAK2-N10-EGFP mutant both the red and green remained co-localized throughout the apoptotic process (Figure 4.3.B). These results suggest that the pTRAMPP vector could readily identify post-translationally myristoylatable caspase-cleaved protein substrates as well as allow the visualization of their post-translational myristoylation in live cells.

Subsequently, we used pTRAMPP to test the myristoylation status of multiple candidates for post-translational myristoylation identified by rationale prediction analysis (Table 4.1.). The pTRAMPP assay reconfirmed the post-translational myristoylation of both CD-IC2 and PKCε, while eliminating Bap31, GCLC and Mst3 [Chapter 3; (Martin et al., 2008)], but adding the apoptotic regulator Mcl-1, CDC6, MACF and the unknown protein YTHDF2 (Figure 4.4.A) to the list of putative post-translationally myristoylated substrates. The addition of the alkyne

myristate to the N-terminal glycine of these proteins was verified by substituting the glycines to alanines in the newly identified proteins. This completely abrogated the incorporation of alkyne myristate into the G2A mutant proteins (Figure 4.4.B).

Due to our previous experience with studying the post-translational myristoylation of the kinase ctPAK2 (Vilas et al., 2006) as well as the robust incorporation and detection of the myristate analogs into ctPKCε-N_{11}-EGFP (Figure 3.7.) and pTRAMPP-ctPKCε (Figure 4.4.), we decided to assess the effect of myristoylation of ctPKCε. The possible effects mediated by post-translational myristoylation on these proteins will be discussed in further detail in Chapter 6.

Like ctPAK2, caspase cleavage of PKCε leads to the cleavage between the N-terminal regulatory domain and release of the constitutively active C-terminal kinase domain (Basu et al., 2002). Exogenous expression of ctPKCε-HA efficiently incorporated the Az-C12, while the mutant form lacking the essential Gly was substituted was not myristoylated. Myristoylation of ctPKCε-HA leads to an association with various compartments within the cell including Golgi, ER, and membrane ruffles whereas non-myristoylated G2ActPKCε-HA remained predominantly diffuse within the cell. The similar distribution of the differentially myristoylated proteins may have been due to a secondary membrane localization signal downstream of the myristoylation site. As mentioned previously, this is a typical characteristic of co-translationally

myristoylated proteins, which require a polybasic domain or a site of palmitoylation to interact with membranes. Of note, ctPKCε has several "patches" of polybasic amino acids, which might represent possible "second" signals involved in membrane binding. It is noteworthy to mention that a recent study demonstrated that PKCε is palmitoylated at two sites; one within the regulatory N-terminal domain and one in C-terminal kinase domain (Dasgupta et al., 2011). Of note, inhibition of palmitoylation at either site by site directed mutagenesis abrogated palmitoylation at both sites. Inhibition of palmitoylation inhibited autophosphorylation of PKCε at Ser729, which suggests that palmitoylation is required for activation of the full-length protein. Regardless, palmitoylation of ctPKCε may explain the relatively large amount of non-myristoylated G2ActPKCε-HA we observed in the membrane fraction following subcellular fractionation.

Myristoylation of ctPKCε-HA leads to an apparent increase in the level of phosphorylation and, therefore, activation of the MAPK signaling pathway Erk1/2. As such, this activation caused a concomitant decrease in the levels of the pro-apoptotic protein Bim as well as an increase in mobility that was associated with phosphorylation on Ser69, which would direct the protein to the proteasome for degradation (O'Reilly et al., 2009). Presumably, the decrease in Bim levels was directly related to its phosphorylation by Erk1/2 (Figure 4.10.). This hypothesis is supported by the inhibition of the upstream activator of Erk1/2, MEK1/2, with U0126,

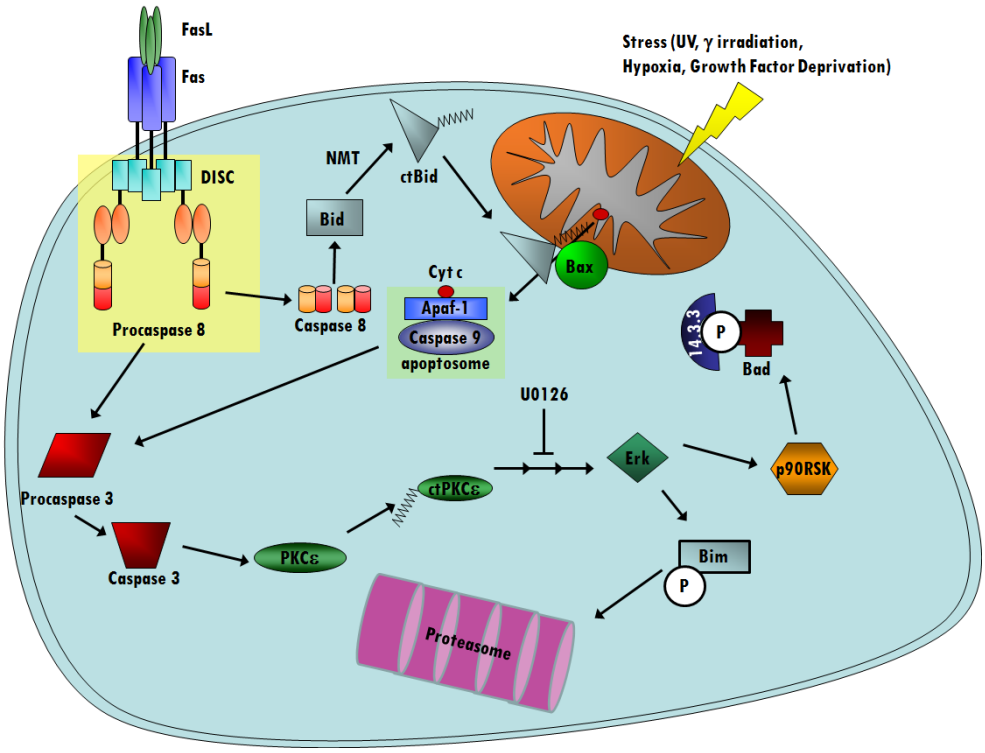

Figure 4.10. - Outline of post-translational myristoylation of ctPKCε and its effect on cell signaling. PKCε is known is to phosphorylate Raf-1 to activate the Erk1/2 pathway. In turn, Erk1/2 phosphorylates Bim at Ser69, which targets the proapoptotic protein for degradation by the proteasome. Alternatively, Erk1/2 may lead to phosphorylation of the proapoptotic protein Bad at Ser112; possibly through p90RSK. Phosphorylation of the two proapoptotic proteins is Erk1/2 dependent as demonstrated by inhibition of phosphorylation by the MEK1/2 inhibitor U0126.

which caused a lower shift in mobility and an increase in total Bim levels suggesting it was phosphorylated and degraded. Phosphorylation of Bim by ctPKCε-HA was confirmed by the co-transfection of ctPKCε-HA and EGFP-Bim_{EL} and the detection phosphorylation of Ser69 of EGFP-Bim_{EL}. Of particular note, in the presence of the MEK inhibitor U0126, the levels of Bim in cells expressing G2A-ctPKCε-HA were much greater than in WT-ctPKCε-HA expressing cells (Figure 4.8.B). This may suggest that ctPKCε-HA may phosphorylate Bim through different pathways based on its myristoylation status. For instance, JNK can also lead to Bim phosphorylation, which is associated with increased cell death (Lei and Davis, 2003; Ley et al., 2005; Putcha et al., 2003). This may also explain why Basu *et al* (Basu et al., 2002) found that an N-terminally tagged version of ctPKCε, which would block myristoylation and consequently mimic G2ActPKCε, appeared to potentiate the effect of TNFα-induced apoptosis in MCF-7 cells.

In a similar fashion to Bim phosphorylation, an increase in the level of Ser112 phosphorylation of the pro-apoptotic protein Bad was detected when myr-ctPKCε-HA was expressed compared to vector alone or G2A-ctPKCε-HA. Typically, this leads to the sequestration of phosphorylated Bad from the mitochondria by 14.3.3 proteins (Outlined in Figure 4.10.), which also leads to suppression of apoptosis. This conclusion is confirmed by the phosphorylation and inactivation of the pro-apoptotic Bim and Bad by myristoylated ctPKCε-HA, which resulted in an increased mitochondrial

TMRE retention in the presence or absence of an apoptotic stimulus (Figure 4.9.), thereby suggesting that the mitochondrial integrity is protected by WTctPKCε-HA.

Overall, the phosphorylation of the pro-apoptotic proteins Bim and Bad during the expression of ctPKCε-HA suggests that ctPKCε-HA has an anti-apoptotic effect, while myristoylation leads to a greater level of phosphorylation of these two proteins compared to its non-myristoylated counterpart. Myr-ctPKCε-HA mediates its protective effect by activating the ERK pathway to promote the phosphorylation of both Bim and Bad which leads to Bim degradation via the proteasome and Bad sequestration from the mitochondria by 14.3.3. proteins. Overall, our results support the possibility that myr-ctPKCε-HA protects mitochondrial integrity and, like myr-ctGelsolin, plays an anti-apoptotic role. This contrasts the established roles of myr-ctBid and myr-ct-PAK2 as pro-apoptotic proteins and identifies post-translational myristoylation of proteins as a potential key regulator of the balance between life and death during apoptosis.

CHAPTER 5

Post-translational myristoylation of caspase cleaved Huntingtin promotes the formation of autophagosome-like vesicles

5.1. Rationale.

In Chapter 4, we described a post-translational assay that identified the first 10 amino acids of a caspase cleaved fragment of Huntingtin (Htt) as a substrate for post-translational myristoylation. Htt is a large 3144 amino acid protein (approximately 350 kDa) that is ubiquitously expressed throughout the body. A mutant form of Htt bearing an extended stretch of glutamines (Q) at the N-terminus initiates the aggregation of the protein in cells and is thought to be the causative agent of Huntington's disease (HD) (reviewed in (Huntington's Disease Collaborative Research Group 1993; Pattison et al., 2006; Sarkar and Rubinsztein, 2008)). Normal Htt has 15 Q within its N-terminus while tandem repeats of greater than 35 Q causes the disease, although a repeat of 39 or higher essentially makes the disease inevitable. In fact, the longer the number of tandem repeats, the younger the onset of the disease (Huntington's Disease Collaborative Research Group 1993; Pattison et al., 2006; Sarkar and Rubinsztein, 2008).

HD is an autosomal dominant disease that affects the central nervous system. It is a progressive disease that leads to the dysfunction and cell death of neuronal cells, primarily within the striatum, which plays a key role in initiating and controlling movements of the body, limbs and eyes. As such, the disease is characterized by a loss of cognitive ability and motor skills, eventually leading to dementia and changes in personality. It is also associated with severe motor dysfunction that leads

to uncoordinated movement known as chorea. Ultimately, the disease leads to death typically within 10 to 20 years after the appearance of the first diagnosable symptoms with an average age of onset of about 35 to 40 years, but juvenile causes have been detected as early as 5 years of age in patients with greater than 135 Q (Ehrnhoefer et al., 2011; Pattison et al., 2006; Sarkar and Rubinsztein, 2008).

Normal Htt plays an important role in cell survival and may mediate its protective effect by preventing the cleavage of PAK2 to its constitutively active and pro-apoptotic form, which is also post-translationally myristoylated (described in Chapter 1) (Luo and Rubinsztein, 2009). In the same study, the authors found that Htt null cells were more sensitive to cell death induced by cell starvation suggesting that Htt may have a protective effect in cells. Moreover, Htt may protect cells by increasing levels of brain derived neurotrophic factor (BDNF), which is essential for the maintenance and differentiation of neurons in the brain (Ehrnhoefer et al., 2011; Gauthier et al., 2004; Zuccato et al., 2001).

Htt undergoes several proteolytic cleavages by caspases under non-apoptotic and apoptotic conditions (Fryer and Zoghbi, 2006; Graham et al., 2006; Kim et al., 2001; Wellington et al., 2002). There are two primary sites of caspase cleavage in Htt, Asp552 and Asp586. Position 552 is cleaved by both caspase-2 and -3 (referred to as the caspase-3 site from now on) while position 586 is cleaved by caspase-6 (Wellington et al., 2002; Wellington et al., 2000). There does not appear to be preferential

cleavage for wildtype or mutant Htt, but the cleavage of mutant Htt may increase caspase-6 activity, providing a feedback mechanism thereby potentiating the effects of mutant Htt (Graham et al., 2006). Inhibition of caspase-6 cleavage of mutant Htt in mice significantly reduces toxicity of mutant Htt demonstrating that cleavage of mutant Htt by caspase-6 is critical for its cytotoxicity. (Wellington et al., 2000).

Interestingly, both caspase cleavage sites result in N-terminal glycines on the C-terminal cleavage products. However, only the Gly553, corresponding to caspase-3, is predicted to be myristoylated (Martin et al., 2010). This results in the release of a 34 amino acid fragment of Htt ($ctHtt_{N34}$) corresponding to the region between the two caspase cleavage sites. Although blocking cleavage of Asp552 did not appear to improve the HD phenotype in mice, this proteolytic event can be detected *in vivo* and may play an important role downstream of the cleavage at Asp586 (Ehrnhoefer et al., 2011; Graham et al., 2006; Kim et al., 2001).

As shown in Chapter 3, using our tandem fluorescent protein reporter assay, we demonstrated that the first 10 amino acids following the Htt caspase-3 cleavage site is post-translationally myristoylated. Herein, we will characterize the role of myristoylation of Htt_{N34} and its potential role in inducing autophagy. Htt has been previously shown to induce the formation of autophagic vesicles and these Htt labeled vacuoles display the same ultrastructural features of early and late autophagosomes. Htt-enriched cytoplasmic vacuoles appear to be more abundant in cells

expressing mutant Htt (Kegel et al., 2000; Nagata et al., 2004; Sarkar and Rubinsztein, 2008). However, a recent study has shown that autophagic vesicles display an apparent deficiency in cargo recognition in HD (Martinez-Vicente et al., 2010). This latter study suggests that the inefficient engulfment of cytosolic proteins and several organelles such as mitochondria and lipid droplets by autophagosomes is responsible for the slower turnover, functional decay and accumulation of damaged proteins and organelles, which is believed to contribute to cellular dysfunction and HD.

5.2. Results.

5.2.1. Detection of post-translational myristoylation of Htt588-YFP.

Cleavage of Htt by caspase-3 and caspase-6 leads to the exposure of two N-terminal glycines that could be post-translationally myristoylated. However, when the amino acid sequences of the two C-terminal fragments with N-terminal glycines were subjected to myristoylation prediction analysis (Bologna et al., 2004; Eisenhaber et al., 2003) only the caspase-3 exposed glycine, corresponding to Gly553 was predicted to be myristoylated (Table 4.1.) (Martin et al., 2010). As described above, the first 10 amino acids corresponding to the N-terminal portion exposed after caspase-3 cleavage of Htt (Htt553-563) was inserted into the dual fluorescent reporter protein TRAMPP (Chapter 4). The TRAMPP reporter contains an N-terminal tdTomato red fluorescent protein and a C-terminal GFP moiety. Cells transiently expressing the reporter protein were induced to undergo apoptosis by the addition of STS and CHX in the presence of the myristate analog, alkyne myristate (Alk-C14). The lysates were subjected to immunoprecipitation using anti-GFP antibodies and the immunoprecipitates were reacted with azido-biotin using click chemistry (Yap et al., 2010). Incorporation of Alk-C14 was detected using NeutrAvidin-HRP by western blotting. As shown in Figure 4.4A, TRAMPP-ctHtt was sufficiently cleaved by caspases and post-translationally

incorporated the Alk-14 analog demonstrating that the Gly553 is a substrate for post-translational myristoylation. This was confirmed by abrogating the incorporation of Alk-C14 by substituting the essential Gly553 to Ala (Figure 4.4.B).

Full length Htt has been shown to translocate to the nucleus to be processed by caspase-6 in the nucleus, but endogenous caspase-3 cleaved Htt is found in a perinuclear localization (Warby et al., 2008). In order to confirm post-translational myristoylation of Htt at Gly553, HeLa cells transiently expressing a previously described (Atwal et al., 2007) version of Htt bearing the first 588 amino acids, which includes both the caspase-3 and -6 cleavage sites, and a C-terminal YFP tag (Figure 5.1.A) were induced to undergo apoptosis with TNFα/CHX in the presence of Alk-C14. C-terminal YFP fragments were immunoprecipitated using anti-GFP antibodies and subjected to click chemistry with azido-biotin. Preliminary data indicated the incorporation of Alk-C14 into a fragment containing YFP at approximately 30 kDa, which correlates with the predicted molecular weight of YFP (~26 kDa) and the 33 amino acid contribution from the caspase-3 cleavage of Htt1-588-YFP at the Asp552 (Figure 5.1.B). To a lesser extent, there appeared to be a small incorporation of Alk-C14 into Gly553 in the absence of apoptotic induction. This can be accounted for by a 10-20% of basal cell death observed in transfected cells in cell culture

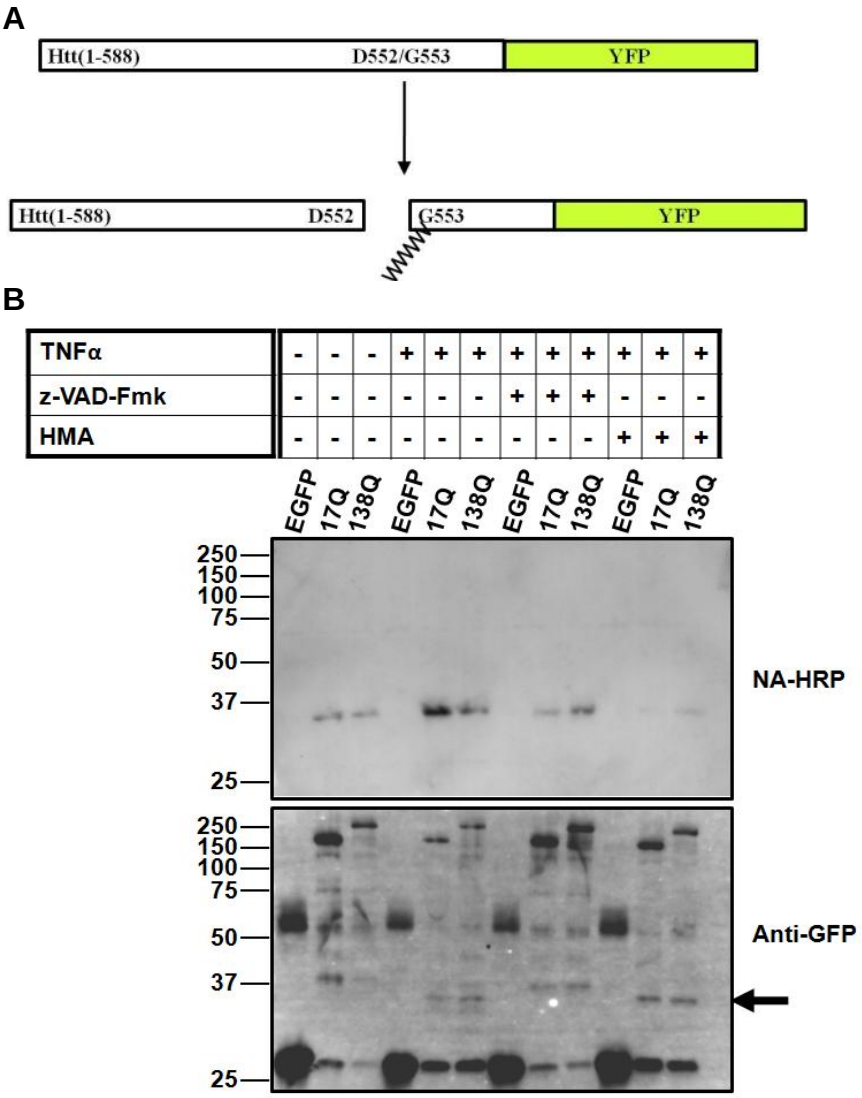
A
Htt(1-588)
D552/G553
YFP
Htt(1-588)
D552
G553
YFP
B
TNFα
z-VAD-Fmk
HMA
EGFP
17Q
138Q
250
150
100
75
50
37
25
NA-HRP
Anti-GFP
C
M.W. (kDa)
1
2
75
50
25
15
10
34 a.a. Htt fragment
migration front
WB: rabbit anti-neo-Htt586

Figure 5.1. – Alkyne-myristoylation of exogenously expressed Htt and detection of the endogenously cleaved ctHttN34 fragment. A Diagram of Htt(1-588)-YFP which contains the first 588 amino acids of the N-terminus of Htt fused to YFP. Like pTRAMPP, cleavage of Htt(1-588)-YFP exposes the N-terminal Gly residue part of a sequence attached to a C-terminal YFP tag. **B** HeLa cells transiently expressing Htt(1-588)-YFP were induced to undergo apoptosis with TNFα in the presence of Alk-Myr. Incorporation of Alk-Myr was inhibited by the addition of caspase inhibitors and HMA (arrow indicates the ctHtt$_{N34}$-YFP fragment released by caspase cleavage). **C** Western blot analysis of lysates obtained from HeLa cells (expressing endogenous WT full length Htt) induced to undergo apoptosis (lane 2) or not (lane 1) probed with rabbit anti-neoHtt586 antibody, which specifically detects the C-terminus of Htt$_{N34}$ released by caspase-6 cleavage (IVLD).

(Goto et al., 2003), which could account for caspase activation and cleavage of the protein. In addition, Htt fragments have been detected in neuronal and HEK293 cell lysates previously (Kim et al., 2001; Ratovitski et al., 2009). Post-translational myristoylation of the Htt-YFP fragment was confirmed by preventing caspase cleavage of the protein in the presence of a general caspase inhibitor, which led to a reduction of the incorporation of Alk-C14 into the appropriate Htt-YFP fragment. In addition, and importantly, the specific inhibitor of NMT, HMA, significantly reduced the incorporation of Alk-C14 into ctHtt-YFP thereby confirming that this is an NMT dependent process.

Of particular note, using a neo-epitope antibody that is specific for the C-terminus of the caspase-6 cleaved fragment of Htt (IVLD) (Warby et al., 2008), we detected a fragment in apoptotic HeLa cells that correlated to the predicted size of HttN34 (approximately 4 kDa) demonstrating the existence of endogenous HttN34 (Figure 5.1.C). The Berthiaume laboratory is currently attempting to label cells to detect post-translational myristoylation of endogenous Htt_{N34} following alkyne myristate labeling, immunoprecipitation and click chemistry.

5.5.2. Co-translational myristoylation of Htt_{N34}-EGFP.

In order to study the effect of myristoylation on the 34 amino acid Htt fragment (Htt_{N34}) released by caspase-3 and -6 cleavage, we append-

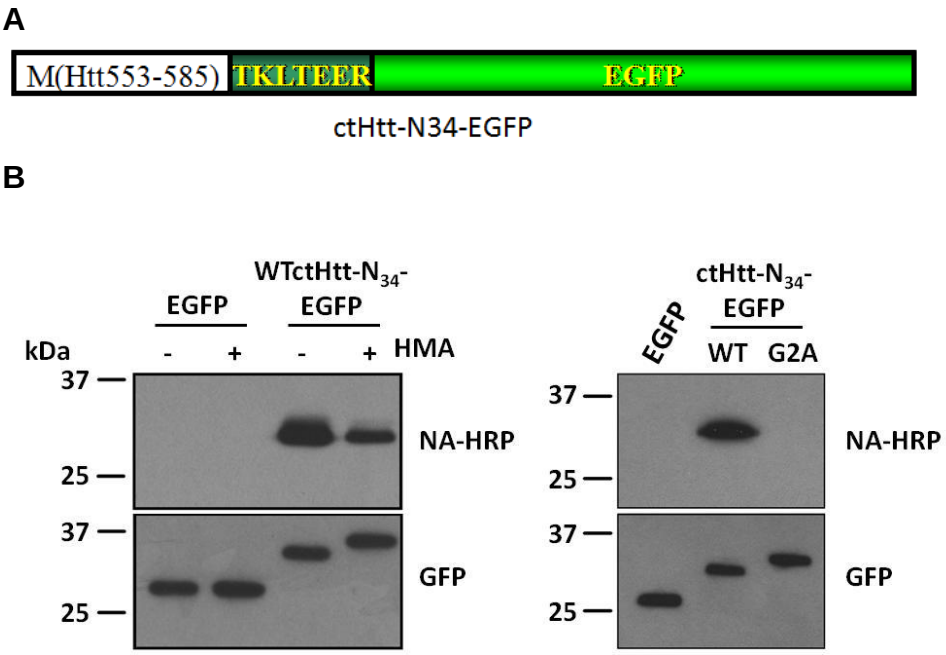

Figure 5.2. Co-translational myristoylation of HttN34-EGFP. A The 33 amino acids between the caspase-3 and -6 sites were appended to GFP and an initiator Met was added (Htt_{N34}-EGFP). The Asp residue in the caspase-6 site was excluded to ensure cleavage between the test sequence and GFP did not occur. **B** WT-HttN34-EGFP incorporated Alk-myr. Incorporation of Alk-myr was decreased by the addition of HMA (left panel) and completed inhibited by substitution of Gly to Ala into ctHttN34-GFP (right panel).

ed Htt553-585 to EGFP with an initiator methionine and the hydrophilic linker TKLTEER, as described above and previously in (Martin et al., 2010; McCabe and Berthiaume, 1999) [Htt_{N34}-EGFP, (Figure 5.2.A)]. Asp586 was excluded to prevent cleavage by caspase-6. As above, HeLa cells were transiently transfected with Htt_{N34}-EGFP, incubated with Alk-14 and subjected to click chemistry with azido-biotin, as described previously. A robust signal was associated with WT-Htt_{N34}-EGFP that was reduced in the presence of the NMT inhibitor HMA (Figure 5.2.B, *Left panel*) or completely blocked by substituting the essential Gly to Ala (Figure 5.2B, *Right panel*). Altogether, these results suggest that Gly553 of ctHtt is a strong candidate for myristoylation. Interestingly, in both cases, blocking myristoylation lead to a mobility shift of Htt_{N34}-GFP. This may be, in part, due to the reduced amount of SDS bound to the non-myristoylated G2A-ctHtt_{N34}-GFP or perhaps the spurious phosphorylation of the non-myristoylated protein. Nearly half of the 34 amino acid sequence is comprised of either Ser or Thr residues, thereby serving as ideal candidates for phosphorylation. In fact, several sites are predicted to be phosphorylated (Figure 5.3.). Interestingly, myr-ctPAK2 was found to migrate at a lower apparent molecular weight when compared to its non-myristoylated G2A counterpart. In that case, G2A-ctPAK2 was hyperphosphorylated (Vilas and Berthiaume, 2004). Therefore, in these cases, myristoylation of these proteins may sequester them away from “inappropriate” kinases or direct them towards phosphatases.

Of particular note, the sequence of amino acids between the caspase-3 and -6 cleavage sites (Htt 549-586) shares 100% sequence identity with ten other mammalian species including mouse, cow and monkey (Table 5.1) (Altschul et al., 1997). This suggests that both the caspase-3 cleavage and post-translational myristoylation of Htt at the newly exposed glycine residue is conserved in many species. In addition, any future identified phosphorylation sites will probably also be conserved.

5.2.3. Localization of Htt_{N34}-EGFP.

To study the localization of Htt_{N34}-EGFP, HeLa cells were transiently transfected for 24 h with Htt_{N34}-EGFP and localization was visualized by several microscopy methods including live cell confocal spinning disc and wide field fluorescence and transmission electron microscopy. Several interesting phenotypes were observed. First, in Figure 5.4A, Htt_{N34}-EGFP appeared to localize in a reticulated manner consistent with ER localization. In addition, a strong perinuclear signal was detected. Interestingly, over time, the formation of small vesicles were observed, which increased in number as time progressed. In this particular case, an unidentified tubular structure which extends as a function of time appeared in the observed cell (Figure 5.4.B).

A

Htt_{N34}: GTQASSPISD$_{10}$SSQTTTEGPD$_{20}$SAVTPSDSSE$_{30}$IVLD

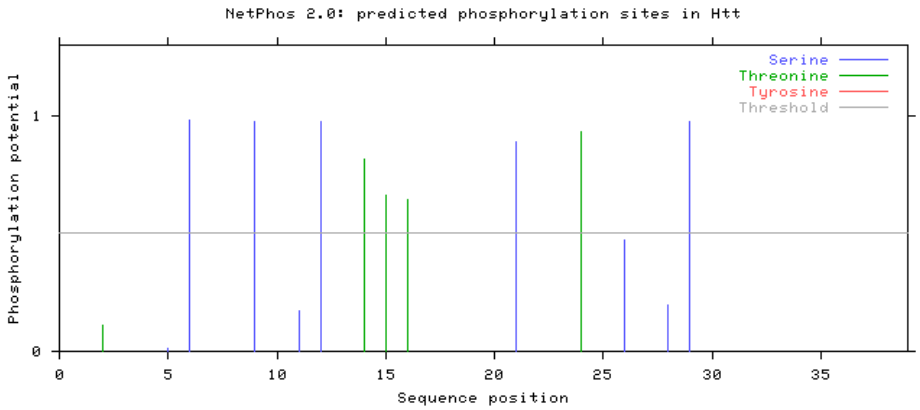

B

Serine predictions

Name	Pos	Context	Score	Pred
Htt	5	GTQASSPIS	0.012	.
Htt	6	TQASSPISD	0.983	*S*
Htt	9	SSPISDSSQ	0.978	*S*
Htt	11	PISDSSQTT	0.172	.
Htt	12	ISDSSQTTT	0.975	*S*
Htt	21	EGPDSAVTP	0.887	*S*
Htt	26	AVTPSDSSE	0.471	.
Htt	28	TPSDSSEIV	0.195	.
Htt	29	PSDSSEIVL	0.976	*S*

Threonine predictions

Name	Pos	Context	Score	Pred
Htt	2	---GTQASS	0.109	.
Htt	14	DSSQTTTEG	0.815	*T*
Htt	15	SSQTTTEGP	0.664	*T*
Htt	16	SQTTTEGPD	0.643	*T*
Htt	24	DSAVTPSDS	0.935	*T*

Figure 5.3. Predicted phosphorylation sites within the Htt_{N34} sequence. A The 34 amino acids between the caspase-3 and caspase-6 cleavage sites of Htt were subjected to phosphorylation prediction analysis using NetPhos (Blom et al., 1999). The predicted sites of phosphorylation are displayed in **B**.

Table 5.1: Sequence alignment of Htt_{N34} between species. The 34 amino acids between the caspase-3 (DLND) and caspase-6 (IVLD) cleavage sites of Htt were subjected to BLAST**.** Sequences show 97-100% sequence identity among several species. Differences in sequences are highlighted in yellow (Altschul et al., 1997).

SPECIES	Amino acid sequence
Homo sapiens	**DLNDGTQASSPISDSSQTTTEGPDSAVTPSDSSEIVLD**
Pongo abelii	**DLNDGTQASSPISDSSQTTTEGPDSAVTPSDSSEIVLD**
Oryctolagus cuniculus	**DLNDGTQASSPISDSSQTTTEGPDSAVTPSDSSEIVLD**
Equus caballus	**DLNDGTQASSPISDSSQTTTEGPDSAVTPSDSSEIVLD**
Pan troglodytes	**DLNDGTQASSPISDSSQTTTEGPDSAVTPSDSSEIVLD**
Callithrix jacchus	**DLNDGTQASSPISDSSQTTTEGPDSAVTPSDSSEIVLD**
Macaca mulatta	**DLNDGTQASSPISDSSQTTTEGPDSAVTPSDSSEIVLD**
Mus musculus	**DLNDGTQASSPISDSSQTTTEGPDSAVTPSDSSEIVLD**
Bos Taurus	**DLNDGTQASSPISDSSQTTTEGPDSAVTPSDSSEIVLD**
Rattus norvegicus	**DLNDGTQASSPISDSSQTTTEGPDSAVTPSDSSEIVLD**
Ovis aries	**DLNDGTQASSPISDSSQTTTEGPDSAVTPSDSSEIVLD**
Canis familiaris	**DLNDGTQASSPVSDSSQTTTEGPDSAVTPSDSSEIVLD**
Ailuropoda melanoleuca	**DLNDGTQASSPVSDSSQTTTEGPDSAVTPSDSSEIVLD**
Sus scrofa	**DLNDGTQASSPISDSSQTTTEGPDSAVTPSDSSEIVLE**
Gallus gallus	**DLNDGTQASSPISDSSQTTTEGPDSAVTPSDSSEIVLE**
Meleagris gallopavo	**DLNDGTQASSPISDSSQTTTEGPDSAVTPSDSSEIVLS**
Monodelphis domestica	**DMNDGTQASSPISDSSQTTTEGPDSAVTPSDSSEIVLD**

In Figure 5.5.A, a greater number of vesicles can be detected in the two highest expressing cells compared to the low expressing cells. Over time, the cell in the middle of the field of view retracted, rounded up and appeared to die. Prior to apparent cellular death, the cytoplasm appeared to rapidly and completely fill up with vesicles, suggesting that the vesicle formation may have a causal role in cell death. Of note, in the two cells expressing lower levels of Htt_{N34}-EGFP on the far right and the top of the field of view, vesicles can still be observed (Figure 5.5.B) suggesting that even at low levels of expression myr-Htt_{N34}-EGFP can induce vesicle formation in these cells and, subsequently, this may become toxic over time. Formation of the small vesicles observed in cells expressing Htt_{N34}-EGFP is shown in Figure 5.6. In particular, the inset in Figure 5.6.B shows the nucleation and complete formation of one of the small vesicles identified in Htt_{N34}-EGFP transfected cells. First, a small sphere formed, which became elongated and eventually circularized to form what appeared to be a complete vesicle. From this sequence of events, we postulate that the resulting vesicle is made of a double membrane, which is consistent with and similar to the formation of an autophagosome from an omegasome (Juhasz and Neufeld, 2006; Tanida, 2011).

In many cases, much larger vesicles were also observed (Figures 5.7. – Figure 5.11.). Regardless, formation and detection of the vesicles observed in Htt_{N34}-EGFP transfected cells appeared to be dependent on myristoylation. This possibility is supported by the fact that we saw a com-

A

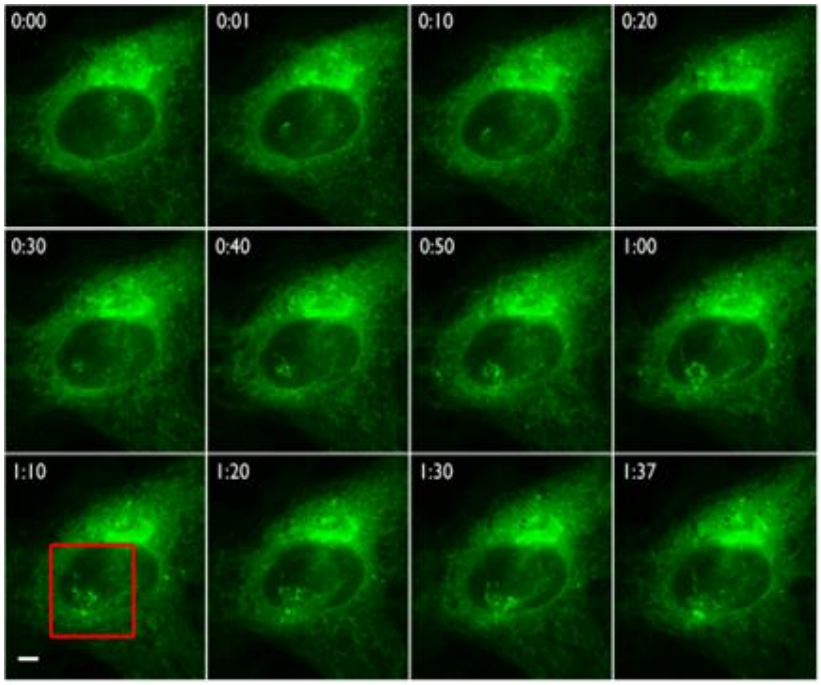

B

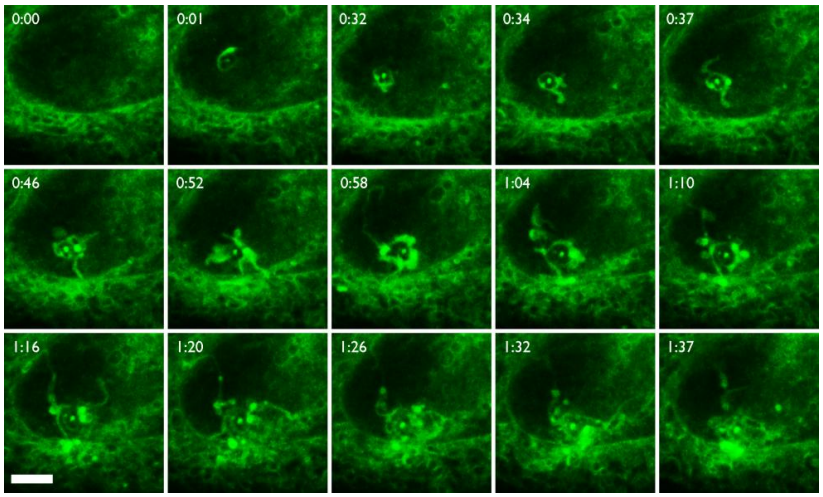

Figure 5.4. – Expression of myr-HttN34-EGFP in HeLa cells. HeLa cells were transiently transfected for 22 h and imaged using live cell confocal spinning disk microscopy. **A** illustrates the formation of a tubulated structure apparently underneath the nucleus. **B** represents the expanded red box inset from (**A**).

A

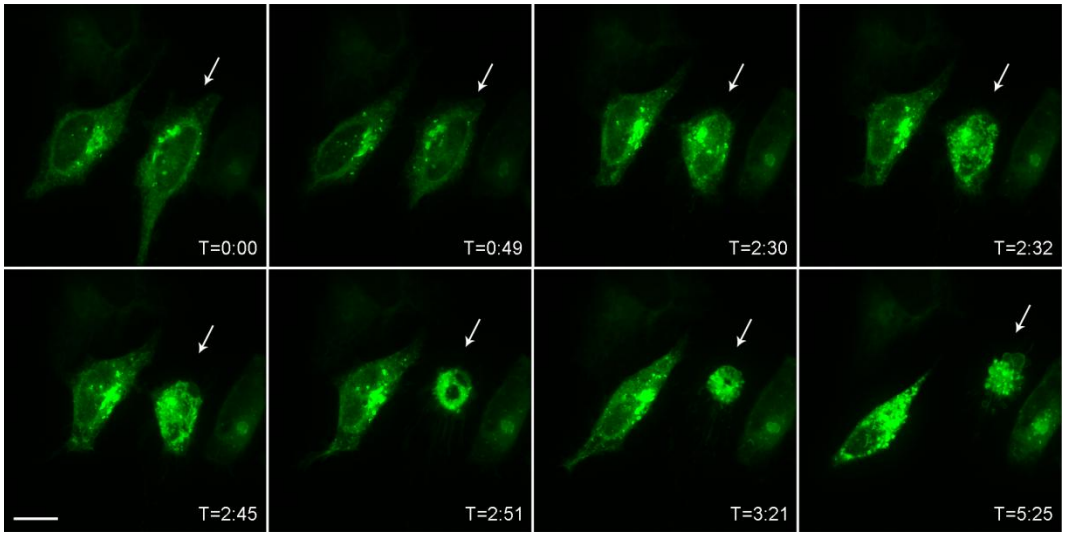

B

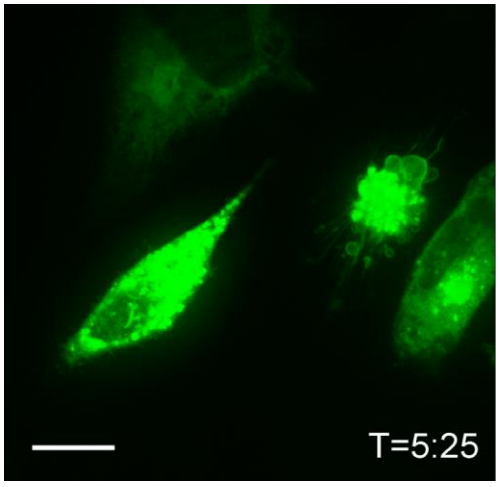

Figure 5.5. - **Expression of myr-ctHtt$_{N34}$-EGFP in HeLa cells leads to cell death.** In **A**, the cell highlighted with an arrow fills with vesicles, retracts and undergoes apparent cell death. **B** shows that the lower expressing cells from **A** also contain vesicles. Images were acquired by spinning disc live cell microscopy. Scale bar represents 20 µm or 2.5 µm in the close-ups.

plete abrogation of vesicle formation when Htt_{N34}-EGFP expressing cells were treated with 1 mM HMA (Figure 5.7.A). In cells treated with 1 mM HMA, Htt_{N34}-EGFP appeared diffuse within the cell, similar to GFP alone. Similarly, non-myristoylatable G2A-Htt_{N34}-EGFP was also found throughout the cytosol (Figure 5.8. - 5.14.).

Further evidence to suggest that the vesicles were dependent on myristoylation of Htt_{N34}-EGFP was shown by immunoelectron microscopy (Figure 5.7.B). HeLa cells transiently expressing Htt_{N34}-EGFP for 24 h were fixed and GFP tagged proteins were detected by immunogold labeling using our anti-GFP antibodies (Manolea et al., 2010). Similar to what was observed by fluorescence microscopy (Figure 5.4. - 5.6.), in cells expressing Htt_{N34}-EGFP the cytoplasm appeared to be filled with vesicles. In addition, these vesicles were immunogold labeled with anti-GFP antibodies demonstrating that myr-Htt_{N34}-EGFP was associated with these vesicles. In contrast, in cells expressing either EGFP or the non-myristoylated Htt_{N34}-EGFP (G2A-Htt_{N34}-EGFP), fewer vesicles were observed and GFP was detected primarily in the cytosol and nucleus; typical of GFP localization (Compare Figure 5.7.B to Figure 5.8. - 5.11.).

Based on the initial reticulated appearance and perinuclear localization of myr-Htt_{N34}-EGFP (Figure 5.4.), which is indicative of ER and Golgi localization, Htt_{N34}-EGFP was co-expressed with ER-RFP and Arf1-mCherry in HeLa cells. Interestingly, myr-Htt_{N34}-EGFP co-localized with Arf1-mCherry prior to the formation of vesicles. However, once vesicles

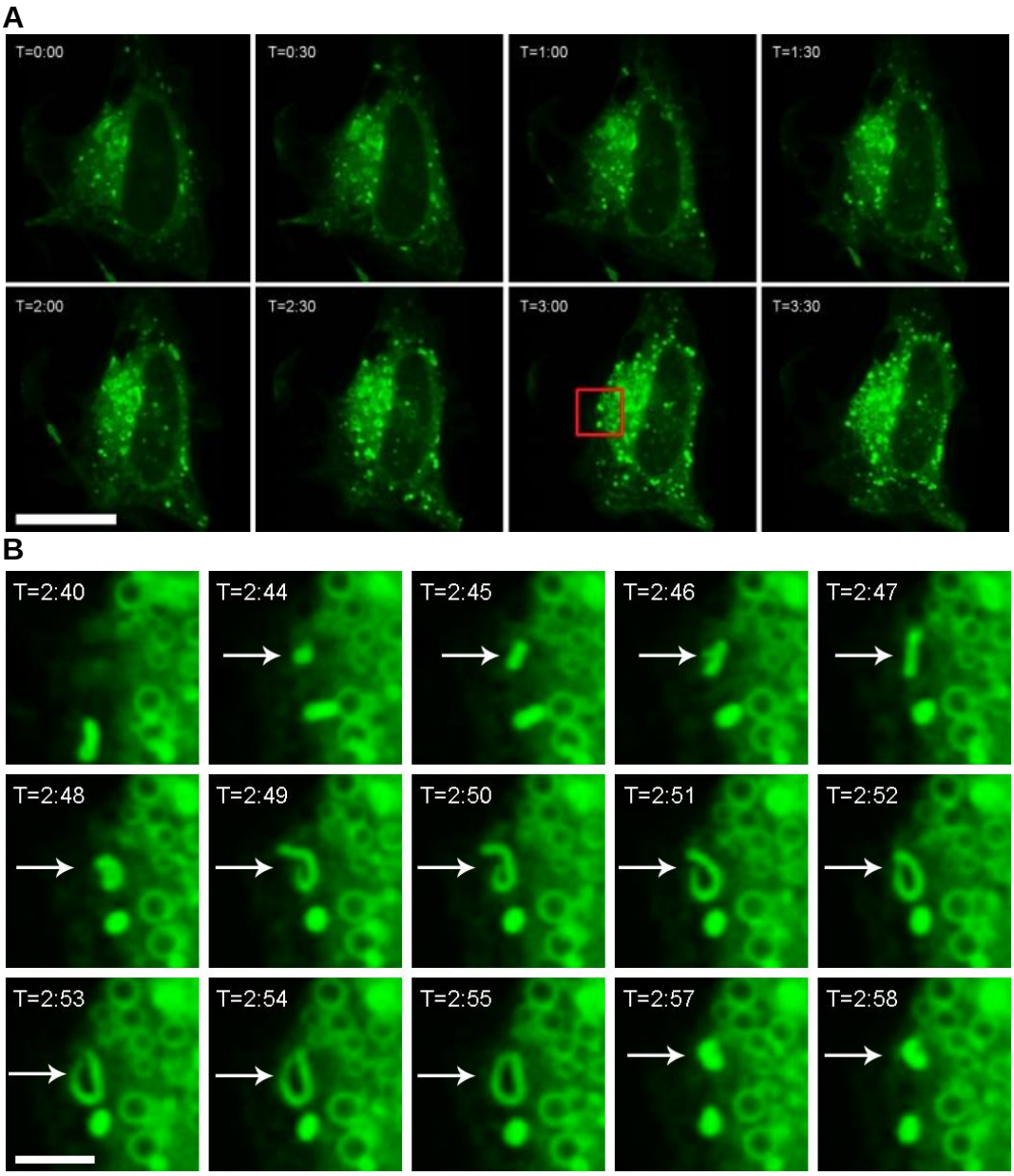

Figure 5.6. – Formation of a vesicle in HeLa cells expressing myr-Htt_{N34}-EGFP. HeLa cells were transiently transfected for 22 h and imaged using live cell confocal spinning disk microscopy. **A** illustrates the increase in vesicle formation within the cell over approximately 3.5 h. **B** represents a close-up of the red-boxed region in (**A**), which follows the generation of a complete vesicle over approximately 30 min (indicated by arrow). Initially, a small punctate green sphere appears which forms a long tubulated structure that, ultimately, circularizes and closes. This process is highly reminiscent of the formation of an autophagosome.

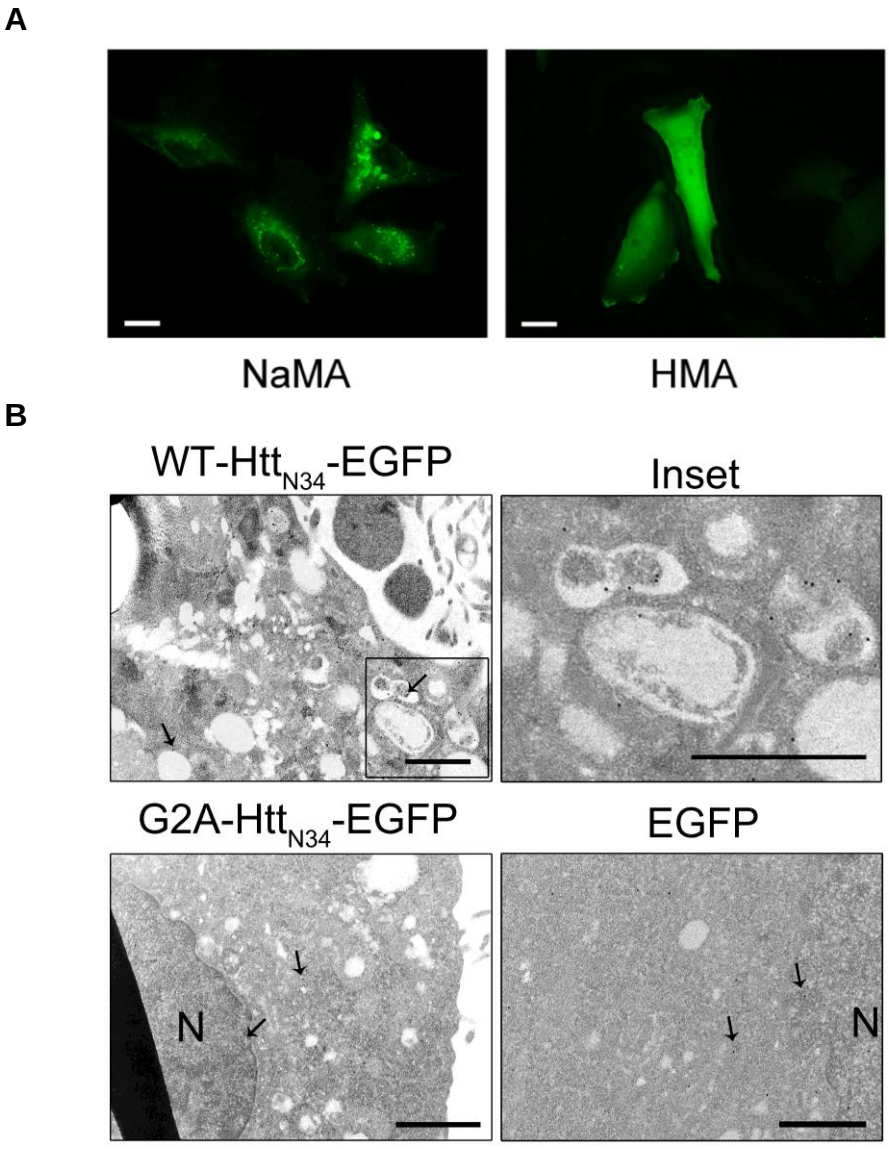

Figure 5.7. – Epifluoresence and immunogold scanning electron microscopy of HttN34-EGFP in HeLa cells. A HeLa cells were transfected for 18 h and treated with either 1 mM NaMA or 1 mM HMA for an additional 6 h. Images were acquired by wide field microscopy and deconvolved using Huygens Deconvolution software from Science Volume Imaging (SVI). Scale bar represents 20 µm or 2.5 µm in the close-ups. **B** HeLa cells transiently expressing HttN34-EGFP for 24 h were fixed and prepared for immunogold EM using anti-GFP antibodies (1:10,000) and 18 nm beads. The 'inset' illustrates an expanded view of the box area in WT-HttN34-EGFP panel. Arrows indicate gold beads. 'N' marks nucleus and all the scale bars represent 1 µm.

began to form in the cells co-localization between Arf1-mCherry and myr-Htt_{N34}-EGFP decreased (Figure 5.8B). As indicated in Figure 5.9A, a high degree of co-localization was observed between myr-Htt_{N34}-EGFP and ER-RFP.

Like with Arf1-mCherry, in cells co-expressing either EGFP or G2A-Htt_{N34}-EGFP with ER-RFP, the ER appeared unaffected and no co-localization was detected. These results suggest that the vesicles formed by overexpression of myr-Htt_{N34}-EGFP may originate from the ER and, ultimately, may distort the ER morphology.

Although there is evidence to support that phagosomes can originate from mitochondria (Hailey et al., 2010) or the plasma membrane (Ravikumar et al., 2010a), the ER is thought to be main membrane donor for autophagy (Axe et al., 2008). In Figure 5.9B, HeLa cells transiently expressing both myr-Htt_{N34}-EGFP and ER-RFP were observed by spinning disc fluorescence microscopy after starving the cells in Hank's Buffering Salt Solution (HBSS) for approximately 4 h. HBSS was used to starve cells and promote autophagy. In Figure 5.9B, the formation of what appeared to be an autophagosome is depicted and is composed of both myr-Htt_{N34}-EGFP and ER-RFP, thereby suggesting that myr-Htt_{N34}-EGFP is not only localized to the ER but is also associated with the formation of autophagosomes and that the ER acts as the membrane donor for this process.

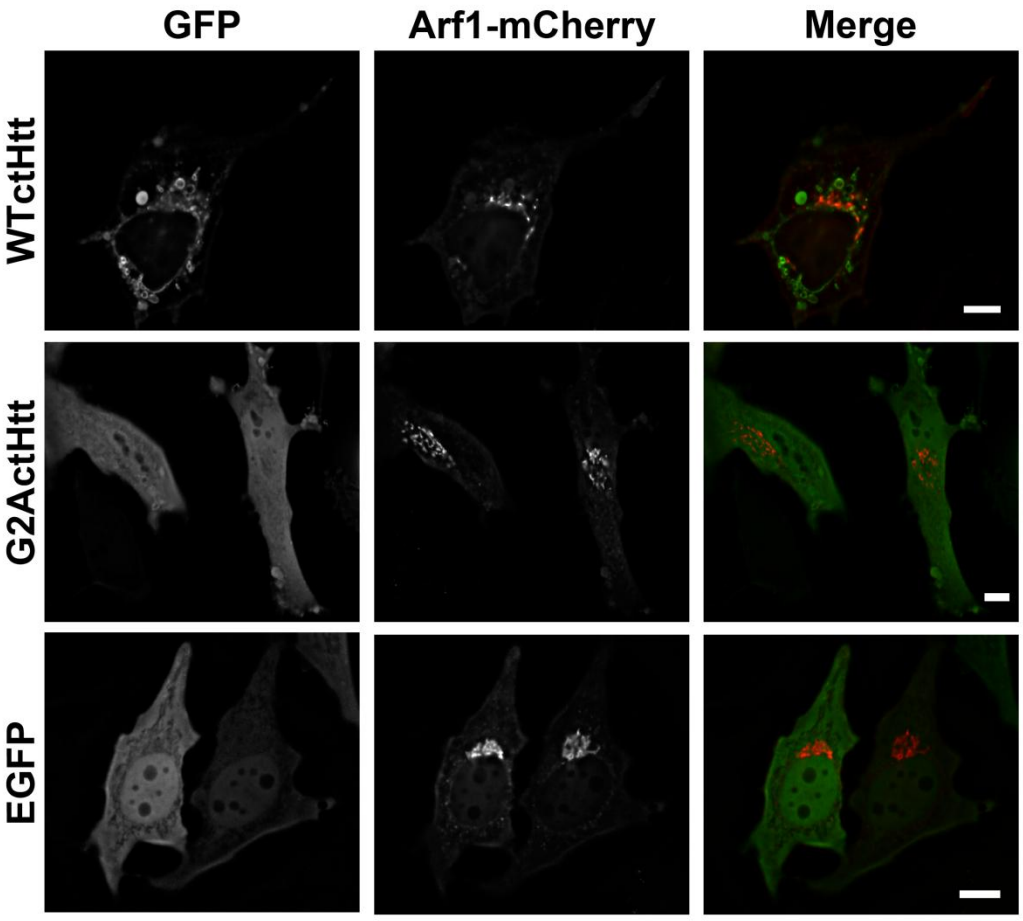

Figure 5.8. – Arf-1-mCherry does not co-localize with large vesicular structures containing and Htt_{N34}-EGFP. HeLa cells were co-transfected with Arf1-mCherry and Htt_{N34}-EGFP. Images were acquired by wide field fluorescence microscopy and deconvolved using SVI Huygens deconvolution software. Images are presented as 3D z-stacks. Scale bars represent 10 µm.

A

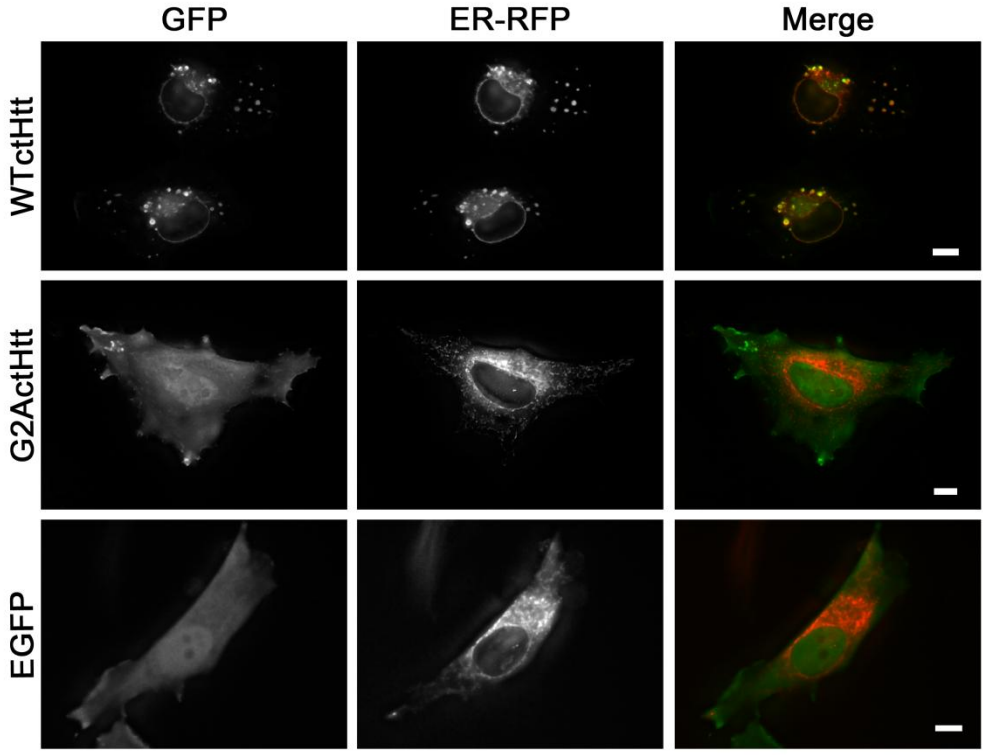
GFP
ER-RFP
Merge
WTctHtt
G2ActHtt
EGFP

B

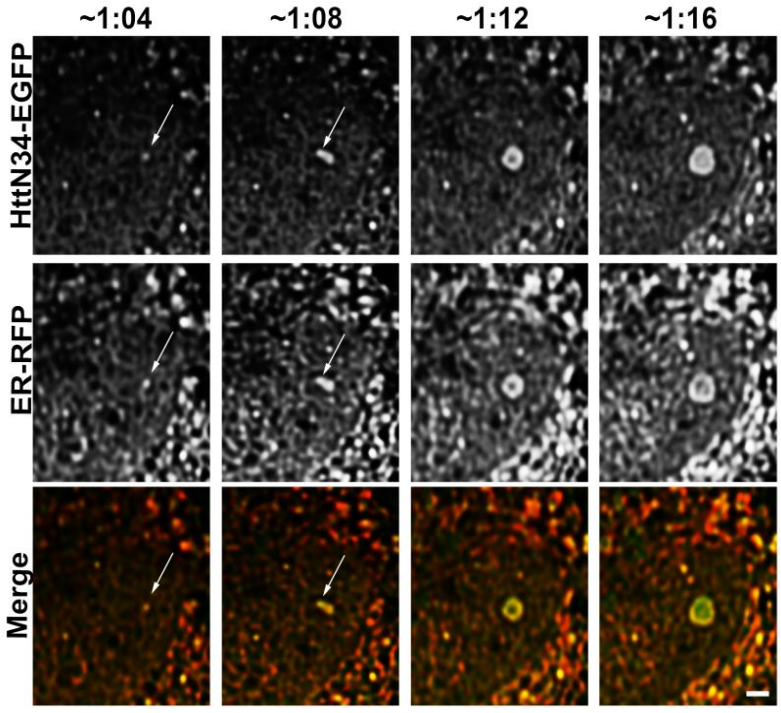
~1:04
~1:08
~1:12
~1:16
HttN34-EGFP
ER-RFP
Merge

Figure 5.9. - Htt_{N34}-EGFP co-localizes with ER marker ER-RFP in HeLa cells. HeLa cells were co-transfected with ER-RFP and Htt_{N34}-EGFP. Images in **A** were acquired by wide field microscopy and deconvolved using SVI Huygens deconvolution software. Images are presented as 3D z-stacks. Scale bars represent 10 µm. **B** HeLa cells transiently expressing ER-RFP and myr-Htt_{N34}-EGFP were starved in HBSS media and viewed using live cell confocal spinning disc fluorescence microscopy. The arrow indicates the initiation of the formation of a myr-Htt_{N34}-EGFP induced vesicle that co-localizes with ER-RFP. Scale bar is representative of 1 µm.

Ultimately, autophagosomes fuse with lysosomes to become autophagolysosomes (Kimura et al., 2007; Klionsky et al., 2008b). Consequently, to further investigate the possibility that myr-Htt_{N34}-EGFP induces the formation of autophagosomes able to fuse with lysosomes myr-Htt_{N34}-EGFP was co-localized with two lysosome markers; LAMP1-RFP and LysoTracker® Red (Figure 5.10) in live cells. LAMP1 is a single spanning transmembrane protein of the lysosome (Eskelinen, 2006). In myr-Htt_{N34}-EGFP expressing cells, LAMP1-RFP was clearly associated with the membranes of the large vesicles that contained membrane localized myr-Htt_{N34}-EGFP in the vast majority of cases. There remained many independent small punctate structures that are indicative of normal lysosome also seen in cells expressing EGFP or G2A-Htt_{N34}-EGFP. Again, the large vesicles that contained LAMP1-RFP were absent in EGFP and G2A-Htt_{N34}-EGFP transfected cells (Figure 5.10.A). LysoTracker® is an acidotrophic dye that accumulates in acidic organelles in live cells (Freundt et al., 2007). In cells expressing myr-Htt_{N34}-EGFP, LysoTracker® was detected inside the large vesicles coated with myr-Htt_{N34}-EGFP (Figure 5.10.B). Because lysosomes are the ultimate destination for autophagosomes and subsequent degradation of their cellular contents, the lysosome co-localization suggests, once again, that myr-Htt_{N34}-EGFP may have a role in autophagy. However, because of the abnormal size of the resulting autophagolysosomes, myr-Htt_{N34}-EGFP

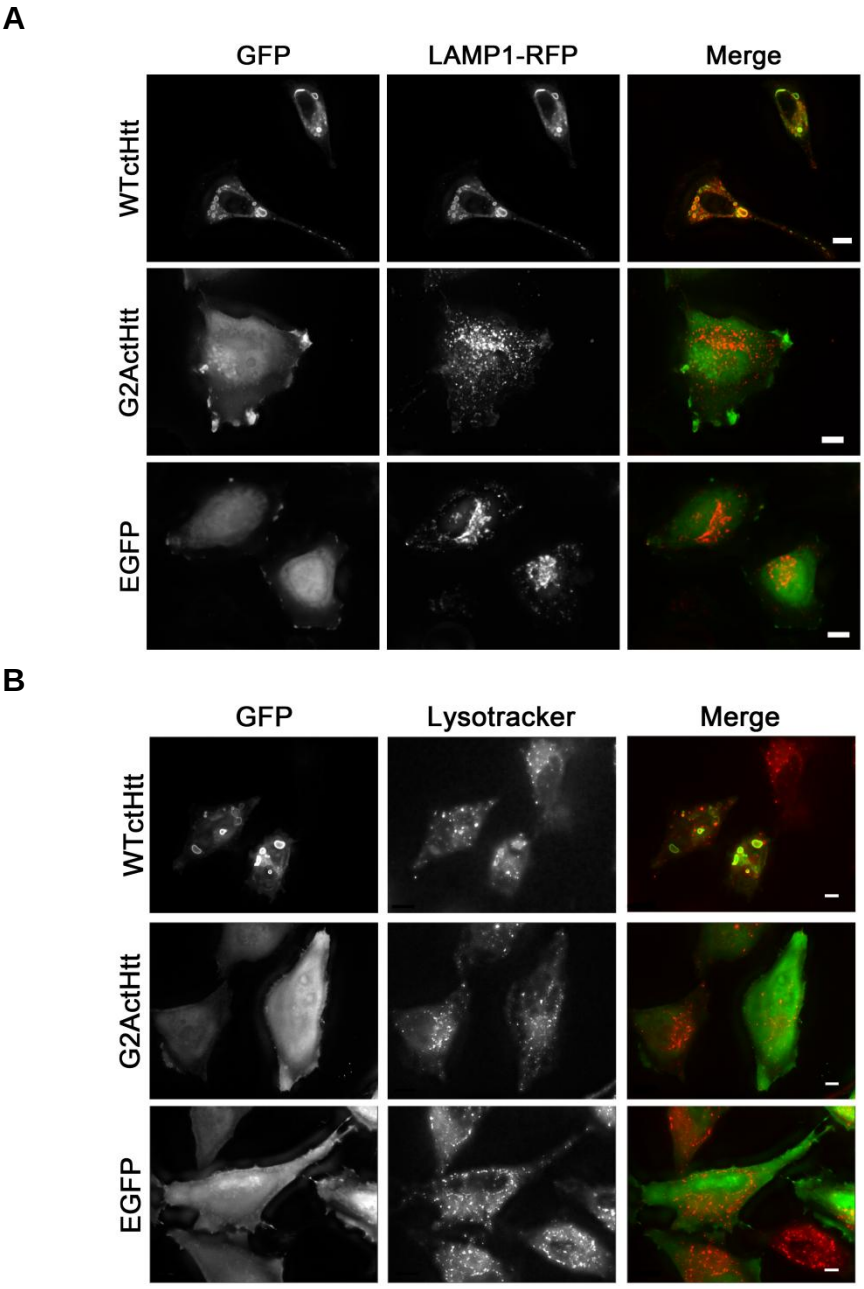

Figure 5.10. – Co-localization of myr-Htt$_{N34}$-EGFP with the lysosome markers LAMP1 and LysoTracker®. HeLa cells were transiently transfected for 24 h with myr-Htt$_{N34}$-EGFP and **A** LAMP1-RFP or **B** stained with 1 µM LysoTracker® for 30 min. Images were acquired by live cell wide field microscopy and deconvolved using SVI Huygens deconvolution software. Images are presented as 3D z-stacks. Scale bars are representative of 10 µm.

somehow alters their morphology and perhaps negatively affects autophagy.

5.2.4. Myr-HttN34-EGFP and mitochondrial integrity.

Huntington's disease is commonly linked to mitochondrial abnormalities and, subsequently, can lead to lose of mitochondrial potential, which may contribute to neurodegeneration (Costa et al., 2010; Martinez-Vicente et al., 2010; Shirendeb et al., 2011; Song et al., 2011). As suggested by Figure 5.5A, the excessive vesicle formation induced by myr-Htt_{N34}-EGFP may have a cytotoxic effect leading to cellular death. Consequently, this led us to evaluate mitochondrial morphology and integrity in myr-Htt_{N34}-EGFP transfected cells. First, HeLa cells transiently expressing myr-Htt_{N34}-EGFP were labeled with the mitochondrial dye MitoTracker® Orange CM-H_2TMRos (Figure 5.11.). This form of MitoTracker® is a reduced, non-fluorescent marker that fluoresces upon oxidation. Thus, this dye stains mitochondria in live cells and its accumulation is dependent upon mitochondrial membrane potential (Kweon et al., 2001). In cells expressing myr-Htt_{N34}-EGFP for 24 h the mitochondria appeared fragmented (Figure 5.11.A) suggesting they were not healthy whereas the mitochondria appeared long and filamentous in cells expressing EGFP and G2A-Htt_{N34}-EGFP. In one particular case following 48 h of transfec-

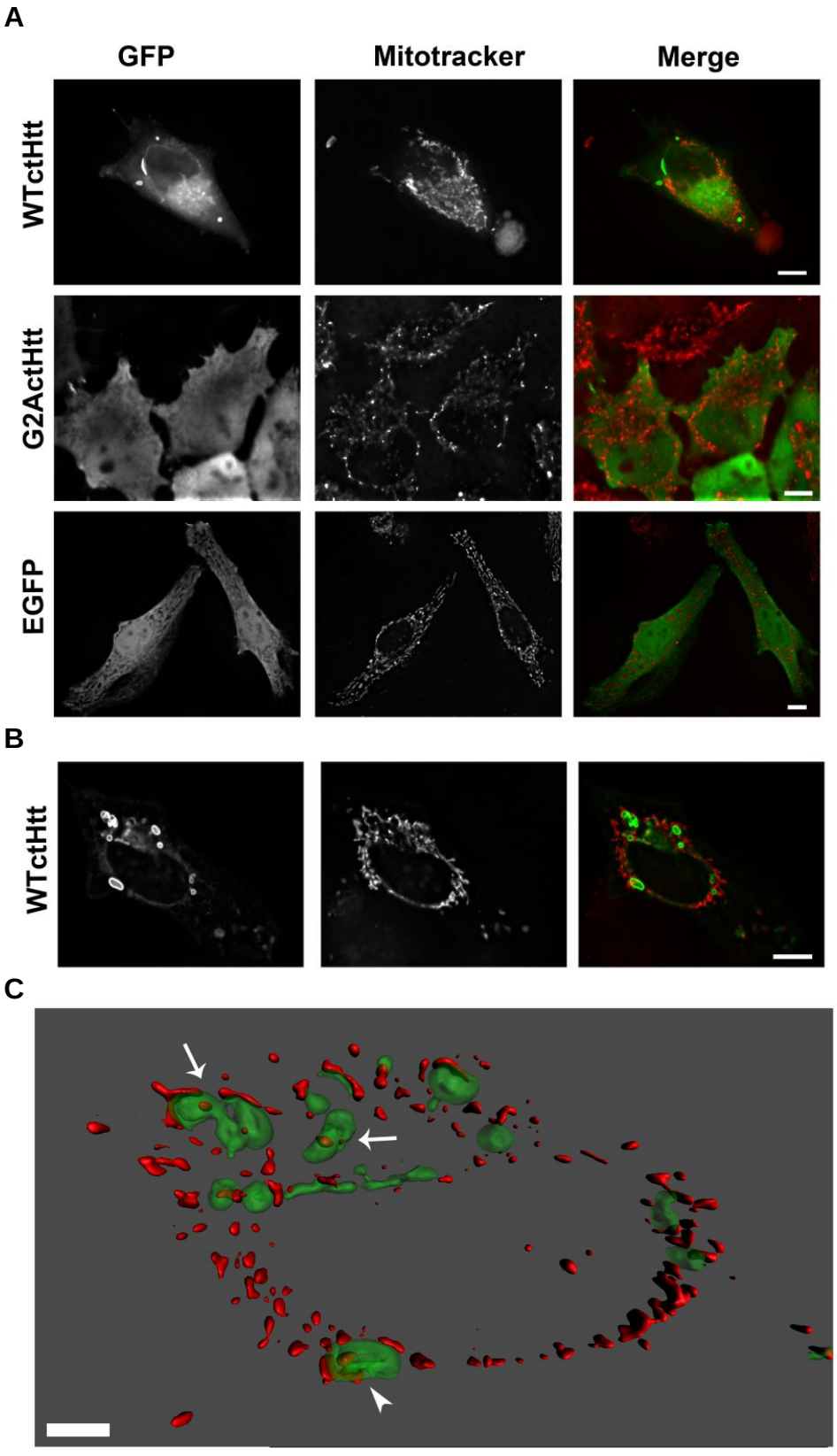
A
GFP
Mitotracker
Merge
WTctHtt
G2ActHtt
EGFP
B
WTctHtt
C

Figure 5.11 – Effect of myr-Htt_{N34}-EGFP on mitochondria in HeLa cells. A HeLa cells were transiently transfected for 24 h or **B** 48 h with myr-Htt_{N34}-EGFP and stained with MitoTracker® Orange CM-H_2TMRos for 30 min. Images were acquired by live cell wide field microscopy and deconvolved using SVI Huygens Deconvolution software. Images are presented as single z-planes. **C** 3D-representation of the cell shown in **B** The arrows indicate the presence of mitochondria within large vesicular structures. Arrowhead indicates partially engulfed mitochondria. Scale bars are 10 µm.

tion, mitochondrial fragments appeared to co-localize with the larger myr-Htt_{N34}-EGFP-induced vesicles (Figure 5.11.B). Following 3D-reconstruction, it was noted the MitoTracker® stained fragments were, in fact, located inside the large vesicles (Figure 5.11.C, arrowhead).

One mitochondrial fragment appeared to be in the process of being engulfed (Figure 5.11C, arrow). This may indicate that myr-Htt_{N34}-EGFP may have a role in a form of autophagy that involves the engulfment of mitochondria referred to as mitophagy (Kim et al., 2007; Kissova et al., 2004; Lemasters, 2005).

Due to the effect on mitochondrial morphology, we next sought to evaluate the effect of myr-Htt_{N34}-EGFP on mitochondrial potential and, consequently, towards cell death. To do so, the mitochondrial potential was measured by tetramethylrhodamine, ethyl ester (TMRE) from mitochondria by flow assisted cell sorting (FACS) in Htt_{N34}-EGFP expressing HeLa cells and (Figure 5.12.). TMRE is a cell-permeant, cationic, red-orange fluorescent dye that is readily sequestered by active mitochondria (Distelmaier et al., 2008). After 24 h transfection, a significantly higher number of myr-Htt_{N34}-EGFP transfected cells lost their mitochondrial potential, as indicated by TMRE loss, compared to EGFP alone ($p=0.0002$) or G2A-Htt_{N34}-EGFP ($p=0.003$). This suggests that the myristoylation of Htt_{N34}-EGFP may promote a toxic environment in cells.

Htt protein is expressed ubiquitously, but HD is a neurodegenerative disease that primarily affects striatal neurons.

A

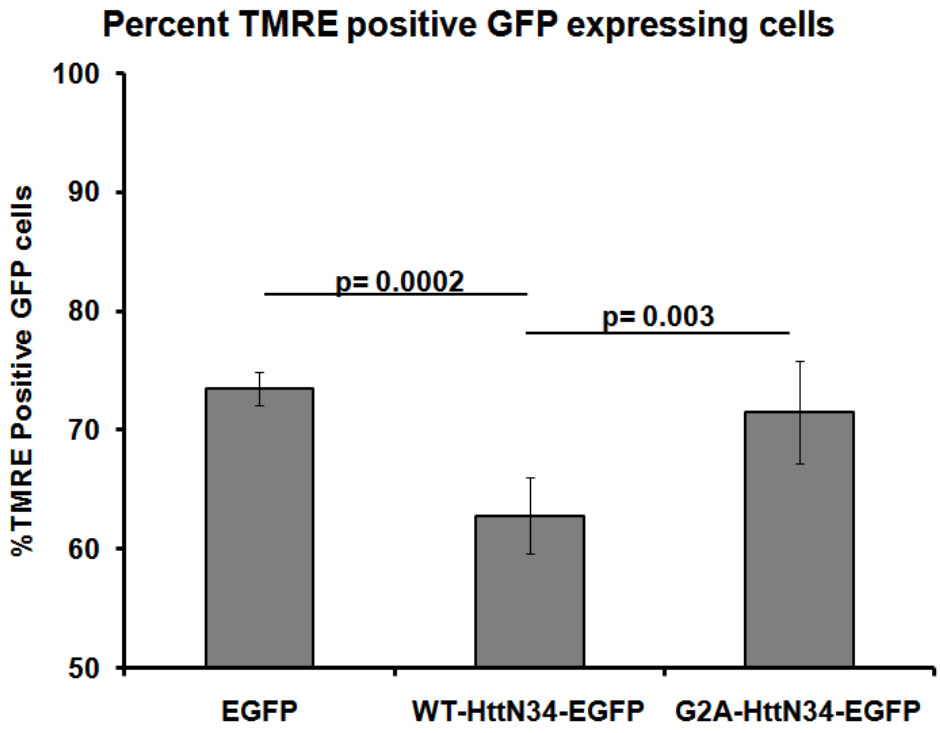

B

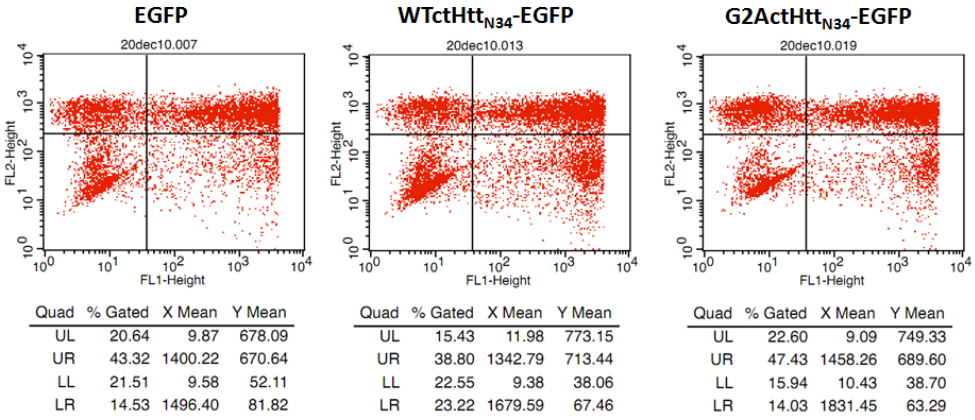

Quad	% Gated	X Mean	Y Mean
UL	20.64	9.87	678.09
UR	43.32	1400.22	670.64
LL	21.51	9.58	52.11
LR	14.53	1496.40	81.82

Quad	% Gated	X Mean	Y Mean
UL	15.43	11.98	773.15
UR	38.80	1342.79	713.44
LL	22.55	9.38	38.06
LR	23.22	1679.59	67.46

Quad	% Gated	X Mean	Y Mean
UL	22.60	9.09	749.33
UR	47.43	1458.26	689.60
LL	15.94	10.43	38.70
LR	14.03	1831.45	63.29

Figure 5.12. – Mitochondrial membrane potential decreases in cells expressing myr-Htt$_{N34}$-EGFP. The mitochondrial membrane potential of cells expressing EGFP, myr-Htt$_{N34}$-EGFP, or G2A-Htt$_{N34}$-EGFP was assessed using the potentiometric dye TMRE. 24 h post-transfection, cells were sorted by FACS. **A** Data is represented as percent of TMRE retained in EGFP expressing cells (n=3). Error bars represent standard deviation. **B** Example of representative data from FACS analysis. FL-1 and FL-2 represent GFP and TMRE fluorescence, respectively.

Therefore, Htt_{N34}-EGFP was expressed in ST14A cells. ST14A cells are cells derived from rat striatal primordia at embryonic day 14 and display characteristics of medium-size spiny neurons (Ehrlich et al., 2001). As seen in HeLa cells, ST14A cells transiently expressing myr-Htt_{N34}-EGFP (Figure 5.13.A) contained large vesicles comprised of myr-Htt_{N34}-EGFP and MitoTracker® Orange CM-H_2TMRos stained mitochondria appeared fragmented. Once again, no abnormal vesicles were seen in cells expressing either EGFP or G2A-Htt_{N34}-EGFP and their mitochondria appeared long and filamentous suggesting they remained healthy after transfection. Once again, MitoTracker® stained fragments were detected inside the large vesicles (Figure 5.13.B).

5.2.5. Myr-Htt_{N34}-EGFP-induced vesicles are autophagosomes.

In Figure 5.5, formation of the vesicle followed the characteristic generation of autophagosomes seen in autophagy (described in Chapter 1.4.3.4.). This was confirmed by co-localization of myr-Htt_{N34}-EGFP with ER-RFP during the formation of one of these vesicles (Figure 5.8.B). In addition, in Figures 5.11 and 5.13, mitochondria were found within the larger vesicles and even being engulfed, which suggests that the vesicles may be involved in mitophagy, a specific form of autophagy.

LC3 is a critical component of conventional autophagy and is often used as a marker for autophagy (Kimura et al., 2007; Tanida, 2011).

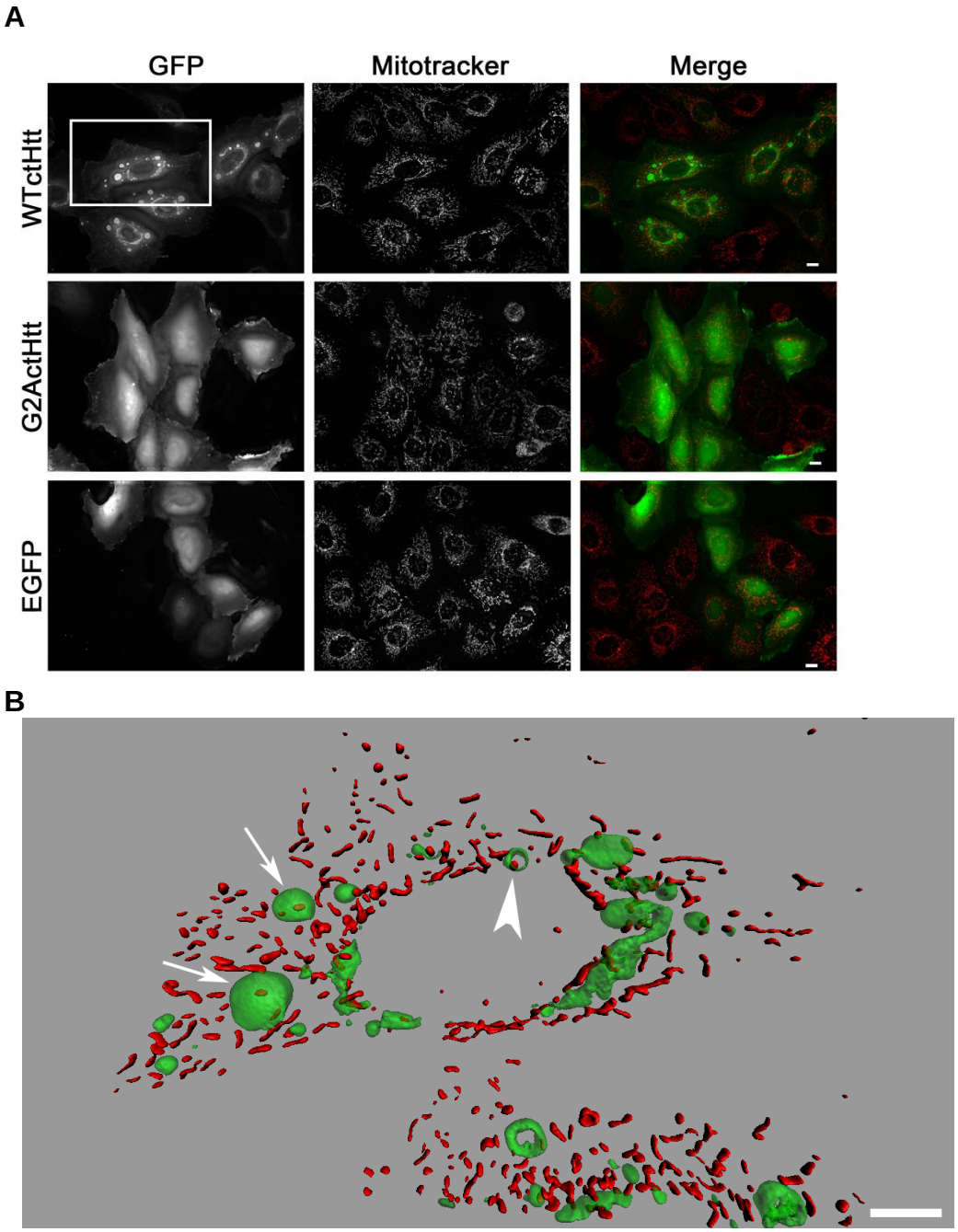

Figure 5.13. - Effect of myr-Htt$_{N34}$-EGFP on mitochondria in rat neuronal ST14A cells. A ST14A cells were transiently transfected for 24 h or with myr-Htt$_{N34}$-EGFP stained with MitoTracker® Orange CM-H_2TMRos for 30 min. Images were acquired by live cell wide field microscopy and deconvolved using SVI Huygens Deconvolution software. Images are presented as 3D z-stacks. **B** 3D-representation of the boxed area in **A**. Scale bars are representative of 10 µm.

Consequently, experiments were performed to visualize LC3 by Western blot analysis and by fluorescence microscopy in the presence or absence of bafilomycin. Bafilomycin (Baf) is a potent and specific inhibitor of vacuolar H^+ ATPase (V-ATPase) and blocks the acidification of organelles containing this enzyme thereby preventing the fusion of autophagosomes and lysosomes. Consequently, the degradation of LC3-II is prevented, which leads to its accumulation (Klionsky et al., 2008b; Kuma et al., 2007; Mizushima and Yoshimori, 2007). LC3-II is the phosphatidylethanolamine-modified form of LC3 and is the "active" form of LC3 in autophagy (Mizushima and Yoshimori, 2007). The levels of LC3 in myr-Htt_{N34}-EGFP transfected cells treated in the presence or absence of bafilomycin (Baf) were visualized by western blotting analysis. In cells treated in the presence of Baf for 4 h, a small increase in the levels of LC3-II was detected (Figure 5.14.B). Therefore, LC3 may be involved in the formation of vesicles induced by the expression of myr-Htt_{N34}-EGFP.

Subsequently, the effect of Baf on the localization of RFP-LC3 in HeLa cells transiently expressing myr-Htt_{N34}-EGFP was explored.

Cathepsin B-BFP was included as a lysosomal marker to follow the effect of co-localization of myr-Htt_{N34}-EGFP and lysosomes. Cathepsin B is a luminal lysosomal protease (Nishimura et al., 1988) that can localize to lysosomal membranes when overexpressed (Sloane et al., 1994). In the absence of Baf little to no co-localization was detected between RFP-LC3 and myr-Htt_{N34}-EGFP-induced vesicles (Figure 5.14.A).

A

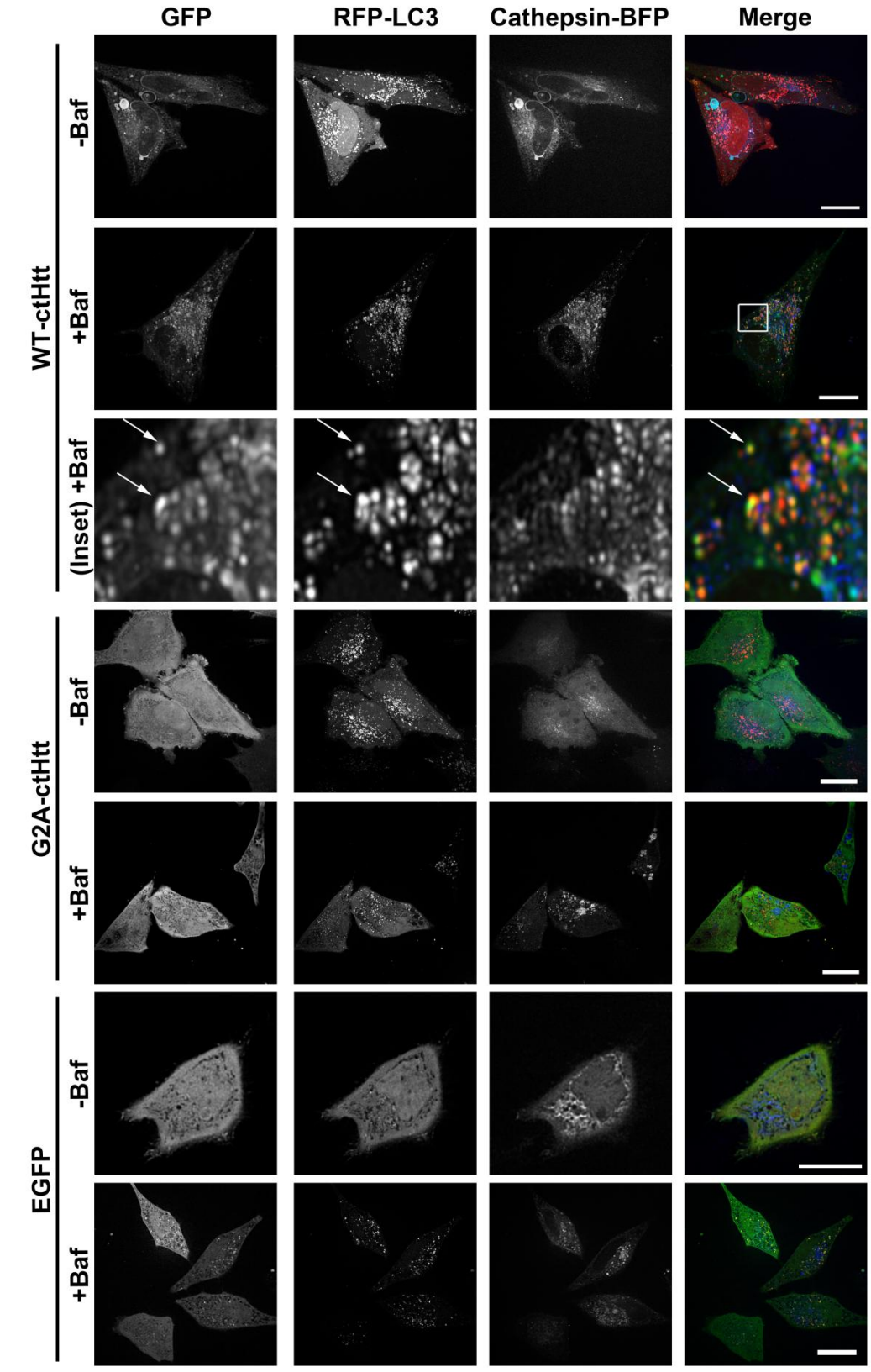
GFP
RFP-LC3
Cathepsin-BFP
Merge
WT-ctHtt
-Baf
+Baf
(Inset) +Baf
G2A-ctHtt
-Baf
+Baf
EGFP
-Baf
+Baf

B

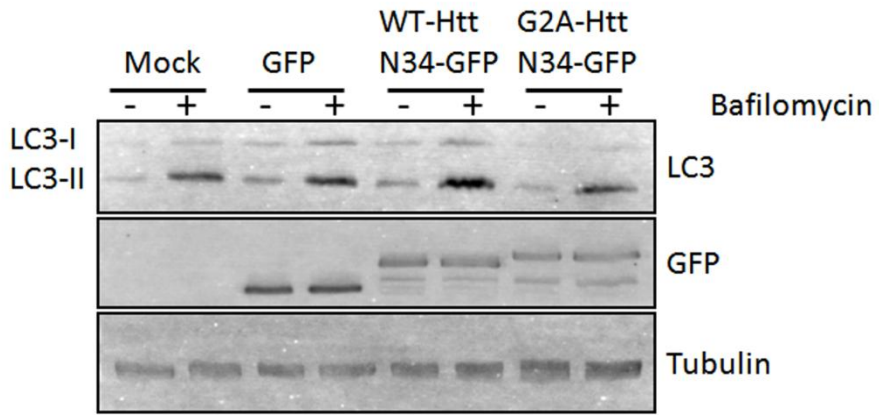

Figure 5.14. – Effect of bafilomycin on LC3 distribution and electrophoretic migration in HeLa cells expressing myr-Htt$_{N34}$-EGFP. **A** HeLa cells were transiently co-transfected with the lysosomal marker Cathepsin B-BFP and the autophagosomal marker RFP-LC3 for 24 h with the indicated EGFP constructs and treated with 0.5 µM Baf for an additional 24 h. Images were acquired by live cell fluorescence spinning disc microscopy and deconvolved using SVI Huygens Deconvolution software. Images are presented as 3D z-stacks. Scale bars represent 10 µm. **B** HeLa cells were transiently transfected with myr-Htt$_{N34}$-EGFP for 20 h and treated in the presence or absence of 0.5 µM Baf for 4 h. Cell lysates were subjected to SDS-PAGE and Western blot analysis. Tubulin is included as a loading control. PVDF membranes were scanned with a Storm 840 Phosphor imager in the Blue fluorescence mode following treatment with ECL Plus®.

However, there was a large degree of co-localization between myr-Htt_{N34}-EGFP and the lysosomal marker cathepsin B-BFP upon treatment of cells with Baf for up to 24 h a reversal of co-localization occurred (Figure 5.14A). More LC3-RFP co-localized in punctate structures that also contained myr-Htt_{N34}-EGFP (Figure 5.14.A, inset) and no co-localization was observed between myr-Htt_{N34}-EGFP and cathepsin-BFP. In addition, no large vesicles containing myr-Htt_{N34}-EGFP were detected in any cells treated with Baf for 24 h. The vesicles were always much smaller. These data suggest that the addition of Baf prevents the fusion of the myr-Htt_{N34}-EGFP-induced vesicles with lysosomes and that these vesicles are, in fact, autophagosomes. Therefore, it appears that myr-Htt_{N34}-EGFP induces the formation of autophagosomes in the absence of the characteristic inducers of autophagy such as starvation and may do so by stimulating heterotypic fusion between autophagosomes and lysosomes.

5.3. Discussion

Previously, using our tandem fluorescent protein reporter assay (TRAMPP; described in Chapter 4) we identified the N-terminal glycine residue that is exposed following caspase-3 cleavage of Htt as a target of post-translational myristoylation. In addition, our preliminary data suggests that a truncated version of Htt fused to YFP retaining both the caspase-3 and -6 cleavage sites could be cleaved in cells undergoing apoptosis and subsequently myristoylated (Figure 5.1.). This was specific for both caspase cleavage and myristoylation as shown by inhibition of myristoylation with either a general caspase inhibitor or the NMT inhibitor HMA. This suggests that caspase cleaved fragment of Htt is post-translationally myristoylated at Gly553. In addition, we have detected the presence of the endogenous HttN34 fragment in cultured HeLa cells (Figure 5.1.C) induced to undergo apoptosis. Currently, our lab is actively seeking to detect the presence of this fragment in normal and HD mouse brain lysates as well as to demonstrate the post-translational myristoylation of this endogenous fragment using click chemistry. The shared homology of this sequence shown in Table 5.1 suggests that this modification may be shared among many species.

In order to evaluate the effect of the myristoylated Htt fragment, we generated an EGFP chimera protein bearing the 33 amino acids between the two caspase sites excluding Asp586 to prevent caspase-6 cleavage,

and included an initiator methionine and a hydrophilic linker. Like the ctHtt-TRAMPP and Htt1-588-YFP, Htt_{N34}-EGFP was shown to be myristoylated. When viewed by fluorescence microscopy myristoylated Htt_{N34}-EGFP localized to ER (Figures 5.9.) and, surprisingly, induced the formation of small and large vesicular structures (Figures 5.4. - 5.14.), which was dependent on myristoylation. Electron microscopy demonstrated that the vesicles containing electron dense material were only present in cells expressing myr-Htt_{N34}-EGFP (Figure 5.7.B) and are reminiscent of autophagosomes in spite of their larger sizes (1-10 µm) in comparison to typical autophagosomes which range from 1-2 µm in size (Mohlig et al., 2007). Therefore, our data demonstrate that the vesicles detected by fluorescence microscopy are induced by the expression of the myristoylated Htt chimera and possibly represent vesicles that are a part of the autophagy pathway. Vesicles were not detected when myristoylation was abrogated by the substitution of the essential glycine to alanine (Figure 5.7.) or in the presence of the NMT inhibitor HMA (Figure 5.7.A).

The biogenesis of one of these enlarged vesicular structures is shown in Figure 5.4. It is also highly reminiscent of the formation of an autophagosome beginning with the tubulated structure and cup-shaped omegasome (Axe et al., 2008; Tanida, 2011). Eventually, the tubule circularized upon itself and formed a complete vesicle. This was also recapitulated in Figure 5.9.C in starved cells co-expressing myr-Htt_{N34}-

EGFP and ER-RFP. In this case, the formation of the myr-Htt_{N34}-EGFP-derived vesicles completely co-localized with ER-RFP. In addition to mitochondria and plasma membrane, the ER is also known as a donor of membranes during the formation of autophagosomes (Axe et al., 2008; Hailey et al., 2010; Ravikumar et al., 2010a). Because the ER is considered a major donor of membranes for autophagosomes (Axe et al., 2008), our results showing extensive co-localization of myr-Htt_{N34}-EGFP and ER-RFP during the biogenesis of the large vesicular structures, reminiscent of autophagosomes, suggest that myr-Htt_{N34}-EGFP induces the formation of the autophagocytic vesicles and that the ER acts as the membrane source. The fact that the size of these apparent autophagic vesicular structures is larger than typical autophagosomes or lysosomes (Figure 5.10.) early on in their biogenesis suggests a defect in the primordial control of vesicular morphology. The fact that myr-Htt_{N34}-EGFP induces the formation of autophagosome-related vesicular structures was further corroborated by the addition of Baf in the cells co-expressing myr-Htt_{N34}-EGFP, RFP-LC3 and cathepsin B-BFP (Figure 5.14.). In the absence of Baf, myr-Htt_{N34}-EGFP and cathepsin B-BFP almost completely co-localized whereas there was little to no co-localization of myr-Htt_{N34}-EGFP and RFP-LC3 suggesting that myr-Htt_{N34}-EGFP induces the formation of autophagosome-related vesicular structures that can eventually fuse with lysosomes to form autophagolysosomes. Upon the addition of Baf for 24 h, co-localization of myr-Htt_{N34}-EGFP with the two

markers studied was the opposite of what was first observed. First, when fusion of autophagosomes with lysosomes is abrogated by Baf, there was a marked increase in the co-localization between myr-Htt_{N34}-EGFP and RFP-LC3, which further supports the possibility that the vesicular structures containing myr-Htt_{N34}-EGFP are *bona fide* autophagosomes. Second, co-localization of myr-Htt_{N34}-EGFP with cathepsin B-BFP was completely lost when acidification of lysosomes was abrogated and the morphology of vesicles structures containing myr-Htt_{N34}-EGFP and cathepsin B-BFP was altered from large vesicular structures to small vesicles. This suggests that myr-Htt_{N34}-EGFP-induced autophagosome-related vesicles can no longer fuse with lysosomes and also indicates that the myr-Htt_{N34}-EGFP might have a fusogenic property that may promote the rate of heterotypic fusion between autophagosomes and lysosomes resulting in enlarged autophagolysosomes.

When HeLa cells (Figure 5.11.) or rat neuronal ST14A cells (Figure 5.13.) were transfected with myr-Htt_{N34}-EGFP and stained with MitoTracker® Orange CM-H_2TMRos to assess mitochondrial integrity, the mitochondria appeared fragmented and unhealthy compared to cells expressing EGFP or the non-myristoylated G2A-Htt_{N34}-EGFP. This suggests that overexpression of myr-Htt_{N34}-EGFP may be detrimental to cells.

This possibility that the fragmentation of mitochondria observed in cells expressing myr-Htt_{N34}-EGFP led to some sort of cytotoxicity was

confirmed when we showed that there was a highly significant decrease in mitochondrial potential as assessed by TMRE retention in HeLa cells myr-Htt_{N34}-EGFP in comparison to controls (Figure 5.12.). After 24 h of transient transfection, up to 11% fewer cells retained TMRE (EGFP compared to myr-Htt_{N34}-EGFP, p= 0.0002) thereby suggesting that the overexpression of myr-Htt_{N34}-EGFP leads to a loss of mitochondrial potential and eventually cell death. However, additional cell death assays will have to be performed to confirm that the decrease in TMRE is associated with cell death.

In addition, in both cell types fragments of mitochondria were detected inside the myr-Htt_{N34}-EGFP-induced vesicles (Figure 5.11.C and Figure 5.13.B). This further suggests that myr-Htt_{N34}-EGFP-induced vesicles are autophagosomes and may represent a particular form of autophagy specific for mitochondria referred to as mitophagy (Outlined in Figure 5.15.).

Overall, the data strongly suggest that myr-Htt_{N34}-EGFP induces the formation of autophagosomes. The prolonged build up of myr-Htt_{N34}-EGFP-induced autophagosomes appear to promote cell death (Figure 5.15.). Because HD is a slow progressing disease that occurs over a long period of time, the post-translational myristoylation of ctHtt at Gly553 may induce toxicity to cells over a long period of time. As mentioned previously,

A

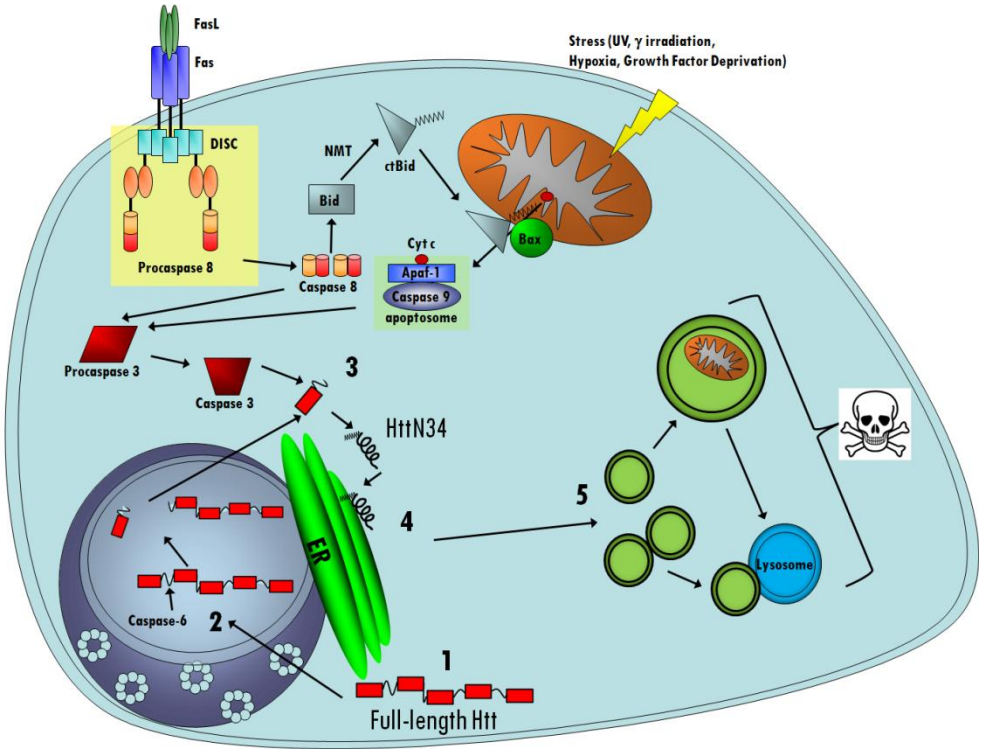
FasL
Fas
DISC
Procaspase 8
Caspase 8
NMT
Bid
ctBid
Stress (UV, γ irradiation,
Hypoxia, Growth Factor Deprivation)
Bax
Cyt c
Apaf-1
Caspase 9
apoptosome
Procaspase 3
Caspase 3
3
HttN34
4
5
Lysosome
ER
Caspase-6
2
1
Full-length Htt

B

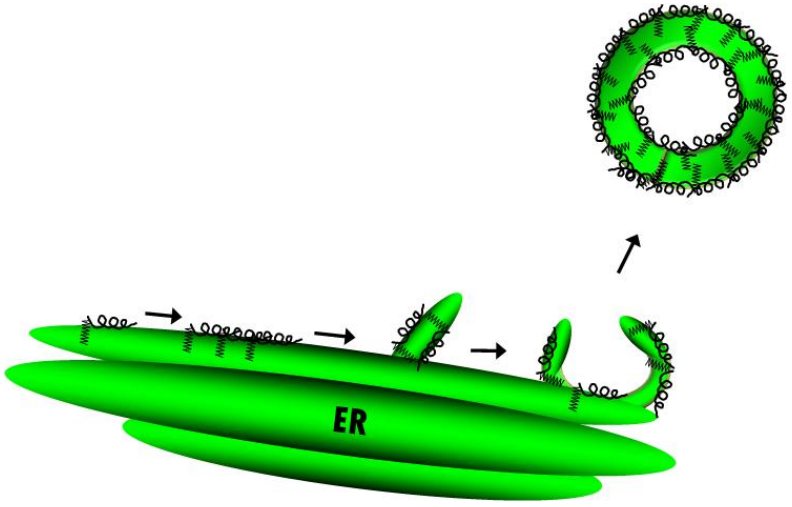
ER

Figure 5.15. – Outline of post-translational myristoylation of ctHtt$_{N34}$ and the formation of autophagosomal–like vesicles by myr-ctHtt$_{N34}$-EGFP. A Full-length Htt translocates to the nucleus (1) where it is cleaved at position 586 by caspase-6 (2). This releases the N-terminal Htt1-586, which translocates to the cytosol where it is cleaved by caspase-3 (3). Caspase-3 cleavage of Htt1-586 at position 552 results in the generation of the Htt$_{N34}$ that is post-translationally myristoylated and translocates to the ER (4, expanded in **B**). Subsequently, myr-ctHtt$_{N34}$ promotes the generation of autophagosomal-like vesicles that accumulate in the cell, envelop mitochondria and/or fuse with lysosomes (5). **B** Myr-ctHtt$_{N34}$-EGFP accumulates on the ER, where it may oligomerize with other molecules of myr-ctHtt$_{N34}$-EGFP to promote membrane curvature and form vesicles that originate from the ER. Myr-ctHtt$_{N34}$-EGFP may be found on the outer and inner leaflet of the vesicles.

caspase-3 and caspase-6 are constitutively active in the brain (Ehrnhoefer et al., 2011) and, therefore, would presumably lead to an accumulation of myr-Htt_{N34} and possibly contribute to the slow progression of the disease. Consequently, the post-translational myristoylation of Htt_{N34} may serve as a potential marker for HD or perhaps a therapeutic target in the future.

CHAPTER 6

DISCUSSION

6.1. Overview.

Since the discovery of post-translational myristoylation of the pro-apoptotic protein Bid over ten years ago (Zha et al., 2000), post-translational myristoylation is emerging as a regulator of apoptosis. The cytoskeletal protein actin, the actin-severing protein gelsolin and regulator of cytoskeletal dynamics PAK2 were subsequently identified as post-translationally myristoylated (Sakurai and Utsumi, 2006; Utsumi et al., 2003; Vilas et al., 2006). Ectopic expression of myr-ctGelsolin protected cells from undergoing etoposide-induced apoptosis and was therefore shown to be cytoprotective (Sakurai and Utsumi, 2006) while the function of myr-ctActin remains unclear (Utsumi et al., 2003). Like myr-ctBid, myr-ctPAK2 is pro-apoptotic when expressed in cells (Vilas et al., 2006). The effects of these proteins in cells are highly dependent on their myristoylation.

In each case, identification of the myristoylation sites required the use of [^{3}H]-myristic acid for labelling of proteins and detection by fluorography, which required weeks to months of exposure to acquire and constantly posed a health hazard.

6.2. Identification of new substrates for post-translational myristoylation using novel chemical biology techniques.

In order to circumvent the long waits associated with the use of radiolabeled fatty acids, we and other laboratories developed a number of non-radioactive techniques for the labeling of myristoylated proteins taking advantage of bio-orthogonal analogs of fatty acids that can be incorporated into proteins and selectively reacted with probes facilitating their detection (Charron et al., 2009; Hang et al., 2007; Hannoush and Arenas-Ramirez, 2009; Heal et al., 2008a; Heal et al., 2008b; Martin and Cravatt, 2009; Martin et al., 2008; Yap et al., 2010). Because the fatty acid analogs attached to proteins can be modified by biotinylating agents, these new techniques have the potential to ultimately be used for affinity purification using avidin-based technology and identification of co- and post-translationally myristoylated proteins. These approaches are being undertaken and optimized for myristoylation in the Berthiaume laboratory. Within this thesis I have described the development of the very specific reaction between an alkyl-azide and a phosphine using the Staudinger ligation (Figure 3.1.) which was exploited to detect myristoylation of various fatty acylated proteins (Martin et al., 2008). In this method, the isosteric and bio-orthogonal analog of myristate, azido-myristate (12 carbon with an ω-azido group; Az-C12), can be specifically incorporated co- or post-translationally into proteins at the N-terminal glycine residues of

various proteins. Subsequently, the azido moiety was chemoselectively ligated to triarylphosphines bearing FLAG or biotin and detected by western blotting with short exposure times to film [Figure 3.4; (Martin et al., 2008)]. For instance, detection of azido-myristoylated ctPAK2 in apoptotic Jurkat cell lysates was reduced from 2 months using [^{3}H]-myristic acid to one second after ligation and detection of the biotin-phosphine probe [Figure 3.5.; (Martin et al., 2008)]. This represented over a million-fold signal amplification in comparison to using radioactive labeling methods. This novel use of a myristate analog that can be chemically ligated to probes was shown to be specific for N-terminal glycine residues of exogenously expressed proteins (Yes-$_{N11}$-EGFP, FL-ctPAK2-EGFP, ctPAK2-$_{N15}$-EGFP; Figures 3.3 and 3.4,). Furthermore, as demonstrated with endogenous ctPAK2 in Jurkat T cells, the presence of the NMT inhibitor HMA prevented the incorporation of Az-C12, thereby proving that the analog relies on N-myristoyl transferases for its incorporation into N-terminal glycine residues of proteins [Figure 3.5; (Martin et al., 2008)].

In order to discover new post-translationally myristoylated proteins, from a review listing 280 caspase substrates we identified 48 protein candidates that exposed an N-terminal glycine after their caspase cleavage sites (Fischer et al., 2003). The complete C-terminal amino acid sequences downstream of the caspase cleavage sites of the 48 candidates were subjected to myristoylation prediction analysis using Myr Predictor and Myristoylator and 9 proteins were predicted to be

myristoylatable (Bologna et al., 2004; Eisenhaber et al., 2003) (Table 3.1.). Following an initiator methionine, the first ten amino acids of the C-terminal fragment of these 9 potential substrates were appended to the N-terminus of EGFP. Using metabolic labeling of COS-7 cells transiently expressing the chimeric GFPs with the Az-C12 analog, the incorporation of the Az-C12 into proteins was monitored by chemical labeling with a biotinylated triarylphosphine, as described in Chapter 3. Doing so, we identified 5 new post-translationally myristoylatable proteins [Protein Kinase C ε (PKCε), cytoplasmic dynein intermediate chain 2A (CD-IC2A), the pro-apoptotic protein Bap31, mammalian Ste-20 like kinase (MST3), and the catalytic subunit of glutamate cysteine ligase (GCLC)][Figure 3.7; (Martin et al., 2008)]. Because myristoylation is typically necessary and sufficient to exclude GFP from the nucleus (McCabe and Berthiaume, 1999), we used this exclusion criteria to assess whether our chimeric EGFPs were *bona fide* myristoylated proteins. We demonstrated that chimeric EGFP bearing N-terminal sequences of caspase cleaved fragments of PAK2, PKCε and CD-IC2A were extensively excluded from the nucleus while chimeras of Bap31, MST3 and GCLC led to little to no nuclear exclusion of EGFP (Figure 3.8.). Therefore, ctPAK2, ctPKCε and ctCD-IC2A chimeric EGFPs were assessed as strong candidates for myristoylation based on our criteria while the Bap31, MST3 and GCLC chimeric EGFPs may not be efficiently myristoylated or strong candidates for myristoylation. Critically, in our approach we originally used an

expression system relying on co-translational myristoylation to investigate and assess the post-translational myristoylation potential of caspase-cleaved protein sequences. Some of the observed discrepancies may thus be attributed, in part, to the substrate specificity of methionine aminopeptidase and its ability to remove the initiator methionine in these artificial substrates. Alternatively, post-translational myristoylation may rely selectively on one of the two NMT isoforms. Since NMT1 associates with ribosomes (Farazi et al., 2001) and thus may play a more predominant role in co-translational myristoylation, NMT2 might be the key NMT required for post-translational myristoylation. Supporting this possibility, immunoprecipitation studies have shown that NMT2 interacts with caspase-3 (Selvakumar et al., 2007). Therefore, the myristoylation of a protein normally post-translationally myristoylated by NMT2 might be difficult to assess using a co-translational expression system possibly relying preferentially on NMT1.

Consequently, we designed a post-translational assay to confirm the myristoylation status of the proteins identified above as well as to identify new post-translationally myristoylatable substrates. Our novel post-translational myristoylation assay was based on the co-translational assay using a tandem of fluorescent proteins described in Chapter 4. In this case, we replaced the initiator methionine in the original vector with the tdTomato fluorescent protein followed by a caspase cleavage site directly upstream of the Gly of putative myristoylation sequences attached

to GFP. As such, we have created a Tandem Reporter Assay for Myristoylation of Proteins Post-translationally and coined the acronym (TRAMPP) (Figure 4.1.A). This assay was combined with an updated chemical biology detection method developed in our lab and others (Charron et al., 2009; Martin and Cravatt, 2009; Yap et al., 2010) to discover new post-translationally myristoylatable substrates.

The newer detection method is based on a chemical ligation technique that relies on the Cu (I) – catalyzed [3+2] Huisgen cycloaddition reaction (commonly referred to as click chemistry) that uses an ω-alkynyl myristate analog (Alk-C14) and various azido-probes (Figure 4.1B) (Charron et al., 2009; Hannoush and Arenas-Ramirez, 2009; Martin and Cravatt, 2009; Yap et al., 2010). Like Az-C12, Alk-C14 is an isosteric analog of myristate that is readily taken up by cells and incorporated into proteins (Yap et al., 2010). Subsequently, the alkynyl moiety of the fatty acid analog can be covalently linked to an azido-probe using click chemistry (Figure 4.1.B).

By combining our post-translational TRAMPP assay with our highly sensitive detection method, we demonstrated that the newly exposed Gly residue of ctPAK2-N_{10}-EGFP released from pTRAMPP-ctPAK2 under apoptotic conditions could be specifically post-translationally myristoylated (Figure 4.2.). Furthermore, for the first time, we were able to visualise post-translational myristoylation of pTRAMPP-ctPAK2 as it occurred in live cells undergoing apoptosis (Figure 4.3.). In apoptotic pTRAMPP-ctPAK2

transfected cells, the caspase-cleaved myristoylated ctPAK2-N_{10}-EGFP fragment released from pTRAMPP-ctPAK2 specifically localised to the membranes of apoptotic bodies while the N-terminal fragment containing tdTomato remained cytosolic.

Since the identification of the new post-translationally myristoylatable substrates described above [Chapter 3; (Martin et al., 2008)], the number of identified caspase substrates with known caspase cleavage sites had increased from 280 (Fischer et al., 2003) to well over 400 (Dix et al., 2008; Luthi and Martin, 2007; Mahrus et al., 2008). Subsequently, the newly identified caspase substrates from these studies were investigated for their potential myristoylation as we did before using a combination of myristoylation prediction programs (e.g. Myr Predictor and Myristoylator) (Bologna et al., 2004; Eisenhaber et al., 2003). By doing so, we identified nearly a dozen new potential substrates for post-translational myristoylation in Table 4.1. These new substrates along with the five identified in the previous study [Chapter 3, (Martin et al., 2008)] were inserted into pTRAMPP and tested for post-translational myristoylation using click chemistry. As shown in Figure 4.4.A, we confirmed the myristoylation of ctCD-IC2A- and ctPKCε-N_{10}-EGFP while essentially eliminating ctBap31-, ctGCLC- and ctMst3-N_{10}-EGFP. In addition, we identified five new substrates for post-translational myristoylation including Huntingtin (Htt), cell division control protein 6 homolog (Cdc6), microtubule-actin crosslinking factor 1 (MACF1), the apoptotic regulator

induced myeloid leukemia cell differentiation protein (Mcl-1), and isoform 1 of YTH domain family protein 2 (YTHDF2) (Figure 4.4.).

Moreover, we also demonstrated the existence of at least 15 post-translationally myristoylated proteins in apoptotic Jurkat T cell lysates using the Staudinger ligation approach [Chapter 3, Figure 3.6. (Martin et al., 2008)], an observation our lab corroborated using click chemistry (Yap et al., 2010). Thus, the presence of numerous post-translationally myristoylated proteins in apoptotic cells suggests an underappreciated role for post-translational myristoylation in the regulation of cell death. Altogether these new techniques at the chemical biology forefront will accelerate the data acquisition process not only for myristoylated proteins but also for NMTs as well as other types of acylated and acylating proteins. In our specific case, the pTRAMPP vector will be invaluable to identify and validate newly discovered myristoylated proteins using computer based approaches as we did before or putative myristoylated proteins discovered using proteomic type approaches currently being carried out in the Berthiaume laboratory.

6.3. Potential roles of recently identified putative post-translationally myristoylated proteins in apoptosis.

Overall, our two screens identified 7 proteins that are strong candidates for post-translational myristoylation. They include an eclectic

assortment of proteins with various cellular functions such as regulators of apoptosis and cell signaling, molecular motors, and disease associated proteins, which are described below.

6.3.1. CD-IC2A

The CD-IC proteins are required for the interaction between cytoplasmic dynein and dynactin through binding of p150^{Glued}, via their N-termini. Dynein and dynactin regulate the secretory and endocytic pathways, microtubule organization at interphase, and the ER serves as cargo for cytoplasmic dynein in *Xenopus* egg extracts. During apoptosis, CD-IC2A is cleaved within the p150^{Glued} binding domain, but remains associated with the heavy and intermediate light chains of dynein, probably via its overlapping WD-40 repeats (Lane et al., 2001). Very interestingly, light chain 8 of dynein associates with the pro-apoptotic protein Bcl-2 interacting mediator of cell death (Bim) in normal cells and during apoptosis this complex translocates to membranes of various organelles, including mitochondria, where it binds and inhibits BCL-2 or functional homologs (Puthalakath et al., 1999). Alternatively, during apoptosis, molecular motors promote the perinuclear clustering of mitochondria, which promotes apoptosis (Aslan and Thomas, 2009). It is possible that myr-ctCD-IC2A may be involved in either of these processes to direct the progression of apoptosis.

6.3.2. Mcl-1

In the case of anti-apoptotic full-length Mcl-1, cleavage leads to the release of a pro-apoptotic fragment that interacts with tBid and associates with the VDAC at the mitochondria to promote an open pore conformation and to promote the release of cytochrome c and, therefore, apoptosis (Martin et al., 2010; Weng et al., 2005; Zha et al., 2000). It would be pertinent to verify the detection of myr-ctMcl-1 at the mitochondria or in association with myr-ctBid. Interestingly, even though the anti-apoptotic myr-ctGelsolin was shown to be cytosolic, ctGelsolin has been shown previously to interact with VDAC to promote a closed formation to protect against apoptosis (Koya et al., 2000; Kusano et al., 2000). Thus, along with myr-ctBid it would appear that post-translational myristoylation may promote the association with the VDAC at the mitochondria, perhaps via an association with cardiolipin (Martin et al., 2010; Wright et al., 2004). Although no specific function for myr-ctActin has been assigned, it too has been shown to translocate to the mitochondria (Utsumi et al., 2003). It may interact at the VDAC to regulate apoptosis as well. Therefore, post-translational myristoylation may provide mitochondrial targeting information to some proteins to regulate VDAC pore formation.

6.3.3. Cdc6

Cdc6 is an essential initiation factor for DNA replication. It contains two caspase-3 cleavage sites (D290S and D442G) that produce either a 32 or 49 kDa N-terminal fragment, respectively (Yim et al., 2006; Yim et al., 2003). The putatively myristoylated 13 kDa C-terminal domain released from the 49 kDa fragment contains the nuclear export signal. Although the N-terminal 49 kDa fragment has been shown to promote apoptosis in HeLa cells (Yim et al., 2003), the effect of the C-terminal domain on apoptotic cells is unknown. However, the lipid moiety may act as a signal to remove the C-terminal fragment from the N-terminal fragments, which could lead to the promotion of apoptosis by the N-terminal fragments, which remain in the nucleus following cleavage (Yim et al., 2006).

6.3.4. MACF1

MACF1 is a multidomain protein that can associate with microfilaments and microtubules. It has been shown to play a role in Wnt signaling. MACF associates with the complex containing Axin, β-catenin, APC and GSK3β. Upon Wnt binding to the receptor Frizzled and its co-receptor LRP-5/6, MACF1 is involved in the translocation of the complex containing Axin, β-catenin, and GSK3β, but not APC from the cytosol to the plasma membrane thereby allowing release of β-catenin, which translocates to the nucleus where it activates Wnt-responsive genes (Chen et al., 2006). MACF1 is cleaved by caspases within the spectrin

repeats (Dix et al., 2008). Based on a study evaluating the binding of truncated forms of MACF1 to the Axin complex, the remainder of ctMACF1 contains all the binding elements required to associate with Axin, APC, β-catenin and GSK3β, but not the co-receptor LRP-5/6 (Chen et al., 2006). Theoretically, ctMACF1 could still associate with the Axin complex, but not the receptor, which is required for the release of β-catenin and the translocation of β-catenin to the nucleus where it activates Wnt-responsive genes. Therefore, cleavage of MACF1 would prevent activation of Wnt signaling genes, which are required for development, cell movement and polarity. However, it is unclear what effect cleavage and post-translational myristoylation of ctMACF1 would have on Wnt signaling during apoptosis.

6.3.5. PKCε

Like PAK2, caspase cleavage of PKCε releases the regulatory N-terminal domain from the kinase domain and leads to a constitutively active kinase (Basu et al., 2002). In Chapter 4, we demonstrated that exogenously expressed ctPKCε-HA specifically incorporates the Az-C12 analog. Myr-ctPKCε-HA localized to the plasma membrane, Golgi and ER while its non-myristoylated counterpart G2A-ctPKCε-HA remained primarily diffuse within the cell (Figure 4.6. and 4.7.). Transient transfection of myr-ctPKCε-HA lead to an increase in Erk signaling, which correlated with an increase in phosphorylation of the pro-apoptotic proteins Bim and Bad at Ser69 and Ser112, respectively (Figure 4.8.).

Phosphorylation of Bim at Ser69 has been shown to lead to degradation of Bim by the proteasome (Luciano et al., 2003). Of particular note, in the presence of the MEK inhibitor U0126, the levels of Bim in cells expressing G2A-ctPKCε-HA were much greater than in WT-ctPKCε-HA expressing cells (Figure 4.8.B). This may suggest that ctPKCε-HA may phosphorylate Bim through different pathways based on its myristoylation status. For instance, JNK can also lead to Bim phosphorylation, which is associated with increased cell death (Lei and Davis, 2003; Ley et al., 2005; Putcha et al., 2003).

Phosphorylation of Bad at Ser112 acts as a binding site for 14.3.3. proteins, which sequesters Bad from mitochondria to prevent cell death (Tan et al., 1999). Therefore, phosphorylation of Bim and Bad should protect the cell from cell death by maintaining the integrity of the mitochondrial membrane. In fact, FACS analysis of HeLa cells transiently expressing myr-ctPKCε-HA demonstrated that cells retain more of the potentiometric dye TMRE than when expressing G2A-ctPKCε-HA or vector alone. This trend was seen in non-apoptotic cells and was significant in cells induced to undergo cell death with anti-Fas (Figure 4.9.). This suggests that myr-ctPKCε-HA protects cells from cell death by maintaining mitochondrial integrity through phosphorylation and inactivation of the pro-apoptotic proteins Bim and Bad (Outlined in Figure 4.10.).

6.3.5.1. - Future Directions for myr-ctPKCε-HA

Due to ineffective immunoprecipitations using commercially available antibodies, post-translational myristoylation of endogenous ctPKCε could not be assessed. Therefore, we will attempt to remedy this in two ways. First, we have had great success performing immunoprecipitations with antibodies generated in the Berthiaume laboratory. Therefore, we are currently in the process of designing antigenic peptides corresponding to ctPKCε for antibody production. Alternatively, the Berthiaume laboratory is working on affinity purification of post-translationally myristoylated proteins.

Based on the difference of Bim levels between cells expressing myristoylated and non-myristoylated ctPKCε-HA (Figure 4.8.A), especially in the presence of the MEK inhibitor (Figure 4.8.B), and the fact that JNK can also phosphorylate Bim at Ser69, it would be of interest to perform similar studies using JNK inhibitors. Alternatively, we could use siRNA to down regulate JNK and/or Erk to study the effects of phosphorylation of Ser69 of Bim in the presence of the myristoylated or non-myristoylated forms of ctPKCε-HA. In addition, co-transfections including ctPKCε-HA and EGFP-Bim_{EL} can be used in the presence and absence of these inhibitors and siRNA to study the effects on the phosphorylation of Ser69 of Bim and the subsequent degradation of Bim. Moreover, these studies can be done in the presence or absence of proteasomal inhibitors to

prevent the degradation of Bim_{EL}. Finally, mitochondrial integrity of cells co-expressing EFGP-Bim_{EL} and ctPKCε-HA can be measured by FACS analysis as shown in Chapter 4 (Figure 4.10.) or by microscopy.

6.3.6. Huntingtin

In contrast to myr-ctPKCε-HA, we found the post-translationally myristoylated fragment of Htt553-586 (Htt_{N34}) to have a cytotoxic effect on cells (Chapter 5). Herein, we identified the newly exposed Gly released by caspase-3 cleavage found at position 553 of Htt to be myristoylated using the TRAMPP assay (Figure 4.4.). Subsequently, we showed that post-translational myristoylation of Htt_{N34} released by a truncated Htt construct Htt1-586-YFP was both caspase and NMT dependent (Figure 5.1).

Subsequently, we used ctHtt_{N34}-EGFP to further confirm myristoylation of Htt_{N34} (Figure 5.2.) and assess the contribution of myristoylation to the localization of Htt_{N34}. Surprisingly, the exogenous expression of myr-ctHtt_{N34}-EGFP led to the formation of vesicles of various sizes in HeLa cells that co-localized with the ER and lysosomes (Figures 5.8. and 5.9.). The biogenesis of the vesicles was highly reminiscent of that of an autophagosome (Figure 1.5. and Figure 5.5.). Further evidence that myr-ctHtt_{N34}-EGFP induces the formation of autophagosomes was provided by the co-localization of myr-ctHtt_{N34}-EGFP and ER-RFP in starved HeLa cells (Figure 5.9.B). ER represents a major membrane contributor to autophagosomes (Axe et al., 2008). Autophagosomes

eventually fuse with lysosomes (Ravikumar et al., 2010a), much like we see with the near complete co-localization of myr-ctHtt$_{N34}$-EGFP with the lysosome markers Lysotracker Red®, LAMP1-RFP (Figure 5.10.) and cathepsin B-BFP (Figure 5.14.). The fusion between autophagosomes can be blocked by the addition of bafilomycin (Klionsky et al., 2008b; Tanida, 2011). The addition of bafilomycin to HeLa cells expressing myr-ctHtt$_{N34}$-EGFP and the lysosomal marker cathepsin B-BFP completely abrogated co-localization between the two proteins (Figure 5.13.). Moreover, the addition of bafilomycin increased the co-localization between myr-ctHtt$_{N34}$-EGFP and the autophagosomal marker RFP-LC3 (Figure 5.13.). Therefore, it appears that the myr-ctHtt$_{N34}$-EGFP-induced vesicles are, in fact, autophagosomes. This is supported by the fact that mitochondria were detected inside the myr-ctHtt$_{N34}$-EGFP-induced vesicles in both HeLa cell and the rat neuronal ST14A cells (Figure 5.10. and 5.12.). Autophagy is typically considered to be a cytoprotective process, which operates by delivering toxic or aggregated proteins, damaged organelles and sometimes viruses or bacteria to the lysosome for degradation (Todde, Veenhuis et al. 2009; Chen and Klionsky 2011). However, although the overexpression of myr-ctHtt$_{N34}$-EGFP promoted the formation of what appeared to be autophagosomes, myr-ctHtt$_{N34}$-EGFP nonetheless promoted loss of mitochondrial potential in HeLa cells (Figure 5.11), suggesting that its expression may impede the removal of damaged mitochondria, alter their membrane potential indirectly (since there was no

co-localization with mitochondria) and potentially be toxic to cells. This is perhaps mediated by an overproduction of 'immature' autophagosomes, which can still promote type II programmed cell death (Todde, Veenhuis et al. 2009; Chen and Klionsky 2011).

Mechanistically speaking, how myr-ctHtt induces the formation of these autophagosome-like vesicles remains unclear. One possible explanation includes increased recruitment of PI3K complexes or other members of the autophagy machinery to the phagophore assembly site (PAS) to serve as the platform for autophagosome formation [Chapter 1, (Axe et al., 2008; Tanida, 2011)]. Alternatively, the binding of myr-ctHtt$_{N34}$-EGFP to the ER may initiate the promotion of membrane curvature that may be a prerequisite for PAS formation. Myr-ctHtt$_{N34}$-EGFP may act as a membrane sensing curvature (MCS) protein, which include amphipathic α-helical proteins and acylated proteins that play a role in ER morphology (Barlowe, 2010; Cui et al., 2011; Shibata et al., 2010). MCS proteins can be inserted into membranes of high curvature, or can promote membrane curvature upon binding to membranes (Cui et al., 2011). As such, myr-ctHtt$_{N34}$-EGFP may insert its myristoylated moiety and hydrophobic residues into the curved membranes of the ER (Figure 5.15.). As myr-ctHtt$_{N34}$-EGFP builds up on a curved membrane the myr-ctHtt$_{N34}$-EGFP molecules may associate with one another and further promote increased curvature of the membrane (Figure 5.15.). This may act to promote autophagy by serving as a platform for the PAS as suggested above or myr-ctHtt$_{N34}$-EGFP-induced vesicles may act independently of autophagy

but mediate the engulfment of mitochondria (Figures 5.11. and 5.13.), especially because of the often close association of mitochondria and the ER. It is important to note that overexpression of some ER-resident proteins can induce the ER to transform from a network of branching tubules into stacked membrane arrays termed organized smooth ER (OSER). Overexpression of these OSER-inducing proteins can lead to stacks of paired membranes closely associated with the nuclear envelope termed 'karmellae' or spirals of ER referred to as 'whorls' (Snapp et al., 2003; Wright et al., 1988). However, the immunoelectron microscopy results presented in Figure 5.7B, which clearly indicated the formation of vesicles and no whorls or karmellae, suggest that the formation of OSER apparently does not occur when overexpressing myr-ctHtt$_{N34}$-EGFP in HeLa cells.

Alternatively, myr-ctHtt$_{N34}$-EGFP may promote cell death through paraptosis. Paraptosis is associated with extensive cytoplasmic vacuolation, ER swelling and mitochondrial swelling with an absence of caspase activation and nuclear changes (Kar et al., 2009; Sperandio et al., 2000).

Expression of full length Htt protein has been associated with ER stress (Atwal and Truant, 2008; Atwal et al., 2007) (Vidal et al., 2011) and ER stress response has recently been linked to autophagy (de Haan et al., 2010). It is possible that myr-ctHtt$_{N34}$-EGFP may cause an upregulation of proteins that regulate the unfolded protein response (UPR). The UPR is a

pathway that responds to perturbations in endoplasmic reticulum (ER) homeostasis. It is regulated by one master regulator Bip, which binds and inactivates transducers of the UPR (Bertolotti et al., 2000; Breckenridge et al., 2003; Zhang and Kaufman, 2004).

Dilated ER and ER stress is also associated with Russell bodies. Russell bodies are dilated ER cisternae containing condensed mutated immunoglobulins that are neither secreted nor degraded (Kopito and Sitia, 2000). These can be identified by containing Calnexin, but lacking soluble ER proteins such as BiP, PDI or ERp72 (Kopito and Sitia, 2000).

6.3.6.1. Future Directions for ctHtt

Future studies to confirm that myr-Htt_{N34}-EGFP-induced vesicles are autophagosomes will include transmission EM of cells sorted specifically for GFP expressing cells to look for double-membraned vesicles, which are representative of autophagosomes, in myr-Htt_{N34}-EGFP expressing cells. To determine how myr-Htt_{N34}-EGFP may be inducing autophagy HeLa and ST14A cells transiently expressing myr-Htt_{N34}-EGFP will be treated with various pharmacological inhibitors and activators of autophagy including wortmannin, 3-methyladenine and rapamycin and observed by fluorescence microscopy to determine if vesicles continue to form. Wortmannin and 3-methyladenine are inhibitors of PI-3K and, therefore, inhibit autophagy. In contrast, rapamycin inhibits

the inhibitor of autophagy mTOR and, consequently, activates autophagy. In addition to vesicle formation, LC3-II levels will also be followed to determine levels of autophagy induction. Alternatively, there is a mRFP-GFP-tandem fluorescent protein-LC3-colour change assay that can be employed, which is based on the difference in stability between mRFP and GFP under acidic conditions (Kimura et al., 2007; Klionsky et al., 2008b). Autolysosomes have a lower pH than autophagosomes and mRFP is stable under either condition whereas GFP stability decreases under acidic conditions. Therefore, the reporter protein appears yellow in autophagosomes and only red in autolysosomes (Kimura et al., 2007; Klionsky et al., 2010). A blue fluorescent protein tagged version of myr-Htt_{N34} will be generated and used in conjunction with the LC3-tandem reporter protein. As above, bafilomycin will also be used to prevent fusion between autophagosomes and autolysosomes. In addition, a smaller HA tag will also be appended to $ctHtt_{N34}$ to ensure that the vesiculation seen with myr-$ctHtt_{N34}$-EGFP is independent of the EGFP tag.

In order to determine how myr-$ctHtt_{N34}$-EGFP may be inducing cell death, we will use various markers of paraptosis, apoptosis and ER stress. For instance, PARP cleavage is a common marker for apoptosis, but it is also cleaved during paraptosis, but PARP cleavage fragments differ between the two cell death pathways (Galluzzi et al., 2009; Sperandio et al., 2000). In addition, during apoptosis, caspases are cleaved, but not

during paraptosis. These markers will be evaluated by western blotting in the presence or absence of the appropriate inducers of cell death.

In addition, the E3-ubiquitin ligase Parkin translocates from the cytosol to mitochondria with low mitochondrial membrane potential to induce mitophagy. Fluorescently tagged Parkin will be used in conjunction with myr-Htt_{N34}-EGFP to identify damaged mitochondria (Klionsky et al., 2010; Narendra et al., 2008). In order to further assess the potential toxicity of the post-translational myristoylation of Htt_{N34}, cells will be transfected with truncated versions of Htt from amino acids 1-585 bearing Gly to Ala mutations to prevent myristoylation. Both wild type and the poly Q mutant Htt will be used.

During ER stress the levels of expression and activation of its key effectors including BiP/GRP78, GRP94, and XBP1 as well as the cleavage of CHOP (Schroder and Kaufman, 2005) can be visualized by western blotting.

Of particular importance, we will evaluate the potential contribution of myr-$ctHtt_{N34}$ to the formation of Htt aggregates in HeLa cells and rat ST14A cells by expressing full-length wildtype Htt and mutant Htt with an extended polyglutamine tract that can be cleaved by caspase-3, but not myristoylated by substituting the N-terminal glycine to alanine. We will also generate a caspase-6 non-cleavable version to assess whether the myr-$ctHtt_{N34}$ can still form vesicles in the presence of the extended C-terminus. We can follow the generation of $ctHtt_{N34}$ fragment in these experiments

using the neo-epitope antibody that is specific for the C-terminus of $ctHtt_{N34}$, as shown in Figure 5.1.C. In addition, we will use this antibody for the detection of of $ctHtt_{N34}$ in human brain lysates with HD and normal human brains lysates post-necropsy. In this way, we will be able to compare the levels of $ctHtt_{N34}$ between normal and diseased tissues. This will allow us to assess how the levels of $ctHtt_{N34}$ correlate to the disease phenotype.

6.4. On the prevalence of post-translationally myristoylated proteins.

During the studies described herein, the number of known caspase substrates has increased from 280 (Fischer et al., 2003) to well over 400 (Dix et al., 2008; Luthi and Martin, 2007; Mahrus et al., 2008). Likewise, the number of cleaved protein products with N-terminally exposed glycine residues has increased from 48 to 72. This accounts for ~17% of all the known caspase substrates, suggesting that many more potential substrates for post-translational myristoylation may exist. In addition, a recent study looking at preferred caspase cleavage sites demonstrated that glycine was the most favoured amino acid adjacent to the aspartate residue (DXXDG) further strengthening the idea that more post-translationally myristoylated substrates exist (Mahrus et al., 2008). Unfortunately, in the same study (Mahrus et al., 2008) the technique used for the labelling, affinity purification and identification of caspase-cleaved

proteins by mass spectrometry relied on subtiligase, a modified form of the bacterial protease subtilisin BPN, which can perform ligation of peptides. Unfortunately, subtiligase requires a free N-terminus for its activity and, therefore, myristoylation would abrogate the addition of an affinity purification tag by subtiligase and prevent the identification of post-translationally myristoylated proteins by this method. Therefore, this method may have missed post-translationally myristoylated proteins that remain to be identified.

The eventual combination of a post-translational myristoylation detection assay and click chemistry with azido-probes will lead to the identification and characterization of many more post-translationally myristoylated proteins. These pull-down methods are currently being optimized in the Berthiaume laboratory.

6.5. New regulatory roles for myristoylation during cell death and development.

The fact that some post-translationally myristoylated proteins promote apoptosis (myr-ctBid, myr-ctPAK2, and myr-ctHtt$_{N34}$) (Vilas et al., 2006; Zha et al., 2000) while others prevent it (myr-ctGelsolin and myr-ctPKCε) (Sakurai and Utsumi, 2006) is paradoxical and suggests antagonistic roles for post-translational myristoylation. This again suggests

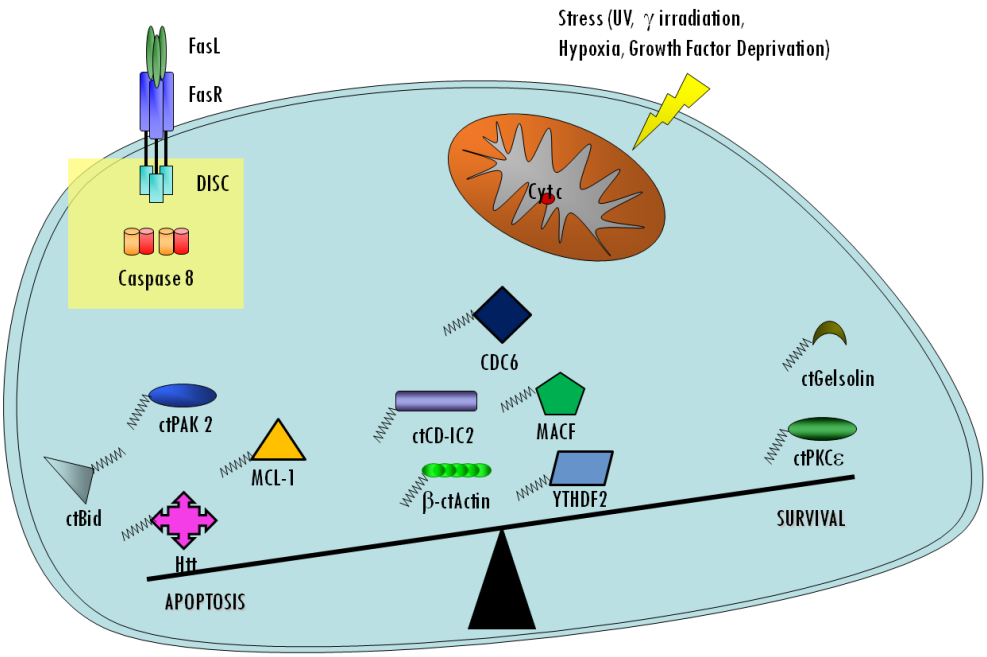

Figure 6.1. - Effect of post-translationally myristoylated proteins on cell death and survival. To date, eleven substrates for post-translational myristoylation have been identified; seven of which have been identified in this study. For the proteins whose functions have been characterized, three have been shown to promote apoptosis or have a cytotoxic effect in cells (ctBid, ctPAK2 and ctHtt. ctMcl-1 is included as pro-apoptotic based on previous studies on ctMcl-1. These studies did not look at myristoylation of Mcl-1 (Weng et al., 2005)) while two more have been shown to have protective effects against apoptotic induction (ctGelsolin and ctPKCε). In every case, the effect of the caspase cleaved proteins is highly dependent on myristoylation. This paradoxical situation suggests that post-translational myristoylation plays a more diverse role in cell fate than previously thought.

a potential regulatory role for post-translational myristoylation in cell death and survival (Figure 6.1.).

The final outcome may be decided by the identity and function of newly post-translationally myristoylated proteins. In addition, the fact that caspases are active and essential for cell proliferation and differentiation in various cell lines may suggest a potential involvement of post-translationally myristoylated proteins in the developmental context as well (Droin et al., 2008; Fujita et al., 2008; Lamkanfi et al., 2007; Schwerk and Schulze-Osthoff, 2003). For example, caspase-8 activity was shown to be required for the differentiation of monocytes into macrophages and PAK2 has been proven to be cleaved in a caspase-dependent manner, at what appears to be at very low levels in those cells during this process (Cathelin et al., 2006). Excitingly, alkyne-myristate labelling of differentiating U937 cells suggests that ctPAK2 is in fact post-translationally myristoylated under these conditions (unpublished results from our laboratory). Furthermore, gelsolin is also cleaved during the differentiation of megakaryocytes (De Botton et al., 2002). It seems likely that these proteins would be post-translationally myristoylated in these contexts. Again, myr-ctGelsolin may aid in cell survival while myr-ctPAK2 may promote cytoskeletal or morphological changes required for both apoptosis and differentiation, depending on the level of cleavage or activation of myr-ctPAK2. Differentiation and proliferation may provide yet another potential pool of post-translationally myristoylated proteins to

discover and another level of cellular regulation by NMTs and myristoylation.

Because cancer occurs due to mutations of various components of the apoptotic machinery and thereby avoiding cell death, in addition to over proliferation, we postulate that post-translational myristoylation may play an important role in cancer progression. Moreover, because different components of the apoptotic pathway are affected we think that the post-translational myristoylation profiles may differ between cancers and between normal versus cancer cells. Therefore, our laboratory is currently working to establish the post-translational myristoylation profiles of various normal and cancer cells. As such, we predict that we will identify more important regulators of apoptosis and make key contributions towards a better understanding of cancer.

6.6. CONCLUSION.

Myristoylation has been known to play an important role in a myriad of processes within the cell and, as described herein, several new aspects of myristoylation have emerged within the last decade. One of the most rapidly expanding areas of myristoylation in the upcoming years will involve the identification of post-translationally myristoylated proteins following caspase cleavage during apoptosis, proliferation or development (Martin et al., 2008; Sakurai and Utsumi, 2006; Utsumi et al., 2003; Vilas

et al., 2006; Yap et al., 2010; Zha et al., 2000). These proteins are proving to have important roles in apoptosis that are intricately linked to their post-translational myristoylation. So far, apoptosis induced by myr-ctBid and myr-ctPAK2 can be significantly reduced by abrogating myristoylation of these proteins (Vilas et al., 2006; Zha et al., 2000). In addition, the vesicles produced by myr-ctHtt$_{N34}$-EGFP were completely dependent on myristoylation. Paradoxically, the anti-apoptotic effect of myr-ctGelsolin and myr-ctPKCε is also linked to their myristoylation statuses (Sakurai and Utsumi, 2006). This suggests that there may be dual roles for post-translationally myristoylated proteins. It is possible that some proteins promote cell survival until the cell has reached an apoptotic threshold and has committed to cell death. Alternatively, some of the pro-survival factors may have a greater role in cell differentiation and proliferation where caspase cleavage is essential and at least PAK2 and gelsolin are targets for caspase cleavage and most likely post-translationally myristoylated (Cathelin et al., 2006; De Botton et al., 2002). With PAK2, it appears that the level of cleavage is not as great in differentiating cells as in apoptosis, which may suggest that lower levels of constitutively active myr-ctPAK2 in differentiating cells may not be toxic or is tightly regulated to prevent apoptosis (Cathelin et al., 2006; Vilas et al., 2006). As such, it may provide a structural role in differentiation and proliferation while myr-ctGelsolin would act as a pro-survival factor in this scenario.

Several new findings suggest that there remains many more, as of yet, unidentified co- and post-translationally myristoylated proteins. For instance, in a cell free rabbit reticulocyte lysate assay described by Utsumi's group identified 1.4% of the proteins as myristoylated of the 1929 proteins in the query proteome they investigated (Suzuki et al., 2010). Therefore, this may suggest that the myristoylome is larger than previously predicted (0.5%) (Maurer-Stroh et al., 2002a; Maurer-Stroh et al., 2002b). Interestingly, and of particular note, they found that the two commonly used prediction analysis programs used for myristoylation were strong predictors of myristoylation. However, while Myr Predictor (Eisenhaber et al., 2003) had more false-negative predictions, Myristoylator (Bologna et al., 2004) had more false-positive predictions, and both programs missed two proteins that were shown to be myristoylated (Suzuki et al., 2010). This demonstrates the importance of testing for myristoylation *in vitro* and *in vivo.* Again, this suggests that there may be some potential substrates overlooked in our studies. Some of the more interesting candidates that were eliminated by the prediction analysis programs may be inserted into our pTRAMPP vector and assessed for post-translational myristoylation in the future.

In the future, we will perform an "unbiased" screen independent of the *in silico* myristoylation prediction analysis step. In that screen, all sequences starting with a Gly residue after their caspase cleavage site will be converted to a pair of oligonucleotides, cloned into pTRAMPP and

tested for myristoylation *in cellulo*, as above. The rationale for this "unbiased" screen is that some candidates for myristoylation might have been missed depending on the accuracy of the myristoylation algorithms (Bologna et al., 2004; Eisenhaber et al., 2003). Should any new substrates emerge from our screen, this could mean that the substrate specificity of the NMTs may be altered in apoptotic cells and cannot be efficiently predicted by current algorithms. Analysis of the new myristoylated sequences will also give us insights into NMT substrate specificities during apoptosis, which could therefore lead to updated prediction analysis programs.

Furthermore, we also showed that there is a clear difference in the cellular contents of co- and post-translationally myristoylated proteins in non-apoptotic and apoptotic Jurkat T cells (Figure 3.2, 3.5 and 3.6) and the identification of these myristoylated proteins awaits. Moreover, the fact that several studies have demonstrated that the preferred amino acid following caspase cleavage sites is glycine, further suggests the existence of more potential sites for post-translational myristoylation. In addition, cryptic myristoylation sites might also be found downstream of other proteolytic sites (e.g. calpain, Granzyme B, cathepsins, etc.). Using chemical biology as a means to speed up detection and isolation of post-translationally myristoylated proteins, the first proteomic analyses of the post-translational-"myristoylomes" of normal and metabolically compromised cells should emerge in the near future.

The chemical biology methods described herein will significantly accelerate the field of myristoylation by decreasing the detection time required for myristoylated proteins from months to near instantaneous. Furthermore, we have identified 7 new substrates for post-translational myristoylation during apoptosis thereby almost tripling the amount of known post-translationally myristoylated proteins from 4 to 11 (Figure 6.1). Moreover, we have touched on the effects of two of these proteins. Myr-ctPKCε-HA was shown to protect mitochondrial integrity and, conversely, myr-ctHtt$_{N34}$-EGFP may have a cytotoxic effect by inducing the formation of autophagosomes and may ultimately contribute to Huntington's disease.

Such proteomics studies have helped delineate new roles for myristoylation of proteins and will continue to do so as we work to further describe the roles of the remaining substrates identified in this study. Indeed, we have shown that many post-translationally myristoylated proteins are found in the cytosol while most co-translationally myristoylated proteins were found attached to membranes (Figure 3.6.). This suggests that myristoylation of proteins may serve additional roles other than membrane tethering during apoptosis.

Because post-translational myristoylation occurs in apoptotic cells and apoptosis is often deregulated in cancer and neurodegenerative diseases (Evan and Vousden, 2001; Leist and Jaattela, 2001; Thompson, 1995), the importance of identifying and characterizing post-translationally myristoylated proteins is undeniable. A better understanding of novel

molecular components involved in apoptosis will not only offer insights into pathogenesis but could also allow for the development of diagnostic, prognostic and therapeutic tools. This study has set the groundwork for future work in these areas.

CHAPTER 7

BIBLIOGRAPHY

Ai, H. W., Hazelwood, K. L., Davidson, M. W. and Campbell, R. E. (2008). Fluorescent protein FRET pairs for ratiometric imaging of dual biosensors. *Nat Methods* **5**, 401-3.

Aitken, A., Cohen, P., Santikarn, S., Williams, D. H., Calder, A. G., Smith, A. and Klee, C. B. (1982). Identification of the NH2-terminal blocking group of calcineurin B as myristic acid. *FEBS Lett* **150**, 314-8.

Akita, Y. (2002). Protein kinase C-epsilon (PKC-epsilon): its unique structure and function. *J Biochem* **132**, 847-52.

Altschul, S. F., Madden, T. L., Schaffer, A. A., Zhang, J., Zhang, Z., Miller, W. and Lipman, D. J. (1997). Gapped BLAST and PSI-BLAST: a new generation of protein database search programs. *Nucleic Acids Res* **25**, 3389-402.

Ames, J. B., Tanaka, T., Stryer, L. and Ikura, M. (1996). Portrait of a myristoyl switch protein. *Curr Opin Struct Biol* **6**, 432-8.

Amor, J. C., Harrison, D. H., Kahn, R. A. and Ringe, D. (1994). Structure of the human ADP-ribosylation factor 1 complexed with GDP. *Nature* **372**, 704-8.

Antonsson, A. and Persson, J. L. (2009). Induction of apoptosis by staurosporine involves the inhibition of expression of the major cell cycle proteins at the G(2)/m checkpoint accompanied by alterations in Erk and Akt kinase activities. *Anticancer Res* **29**, 2893-8.

Armah, D. A. and Mensa-Wilmot, K. (1999). S-myristoylation of a glycosylphosphatidylinositol-specific phospholipase C in Trypanosoma brucei. *J Biol Chem* **274**, 5931-8.

Aslan, J. E. and Thomas, G. (2009). Death by committee: organellar trafficking and communication in apoptosis. *Traffic* **10**, 1390-404.

Atwal, R. S. and Truant, R. (2008). A stress sensitive ER membrane-association domain in Huntingtin protein defines a potential role for Huntingtin in the regulation of autophagy. *Autophagy* **4**, 91-3.

Atwal, R. S., Xia, J., Pinchev, D., Taylor, J., Epand, R. M. and Truant, R. (2007). Huntingtin has a membrane association signal that can modulate huntingtin aggregation, nuclear entry and toxicity. *Hum Mol Genet* **16**, 2600-15.

Axe, E. L., Walker, S. A., Manifava, M., Chandra, P., Roderick, H. L., Habermann, A., Griffiths, G. and Ktistakis, N. T. (2008). Autophagosome formation from membrane compartments enriched in

phosphatidylinositol 3-phosphate and dynamically connected to the endoplasmic reticulum. *J Cell Biol* **182**, 685-701.

Bagrodia, S., Taylor, S. J. and Shalloway, D. (1993). Myristylation is required for Tyr-527 dephosphorylation and activation of pp60c-src in mitosis. *Mol Cell Biol* **13**, 1464-70.

Baines, C. P., Zhang, J., Wang, G. W., Zheng, Y. T., Xiu, J. X., Cardwell, E. M., Bolli, R. and Ping, P. (2002). Mitochondrial PKCepsilon and MAPK form signaling modules in the murine heart: enhanced mitochondrial PKCepsilon-MAPK interactions and differential MAPK activation in PKCepsilon-induced cardioprotection. *Circ Res* **90**, 390-7.

Barlowe, C. (2010). ER sheets get roughed up. *Cell* **143**, 665-6.

Basso, A. D., Kirschmeier, P. and Bishop, W. R. (2006). Lipid posttranslational modifications. Farnesyl transferase inhibitors. *J Lipid Res* **47**, 15-31.

Basu, A., Lu, D., Sun, B., Moor, A. N., Akkaraju, G. R. and Huang, J. (2002). Proteolytic activation of protein kinase C-epsilon by caspase-mediated processing and transduction of antiapoptotic signals. *J Biol Chem* **277**, 41850-6.

Bayer, E. A. and Wilchek, M. (1990). Application of avidin-biotin technology to affinity-based separations. *J Chromatogr* **510**, 3-11.

Beauchamp, E., Goenaga, D., Le Bloc'h, J., Catheline, D., Legrand, P. and Rioux, V. (2007). Myristic acid increases the activity of dihydroceramide Delta4-desaturase 1 through its N-terminal myristoylation. *Biochimie* **89**, 1553-61.

Beauchamp, E., Tekpli, X., Marteil, G., Lagadic-Gossmann, D., Legrand, P. and Rioux, V. (2009). N-Myristoylation targets dihydroceramide Delta4-desaturase 1 to mitochondria: partial involvement in the apoptotic effect of myristic acid. *Biochimie* **91**, 1411-9.

Bereta, G. and Palczewski, K. (2011). Heterogeneous N-terminal Acylation of Retinal Proteins Results from the Retina's Unusual Lipid Metabolism. *Biochemistry*.

Bergo, M. O., Lieu, H. D., Gavino, B. J., Ambroziak, P., Otto, J. C., Casey, P. J., Walker, Q. M. and Young, S. G. (2004). On the physiological importance of endoproteolysis of CAAX proteins: heart-specific RCE1 knockout mice develop a lethal cardiomyopathy. *J Biol Chem* **279**, 4729-36.

Bergsbaken, T., Fink, S. L. and Cookson, B. T. (2009). Pyroptosis: host cell death and inflammation. *Nat Rev Microbiol* **7**, 99-109.

Berthiaume, L., Deichaite, I., Peseckis, S. and Resh, M. D. (1994). Regulation of enzymatic activity by active site fatty acylation. A new role for long chain fatty acid acylation of proteins. *J Biol Chem* **269**, 6498-505.

Bertolotti, A., Zhang, Y., Hendershot, L. M., Harding, H. P. and Ron, D. (2000). Dynamic interaction of BiP and ER stress transducers in the unfolded-protein response. *Nat Cell Biol* **2**, 326-32.

Bertolotto, C., Maulon, L., Filippa, N., Baier, G. and Auberger, P. (2000). Protein kinase C theta and epsilon promote T-cell survival by a rsk-dependent phosphorylation and inactivation of BAD. *J Biol Chem* **275**, 37246-50.

Bhatnagar, R. S., Futterer, K., Waksman, G. and Gordon, J. I. (1999). The structure of myristoyl-CoA:protein N-myristoyltransferase. *Biochim Biophys Acta* **1441**, 162-72.

Bhatnagar, R. S., Jackson-Machelski, E., McWherter, C. A. and Gordon, J. I. (1994). Isothermal titration calorimetric studies of Saccharomyces cerevisiae myristoyl-CoA:protein N-myristoyltransferase. Determinants of binding energy and catalytic discrimination among acyl-CoA and peptide ligands. *J Biol Chem* **269**, 11045-53.

Blom, N., Gammeltoft, S. and Brunak, S. (1999). Sequence and structure-based prediction of eukaryotic protein phosphorylation sites. *J Mol Biol* **294**, 1351-62.

Boisson, B., Giglione, C. and Meinnel, T. (2003). Unexpected protein families including cell defense components feature in the N-myristoylome of a higher eukaryote. *J Biol Chem* **278**, 43418-29.

Bokoch, G. M. (2003). Biology of the p21-activated kinases. *Annu Rev Biochem* **72**, 743-81.

Bologna, G., Yvon, C., Duvaud, S. and Veuthey, A. L. (2004). N-Terminal myristoylation predictions by ensembles of neural networks. *Proteomics* **4**, 1626-32.

Bonham, K. and Fujita, D. J. (1993). Organization and analysis of the promoter region and 5' non-coding exons of the human c-src proto-oncogene. *Oncogene* **8**, 1973-81.

Boutin, J. A. (1997). Myristoylation. *Cell Signal* **9**, 15-35.

Bowyer, P. W., Gunaratne, R. S., Grainger, M., Withers-Martinez, C., Wickramsinghe, S. R., Tate, E. W., Leatherbarrow, R. J., Brown, K. A., Holder, A. A. and Smith, D. F. (2007). Molecules incorporating a benzothiazole core scaffold inhibit the N-myristoyltransferase of Plasmodium falciparum. *Biochem J* **408**, 173-80.

Brannigan, J. A., Smith, B. A., Yu, Z., Brzozowski, A. M., Hodgkinson, M. R., Maroof, A., Price, H. P., Meier, F., Leatherbarrow, R. J., Tate, E. W. et al. (2010). N-myristoyltransferase from Leishmania donovani: structural and functional characterisation of a potential drug target for visceral leishmaniasis. *J Mol Biol* **396**, 985-99.

Bratton, S. B. and Cohen, G. M. (2001). Apoptotic death sensor: an organelle's alter ego? *Trends Pharmacol Sci* **22**, 306-15.

Breckenridge, D. G., Germain, M., Mathai, J. P., Nguyen, M. and Shore, G. C. (2003). Regulation of apoptosis by endoplasmic reticulum pathways. *Oncogene* **22**, 8608-18.

Buglino, J. A. and Resh, M. D. (2008). Hhat is a palmitoylacyltransferase with specificity for N-palmitoylation of Sonic Hedgehog. *J Biol Chem* **283**, 22076-88.

Bursten, S. L., Locksley, R. M., Ryan, J. L. and Lovett, D. H. (1988). Acylation of monocyte and glomerular mesangial cell proteins. Myristyl acylation of the interleukin 1 precursors. *J Clin Invest* **82**, 1479-88.

Burtnick, L. D., Urosev, D., Irobi, E., Narayan, K. and Robinson, R. C. (2004). Structure of the N-terminal half of gelsolin bound to actin: roles in severing, apoptosis and FAF. *EMBO J* **23**, 2713-22.

Cagnol, S. and Chambard, J. C. (2010). ERK and cell death: mechanisms of ERK-induced cell death--apoptosis, autophagy and senescence. *FEBS J* **277**, 2-21.

Cain, K., Bratton, S. B., Langlais, C., Walker, G., Brown, D. G., Sun, X. M. and Cohen, G. M. (2000). Apaf-1 oligomerizes into biologically active approximately 700-kDa and inactive approximately 1.4-MDa apoptosome complexes. *J Biol Chem* **275**, 6067-70.

Carr, S. A., Biemann, K., Shoji, S., Parmelee, D. C. and Titani, K. (1982). n-Tetradecanoyl is the NH2-terminal blocking group of the catalytic subunit of cyclic AMP-dependent protein kinase from bovine cardiac muscle. *Proc Natl Acad Sci U S A* **79**, 6128-31.

Cathelin, S., Rebe, C., Haddaoui, L., Simioni, N., Verdier, F., Fontenay, M., Launay, S., Mayeux, P. and Solary, E. (2006). Identification of proteins cleaved downstream of caspase activation in

monocytes undergoing macrophage differentiation. *J Biol Chem* **281**, 17779-88.

Cenni, V., Doppler, H., Sonnenburg, E. D., Maraldi, N., Newton, A. C. and Toker, A. (2002). Regulation of novel protein kinase C epsilon by phosphorylation. *Biochem J* **363**, 537-45.

Charron, G., Zhang, M. M., Yount, J. S., Wilson, J., Raghavan, A. S., Shamir, E. and Hang, H. C. (2009). Robust fluorescent detection of protein fatty-acylation with chemical reporters. *J Am Chem Soc* **131**, 4967-75.

Chatterjee, S., Han, H., Rollins, S. and Cleveland, T. (1999). Molecular cloning, characterization, and expression of a novel human neutral sphingomyelinase. *J Biol Chem* **274**, 37407-12.

Chen, H. J., Lin, C. M., Lin, C. S., Perez-Olle, R., Leung, C. L. and Liem, R. K. (2006). The role of microtubule actin cross-linking factor 1 (MACF1) in the Wnt signaling pathway. *Genes Dev* **20**, 1933-45.

Chen, Y. and Klionsky, D. J. (2011). The regulation of autophagy - unanswered questions. *J Cell Sci* **124**, 161-70.

Coleman, M. L., Sahai, E. A., Yeo, M., Bosch, M., Dewar, A. and Olson, M. F. (2001). Membrane blebbing during apoptosis results from caspase-mediated activation of ROCK I. *Nat Cell Biol* **3**, 339-45.

Colombo, S., Longhi, R., Alcaro, S., Ortuso, F., Sprocati, T., Flora, A. and Borgese, N. (2005). N-myristoylation determines dual targeting of mammalian NADH-cytochrome b5 reductase to ER and mitochondrial outer membranes by a mechanism of kinetic partitioning. *J Cell Biol* **168**, 735-45.

Cordeddu, V., Di Schiavi, E., Pennacchio, L. A., Ma'ayan, A., Sarkozy, A., Fodale, V., Cecchetti, S., Cardinale, A., Martin, J., Schackwitz, W. et al. (2009). Mutation of SHOC2 promotes aberrant protein N-myristoylation and causes Noonan-like syndrome with loose anagen hair. *Nat Genet* **41**, 1022-6.

Corvi, M. M., Soltys, C. L. and Berthiaume, L. G. (2001). Regulation of mitochondrial carbamoyl-phosphate synthetase 1 activity by active site fatty acylation. *J Biol Chem* **276**, 45704-12.

Costa, V., Giacomello, M., Hudec, R., Lopreiato, R., Ermak, G., Lim, D., Malorni, W., Davies, K. J., Carafoli, E. and Scorrano, L. (2010). Mitochondrial fission and cristae disruption increase the response of cell models of Huntington's disease to apoptotic stimuli. *EMBO Mol Med* **2**, 490-503.

Cross, F. R., Garber, E. A., Pellman, D. and Hanafusa, H. (1984). A short sequence in the p60src N terminus is required for p60src myristylation and membrane association and for cell transformation. *Mol Cell Biol* **4**, 1834-42.

Crowell, D. N. and Huizinga, D. H. (2009). Protein isoprenylation: the fat of the matter. *Trends Plant Sci* **14**, 163-70.

Cui, H., Lyman, E. and Voth, G. A. (2011). Mechanism of membrane curvature sensing by amphipathic helix containing proteins. *Biophys J* **100**, 1271-9.

Curtin, J. F. and Cotter, T. G. (2003). Live and let die: regulatory mechanisms in Fas-mediated apoptosis. *Cell Signal* **15**, 983-92.

Danial, N. N. (2007). BCL-2 family proteins: critical checkpoints of apoptotic cell death. *Clin Cancer Res* **13**, 7254-63.

Dasgupta, S., Bhattacharya, S., Maitra, S., Pal, D., Majumdar, S. S. and Datta, A. (2011). Mechanism of lipid induced insulin resistance: activated PKCepsilon is a key regulator. *Biochim Biophys Acta* **1812**, 495-506.

De Botton, S., Sabri, S., Daugas, E., Zermati, Y., Guidotti, J. E., Hermine, O., Kroemer, G., Vainchenker, W. and Debili, N. (2002). Platelet formation is the consequence of caspase activation within megakaryocytes. *Blood* **100**, 1310-7.

de Haan, C. A., Molinari, M. and Reggiori, F. (2010). Autophagy-independent LC3 function in vesicular traffic. *Autophagy* **6**, 994-6.

Dehm, S., Senger, M. A. and Bonham, K. (2001). SRC transcriptional activation in a subset of human colon cancer cell lines. *FEBS Lett* **487**, 367-71.

Dehm, S. M. and Bonham, K. (2004). SRC gene expression in human cancer: the role of transcriptional activation. *Biochem Cell Biol* **82**, 263-74.

Deichaite, I., Berthiaume, L., Peseckis, S. M., Patton, W. F. and Resh, M. D. (1993). Novel use of an iodo-myristyl-CoA analog identifies a semialdehyde dehydrogenase in bovine liver. *J Biol Chem* **268**, 13738-47.

Deichaite, I., Casson, L. P., Ling, H. P. and Resh, M. D. (1988). In vitro synthesis of pp60v-src: myristylation in a cell-free system. *Mol Cell Biol* **8**, 4295-301.

Dekker, F. J., Rocks, O., Vartak, N., Menninger, S., Hedberg, C., Balamurugan, R., Wetzel, S., Renner, S., Gerauer, M., Scholermann, B. et al. (2010). Small-molecule inhibition of APT1 affects Ras localization and signaling. *Nat Chem Biol* **6**, 449-56.

DeMar, J. C., Jr., Rundle, D. R., Wensel, T. G. and Anderson, R. E. (1999). Heterogeneous N-terminal acylation of retinal proteins. *Prog Lipid Res* **38**, 49-90.

Devadas, B., Freeman, S. K., McWherter, C. A., Kishore, N. S., Lodge, J. K., Jackson-Machelski, E., Gordon, J. I. and Sikorski, J. A. (1998). Novel biologically active nonpeptidic inhibitors of myristoylCoA:protein N-myristoyltransferase. *J Med Chem* **41**, 996-1000.

DiFiglia, M., Sapp, E., Chase, K. O., Davies, S. W., Bates, G. P., Vonsattel, J. P. and Aronin, N. (1997). Aggregation of huntingtin in neuronal intranuclear inclusions and dystrophic neurites in brain. *Science* **277**, 1990-3.

Distelmaier, F., Koopman, W. J., Testa, E. R., de Jong, A. S., Swarts, H. G., Mayatepek, E., Smeitink, J. A. and Willems, P. H. (2008). Life cell quantification of mitochondrial membrane potential at the single organelle level. *Cytometry A* **73**, 129-38.

Dix, M. M., Simon, G. M. and Cravatt, B. F. (2008). Global mapping of the topography and magnitude of proteolytic events in apoptosis. *Cell* **134**, 679-91.

Droin, N., Cathelin, S., Jacquel, A., Guery, L., Garrido, C., Fontenay, M., Hermine, O. and Solary, E. (2008). A role for caspases in the differentiation of erythroid cells and macrophages. *Biochimie* **90**, 416-22.

Ducker, C. E., Upson, J. J., French, K. J. and Smith, C. D. (2005). Two N-myristoyltransferase isozymes play unique roles in protein myristoylation, proliferation, and apoptosis. *Mol Cancer Res* **3**, 463-76.

Durgan, J., Cameron, A. J., Saurin, A. T., Hanrahan, S., Totty, N., Messing, R. O. and Parker, P. J. (2008). The identification and characterization of novel PKCepsilon phosphorylation sites provide evidence for functional cross-talk within the PKC superfamily. *Biochem J* **411**, 319-31.

Duronio, R. J., Towler, D. A., Heuckeroth, R. O. and Gordon, J. I. (1989). Disruption of the yeast N-myristoyl transferase gene causes recessive lethality. *Science* **243**, 796-800.

Dyda, F., Klein, D. C. and Hickman, A. B. (2000). GCN5-related N-acetyltransferases: a structural overview. *Annu Rev Biophys Biomol Struct* **29**, 81-103.

Ehrlich, M. E., Conti, L., Toselli, M., Taglietti, L., Fiorillo, E., Taglietti, V., Ivkovic, S., Guinea, B., Tranberg, A., Sipione, S. et al. (2001). ST14A cells have properties of a medium-size spiny neuron. *Exp Neurol* **167**, 215-26.

Ehrnhoefer, D. E., Sutton, L. and Hayden, M. R. (2011). Small Changes, Big Impact: Posttranslational Modifications and Function of Huntingtin in Huntington Disease. *Neuroscientist*.

Eisenhaber, B., Eisenhaber, F., Maurer-Stroh, S. and Neuberger, G. (2004). Prediction of sequence signals for lipid post-translational modifications: insights from case studies. *Proteomics* **4**, 1614-25.

Eisenhaber, F., Eisenhaber, B., Kubina, W., Maurer-Stroh, S., Neuberger, G., Schneider, G. and Wildpaner, M. (2003). Prediction of lipid posttranslational modifications and localization signals from protein sequences: big-Pi, NMT and PTS1. *Nucleic Acids Res* **31**, 3631-4.

Enari, M., Sakahira, H., Yokoyama, H., Okawa, K., Iwamatsu, A. and Nagata, S. (1998). A caspase-activated DNase that degrades DNA during apoptosis, and its inhibitor ICAD. *Nature* **391**, 43-50.

Eskelinen, E. L. (2006). Roles of LAMP-1 and LAMP-2 in lysosome biogenesis and autophagy. *Mol Aspects Med* **27**, 495-502.

Evan, G. I. and Vousden, K. H. (2001). Proliferation, cell cycle and apoptosis in cancer. *Nature* **411**, 342-8.

Faergeman, N. J. and Knudsen, J. (1997). Role of long-chain fatty acyl-CoA esters in the regulation of metabolism and in cell signalling. *Biochem J* **323 (Pt 1)**, 1-12.

Farazi, T. A., Waksman, G. and Gordon, J. I. (2001). The biology and enzymology of protein N-myristoylation. *J Biol Chem* **276**, 39501-4.

Fischer, U., Janicke, R. U. and Schulze-Osthoff, K. (2003). Many cuts to ruin: a comprehensive update of caspase substrates. *Cell Death Differ* **10**, 76-100.

Frearson, J. A., Brand, S., McElroy, S. P., Cleghorn, L. A., Smid, O., Stojanovski, L., Price, H. P., Guther, M. L., Torrie, L. S., Robinson, D. A. et al. (2010). N-myristoyltransferase inhibitors as new leads to treat sleeping sickness. *Nature* **464**, 728-32.

Freundt, E. C., Czapiga, M. and Lenardo, M. J. (2007). Photoconversion of Lysotracker Red to a green fluorescent molecule. *Cell Res* **17**, 956-8.

Frottin, F., Martinez, A., Peynot, P., Mitra, S., Holz, R. C., Giglione, C. and Meinnel, T. (2006). The proteomics of N-terminal methionine cleavage. *Mol Cell Proteomics* **5**, 2336-49.

Fryer, J. D. and Zoghbi, H. Y. (2006). Huntingtin's critical cleavage. *Nat Neurosci* **9**, 1088-9.

Fujita, J., Crane, A. M., Souza, M. K., Dejosez, M., Kyba, M., Flavell, R. A., Thomson, J. A. and Zwaka, T. P. (2008). Caspase activity mediates the differentiation of embryonic stem cells. *Cell Stem Cell* **2**, 595-601.

Fukata, Y. and Fukata, M. (2010). Protein palmitoylation in neuronal development and synaptic plasticity. *Nat Rev Neurosci* **11**, 161-75.

Furuishi, K., Matsuoka, H., Takama, M., Takahashi, I., Misumi, S. and Shoji, S. (1997). Blockage of N-myristoylation of HIV-1 gag induces the production of impotent progeny virus. *Biochem Biophys Res Commun* **237**, 504-11.

Galbiati, F., Guzzi, F., Magee, A. I., Milligan, G. and Parenti, M. (1996). Chemical inhibition of myristoylation of the G-protein Gi1 alpha by 2-hydroxymyristate does not interfere with its palmitoylation or membrane association. Evidence that palmitoylation, but not myristoylation, regulates membrane attachment. *Biochem J* **313 (Pt 3)**, 717-20.

Galluzzi, L., Aaronson, S. A., Abrams, J., Alnemri, E. S., Andrews, D. W., Baehrecke, E. H., Bazan, N. G., Blagosklonny, M. V., Blomgren, K., Borner, C. et al. (2009). Guidelines for the use and interpretation of assays for monitoring cell death in higher eukaryotes. *Cell Death Differ* **16**, 1093-107.

Galluzzi, L. and Kroemer, G. (2008). Necroptosis: a specialized pathway of programmed necrosis. *Cell* **135**, 1161-3.

Garcia-Ruiz, C., Colell, A., Mari, M., Morales, A. and Fernandez-Checa, J. C. (1997). Direct effect of ceramide on the mitochondrial electron transport chain leads to generation of reactive oxygen species. Role of mitochondrial glutathione. *J Biol Chem* **272**, 11369-77.

Garczarczyk, D., Toton, E., Biedermann, V., Rosivatz, E., Rechfeld, F., Rybczynska, M. and Hofmann, J. (2009). Signal

transduction of constitutively active protein kinase C epsilon. *Cell Signal* **21**, 745-52.

Gauthier, L. R., Charrin, B. C., Borrell-Pages, M., Dompierre, J. P., Rangone, H., Cordelieres, F. P., De Mey, J., MacDonald, M. E., Lessmann, V., Humbert, S. et al. (2004). Huntingtin controls neurotrophic support and survival of neurons by enhancing BDNF vesicular transport along microtubules. *Cell* **118**, 127-38.

Giang, D. K. and Cravatt, B. F. (1998). A second mammalian N-myristoyltransferase. *J Biol Chem* **273**, 6595-8.

Gorin, M. A. and Pan, Q. (2009). Protein kinase C epsilon: an oncogene and emerging tumor biomarker. *Mol Cancer* **8**, 9.

Goto, H., Yang, B., Petersen, D., Pepper, K. A., Alfaro, P. A., Kohn, D. B. and Reynolds, C. P. (2003). Transduction of green fluorescent protein increased oxidative stress and enhanced sensitivity to cytotoxic drugs in neuroblastoma cell lines. *Mol Cancer Ther* **2**, 911-7.

Gozuacik, D. and Kimchi, A. (2004). Autophagy as a cell death and tumor suppressor mechanism. *Oncogene* **23**, 2891-906.

Graham, R. K., Deng, Y., Slow, E. J., Haigh, B., Bissada, N., Lu, G., Pearson, J., Shehadeh, J., Bertram, L., Murphy, Z. et al. (2006). Cleavage at the caspase-6 site is required for neuronal dysfunction and degeneration due to mutant huntingtin. *Cell* **125**, 1179-91.

Griner, E. M. and Kazanietz, M. G. (2007). Protein kinase C and other diacylglycerol effectors in cancer. *Nat Rev Cancer* **7**, 281-94.

Group, H. s. D. C. R. (1993). A novel gene containing a trinucleotide repeat that is expanded and unstable on Huntington's disease chromosomes. The Huntington's Disease Collaborative Research Group. *Cell* **72**, 971-83.

Guasch, R. M., Guerri, C. and O'Connor, J. E. (1993). Flow cytometric analysis of concanavalin A binding to isolated Golgi fractions from rat liver. *Exp Cell Res* **207**, 136-41.

Gudz, T. I., Tserng, K. Y. and Hoppel, C. L. (1997). Direct inhibition of mitochondrial respiratory chain complex III by cell-permeable ceramide. *J Biol Chem* **272**, 24154-8.

Hailey, D. W., Rambold, A. S., Satpute-Krishnan, P., Mitra, K., Sougrat, R., Kim, P. K. and Lippincott-Schwartz, J. (2010). Mitochondria supply membranes for autophagosome biogenesis during starvation. *Cell* **141**, 656-67.

Hang, H. C., Geutjes, E. J., Grotenbreg, G., Pollington, A. M., Bijlmakers, M. J. and Ploegh, H. L. (2007). Chemical probes for the rapid detection of Fatty-acylated proteins in Mammalian cells. *J Am Chem Soc* **129**, 2744-5.

Hannoush, R. N. and Arenas-Ramirez, N. (2009). Imaging the lipidome: omega-alkynyl fatty acids for detection and cellular visualization of lipid-modified proteins. *ACS Chem Biol* **4**, 581-7.

Hantschel, O., Nagar, B., Guettler, S., Kretzschmar, J., Dorey, K., Kuriyan, J. and Superti-Furga, G. (2003). A myristoyl/phosphotyrosine switch regulates c-Abl. *Cell* **112**, 845-57.

Heal, W. P., Wickramasinghe, S. R., Bowyer, P. W., Holder, A. A., Smith, D. F., Leatherbarrow, R. J. and Tate, E. W. (2008a). Site-specific N-terminal labelling of proteins in vitro and in vivo using N-myristoyl transferase and bioorthogonal ligation chemistry. *Chem Commun (Camb)*, 480-2.

Heal, W. P., Wickramasinghe, S. R., Leatherbarrow, R. J. and Tate, E. W. (2008b). N-Myristoyl transferase-mediated protein labelling in vivo. *Org Biomol Chem* **6**, 2308-15.

Hedo, J. A., Collier, E. and Watkinson, A. (1987). Myristyl and palmityl acylation of the insulin receptor. *J Biol Chem* **262**, 954-7.

Hill, B. T. and Skowronski, J. (2005). Human N-myristoyltransferases form stable complexes with lentiviral nef and other viral and cellular substrate proteins. *J Virol* **79**, 1133-41.

Hoppe, J., Hoppe, V. and Schafer, R. (2001). Selective degradation of the PKC-epsilon isoform during cell death in AKR-2B fibroblasts. *Exp Cell Res* **266**, 64-73.

Hornung, V., Ablasser, A., Charrel-Dennis, M., Bauernfeind, F., Horvath, G., Caffrey, D. R., Latz, E. and Fitzgerald, K. A. (2009). AIM2 recognizes cytosolic dsDNA and forms a caspase-1-activating inflammasome with ASC. *Nature* **458**, 514-8.

Isenberg, J. S., Jia, Y., Fukuyama, J., Switzer, C. H., Wink, D. A. and Roberts, D. D. (2007). Thrombospondin-1 inhibits nitric oxide signaling via CD36 by inhibiting myristic acid uptake. *J Biol Chem* **282**, 15404-15.

Jackson, P. and Baltimore, D. (1989). N-terminal mutations activate the leukemogenic potential of the myristoylated form of c-abl. *EMBO J* **8**, 449-56.

Jeong, H., Then, F., Melia, T. J., Jr., Mazzulli, J. R., Cui, L., Savas, J. N., Voisine, C., Paganetti, P., Tanese, N., Hart, A. C. et al. (2009). Acetylation targets mutant huntingtin to autophagosomes for degradation. *Cell* **137**, 60-72.

Jiang, X. and Wang, X. (2004). Cytochrome C-mediated apoptosis. *Annu Rev Biochem* **73**, 87-106.

Jin, S., Zhuo, Y., Guo, W. and Field, J. (2005). p21-activated Kinase 1 (Pak1)-dependent phosphorylation of Raf-1 regulates its mitochondrial localization, phosphorylation of BAD, and Bcl-2 association. *J Biol Chem* **280**, 24698-705.

Johnson, D. R., Bhatnagar, R. S., Knoll, L. J. and Gordon, J. I. (1994). Genetic and biochemical studies of protein N-myristoylation. *Annu Rev Biochem* **63**, 869-914.

Juhasz, G. and Neufeld, T. P. (2006). Autophagy: a forty-year search for a missing membrane source. *PLoS Biol* **4**, e36.

Kar, R., Singha, P. K., Venkatachalam, M. A. and Saikumar, P. (2009). A novel role for MAP1 LC3 in nonautophagic cytoplasmic vacuolation death of cancer cells. *Oncogene* **28**, 2556-68.

Kaushik, S., Singh, R. and Cuervo, A. M. (2010). Autophagic pathways and metabolic stress. *Diabetes Obes Metab* **12 Suppl 2**, 4-14.

Kegel, K. B., Kim, M., Sapp, E., McIntyre, C., Castano, J. G., Aronin, N. and DiFiglia, M. (2000). Huntingtin expression stimulates endosomal-lysosomal activity, endosome tubulation, and autophagy. *J Neurosci* **20**, 7268-78.

Kho, Y., Kim, S. C., Jiang, C., Barma, D., Kwon, S. W., Cheng, J., Jaunbergs, J., Weinbaum, C., Tamanoi, F., Falck, J. et al. (2004). A tagging-via-substrate technology for detection and proteomics of farnesylated proteins. *Proc Natl Acad Sci U S A* **101**, 12479-84.

Khosravi-Far, R. and Esposti, M. D. (2004). Death receptor signals to mitochondria. *Cancer Biol Ther* **3**, 1051-7.

Kim, I., Rodriguez-Enriquez, S. and Lemasters, J. J. (2007). Selective degradation of mitochondria by mitophagy. *Arch Biochem Biophys* **462**, 245-53.

Kim, R., Emi, M. and Tanabe, K. (2006). Role of mitochondria as the gardens of cell death. *Cancer Chemother Pharmacol* **57**, 545-53.

Kim, Y. J., Yi, Y., Sapp, E., Wang, Y., Cuiffo, B., Kegel, K. B., Qin, Z. H., Aronin, N. and DiFiglia, M. (2001). Caspase 3-cleaved N-terminal fragments of wild-type and mutant huntingtin are present in normal and Huntington's disease brains, associate with membranes, and undergo calpain-dependent proteolysis. *Proc Natl Acad Sci U S A* **98**, 12784-9.

Kimura, S., Fujita, N., Noda, T. and Yoshimori, T. (2009). Monitoring autophagy in mammalian cultured cells through the dynamics of LC3. *Methods Enzymol* **452**, 1-12.

Kimura, S., Noda, T. and Yoshimori, T. (2007). Dissection of the autophagosome maturation process by a novel reporter protein, tandem fluorescent-tagged LC3. *Autophagy* **3**, 452-60.

King, M. J. and Sharma, R. K. (1993). Identification, purification and characterization of a membrane-associated N-myristoyltransferase inhibitor protein from bovine brain. *Biochem J* **291 (Pt 2)**, 635-9.

Kirchner, H., Gutierrez, J. A., Solenberg, P. J., Pfluger, P. T., Czyzyk, T. A., Willency, J. A., Schurmann, A., Joost, H. G., Jandacek, R. J., Hale, J. E. et al. (2009). GOAT links dietary lipids with the endocrine control of energy balance. *Nat Med* **15**, 741-5.

Kishore, N. S., Lu, T. B., Knoll, L. J., Katoh, A., Rudnick, D. A., Mehta, P. P., Devadas, B., Huhn, M., Atwood, J. L., Adams, S. P. et al. (1991). The substrate specificity of Saccharomyces cerevisiae myristoyl-CoA:protein N-myristoyltransferase. Analysis of myristic acid analogs containing oxygen, sulfur, double bonds, triple bonds, and/or an aromatic residue. *J Biol Chem* **266**, 8835-55.

Kishore, N. S., Wood, D. C., Mehta, P. P., Wade, A. C., Lu, T., Gokel, G. W. and Gordon, J. I. (1993). Comparison of the acyl chain specificities of human myristoyl-CoA synthetase and human myristoyl-CoA:protein N-myristoyltransferase. *J Biol Chem* **268**, 4889-902.

Kissova, I., Deffieu, M., Manon, S. and Camougrand, N. (2004). Uth1p is involved in the autophagic degradation of mitochondria. *J Biol Chem* **279**, 39068-74.

Kleuss, C. and Krause, E. (2003). Galpha(s) is palmitoylated at the N-terminal glycine. *EMBO J* **22**, 826-32.

Klionsky, D. J. Abeliovich, H. Agostinis, P. Agrawal, D. K. Aliev, G. Askew, D. S. Baba, M. Baehrecke, E. H. Bahr, B. A. Ballabio, A. et al. (2008a). Guidelines for the use and interpretation of assays for monitoring autophagy in higher eukaryotes. *Autophagy* **4**, 151-75.

Klionsky, D. J., Codogno, P., Cuervo, A. M., Deretic, V., Elazar, Z., Fueyo-Margareto, J., Gewirtz, D. A., Kroemer, G., Levine, B., Mizushima, N. et al. (2010). A comprehensive glossary of autophagy-related molecules and processes. *Autophagy* **6**.

Klionsky, D. J., Elazar, Z., Seglen, P. O. and Rubinsztein, D. C. (2008b). Does bafilomycin A1 block the fusion of autophagosomes with lysosomes? *Autophagy* **4**, 849-950.

Knaus, U. G., Morris, S., Dong, H. J., Chernoff, J. and Bokoch, G. M. (1995). Regulation of human leukocyte p21-activated kinases through G protein--coupled receptors. *Science* **269**, 221-3.

Kojima, M., Hosoda, H., Date, Y., Nakazato, M., Matsuo, H. and Kangawa, K. (1999). Ghrelin is a growth-hormone-releasing acylated peptide from stomach. *Nature* **402**, 656-60.

Kojima, M. and Kangawa, K. (2005). Ghrelin: structure and function. *Physiol Rev* **85**, 495-522.

Kon, M. and Cuervo, A. M. (2010). Chaperone-mediated autophagy in health and disease. *FEBS Lett* **584**, 1399-404.

Kopito, R. R. and Sitia, R. (2000). Aggresomes and Russell bodies. Symptoms of cellular indigestion? *EMBO Rep* **1**, 225-31.

Koriyama, H., Kouchi, Z., Umeda, T., Saido, T. C., Momoi, T., Ishiura, S. and Suzuki, K. (1999). Proteolytic activation of protein kinase C delta and epsilon by caspase-3 in U937 cells during chemotherapeutic agent-induced apoptosis. *Cell Signal* **11**, 831-8.

Kostiuk, M. A., Keller, B. O. and Berthiaume, L. G. (2009). Non-radioactive detection of palmitoylated mitochondrial proteins using an azido-palmitate analogue. *Methods Enzymol* **457**, 149-65.

Kostiuk, M. A., Keller, B. O. and Berthiaume, L. G. (2010). Palmitoylation of ketogenic enzyme HMGCS2 enhances its interaction with PPARalpha and transcription at the Hmgcs2 PPRE. *FASEB J* **24**, 1914-24.

Koya, R. C., Fujita, H., Shimizu, S., Ohtsu, M., Takimoto, M., Tsujimoto, Y. and Kuzumaki, N. (2000). Gelsolin inhibits apoptosis by blocking mitochondrial membrane potential loss and cytochrome c release. *J Biol Chem* **275**, 15343-9.

Kuma, A., Matsui, M. and Mizushima, N. (2007). LC3, an autophagosome marker, can be incorporated into protein aggregates

independent of autophagy: caution in the interpretation of LC3 localization. *Autophagy* **3**, 323-8.

Kusano, H., Shimizu, S., Koya, R. C., Fujita, H., Kamada, S., Kuzumaki, N. and Tsujimoto, Y. (2000). Human gelsolin prevents apoptosis by inhibiting apoptotic mitochondrial changes via closing VDAC. *Oncogene* **19**, 4807-14.

Kweon, S. M., Kim, H. J., Lee, Z. W., Kim, S. J., Kim, S. I., Paik, S. G. and Ha, K. S. (2001). Real-time measurement of intracellular reactive oxygen species using Mito tracker orange (CMH2TMRos). *Biosci Rep* **21**, 341-52.

Laemmli, U. K. (1970). Cleavage of structural proteins during the assembly of the head of bacteriophage T4. *Nature* **227**, 680-5.

Lamkanfi, M., Festjens, N., Declercq, W., Vanden Berghe, T. and Vandenabeele, P. (2007). Caspases in cell survival, proliferation and differentiation. *Cell Death Differ* **14**, 44-55.

Lane, J. D., Vergnolle, M. A., Woodman, P. G. and Allan, V. J. (2001). Apoptotic cleavage of cytoplasmic dynein intermediate chain and p150(Glued) stops dynein-dependent membrane motility. *J Cell Biol* **153**, 1415-26.

Lei, K. and Davis, R. J. (2003). JNK phosphorylation of Bim-related members of the Bcl2 family induces Bax-dependent apoptosis. *Proc Natl Acad Sci U S A* **100**, 2432-7.

Leist, M. and Jaattela, M. (2001). Four deaths and a funeral: from caspases to alternative mechanisms. *Nat Rev Mol Cell Biol* **2**, 589-98.

Lemasters, J. J. (2005). Selective mitochondrial autophagy, or mitophagy, as a targeted defense against oxidative stress, mitochondrial dysfunction, and aging. *Rejuvenation Res* **8**, 3-5.

Leverrier, S., Vallentin, A. and Joubert, D. (2002). Positive feedback of protein kinase C proteolytic activation during apoptosis. *Biochem J* **368**, 905-13.

Ley, R., Ewings, K. E., Hadfield, K. and Cook, S. J. (2005). Regulatory phosphorylation of Bim: sorting out the ERK from the JNK. *Cell Death Differ* **12**, 1008-14.

Li, Y., Urban, J. M., Cayer, M. L., Plummer, H. K., 3rd and Heckman, C. A. (2006). Actin-based features negatively regulated by protein kinase C-epsilon. *Am J Physiol Cell Physiol* **291**, C1002-13.

Liang, X., Lu, Y., Wilkes, M., Neubert, T. A. and Resh, M. D. (2004). The N-terminal SH4 region of the Src family kinase Fyn is modified by methylation and heterogeneous fatty acylation: role in membrane targeting, cell adhesion, and spreading. *J Biol Chem* **279**, 8133-9.

Liston, P., Fong, W. G. and Korneluk, R. G. (2003). The inhibitors of apoptosis: there is more to life than Bcl2. *Oncogene* **22**, 8568-80.

Lodge, J. K., Johnson, R. L., Weinberg, R. A. and Gordon, J. I. (1994). Comparison of myristoyl-CoA:protein N-myristoyltransferases from three pathogenic fungi: Cryptococcus neoformans, Histoplasma capsulatum, and Candida albicans. *J Biol Chem* **269**, 2996-3009.

Lu, Y., Selvakumar, P., Ali, K., Shrivastav, A., Bajaj, G., Resch, L., Griebel, R., Fourney, D., Meguro, K. and Sharma, R. K. (2005). Expression of N-myristoyltransferase in human brain tumors. *Neurochem Res* **30**, 9-13.

Luciano, F., Jacquel, A., Colosetti, P., Herrant, M., Cagnol, S., Pages, G. and Auberger, P. (2003). Phosphorylation of Bim-EL by Erk1/2 on serine 69 promotes its degradation via the proteasome pathway and regulates its proapoptotic function. *Oncogene* **22**, 6785-93.

Luo, S. and Rubinsztein, D. C. (2009). Huntingtin promotes cell survival by preventing Pak2 cleavage. *J Cell Sci* **122**, 875-85.

Luthi, A. U. and Martin, S. J. (2007). The CASBAH: a searchable database of caspase substrates. *Cell Death Differ* **14**, 641-50.

Mackay, H. J. and Twelves, C. J. (2007). Targeting the protein kinase C family: are we there yet? *Nat Rev Cancer* **7**, 554-62.

Magnuson, B. A., Raju, R. V., Moyana, T. N. and Sharma, R. K. (1995). Increased N-myristoyltransferase activity observed in rat and human colonic tumors. *J Natl Cancer Inst* **87**, 1630-5.

Mahrus, S., Trinidad, J. C., Barkan, D. T., Sali, A., Burlingame, A. L. and Wells, J. A. (2008). Global sequencing of proteolytic cleavage sites in apoptosis by specific labeling of protein N termini. *Cell* **134**, 866-76.

Majewski, N., Nogueira, V., Robey, R. B. and Hay, N. (2004). Akt inhibits apoptosis downstream of BID cleavage via a glucose-dependent mechanism involving mitochondrial hexokinases. *Mol Cell Biol* **24**, 730-40.

Mann, R. K. and Beachy, P. A. (2000). Cholesterol modification of proteins. *Biochim Biophys Acta* **1529**, 188-202.

Manolea, F., Chun, J., Chen, D. W., Clarke, I., Summerfeldt, N., Dacks, J. B. and Melancon, P. (2010). Arf3 is activated uniquely at the trans-Golgi network by brefeldin A-inhibited guanine nucleotide exchange factors. *Mol Biol Cell* **21**, 1836-49.

Marino, G., Madeo, F. and Kroemer, G. (2010). Autophagy for tissue homeostasis and neuroprotection. *Curr Opin Cell Biol*.

Martelli, A. M., Evangelisti, C., Nyakern, M. and Manzoli, F. A. (2006). Nuclear protein kinase C. *Biochim Biophys Acta* **1761**, 542-51.

Martin, B. R. and Cravatt, B. F. (2009). Large-scale profiling of protein palmitoylation in mammalian cells. *Nat Methods* **6**, 135-8.

Martin, D. D., Beauchamp, E. and Berthiaume, L. G. (2010). Post-translational myristoylation: Fat matters in cellular life and death. *Biochimie*.

Martin, D. D., Vilas, G. L., Prescher, J. A., Rajaiah, G., Falck, J. R., Bertozzi, C. R. and Berthiaume, L. G. (2008). Rapid detection, discovery, and identification of post-translationally myristoylated proteins during apoptosis using a bio-orthogonal azidomyristate analog. *FASEB J* **22**, 797-806.

Martinez-Vicente, M. and Cuervo, A. M. (2007). Autophagy and neurodegeneration: when the cleaning crew goes on strike. *Lancet Neurol* **6**, 352-61.

Martinez-Vicente, M., Talloczy, Z., Wong, E., Tang, G., Koga, H., Kaushik, S., de Vries, R., Arias, E., Harris, S., Sulzer, D. et al. (2010). Cargo recognition failure is responsible for inefficient autophagy in Huntington's disease. *Nat Neurosci* **13**, 567-76.

Matheson, A. T., Yaguchi, M. and Visentin, L. P. (1975). The conservation of amino acids in the n-terminal position of ribosomal and cytosol proteins from Escherichia coli, Bacillus stearothermophilus, and Halobacterium cutirubrum. *Can J Biochem* **53**, 1323-7.

Maurer-Stroh, S., Eisenhaber, B. and Eisenhaber, F. (2002a). N-terminal N-myristoylation of proteins: prediction of substrate proteins from amino acid sequence. *J Mol Biol* **317**, 541-57.

Maurer-Stroh, S., Eisenhaber, B. and Eisenhaber, F. (2002b). N-terminal N-myristoylation of proteins: refinement of the sequence motif and its taxon-specific differences. *J Mol Biol* **317**, 523-40.

Maurer-Stroh, S. and Eisenhaber, F. (2004). Myristoylation of viral and bacterial proteins. *Trends Microbiol* **12**, 178-85.

Maurer-Stroh, S., Gouda, M., Novatchkova, M., Schleiffer, A., Schneider, G., Sirota, F. L., Wildpaner, M., Hayashi, N. and Eisenhaber, F. (2004). MYRbase: analysis of genome-wide glycine myristoylation enlarges the functional spectrum of eukaryotic myristoylated proteins. *Genome Biol* **5**, R21.

Mayor, S. and Riezman, H. (2004). Sorting GPI-anchored proteins. *Nat Rev Mol Cell Biol* **5**, 110-20.

Mazzanti, L., Cacciari, E., Cicognani, A., Bergamaschi, R., Scarano, E. and Forabosco, A. (2003). Noonan-like syndrome with loose anagen hair: a new syndrome? *Am J Med Genet A* **118A**, 279-86.

McCabe, J. B. and Berthiaume, L. G. (1999). Functional roles for fatty acylated amino-terminal domains in subcellular localization. *Mol Biol Cell* **10**, 3771-86.

McCabe, J. B. and Berthiaume, L. G. (2001). N-terminal protein acylation confers localization to cholesterol, sphingolipid-enriched membranes but not to lipid rafts/caveolae. *Mol Biol Cell* **12**, 3601-17.

McLaughlin, S. and Aderem, A. (1995). The myristoyl-electrostatic switch: a modulator of reversible protein-membrane interactions. *Trends Biochem Sci* **20**, 272-6.

McTaggart, S. J. (2006). Isoprenylated proteins. *Cell Mol Life Sci* **63**, 255-67.

Menard, R., Sansonetti, P. and Parsot, C. (1994). The secretion of the Shigella flexneri Ipa invasins is activated by epithelial cells and controlled by IpaB and IpaD. *EMBO J* **13**, 5293-302.

Mischak, H., Goodnight, J. A., Kolch, W., Martiny-Baron, G., Schaechtle, C., Kazanietz, M. G., Blumberg, P. M., Pierce, J. H. and Mushinski, J. F. (1993). Overexpression of protein kinase C-delta and -epsilon in NIH 3T3 cells induces opposite effects on growth, morphology, anchorage dependence, and tumorigenicity. *J Biol Chem* **268**, 6090-6.

Mishkind, M. (2001). Morbid myristoylation. *Trends Cell Biol* **11**, 191.

Mizuno, K., Noda, K., Araki, T., Imaoka, T., Kobayashi, Y., Akita, Y., Shimonaka, M., Kishi, S. and Ohno, S. (1997). The proteolytic cleavage of protein kinase C isotypes, which generates kinase and regulatory fragments, correlates with Fas-mediated and 12-O-tetradecanoyl-phorbol-13-acetate-induced apoptosis. *Eur J Biochem* **250**, 7-18.

Mizushima, N. and Yoshimori, T. (2007). How to interpret LC3 immunoblotting. *Autophagy* **3**, 542-5.

Mohlig, H., Mathieu, S., Thon, L., Frederiksen, M. C., Ward, D. M., Kaplan, J., Schutze, S., Kabelitz, D. and Adam, D. (2007). The WD repeat protein FAN regulates lysosome size independent from abnormal downregulation/membrane recruitment of protein kinase C. *Exp Cell Res* **313**, 2703-18.

Nadler, M. J., Harrison, M. L., Ashendel, C. L., Cassady, J. M. and Geahlen, R. L. (1993). Treatment of T cells with 2-hydroxymyristic acid inhibits the myristoylation and alters the stability of p56lck. *Biochemistry* **32**, 9250-5.

Nadolski, M. J. and Linder, M. E. (2007). Protein lipidation. *FEBS J* **274**, 5202-10.

Nagar, B., Hantschel, O., Young, M. A., Scheffzek, K., Veach, D., Bornmann, W., Clarkson, B., Superti-Furga, G. and Kuriyan, J. (2003). Structural basis for the autoinhibition of c-Abl tyrosine kinase. *Cell* **112**, 859-71.

Nagata, E., Sawa, A., Ross, C. A. and Snyder, S. H. (2004). Autophagosome-like vacuole formation in Huntington's disease lymphoblasts. *Neuroreport* **15**, 1325-8.

Nagata, S. (2000). Apoptotic DNA fragmentation. *Exp Cell Res* **256**, 12-8.

Narendra, D., Tanaka, A., Suen, D. F. and Youle, R. J. (2008). Parkin is recruited selectively to impaired mitochondria and promotes their autophagy. *J Cell Biol* **183**, 795-803.

Newton, P. M. and Messing, R. O. (2010). The substrates and binding partners of protein kinase Cepsilon. *Biochem J* **427**, 189-96.

Nicholson, D. W. (1999). Caspase structure, proteolytic substrates, and function during apoptotic cell death. *Cell Death Differ* **6**, 1028-42.

Nimchuk, Z., Marois, E., Kjemtrup, S., Leister, R. T., Katagiri, F. and Dangl, J. L. (2000). Eukaryotic fatty acylation drives plasma membrane targeting and enhances function of several type III effector proteins from Pseudomonas syringae. *Cell* **101**, 353-63.

Nishimura, Y., Kawabata, T. and Kato, K. (1988). Identification of latent procathepsins B and L in microsomal lumen: characterization of enzymatic activation and proteolytic processing in vitro. *Arch Biochem Biophys* **261**, 64-71.

Ntwasa, M., Aapies, S., Schiffmann, D. A. and Gay, N. J. (2001). Drosophila embryos lacking N-myristoyltransferase have multiple developmental defects. *Exp Cell Res* **262**, 134-44.

Ntwasa, M., Egerton, M. and Gay, N. J. (1997). Sequence and expression of Drosophila myristoyl-CoA: protein N-myristoyl transferase: evidence for proteolytic processing and membrane localisation. *J Cell Sci* **110 (Pt 2)**, 149-56.

O'Reilly, L. A., Kruse, E. A., Puthalakath, H., Kelly, P. N., Kaufmann, T., Huang, D. C. and Strasser, A. (2009). MEK/ERK-mediated phosphorylation of Bim is required to ensure survival of T and B lymphocytes during mitogenic stimulation. *J Immunol* **183**, 261-9.

Paige, L. A., Zheng, G. Q., DeFrees, S. A., Cassady, J. M. and Geahlen, R. L. (1990). Metabolic activation of 2-substituted derivatives of myristic acid to form potent inhibitors of myristoyl CoA:protein N-myristoyltransferase. *Biochemistry* **29**, 10566-73.

Panethymitaki, C., Bowyer, P. W., Price, H. P., Leatherbarrow, R. J., Brown, K. A. and Smith, D. F. (2006). Characterization and selective inhibition of myristoyl-CoA:protein N-myristoyltransferase from Trypanosoma brucei and Leishmania major. *Biochem J* **396**, 277-85.

Pattison, L. R., Kotter, M. R., Fraga, D. and Bonelli, R. M. (2006). Apoptotic cascades as possible targets for inhibiting cell death in Huntington's disease. *J Neurol* **253**, 1137-42.

Patwardhan, P. and Resh, M. D. (2010). Myristoylation and Membrane binding regulate c-Src Stability and Kinase Activity. *Mol Cell Biol*.

Paulick, M. G. and Bertozzi, C. R. (2008). The glycosylphosphatidylinositol anchor: a complex membrane-anchoring structure for proteins. *Biochemistry* **47**, 6991-7000.

Peitzsch, R. M. and McLaughlin, S. (1993). Binding of acylated peptides and fatty acids to phospholipid vesicles: pertinence to myristoylated proteins. *Biochemistry* **32**, 10436-43.

Pepinsky, R. B., Zeng, C., Wen, D., Rayhorn, P., Baker, D. P., Williams, K. P., Bixler, S. A., Ambrose, C. M., Garber, E. A., Miatkowski, K. et al. (1998). Identification of a palmitic acid-modified form of human Sonic hedgehog. *J Biol Chem* **273**, 14037-45.

Podell, S. and Gribskov, M. (2004). Predicting N-terminal myristoylation sites in plant proteins. *BMC Genomics* **5**, 37.

Pollard, T. D., Blanchoin, L. and Mullins, R. D. (2000). Molecular mechanisms controlling actin filament dynamics in nonmuscle cells. *Annu Rev Biophys Biomol Struct* **29**, 545-76.

Porter, J. A., Young, K. E. and Beachy, P. A. (1996). Cholesterol modification of hedgehog signaling proteins in animal development. *Science* **274**, 255-9.

Price, H. P., Menon, M. R., Panethymitaki, C., Goulding, D., McKean, P. G. and Smith, D. F. (2003). Myristoyl-CoA:protein N-myristoyltransferase, an essential enzyme and potential drug target in kinetoplastid parasites. *J Biol Chem* **278**, 7206-14.

Putcha, G. V., Le, S., Frank, S., Besirli, C. G., Clark, K., Chu, B., Alix, S., Youle, R. J., LaMarche, A., Maroney, A. C. et al. (2003). JNK-mediated BIM phosphorylation potentiates BAX-dependent apoptosis. *Neuron* **38**, 899-914.

Puthalakath, H., Huang, D. C., O'Reilly, L. A., King, S. M. and Strasser, A. (1999). The proapoptotic activity of the Bcl-2 family member Bim is regulated by interaction with the dynein motor complex. *Mol Cell* **3**, 287-96.

Rajala, R. V., Datla, R. S., Carlsen, S. A., Anderson, D. H., Qi, Z., Wang, J. H. and Sharma, R. K. (2001). Phosphorylation of human N-myristoyltransferase by N-myristoylated SRC family tyrosine kinase members. *Biochem Biophys Res Commun* **288**, 233-9.

Rajala, R. V., Radhi, J. M., Kakkar, R., Datla, R. S. and Sharma, R. K. (2000). Increased expression of N-myristoyltransferase in gallbladder carcinomas. *Cancer* **88**, 1992-9.

Raju, R. V., Moyana, T. N. and Sharma, R. K. (1997). N-Myristoyltransferase overexpression in human colorectal adenocarcinomas. *Exp Cell Res* **235**, 145-54.

Ramaswamy, M., Cleland, S. Y., Cruz, A. C. and Siegel, R. M. (2009). Many checkpoints on the road to cell death: regulation of Fas-FasL interactions and Fas signaling in peripheral immune responses. *Results Probl Cell Differ* **49**, 17-47.

Ratovitski, T., Gucek, M., Jiang, H., Chighladze, E., Waldron, E., D'Ambola, J., Hou, Z., Liang, Y., Poirier, M. A., Hirschhorn, R. R. et al. (2009). Mutant huntingtin N-terminal fragments of specific size mediate aggregation and toxicity in neuronal cells. *J Biol Chem* **284**, 10855-67.

Ravikumar, B., Moreau, K., Jahreiss, L., Puri, C. and Rubinsztein, D. C. (2010a). Plasma membrane contributes to the formation of pre-autophagosomal structures. *Nat Cell Biol* **12**, 747-57.

Ravikumar, B., Sarkar, S., Davies, J. E., Futter, M., Garcia-Arencibia, M., Green-Thompson, Z. W., Jimenez-Sanchez, M., Korolchuk, V. I., Lichtenberg, M., Luo, S. et al. (2010b). Regulation of mammalian autophagy in physiology and pathophysiology. *Physiol Rev* **90**, 1383-435.

Resh, M. D. (2004). Membrane targeting of lipid modified signal transduction proteins. *Subcell Biochem* **37**, 217-32.

Resh, M. D. (2006). Trafficking and signaling by fatty-acylated and prenylated proteins. *Nat Chem Biol* **2**, 584-90.

Rioux, V., Beauchamp, E., Pedrono, F., Daval, S., Molle, D., Catheline, D. and Legrand, P. (2006). Identification and characterization of recombinant and native rat myristoyl-CoA: protein N-myristoyltransferases. *Mol Cell Biochem* **286**, 161-70.

Rioux, V., Galat, A., Jan, G., Vinci, F., D'Andrea, S. and Legrand, P. (2002). Exogenous myristic acid acylates proteins in cultured rat hepatocytes. *J Nutr Biochem* **13**, 66-74.

Rocque, W. J., McWherter, C. A., Wood, D. C. and Gordon, J. I. (1993). A comparative analysis of the kinetic mechanism and peptide substrate specificity of human and Saccharomyces cerevisiae myristoyl-CoA:protein N-myristoyltransferase. *J Biol Chem* **268**, 9964-71.

Roskoski, R., Jr. (2003). Protein prenylation: a pivotal posttranslational process. *Biochem Biophys Res Commun* **303**, 1-7.

Rostovtseva, T. K., Antonsson, B., Suzuki, M., Youle, R. J., Colombini, M. and Bezrukov, S. M. (2004). Bid, but not Bax, regulates VDAC channels. *J Biol Chem* **279**, 13575-83.

Rubinsztein, D. C. (2006). The roles of intracellular protein-degradation pathways in neurodegeneration. *Nature* **443**, 780-6.

Rudel, T. and Bokoch, G. M. (1997). Membrane and morphological changes in apoptotic cells regulated by caspase-mediated activation of PAK2. *Science* **276**, 1571-4.

Rudnick, D. A., Johnson, R. L. and Gordon, J. I. (1992a). Studies of the catalytic activities and substrate specificities of Saccharomyces cerevisiae myristoyl-coenzyme A: protein N-myristoyltransferase deletion

mutants and human/yeast Nmt chimeras in Escherichia coli and S. cerevisiae. *J Biol Chem* **267**, 23852-61.

Rudnick, D. A., Lu, T., Jackson-Machelski, E., Hernandez, J. C., Li, Q., Gokel, G. W. and Gordon, J. I. (1992b). Analogs of palmitoyl-CoA that are substrates for myristoyl-CoA:protein N-myristoyltransferase. *Proc Natl Acad Sci U S A* **89**, 10507-11.

Rudnick, D. A., McWherter, C. A., Adams, S. P., Ropson, I. J., Duronio, R. J. and Gordon, J. I. (1990). Structural and functional studies of Saccharomyces cerevisiae myristoyl-CoA:protein N-myristoyltransferase produced in Escherichia coli. Evidence for an acyl-enzyme intermediate. *J Biol Chem* **265**, 13370-8.

Rudnick, D. A., McWherter, C. A., Rocque, W. J., Lennon, P. J., Getman, D. P. and Gordon, J. I. (1991). Kinetic and structural evidence for a sequential ordered Bi Bi mechanism of catalysis by Saccharomyces cerevisiae myristoyl-CoA:protein N-myristoyltransferase. *J Biol Chem* **266**, 9732-9.

Rundle, D. R., Rajala, R. V., Alvarez, R. A. and Anderson, R. E. (2004). Myristoyl-CoA:protein N-myristoyltransferases: isoform identification and gene expression in retina. *Mol Vis* **10**, 177-85.

Sakamaki, K. and Satou, Y. (2009). Caspases: evolutionary aspects of their functions in vertebrates. *J Fish Biol* **74**, 727-53.

Sakurai, N. and Utsumi, T. (2006). Posttranslational N-myristoylation is required for the anti-apoptotic activity of human tGelsolin, the C-terminal caspase cleavage product of human gelsolin. *J Biol Chem* **281**, 14288-95.

Sallese, M., Pulvirenti, T. and Luini, A. (2006). The physiology of membrane transport and endomembrane-based signalling. *EMBO J* **25**, 2663-73.

Sarkar, S. and Rubinsztein, D. C. (2008). Huntington's disease: degradation of mutant huntingtin by autophagy. *FEBS J* **275**, 4263-70.

Satoo, K., Noda, N. N., Kumeta, H., Fujioka, Y., Mizushima, N., Ohsumi, Y. and Inagaki, F. (2009). The structure of Atg4B-LC3 complex reveals the mechanism of LC3 processing and delipidation during autophagy. *EMBO J* **28**, 1341-50.

Saurin, A. T., Durgan, J., Cameron, A. J., Faisal, A., Marber, M. S. and Parker, P. J. (2008). The regulated assembly of a PKCepsilon complex controls the completion of cytokinesis. *Nat Cell Biol* **10**, 891-901.

Saxon, E. and Bertozzi, C. R. (2000). Cell surface engineering by a modified Staudinger reaction. *Science* **287**, 2007-10.

Saxon, E., Luchansky, S. J., Hang, H. C., Yu, C., Lee, S. C. and Bertozzi, C. R. (2002). Investigating cellular metabolism of synthetic azidosugars with the Staudinger ligation. *J Am Chem Soc* **124**, 14893-902.

Schey, K. L., Gutierrez, D. B., Wang, Z., Wei, J. and Grey, A. C. (2010). Novel Fatty Acid Acylation of Lens Integral Membrane Protein Aquaporin-0. *Biochemistry*.

Schilling, B., Gafni, J., Torcassi, C., Cong, X., Row, R. H., LaFevre-Bernt, M. A., Cusack, M. P., Ratovitski, T., Hirschhorn, R., Ross, C. A. et al. (2006). Huntingtin phosphorylation sites mapped by mass spectrometry. Modulation of cleavage and toxicity. *J Biol Chem* **281**, 23686-97.

Schroder, M. and Kaufman, R. J. (2005). ER stress and the unfolded protein response. *Mutat Res* **569**, 29-63.

Schubbert, S., Shannon, K. and Bollag, G. (2007). Hyperactive Ras in developmental disorders and cancer. *Nat Rev Cancer* **7**, 295-308.

Schultz, A. M. and Oroszlan, S. (1983). In vivo modification of retroviral gag gene-encoded polyproteins by myristic acid. *J Virol* **46**, 355-61.

Schwerk, C. and Schulze-Osthoff, K. (2003). Non-apoptotic functions of caspases in cellular proliferation and differentiation. *Biochem Pharmacol* **66**, 1453-8.

Seaton, K. E. and Smith, C. D. (2008). N-Myristoyltransferase isozymes exhibit differential specificity for human immunodeficiency virus type 1 Gag and Nef. *J Gen Virol* **89**, 288-96.

Sebbagh, M., Renvoize, C., Hamelin, J., Riche, N., Bertoglio, J. and Breard, J. (2001). Caspase-3-mediated cleavage of ROCK I induces MLC phosphorylation and apoptotic membrane blebbing. *Nat Cell Biol* **3**, 346-52.

Selvakumar, P., Lakshmikuttyamma, A., Shrivastav, A., Das, S. B., Dimmock, J. R. and Sharma, R. K. (2007). Potential role of N-myristoyltransferase in cancer. *Prog Lipid Res* **46**, 1-36.

Selvakumar, P., Smith-Windsor, E., Bonham, K. and Sharma, R. K. (2006). N-myristoyltransferase 2 expression in human colon cancer: cross-talk between the calpain and caspase system. *FEBS Lett* **580**, 2021-6.

Seykora, J. T., Myat, M. M., Allen, L. A., Ravetch, J. V. and Aderem, A. (1996). Molecular determinants of the myristoyl-electrostatic switch of MARCKS. *J Biol Chem* **271**, 18797-802.

Shaner, N. C., Steinbach, P. A. and Tsien, R. Y. (2005). A guide to choosing fluorescent proteins. *Nat Methods* **2**, 905-9.

Shibata, Y., Shemesh, T., Prinz, W. A., Palazzo, A. F., Kozlov, M. M. and Rapoport, T. A. (2010). Mechanisms determining the morphology of the peripheral ER. *Cell* **143**, 774-88.

Shirendeb, U., Reddy, A. P., Manczak, M., Calkins, M. J., Mao, P., Tagle, D. A. and Hemachandra Reddy, P. (2011). Abnormal mitochondrial dynamics, mitochondrial loss and mutant huntingtin oligomers in Huntington's disease: implications for selective neuronal damage. *Hum Mol Genet* **20**, 1438-55.

Shnyder, S. D. and Hubbard, M. J. (2002). ERp29 is a ubiquitous resident of the endoplasmic reticulum with a distinct role in secretory protein production. *J Histochem Cytochem* **50**, 557-66.

Shoji, S., Kurosawa, T., Inoue, H., Funakoshi, T. and Kubota, Y. (1990). Human cellular src gene product: identification of the myristoylated pp60c-src and blockage of its myristoyl acylation with N-fatty acyl compounds resulted in the suppression of colony formation. *Biochem Biophys Res Commun* **173**, 894-901.

Shrivastav, A., Pasha, M. K., Selvakumar, P., Gowda, S., Olson, D. J., Ross, A. R., Dimmock, J. R. and Sharma, R. K. (2003). Potent inhibitor of N-myristoylation: a novel molecular target for cancer. *Cancer Res* **63**, 7975-8.

Shrivastav, A., Varma, S., Senger, A., Khandelwal, R. L., Carlsen, S. and Sharma, R. K. (2009). Overexpression of Akt/PKB modulates N-myristoyltransferase activity in cancer cells. *J Pathol* **218**, 391-8.

Siegel, G., Obernosterer, G., Fiore, R., Oehmen, M., Bicker, S., Christensen, M., Khudayberdiev, S., Leuschner, P. F., Busch, C. J., Kane, C. et al. (2009). A functional screen implicates microRNA-138-dependent regulation of the depalmitoylation enzyme APT1 in dendritic spine morphogenesis. *Nat Cell Biol* **11**, 705-16.

Silverman, L. and Resh, M. D. (1992). Lysine residues form an integral component of a novel NH2-terminal membrane targeting motif for myristylated pp60v-src. *J Cell Biol* **119**, 415-25.

Silvius, J. R. (2002). Peptide-lipid interactions. In *Current topics in membranes,*, pp. xxi, 371-395 p. [15] p. of plates. San Diego, Calif. ; London: Academic Press.

Sinensky, M. (2000). Recent advances in the study of prenylated proteins. *Biochim Biophys Acta* **1484**, 93-106.

Sloane, B. F., Herman, C. J. and Padarathsingh, M. (1994). Molecular mechanisms of progression and metastasis of human tumors: a pathology B study section workshop. Working Report from the Division of Research Grants, NIH. *Cancer Res* **54**, 5241-5.

Snapp, E. L., Hegde, R. S., Francolini, M., Lombardo, F., Colombo, S., Pedrazzini, E., Borgese, N. and Lippincott-Schwartz, J. (2003). Formation of stacked ER cisternae by low affinity protein interactions. *J Cell Biol* **163**, 257-69.

Song, W., Chen, J., Petrilli, A., Liot, G., Klinglmayr, E., Zhou, Y., Poquiz, P., Tjong, J., Pouladi, M. A., Hayden, M. R. et al. (2011). Mutant huntingtin binds the mitochondrial fission GTPase dynamin-related protein-1 and increases its enzymatic activity. *Nat Med* **17**, 377-82.

Spearman, P., Horton, R., Ratner, L. and Kuli-Zade, I. (1997). Membrane binding of human immunodeficiency virus type 1 matrix protein in vivo supports a conformational myristyl switch mechanism. *J Virol* **71**, 6582-92.

Sperandio, S., de Belle, I. and Bredesen, D. E. (2000). An alternative, nonapoptotic form of programmed cell death. *Proc Natl Acad Sci U S A* **97**, 14376-81.

Sprung, R., Nandi, A., Chen, Y., Kim, S. C., Barma, D., Falck, J. R. and Zhao, Y. (2005). Tagging-via-substrate strategy for probing O-GlcNAc modified proteins. *J Proteome Res* **4**, 950-7.

Stiban, J., Fistere, D. and Colombini, M. (2006). Dihydroceramide hinders ceramide channel formation: Implications on apoptosis. *Apoptosis* **11**, 773-80.

Sugii, M., Okada, R., Matsuno, H. and Miyano, S. (2007). Performance improvement in protein N-myristoyl classification by BONSAI with insignificant indexing symbol. *Genome Inform* **18**, 277-86.

Sugiura, M., Kono, K., Liu, H., Shimizugawa, T., Minekura, H., Spiegel, S. and Kohama, T. (2002). Ceramide kinase, a novel lipid kinase. Molecular cloning and functional characterization. *J Biol Chem* **277**, 23294-300.

Summy, J. M. and Gallick, G. E. (2003). Src family kinases in tumor progression and metastasis. *Cancer Metastasis Rev* **22**, 337-58.

Suzuki, T., Ito, M., Ezure, T., Shikata, M., Ando, E., Utsumi, T., Tsunasawa, S. and Nishimura, O. (2007). Preparation of N-acylated proteins modified with fatty acids having a specific chain length using an insect cell-free protein synthesis system. *Biosci Biotechnol Biochem* **71**, 261-4.

Suzuki, T., Moriya, K., Nagatoshi, K., Ota, Y., Ezure, T., Ando, E., Tsunasawa, S. and Utsumi, T. (2010). Strategy for comprehensive identification of human N-myristoylated proteins using an insect cell-free protein synthesis system. *Proteomics* **10**, 1780-93.

Takada, R., Satomi, Y., Kurata, T., Ueno, N., Norioka, S., Kondoh, H., Takao, T. and Takada, S. (2006). Monounsaturated fatty acid modification of Wnt protein: its role in Wnt secretion. *Dev Cell* **11**, 791-801.

Takahashi, Y., Meyerkord, C. L., Hori, T., Runkle, K., Fox, T. E., Kester, M., Loughran, T. P. and Wang, H. G. (2011). Bif-1 regulates Atg9 trafficking by mediating the fission of Golgi membranes during autophagy. *Autophagy* **7**, 61-73.

Takamune, N., Gota, K., Misumi, S., Tanaka, K., Okinaka, S. and Shoji, S. (2008). HIV-1 production is specifically associated with human NMT1 long form in human NMT isozymes. *Microbes Infect* **10**, 143-50.

Tan, Y., Ruan, H., Demeter, M. R. and Comb, M. J. (1999). p90(RSK) blocks bad-mediated cell death via a protein kinase C-dependent pathway. *J Biol Chem* **274**, 34859-67.

Tanida, I. (2011). Autophagy basics. *Microbiol Immunol* **55**, 1-11.

Thompson, C. B. (1995). Apoptosis in the pathogenesis and treatment of disease. *Science* **267**, 1456-62.

Todde, V., Veenhuis, M. and van der Klei, I. J. (2009). Autophagy: principles and significance in health and disease. *Biochim Biophys Acta* **1792**, 3-13.

Towler, D. and Glaser, L. (1986). Protein fatty acid acylation: enzymatic synthesis of an N-myristoylglycyl peptide. *Proc Natl Acad Sci U S A* **83**, 2812-6.

Towler, D. A., Adams, S. P., Eubanks, S. R., Towery, D. S., Jackson-Machelski, E., Glaser, L. and Gordon, J. I. (1987a).

Purification and characterization of yeast myristoyl CoA:protein N-myristoyltransferase. *Proc Natl Acad Sci U S A* **84**, 2708-12.

Towler, D. A., Adams, S. P., Eubanks, S. R., Towery, D. S., Jackson-Machelski, E., Glaser, L. and Gordon, J. I. (1988a). Myristoyl CoA:protein N-myristoyltransferase activities from rat liver and yeast possess overlapping yet distinct peptide substrate specificities. *J Biol Chem* **263**, 1784-90.

Towler, D. A., Eubanks, S. R., Towery, D. S., Adams, S. P. and Glaser, L. (1987b). Amino-terminal processing of proteins by N-myristoylation. Substrate specificity of N-myristoyl transferase. *J Biol Chem* **262**, 1030-6.

Towler, D. A., Gordon, J. I., Adams, S. P. and Glaser, L. (1988b). The biology and enzymology of eukaryotic protein acylation. *Annu Rev Biochem* **57**, 69-99.

Turnay, J., Lecona, E., Fernandez-Lizarbe, S., Guzman-Aranguez, A., Fernandez, M. P., Olmo, N. and Lizarbe, M. A. (2005). Structure-function relationship in annexin A13, the founder member of the vertebrate family of annexins. *Biochem J* **389**, 899-911.

Tyas, L., Brophy, V. A., Pope, A., Rivett, A. J. and Tavare, J. M. (2000). Rapid caspase-3 activation during apoptosis revealed using fluorescence-resonance energy transfer. *EMBO Rep* **1**, 266-70.

Utsumi, T., Nakano, K., Funakoshi, T., Kayano, Y., Nakao, S., Sakurai, N., Iwata, H. and Ishisaka, R. (2004). Vertical-scanning mutagenesis of amino acids in a model N-myristoylation motif reveals the major amino-terminal sequence requirements for protein N-myristoylation. *Eur J Biochem* **271**, 863-74.

Utsumi, T., Sakurai, N., Nakano, K. and Ishisaka, R. (2003). C-terminal 15 kDa fragment of cytoskeletal actin is posttranslationally N-myristoylated upon caspase-mediated cleavage and targeted to mitochondria. *FEBS Lett* **539**, 37-44.

Utsumi, T., Sato, M., Nakano, K., Takemura, D., Iwata, H. and Ishisaka, R. (2001). Amino acid residue penultimate to the amino-terminal gly residue strongly affects two cotranslational protein modifications, N-myristoylation and N-acetylation. *J Biol Chem* **276**, 10505-13.

van der Vusse, G. J., van Bilsen, M., Glatz, J. F., Hasselbaink, D. M. and Luiken, J. J. (2002). Critical steps in cellular fatty acid uptake and utilization. *Mol Cell Biochem* **239**, 9-15.

Vandenabeele, P., Galluzzi, L., Vanden Berghe, T. and Kroemer, G. (2010). Molecular mechanisms of necroptosis: an ordered cellular explosion. *Nat Rev Mol Cell Biol* **11**, 700-14.

Vidal, R., Caballero, B., Couve, A. and Hetz, C. (2011). Converging pathways in the occurrence of endoplasmic reticulum (ER) stress in Huntington's disease. *Curr Mol Med* **11**, 1-12.

Vilas, G. L. and Berthiaume, L. G. (2004). A role for palmitoylation in the quality control, assembly and secretion of apolipoprotein B. *Biochem J* **377**, 121-30.

Vilas, G. L., Corvi, M. M., Plummer, G. J., Seime, A. M., Lambkin, G. R. and Berthiaume, L. G. (2006). Posttranslational myristoylation of caspase-activated p21-activated protein kinase 2 (PAK2) potentiates late apoptotic events. *Proc Natl Acad Sci U S A* **103**, 6542-7.

Warby, S. C., Doty, C. N., Graham, R. K., Carroll, J. B., Yang, Y. Z., Singaraja, R. R., Overall, C. M. and Hayden, M. R. (2008). Activated caspase-6 and caspase-6-cleaved fragments of huntingtin specifically colocalize in the nucleus. *Hum Mol Genet* **17**, 2390-404.

Wellington, C. L., Ellerby, L. M., Gutekunst, C. A., Rogers, D., Warby, S., Graham, R. K., Loubser, O., van Raamsdonk, J., Singaraja, R., Yang, Y. Z. et al. (2002). Caspase cleavage of mutant huntingtin precedes neurodegeneration in Huntington's disease. *J Neurosci* **22**, 7862-72.

Wellington, C. L., Singaraja, R., Ellerby, L., Savill, J., Roy, S., Leavitt, B., Cattaneo, E., Hackam, A., Sharp, A., Thornberry, N. et al. (2000). Inhibiting caspase cleavage of huntingtin reduces toxicity and aggregate formation in neuronal and nonneuronal cells. *J Biol Chem* **275**, 19831-8.

Weng, C., Li, Y., Xu, D., Shi, Y. and Tang, H. (2005). Specific cleavage of Mcl-1 by caspase-3 in tumor necrosis factor-related apoptosis-inducing ligand (TRAIL)-induced apoptosis in Jurkat leukemia T cells. *J Biol Chem* **280**, 10491-500.

Wiegand, R. C., Carr, C., Minnerly, J. C., Pauley, A. M., Carron, C. P., Langner, C. A., Duronio, R. J. and Gordon, J. I. (1992). The Candida albicans myristoyl-CoA:protein N-myristoyltransferase gene. Isolation and expression in Saccharomyces cerevisiae and Escherichia coli. *J Biol Chem* **267**, 8591-8.

Wilcox, C., Hu, J. S. and Olson, E. N. (1987). Acylation of proteins with myristic acid occurs cotranslationally. *Science* **238**, 1275-8.

Willert, K., Brown, J. D., Danenberg, E., Duncan, A. W., Weissman, I. L., Reya, T., Yates, J. R., 3rd and Nusse, R. (2003). Wnt proteins are lipid-modified and can act as stem cell growth factors. *Nature* **423**, 448-52.

Wright, M. M., Howe, A. G. and Zaremberg, V. (2004). Cell membranes and apoptosis: role of cardiolipin, phosphatidylcholine, and anticancer lipid analogues. *Biochem Cell Biol* **82**, 18-26.

Wright, R., Basson, M., D'Ari, L. and Rine, J. (1988). Increased amounts of HMG-CoA reductase induce "karmellae": a proliferation of stacked membrane pairs surrounding the yeast nucleus. *J Cell Biol* **107**, 101-14.

Wyllie, A. H. (1997). Apoptosis: an overview. *Br Med Bull* **53**, 451-65.

Wyllie, A. H., Bellamy, C. O., Bubb, V. J., Clarke, A. R., Corbet, S., Curtis, L., Harrison, D. J., Hooper, M. L., Toft, N., Webb, S. et al. (1999). Apoptosis and carcinogenesis. *Br J Cancer* **80 Suppl 1**, 34-7.

Xia, J., Lee, D. H., Taylor, J., Vandelft, M. and Truant, R. (2003). Huntingtin contains a highly conserved nuclear export signal. *Hum Mol Genet* **12**, 1393-403.

Xu, T. R., He, G. and Rumsby, M. G. (2009). Adenosine triggers the nuclear translocation of protein kinase C epsilon in H9c2 cardiomyoblasts with the loss of phosphorylation at Ser729. *J Cell Biochem* **106**, 633-42.

Xu, T. R. and Rumsby, M. G. (2004). Phorbol ester-induced translocation of PKC epsilon to the nucleus in fibroblasts: identification of nuclear PKC epsilon-associating proteins. *FEBS Lett* **570**, 20-4.

Yanai, A., Huang, K., Kang, R., Singaraja, R. R., Arstikaitis, P., Gan, L., Orban, P. C., Mullard, A., Cowan, C. M., Raymond, L. A. et al. (2006). Palmitoylation of huntingtin by HIP14 is essential for its trafficking and function. *Nat Neurosci* **9**, 824-31.

Yang, J., Brown, M. S., Liang, G., Grishin, N. V. and Goldstein, J. L. (2008). Identification of the acyltransferase that octanoylates ghrelin, an appetite-stimulating peptide hormone. *Cell* **132**, 387-96.

Yang, S., Wang, X., Contino, G., Liesa, M., Sahin, E., Ying, H., Bause, A., Li, Y., Stommel, J. M., Dell'antonio, G. et al. (2011). Pancreatic cancers require autophagy for tumor growth. *Genes Dev* **25**, 717-29.

Yang, S. H., Shrivastav, A., Kosinski, C., Sharma, R. K., Chen, M. H., Berthiaume, L. G., Peters, L. L., Chuang, P. T., Young, S. G. and Bergo, M. O. (2005). N-myristoyltransferase 1 is essential in early mouse development. *J Biol Chem* **280**, 18990-5.

Yap, M. C., Kostiuk, M. A., Martin, D. D., Perinpanayagam, M. A., Hak, P. C., Siddam, A., Majjigapu, J. R., Rajaiah, G., Keller, B. O., Prescher, J. A. et al. (2009). Rapid and selective detection of fatty acylated proteins using {omega}-alkynyl-fatty acids and click chemistry. *J Lipid Res*.

Yap, M. C., Kostiuk, M. A., Martin, D. D., Perinpanayagam, M. A., Hak, P. G., Siddam, A., Majjigapu, J. R., Rajaiah, G., Keller, B. O., Prescher, J. A. et al. (2010). Rapid and selective detection of fatty acylated proteins using omega-alkynyl-fatty acids and click chemistry. *J Lipid Res* **51**, 1566-80.

Yim, H., Hwang, I. S., Choi, J. S., Chun, K. H., Jin, Y. H., Ham, Y. M., Lee, K. Y. and Lee, S. K. (2006). Cleavage of Cdc6 by caspase-3 promotes ATM/ATR kinase-mediated apoptosis of HeLa cells. *J Cell Biol* **174**, 77-88.

Yim, H., Jin, Y. H., Park, B. D., Choi, H. J. and Lee, S. K. (2003). Caspase-3-mediated cleavage of Cdc6 induces nuclear localization of p49-truncated Cdc6 and apoptosis. *Mol Biol Cell* **14**, 4250-9.

Zha, J., Weiler, S., Oh, K. J., Wei, M. C. and Korsmeyer, S. J. (2000). Posttranslational N-myristoylation of BID as a molecular switch for targeting mitochondria and apoptosis. *Science* **290**, 1761-5.

Zhang, K. and Kaufman, R. J. (2004). Signaling the unfolded protein response from the endoplasmic reticulum. *J Biol Chem* **279**, 25935-8.

Zhao, Y., McCabe, J. B., Vance, J. and Berthiaume, L. G. (2000). Palmitoylation of apolipoprotein B is required for proper intracellular sorting and transport of cholesteroyl esters and triglycerides. *Mol Biol Cell* **11**, 721-34.

Zimmermann, K. C., Bonzon, C. and Green, D. R. (2001). The machinery of programmed cell death. *Pharmacol Ther* **92**, 57-70.

Zou, H., Li, Y., Liu, X. and Wang, X. (1999). An APAF-1.cytochrome c multimeric complex is a functional apoptosome that activates procaspase-9. *J Biol Chem* **274**, 11549-56.

Zuccato, C., Ciammola, A., Rigamonti, D., Leavitt, B. R., Goffredo, D., Conti, L., MacDonald, M. E., Friedlander, R. M., Silani,

V., Hayden, M. R. et al. (2001). Loss of huntingtin-mediated BDNF gene transcription in Huntington's disease. *Science* **293**, 493-8.